Mathematical Problems in Engineering

Intelligent Collaborative Decision Making Models, Methods, and Tools

Lead Guest Editor: Goran D. Putnik
Guest Editors: Leonilde Varela and Vladimir Modrak

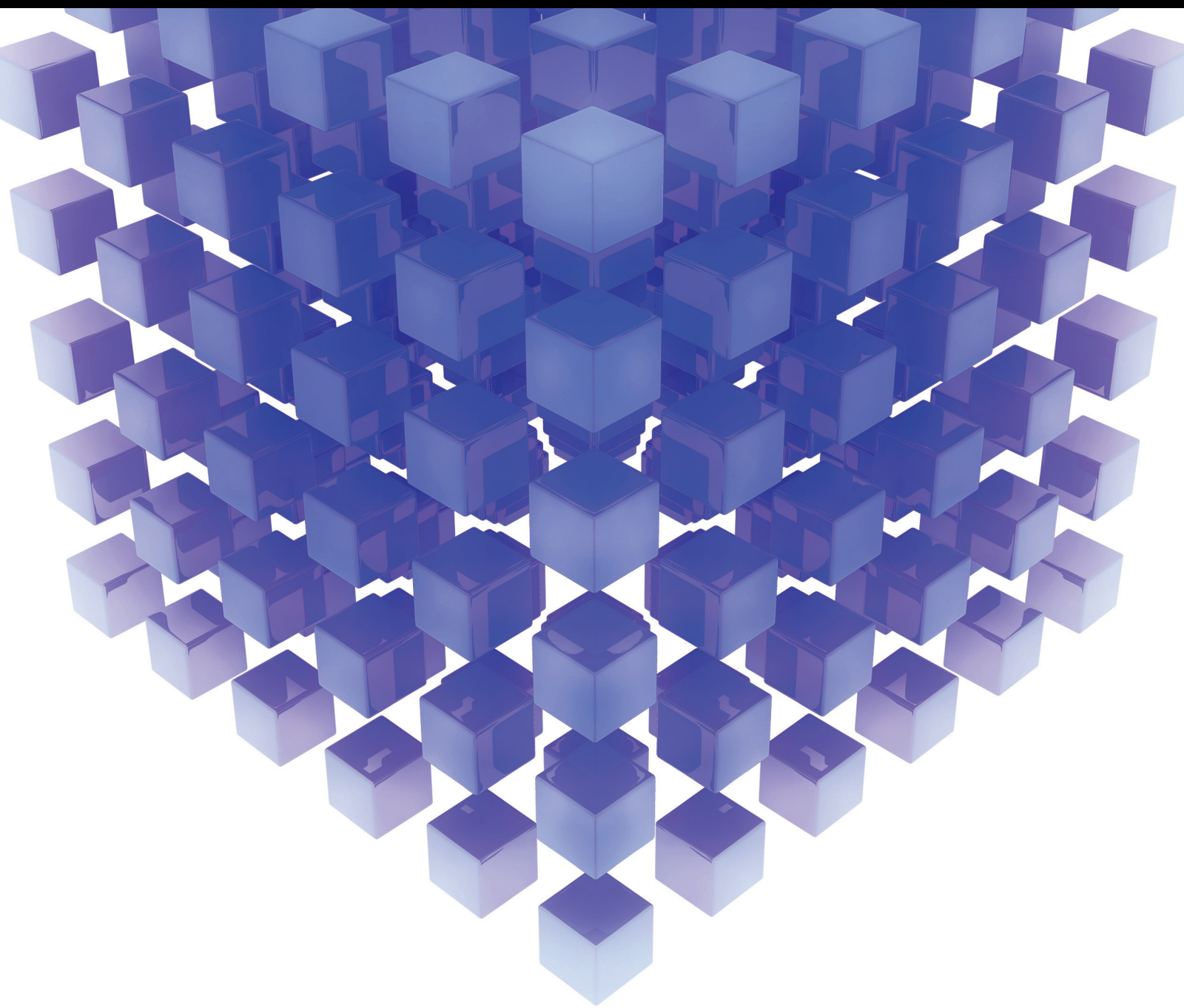

Intelligent Collaborative Decision Making Models, Methods, and Tools

Mathematical Problems in Engineering

Intelligent Collaborative Decision Making Models, Methods, and Tools

Lead Guest Editor: Goran D. Putnik
Guest Editors: Leonilde Varela and Vladimir Modrak

Editorial Board

Contents

Hindawi
Mathematical Problems in Engineering
Volume 2018, Article ID 9627917, 2 pages
https://doi.org/10.1155/2018/9627917

Editorial

Intelligent Collaborative Decision-Making Models, Methods, and Tools

Goran D. Putnik,[1] **Leonilde Varela**,[1] **and Vladimír Modrák**[2]

[1]*University of Minho, Campus of Azurém, Guimarães, Portugal*
[2]*Technical University of Košice Letná 9, 042 00 Košice, Slovakia*

Correspondence should be addressed to Goran D. Putnik; putnikgd@dps.uminho.pt

Received 24 June 2018; Accepted 24 June 2018; Published 5 July 2018

Problems in engineering are usually hard to be modeled and solved through mathematical approaches, due to the complex nature of these problems and the need for specifying effective, efficient, and proper models to consider and approach real-life or empirical and emulated problem scenarios. Many proposals are constantly being put forward, based on different kind of models, specially referring to mathematical models, and formalization approaches, in the context of this journal, ranging from purely linear programming models, algebra or differential equations based models to artificial intelligent (AI) oriented models or based on agents or neural networks. These include a great number of AI tools, such as fuzzy theory, grey theory, neural network model, Genetic Algorithms, and expert systems.

This special issue addresses intelligent, collaborative decision-making models, methods, and tools for enabling improvements towards collaborative management and the optimization of production activities as well as enhancement of supply chain and networked manufacturing processes. One of the biggest problems arising in the context of engineering and production management science, besides the problem of data collection, is related to information modeling and processing in secure and timely manner. Decision support models and tools have to become increasingly more interactive and accurate across software-based systems intended to support business and organizational decision-making activities in order to help decision makers to compile and process information, specify useful business models and processes, and solve production management problems in companies. The advent of the web and cloud computing have enabled interorganizational decision support systems and have given rise to numerous challenges and applications of existing technology as well as many new decision support models, methods, and technologies.

A number of important works have been carried out during the last decade focusing on these issues, and in this special issue on intelligent, collaborative decision-making models, methods, and tools, a set of papers that further explore this issues are incorporated.

One paper of this special issue addresses a time-variant variance and time-variant expected market demand model to investigate order strategies that are used by risk-averse holiday merchants. Through their newsvendor model, the authors were able to capture the unique characteristics of holiday merchandise in the retail market to investigate the display time and the traditional order quantity decision with time-sensitive purchase cost, therefore helping to offer a more detailed understanding of the interaction among these important parameters through numerical analysis.

Another paper puts forward a plant intelligent behaviour optimization algorithm for solving vehicle routing problem. The algorithm is motivated by intelligent behaviour of plants and is implemented to solve benchmark vehicle routing problems of all sizes. The algorithm is able to be applied to very large vehicle routing problem instances due to the ability of the plant to use previously stored memory to respond to new problems and to adjust to changing problem conditions.

The authors of another paper propose network Data Envelopment Analysis models based on slacks-based measure framework which categorize intermediate measures into

input or output type endogenously. Moreover, to incorporate inefficiency associated with intermediate measures in efficiency measurement they propose two alternative slacks-based measure models referred to as Model (I) and Model (II), to address the conflict caused by the dual role of intermediate measures, which can be applied to deal with dynamic network models.

Another study presents a cycle deep belief network model for multivariate time series classification, which is a learning algorithm that can discover the structure hidden in the data and learn representations that are more suitable as input to a supervised machine than the raw input. This kind of contributions is quite important as time series classifications are becoming increasingly more important in a broad range of real world applications.

One of the papers of this special issue addresses secure k-nearest neighbors (kNN) computation and integrity assurance of data outsourcing in the cloud. Therefore, the authors propose a verifiable spatial data index structure (VSS-tree) to improve kNN query efficiency and provide kNN query verification. Moreover, for resisting level 2 attacks, the cloud server can perform a kNN query on encrypted data points and query points.

Another study puts forward a recommendation approach based on simulation for suggesting optimized production conditions, including processing velocity of the automated machine, to overcome and avoid contamination problems, which can very negatively affect production processes, such as in the case of manufacturing head stack assembly (HSA) within a hard disk drive factory. Therefore, the proposed approach is suitable for recommending sustainable optimized production conditions to provide enhanced environmental conditions, along with improved economical manufacturing conditions, with reduced energy consumptions.

One paper performs an analysis of critical-barriers identification and qualitative data analysis to implement sustainable supply chain management by using interpretive structural modeling technique, based on an empirical case study.

Another paper describes a hybrid algorithm combining simulated annealing and genetic algorithm, referred to as simulated annealing genetic algorithm, along with the application of distributed decision-making and principal-agent theory to build a model for scheduling risk management of IT outsourcing projects.

The authors of one of the papers put forward an agent-based modeling and simulation approach of designer's bidirectional behaviour of task selection in open source design process, based on a website recommendation mechanism through a collaborative filtering algorithm based on a three-dimensional matrix including information of design agents, tasks and skills, and an autonomous selection approach, which can be applied in practice benefiting both designers and open source design.

A study of this special issue presents a quite interesting risky multicriteria group decision-making approach based on cloud prospect theory and regret feedback. The approach is based on linguistic variable assessment and proposes a model that considers various and differential psychological behaviour and the ambiguity of linguistic variable assessment across multicriteria risks. Based on the cloud prospect value assessment, a cloud prospect value aggregation method and consensus degree measurement are used. Moreover, an improved feedback adjustment mechanism based on regret theory is employed as the consistency model, which complements prospect theory. The three theoretical methods together constitute the core elements of the authors' proposed cloud prospect value consensus degree decision model.

Goran D. Putnik
Leonilde Varela
Vladimír Modrák

Hindawi
Mathematical Problems in Engineering
Volume 2018, Article ID 7947894, 11 pages
https://doi.org/10.1155/2018/7947894

Research Article

An Empirical Research on Marketing Strategies of Different Risk Preference Merchant

Quan Chen,[1] Jiangtao Wang,[1] Jianjun Yu,[2] and Sang-Bing Tsai[1,3,4,5]

[1]*Zhongshan Institute, University of Electronic Science and Technology of China, Guangdong 528400, China*
[2]*School of Business Administration, South China University of Technology, Guangzhou 510641, China*
[3]*China Academy of Corporate Governance, Nankai University, Tianjin 300071, China*
[4]*Economics and Management College, Civil Aviation University of China, Tianjin 300300, China*
[5]*Business and Law School, Foshan University, Guangdong 528000, China*

Correspondence should be addressed to Jiangtao Wang; jiangtao-w@foxmail.com, Jianjun Yu; yujj@scut.edu.cn, and Sang-Bing Tsai; sangbing@hotmail.com

Received 20 June 2017; Accepted 11 March 2018; Published 24 April 2018

Academic Editor: Leonilde Varela

Holiday merchandise has unique demand characteristics, unofficial start data, and a limited life cycle. In an intensely competitive market, individual merchants are able to get more sales opportunities if they display their products earlier. In this study, a time-variant variance and time-variant expected market demand model are introduced to investigate the order strategies that are used by risk-averse holiday merchants. Our results show that risk preference, market uncertainty, and market power have a significant effect on the merchant's market strategies. Risk-averse merchants prefer to enhance forecast accuracy rather than using an early-display advantage. They can even give up their early-display advantage if they are faced with increased market uncertainty and small market power. Compared with the fixed purchase cost, the time-sensitive purchase cost can stimulate the merchant to purchase in advance, but this can decrease the merchant's profit. Consequently, risk-averse merchants always display their merchandise later, decrease the order quantity, and, finally, miss the market opportunity.

1. Introduction

As a special type of seasonal goods, holiday merchandise has unique demand characteristics, such as an unofficial start date and a finite selling horizon [1]. Most holiday goods are introduced into the retail market over a well-defined and finite selling horizon. They are then removed from display after the special date has passed. For example, as described by Robert Rand, "*Although the holiday shopping season does not 'officially' begin until the Friday after Thanksgiving, artificial trees and holiday wreaths now appears in some store as early as September*" [2]. Similarly, the Chinese Spring Festival shopping season always officially begins on 23 December. However, the New Year's gatepost couplet has recently appeared in the Chinese retail market at the beginning of December. The total amount of money that shoppers spend on holiday merchandise is largely independent of the length of the holiday. In addition, an early display entails opportunity costs. Why then do these merchants put this holiday merchandise on display so early? Frank [2] argued that the rationale behind early display is that, in a fiercely competitive market, any merchants who wait until the Friday after Thanksgiving to display Christmas wreaths will lose out to merchants who display them earlier, allowing them to capture more of the market demand (the early part) and reap the first-mover advantage. This is the reason why some US merchants put Christmas decorations on display as early as Labor Day. However, this phenomenon is limited, and we do not eventually see year-round displays of holiday merchandise.

The early display not only comes at the expense of reduced sales of other merchandise (e.g., because the shelves used for displaying the Christmas decorations cannot be used for displaying other merchandise, which in turn means

reduced sales of the other merchandise and smaller profits for the merchants [2]) but also can face high-demand forecast errors. The previous literature shows that the uncertainty in the market demand for holiday merchandise is problematic for merchants when they have to make a decision for the display time and for the quantities of holiday merchandise to order [3–7]. A Wal-Mart survey has shown that the demand forecast error is 40% if it purchases products from suppliers 26 weeks in advance, while the forecast error is decreased to 10% if it orders products at the beginning of the sales period [8]. Hence, the forecast error is likely to be larger when the date of display is earlier. Therefore, an early display may help the merchant to capture more of the market demand but can reduce the sales of other merchandise (because the shelves are limited) and increase the sales forecast error.

This study aims to investigate the merchant's challenge of optimizing the display time and inventory management of holiday merchandise in a competitive retail market that is characterized by uncertainty, low-salvage values, and high stock-out costs. The merchant's risk preference is introduced to consider how these market strategies vary in an uncertain market environment [9–11]. In this study, a model where both the market sale and the demand forecast accuracy are time-sensitive is introduced into the decision model to numerically analyze the merchant's display time and order quantity.

The rest of this paper is organized as follows. Section 2 provides a brief literature review. Section 3 introduces the basic assumptions for the model and yields the retailer's objective function. Section 4 presents the optimal risk-neutral solutions that will be used as benchmarks. Section 5 will investigate the optimal solutions for a risk-averse merchant. Section 6 gives some numerical examples and outlines the managerial implications. Section 7 concludes with a discussion of the results, and it makes some suggestions for future research.

2. Literature Review

Our models are largely inspired by the holiday merchandise problem and by previous studies of traditional newsvendor models that examine a demand uncertainty environment and a quick response system. In this section, we will briefly review each stream of the literature related to our study.

The first research stream of interest is demand uncertainty. The demand uncertainty of holiday products has been widely recognized as an important issue in the operations management literature. Milner and Rosenblatt tried to reduce the negative effect of uncertain demand using a quantity flexible contract [12]. Weng considered using the coordination mechanism in the supply chain to meet demand uncertainty [13]. In addition, Hua et al. considered the effects of demand uncertainty on supply chain cooperation [14]. The operational environment in this present research is similar to those presented in the previous literature [15–17]. In particular, the modeling approach that is used in this study is related to the traditional newsvendor models that are used in an uncertain market demand environment. Readers can refer to the literature [18] for an extensive review of these models. Demand uncertainty is the basic market characteristic that is faced by decision-makers. Recently, Sana and Goyal incorporated variable purchasing cost of the order quantity, lead-time-dependent partial backordering, and lost sales into the (Q, r, L) model in a random demand environment [19]. Radhi and Zhang studied the optimal configuration of a remanufacturing supply network with stochastic demand [20]. Zhao et al. analyzed the lateral inventory transshipment problem for a dual-channel supply chain with uncertain market demand [21]. A substantial amount of research has assumed that uncertain demand is price sensitive, service sensitive, or both price and promised lead-time sensitive and price and service sensitive. For example, some studies have assumed that uncertain demand is both price and lead-time sensitive [11, 21–24]. Xiao et al. modeled the demand uncertainty with the lead time and considered the effects of lead time and the length of selling on demand uncertainty [24]. In addition, Sana has introduced price-dependent demand with random sales price into the classical newsboy problem [25]. In summary, most of the previous studies of the newsvendor model have either assumed that uncertain market demand is independent of any decision variable or assumed that uncertain demand is price or both price and lead-time sensitive. However, both the expected market sales and the forecast accuracy in the uncertain demand environment for holiday merchandise are affected by the display time. Hence, a time-sensitive expected market and forecast accuracy demand model is introduced in this study.

The second research stream of interest is the time-variant market demand model in a quick response system. This research assumes that the merchant can enhance forecast accuracy in an uncertain market by collecting market information. For example, some literature has assumed that lead-time reduction can help enhance the forecast accuracy in an uncertain demand market [4–6, 26–28]. First, Chen and Chuang pointed out the relationships between the purchasing time and the time variance of uncertain demand and embedded the time-variant variance of demand into the classical newsvendor problem by considering the purchasing time and order quantity as a decision variable [26]. Subsequently, Chuang developed the decision model by extending the demand distribution into an unidentified demand distribution function [29]. Recently, some literature has also introduced the time-variant variance of demand model into the supply chain to consider the time factors [5–7, 30]. For example, Wang et al. used the time-variant demand model in the supply chain to consider the retailer's purchase time and order quantity under different statement strategies [6]. Li et al. investigated the optimal lead-time policy for short life cycle products by assuming that the lead-time reduction can enhance forecast accuracy in an uncertain demand market [5]. However, replenishment lead times are much longer compared with the length of the selling season in some seasonal goods industries, which limits the merchant's opportunity to replenish the inventory during the season. Therefore, the holiday merchant must decide the order inventory by forecasting demand before the selling season. Consequently, this study assumes that not only the forecast

accuracy but also the expected markets sales are related to the timing of displaying holiday products. The model in our study is closest to Wang et al.'s [7], who considered the display time and order quantity with the fixed purchase cost. However, as Chen and Chuang [26] pointed out, suppliers are often more than willing to carry a price discount to stimulate the merchant to purchase earlier and so decrease the inventory level. Hence, we introduce a similar time-sensitive purchase cost as that used by Chen and Chuang [26] into our model to consider the holiday merchant's marketing strategies, which differ from Wang et al.'s [7].

3. Description of the Problem

Consider a merchant who sells a kind of holiday merchandise to the retail market, such as an artificial Christmas tree or Spring Festival merchandise. Although this holiday merchandise does not have an official start date to the market, year-round displays of this holiday merchandise do not occur in practice. Consequently, there must exist a critical time point ($t = 0$) where the potential demand may occur but the probability approximates to zero. However, delaying display after this critical point will come at the expense of less market share because it has been taken by the other merchants. Hence, we assume that the merchant will sell holiday merchandise to the market on a concentrated selling $[0, T]$ and that the market demand D is random and time-sensitive with respect to the display time t. An early-display date can help the merchant to capture more market demand. Thus, the market demand when displaying the holiday merchandise at time t can be expressed as

$$D(t) = d - \alpha e^{-\gamma(T-t)} + \varepsilon(t), \quad 0 \le t \le T, \tag{1}$$

where d represents the maximum market demand potential and α represents the competitive market size (i.e., the merchant's power in the retail market). The exponential-function marketing model $e^{-\gamma(T-t)}$ is used to characterize the possible fraction of the competitive market demand that has been taken by the competitors when displaying at time t. The exponential-function type is widely used in the literature [31–33]. In addition, γ is the coefficient of the elasticity of competition. The stochastic part of market $\varepsilon(t)$ is time-sensitive white noise of the forecast at display time t [34]. Following the model that was used by Chen and Chuang [26], we also assume $\varepsilon(t) = X(\sigma(T-t)/T)$, $X \sim N(0,1)$, with the probability density $f(\cdot)$, and cumulative distribution function $F(\cdot)$ and its inverse function $\overline{F}(\cdot) = 1 - F(\cdot)$. Here, σ represents demand deviation, that is, the market demand uncertainty. Then, we have $E(\varepsilon(t)) = 0, \operatorname{var}(\varepsilon(t)) = \sigma^2(t) = (T-t)^2/T^2\sigma^2$. Generally, we assume that $d - \alpha\varphi(t) (> 0)$ is much larger than σ so that $\Pr\{D(t) \le 0\}$ can be negligible.

Consider the following scenario faced by a merchant: p represents the retail price in a competitive retail market and s is the salvage price for the unsold merchandise at the end of the holiday. The supplier will charge a higher price discount $c(t)$ to stimulate the consumer to purchase earlier to allow the supplier to decrease their inventory level. Hence, it is reasonable to assume that the supplier will charge price discount $c(t) = c + \delta t$ at time t to stimulate the merchant to purchase earlier, while the purchase cost must satisfy $s < c(t) < p$, $\forall t \in [0, T]$. The holiday merchant then faces the challenge of maximizing utility by determining the order inventory and purchase time to display the product on the shelves to capture uncertain market demand, as follows:

$$\begin{aligned}\pi(Q,t) = {} & p\min(Q,D) + s[Q-D]^+ - (c+\delta t)Q \\ & - \theta(T-t),\end{aligned} \tag{2}$$

where $\theta(T-t)$ denotes the opportunity cost because the shelves used for holiday merchandise cannot be used to display other merchandise, $[x]^+ = \max\{x, 0\}$.

4. The Benchmark Model

This section will characterize the risk of the merchant's marketing strategies. Here, we first use a risk-neutral model as a benchmark. The unity for the risk-neutral merchant is the expected profit, as follows:

$$\begin{aligned}& E(\pi(Q,t)) \\ & = (p-s)(\mu - Q) F\left(\frac{T(Q-\mu)}{(T-t)\sigma}\right) \\ & \quad + (p-s)\sigma\frac{T-t}{T}\int_{-\infty}^{T(Q-\mu)/(T-t)\sigma} x f(x)\,dx \\ & \quad + (p-c-\delta t)Q - \theta(T-t),\end{aligned} \tag{3}$$

where $\mu = d - \alpha e^{\gamma(t-T)}$.

Lemma 1. *For any display time t, a risk-neutral merchant's expected profit $E(\pi(Q,t))$ is always a concave function of the order quantity.*

Proof. For any time t, taking the first and second partial derivatives of $E(\pi(Q,t))$ with respect to Q, we obtain $\partial E(\pi(Q,t))/\partial Q = -(p-s)F(T(Q-\mu)/(T-s)\sigma) + (p-c-\delta t)$, $\partial^2 E(\pi(Q,t))/\partial Q^2 = -((p-s)T/(T-t)\sigma) f(T(Q-\mu)/(T-t)\sigma) \le 0$. Hence, the expected profit is a concave function of the order quantity. □

Lemma 2. *For a risk-neutral merchant, the order quantity can be expressed by the purchase time as $Q^*_{RN} = d - \alpha e^{\gamma(t^*_{RN}-T)} + \sigma((T - t^*_{RN})/T)F^{-1}(\beta)$, and the optimal display time t^*_{RN} can be determined by the following algorithm:*

(1) Solve the equation $\alpha e^{\gamma(t-T)}(\delta - \gamma(p-c-\delta t)) - \delta d - ((p-s)\sigma/T)(F^{-1}(\beta)\beta - \int_{-\infty}^{F^{-1}(\beta)} F(x)dx) - ((T-t)\sigma\delta/T)F^{-1}(\beta) + \theta = 0$ to obtain the solutions represented as $t_1, t_2, \ldots, t_n$.

(2) Let $\Theta = \{t_i \mid 0 \le t_i \le T,\ i = 1, 2, \ldots, n\}$.

(3) Compute the values of (3) to obtain the optimal solution as

$$t_{\mathrm{RN}}^{*} = \arg\max \left\{ E\left(\pi\left(Q^{*}, t_i\right)\right), E\left(\pi\left(Q^{*}, 0\right)\right), E\left(\pi\left(Q^{*}, T\right)\right) \mid t_i \in \Theta \right\}, \tag{4}$$

where $\beta \triangleq (p - c - \delta t)/(p - s)$.

Proof. From Lemma 1, it can be seen that the expected profit function $E(\pi(Q,t))$ is a concave function of the order quantity. Consequently, the optimal order quantity can be obtained by solving the derivatives function of $E(\pi(Q,t))$ with respect to Q, and then $Q_{\beta}^{*} = d - \alpha e^{\gamma(t-T)} + \sigma((T - t)/T)F^{-1}(\beta)$, $\beta \triangleq (p - c - \delta t)/(p - s)$.

By substituting Q_{β}^{*} into formula (3), we have $E(\pi(Q_{\beta}^{*}, t)) = (p - c - \delta t)(d - \alpha e^{\gamma(t-T)}) + (p - s)\sigma((T - t)/T)(F^{-1}(\beta)\beta - \int_{-\infty}^{F^{-1}(\beta)} F(x)dx) - \theta(T - t)$. $E(\pi(Q_{\beta}^{*}, t))$ is a continuous and differentiable function of $t \in [0, T]$. However, it is difficult to express the analytical results because they are nonlinear. Therefore, based on algebraic theory, there exists a maximum point $t^{*}(\in [0, T])$ that satisfies $\pi(Q_{\beta}^{*}, t^{*}) = \max_t E(\pi(Q_{\beta}^{*}, t))$. The optimal purchase time can then be found through the following algorithm:

(1) Differentiate the expected function $E(\pi(Q_{\beta}^{*}, t))$ with respect to t as $dE(\pi(Q^{*}, t))/dt = \alpha e^{\gamma(t-T)}(\delta - \gamma(p - c - \delta t)) - \delta d - ((p - s)\sigma/T)(F^{-1}(\beta)\beta - \int_{-\infty}^{F^{-1}(\beta)} F(x)dx) - ((T - t)\sigma\delta/T)F^{-1}(\beta) + \theta$.

(2) Let $dE(\pi(Q^{*}, t))/dt = 0$ to allow us to obtain the solutions expressed as $(t_1, t_2, \ldots, t_n)$.

(3) Obtain the valid extreme values set by excluding the invalid extreme as $\Theta = \{t_i \mid 0 \le t_i \le T,\ i = 1, 2, \ldots, n\}$.

(4) Compute the possible optimal values for the expected function $E(\pi(Q_{\beta}^{*}, t_i))$, $t_i \in \Theta$, and then compare these values to find the optimal time point t_{RN}^{*} that satisfies $t_{\mathrm{RN}}^{*} = \arg\max\{E(\pi(Q^{*}, t_i)), E(\pi(Q^{*}, 0)), E(\pi(Q^{*}, T)) \mid t_i \in \Theta\}$. □

5. The Influence of Risk Reference on a Merchant's Optimal Strategies

The previous literature has shown that decision-makers will tend to be risk-averse because they are faced with an uncertain environment [35, 36]. The risk-aversion issue can be addressed as the expected utility criterion [37], mean-variance objective function [38], and conditional value at risk (CVaR) [39]. In particular, the CVaR criterion measures "the average value of the profit falling below a certain quantile level; it takes into account both reward and risk," which has drawn attention in the study of operational management [10, 39, 40]. In this study, we adopt CVaR to measure the risk-averse merchant's performance.

The merchant's objective is to maximize the following utility function according to the general definition of CVaR [40]:

$$CVaR_{\eta}\left(\pi\left(Q,t\right)\right) = \max_{v \in R}\left\{ v + \frac{1}{\eta} E\left[\min\left(\pi\left(Q,t\right) - v, 0\right)\right]\right\}, \tag{5}$$

where E is the expected operator, R represents the real number set, $\eta \in (0, 1]$ reflects the degree of risk aversion for the merchant (the smaller the value of η is, the more risk-averse the retailer will be), and v represents the possible upper limit of the profit under certain η.

Theorem 3. *For a risk-averse merchant, the order quantity can be expressed by the purchase time as*

$$Q_{RA}^{*} = d - \alpha e^{-\gamma(T - t_{RA}^{*})} + \frac{\left(T - t_{RA}^{*}\right)\sigma F^{-1}\left(\tau\right)}{T}, \tag{6}$$

and the optimal purchase time t_{RA}^{*} can be determined by the following algorithm:

(1) Solve the equation $(-\delta/\eta)\sigma((T - t)/T)F^{-1}(\tau) - (1/\eta T)(p - s)\sigma\int_{-\infty}^{F^{-1}(\tau)} x\,dF(x) - \delta(d - \alpha e^{\gamma(t-T)}) - (p - c - \delta t)\alpha\gamma e^{\gamma(t-T)} + \theta = 0$ to obtain the solutions as $t_1, t_2, \ldots, t_n$.

(2) Let $\Gamma = \{t_i \mid 0 \le t_i \le T,\ i = 1, 2, \ldots, n\}$.

(3) Compute the values of formula (6) to obtain the optimal solution as

$$t_{\mathrm{RA}}^{*} = \arg\max \left\{ E\left(\pi\left(Q^{*}, t_i\right)\right), E\left(\pi\left(Q^{*}, 0\right)\right), E\left(\pi\left(Q^{*}, T\right)\right) \mid t_i \in \Gamma \right\}, \tag{7}$$

where $\tau \triangleq ((p - c - \delta t)/(p - s))\eta = \beta\eta$.

Proof. From the definition of CVaR, substitute $\pi(Q,t)$ into formula (5) and the optimal order quantity satisfying $Q^{*}(t) = \arg\max_{Q \ge 0}\{\max_v g(Q,t,v)\}$. Obviously, $g(Q,t,v) = v - (1/\eta)E[v - \pi(Q,t)]^{+} = v - (1/\eta)\int_0^{Q}[v - (s - c_t)Q - (p - s)x + \theta(T - t)]^{+}d\Phi(t,x) - (1/\eta)\int_{Q}^{+\infty}[v - (p - c_t)Q + \theta(T - t)]^{+}d\Phi(t,x)$, where $\Phi(t,x)$ represents the cumulative distribution function of the market demand $D(t,X)$ and $c_t = c + \delta t$ □

(1) For any given Q, t, we can first solve $\max_v g(Q,t,v)$.

Case 1. If $v < (s - c_t)Q - \theta(T - t)$, then $v - (s - c_t)Q - (p - s)x + \theta(T - t) < 0$, $v - (p - c_t)Q + \theta(T - t) < 0$ and $g(Q,t,v) = v$, and thus $\partial g(Q,t,v)/\partial v = 1 > 0$.

Case 2. If $(s - c_t)Q - \theta(T - t) \le v \le (p - c_t)Q - \theta(T - t)$, then

if $x > (v - (s - c_t)Q + \theta(T - t))/(p - s)$, then $g(Q,t,v) = v$, and thus $\partial g(Q,t,v)/\partial v = 1 > 0$;

if $x \le (v-(s-c_t)Q+\theta(T-t))/(p-s)$, then $g(Q,t,v) = v-(1/\eta)\int_0^{(v-(s-c_t)Q+\theta(T-t))/(p-s)} v-(s-c_t)Q-(p-s)x+\theta(T-t)d\Phi(t,x)$, and thus $\partial g(Q,t,v)/\partial v = 1-(1/\eta)\Phi(t,(v-(s-c_t)Q+\theta(T-t))/(p-s))$ and $(\partial g(Q,t,v)/\partial v)|_{v=(s-c_t)Q-\theta(T-t)} = 1-(1/\eta)\Phi(t,0) = 1 > 0$, $(\partial g(Q,t,v)/\partial v)|_{v=(p-c_t)Q-\theta(T-t)} = 1-(1/\eta)\Phi(t,Q)$.

Case 3. If $v \ge (p-c_t)Q-\theta(T-t)$, then $g(Q,t,v) = v-(1/\eta)\int_0^Q v-(s-c_t)Q+(p-s)x+\theta(T-t)d\Phi(t,x)-(1/\eta)(v-(p-c_t)Q+\theta(T-t))(1-\Phi(t,Q))$, and thus $\partial g(Q,t,v)/\partial v = 1-(1/\eta)(\Phi(t,Q)+1-\Phi(t,Q)) = 1-(1/\eta) < 0$ $(\eta \in (0,1))$.

Combine Case 1 and Case 3; the optimal solutions for given Q and t must then be in the interval $[(s-c_t)Q-\theta(T-t),(p-c_t)Q-\theta(T-t)]$.

(i) If $1-(1/\eta)\Phi(t,Q) \le 0$, that is, $\eta < \Phi^{-1}(t,Q)$, then the optimal solutions $\widetilde{v}$ must satisfy $1-(1/\eta)\Phi(t,(\widetilde{v}-(s-c_t)Q+\theta(T-t))/(p-s)) = 0$, and thus $\widetilde{v} = (s-c_t)Q-\theta(T-t)+(p-s)\Phi^{-1}(t,\eta)$. By substituting into $g(Q,t,v)$ in Case 2, we have $g(Q,t,\widetilde{v}) = (s-c_t)Q-\theta(T-t)+(1/\eta)(p-s)\int_0^{\Phi^{-1}(t,\eta)} x\,d\Phi(t,x)$. We then have $\partial g(Q,t,\widetilde{v})/\partial Q = (s-c_t) < 0$. Hence, there is no extreme value for Q under this situation.

(ii) If $1-(1/\eta)\Phi(t,Q) \ge 0$, that is, $\eta \ge \Phi^{-1}(t,Q)$, then the optimal value $\widetilde{v}$ can be obtained as $\widetilde{v} = (p-c_t)Q-\theta(T-t)$.

(2) By substituting $\widetilde{v}$ into $g(Q,t,v)$ in Case 2, we have $g(Q,t,\widetilde{v}) = (p-c_t)Q-\theta(T-t)-(1/\eta)\int_0^{((p-c_t)Q-\theta(T-t)-(s-c_t)Q+\theta(T-t))/(t-s)}(p-c_t)Q-\theta(T-t)-(s-c_t)Q-(p-s)x+\theta(T-t)d\Phi(t,x) = (p-c_t)Q-\theta(T-t)-(1/\eta)\int_0^Q(p-s)(Q-x)d\Phi(t,x)$. Taking the first and second partial derivatives of $g(Q,t,\widetilde{v})$ with respect to Q yields $\partial g(Q,t,\widetilde{v})/\partial Q = (p-c_t)-(1/\eta)\int_0^Q(p-s)d\Phi(t,x) = (p-c_t)-(1/\eta)(p-s)\Phi(t,Q)$, $\partial^2 g(Q,t,\widetilde{v})/\partial Q^2 = -(1/\eta)(p-s)\phi(t,Q) \le 0$. Hence, $g(Q,t,\widetilde{v})$ is the concave function of the Q. Thus, let $\partial g(Q,t,\widetilde{v})/\partial Q = 0$ to obtain the risk-averse merchants' optimal order quantity $Q_{RA}^* = d-\alpha e^{-\gamma(T-t)}+(T-t)\sigma F^{-1}(\tau)/T$, $\tau \triangleq ((p-c_t)/(p-s))\eta$.

By substituting Q_{RA}^* into $g(Q,t,\widetilde{v})$, we obtain $g(Q_{RA}^*,t,\widetilde{v}) = (p-c_t)Q_{RA}^*-\theta(T-t)-(1/\eta)(p-s)Q_{RA}^*\int_0^{Q_{RA}^*}d\Phi(t,x)+(1/\eta)(p-s)\int_0^{Q_{RA}^*}x\,d\Phi(t,x) = Q_{RA}^*(p-c_t-(1/\eta)(p-s)\Phi(t,Q_{RA}^*))-\theta(T-t)+(1/\eta)(p-s)\int_0^{Q_{RA}^*}x\,d\Phi(t,x) = (1/\eta)(p-s)\int_0^{Q_{RA}^*}x\,d\Phi(t,x)-\theta(T-t) = (1/\eta)(p-s)\int_{-\infty}^{F^{-1}(\tau)}d(t,z)dF(z)-\theta(T-t) = (1/\eta)(p-s)\sigma((T-t)/T)\int_{-\infty}^{F^{-1}(\tau)}x\,dF(x)+(p-c)(d-\alpha\varphi(t))-\theta(T-t)$. Noticeably, $g(Q_{RA}^*,t,\widetilde{v})$ is a nonlinear function and is a continuous and differentiable function of $t \in [0,T]$. Hence, it is difficult to express the analytical optimal solutions. However, based on algebraic theory, there exists a maximum point $t^*(\in [0,T])$ which satisfies $g(Q_{RA}^*,t^*,\widetilde{v}) = \max_t g(Q_{RA}^*,t,\widetilde{v})$. The optimal point t^* can be found through the following algorithm:

(1) Take the first and second partial derivatives of $g(Q_{RA}^*,t,\widetilde{v})$ with respect to t as $\partial g(Q_{RA}^*,t,\widetilde{v})/\partial t = (-1/\eta T)(p-s)\sigma\int_{-\infty}^{F^{-1}(\tau)}x\,dF(x)+(1/\eta)(p-s)\sigma((T-t)/T)F^{-1}(\tau)(d\tau/dt)-\delta(d-\alpha e^{\gamma(t-T)})-(p-c-\delta t)\alpha\gamma e^{\gamma(t-T)}+\theta$.

(2) Let $\partial g(Q_{RA}^*,t,\widetilde{v})/\partial t = 0$ and then obtain the extreme points expressed as $(t_1,t_2,\ldots,t_n)$.

(3) Exclude the invalid extreme points and obtain the valid extreme points set as $\Gamma = \{t_i \mid 0 \le t_i \le T,\ i = 1,2,\ldots,n\}$.

(4) Substitute these valid extreme points into $g(Q_{RA}^*,t,\widetilde{v})$ and compare these values to find the optimal time points t_{RN}^* that satisfy $t_{RA}^* = \arg\max\{g(Q_{RA}^*,t_i),g(Q_{RA}^*,0),g(Q_{RA}^*,T) \mid i = 1,2,\ldots,n\}$.

6. Numerical Examples and Managerial Insights

It is difficult to obtain the analytical solutions for nonlinear decision equations. Thus, we will conduct a numerical analysis to better understand the impact of these parameters on the risk reference of the merchants' market strategies. We will then make some recommendations for holiday merchants. Our focus is on investigating how the risk-averse merchant makes the strategies, display time, and order quantity reflect the various influential parameters. To illustrate the impacts of these important parameters, we assume that $T = 120$, $d = 10000$, $p = 100$, $s = 25$, $\theta = 30$, $c = 50$, and $Y \sim N(0,1)$.

6.1. The Effects of the Degree of Risk Aversion η. In the theoretical analysis, we represent the degree of risk aversion with η; that is, a smaller η means that the merchant is more risk-averse. In particular, the merchant is risk-neutral when $\eta = 1$. Figure 1 suggests that a risk-averse merchant will delay the display time and decrease the order quantity as the merchant becomes more risk-averse. Generally, when the merchant is less risk-averse, the display will be made earlier and the order quantity will be larger. In reality, a risk-averse merchant may prefer spending more time enhancing the forecast accuracy. They may then lose the potential market and they would finally have to order a smaller quantity to meet the follow-up market demand. Risk-averse merchants always lose profit due to their risk preference. Therefore, the risk-averse merchant has to weigh the time-sensitive market demand with the forecast accuracy.

6.2. The Effect of the Uncertainty of Market σ. Figure 2 presents how the market demand uncertainty influences the merchant's display time, order quantity, and profit. From Figure 2, we can see that all of the merchants would opt to delay the display time and decrease the order quantity to meet market demand. Actually, all of the merchants will choose to wait or collect information to further enhance the accuracy of their market forecast when faced with high market demand risk. In particular, the risk-averse merchant may give up the early display entirely when faced with high market demand risk. Meanwhile, the risk-averse merchant would tend to capture the fist-mover advantage when faced with clear market demand. In addition, the merchant's profit decreases as the uncertainty of market demand increases. However, the risk-neutral merchant's profit decreases sharply and will finally tend toward the risk-averse merchant's profit with large market uncertainty. A comparison of the strategies

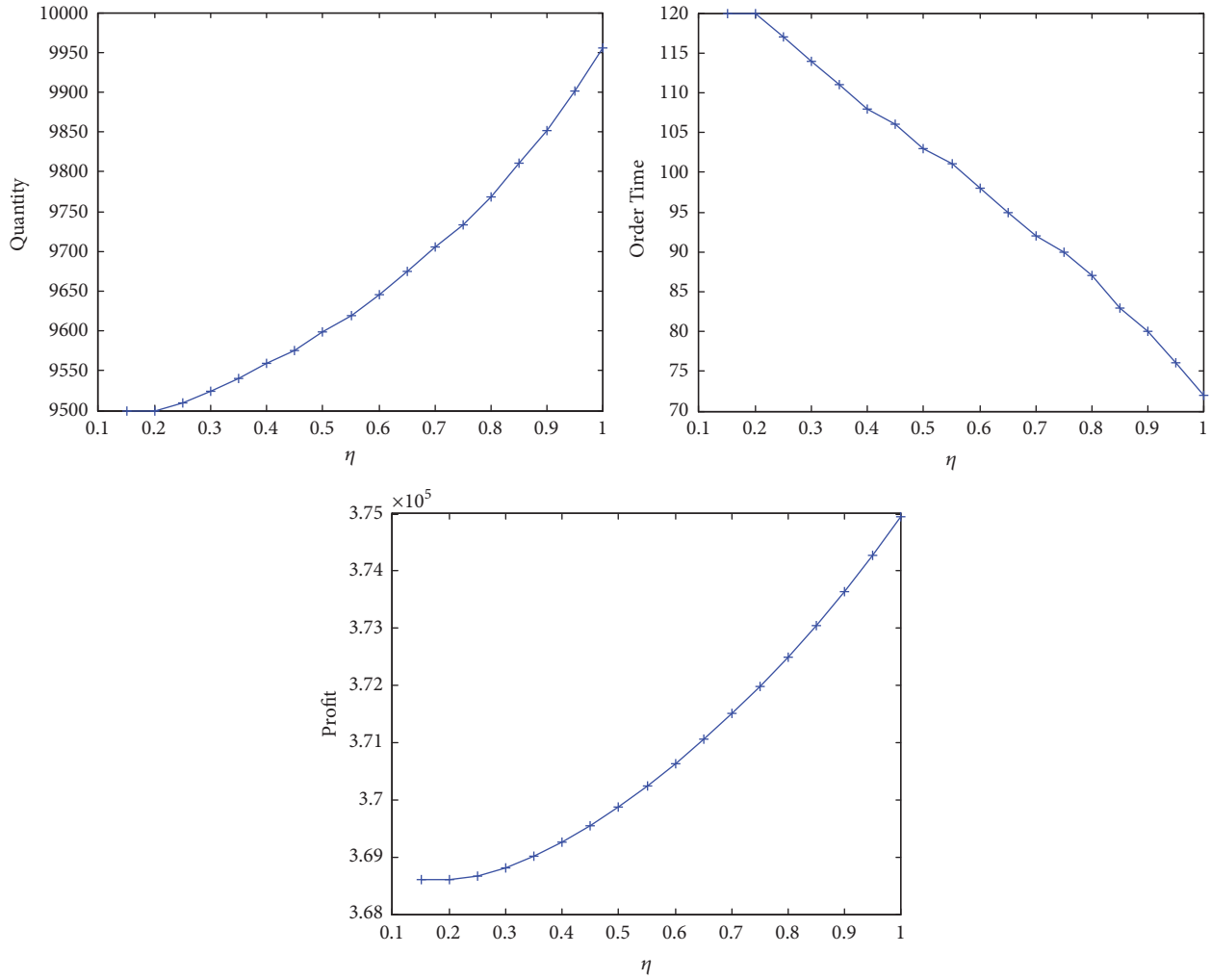

Figure 1: The effects of degree of risk aversion η with $\alpha = 500$, $\sigma = 1000$, and $\gamma = 0.025$.

used by these two types of merchants shows that risk-neutral merchants order more holiday merchandise to capture the early-display advantage and will capture more profit than the risk-averse merchant, even with increased market uncertainty.

6.3. The Effect of the Coefficient of Elasticity of Competitive γ. Here, γ represents the coefficient of the elasticity of competition; that is, a larger γ means that the market demand will make a loss due to the late display at the early stage less likely. Figure 3 shows the effects of the coefficient of the elasticity of competition on the merchant's market strategies. From Figure 3, we can see that if the market demand is less likely to be taken by competitors, then all rational merchants will choose the delay display time to decrease the opportunity cost and enhance the forecast accuracy. Meanwhile, all rational merchants will choose an early display to capture the fist-mover advantage. Hence, the merchants of different risk preferences tend to display their holiday products at the same time with larger γ. Although the certainty level of risk-neutral merchant's order quantity fluctuates, the risk-averse merchant's order quantity increases with γ. This may happen because a large γ only coincides with the risk-averse merchant's order strategies, so the risk-averse merchant's order quantity is more sensitive to γ than that of the risk-neutral merchants. Finally, the merchant's profits will benefit from high forecast accuracy and a decrease of the opportunity cost.

6.4. Effect of Purchase Discount Factor δ. As described previously, the aim of the price discount provided by the supplier is to stimulate the merchant to purchase earlier. When δ is larger, the cost charged by the supplier due to the delayed purchase will be higher. All holiday merchants are sensitive to the purchase cost. Figure 4 suggests that risk preference merchants will purchase in advance with the increase of δ. Consequently, the time-sensitive purchase cost can stimulate the merchant to purchase the order earlier. In particular, the risk-neutral merchant purchases their order

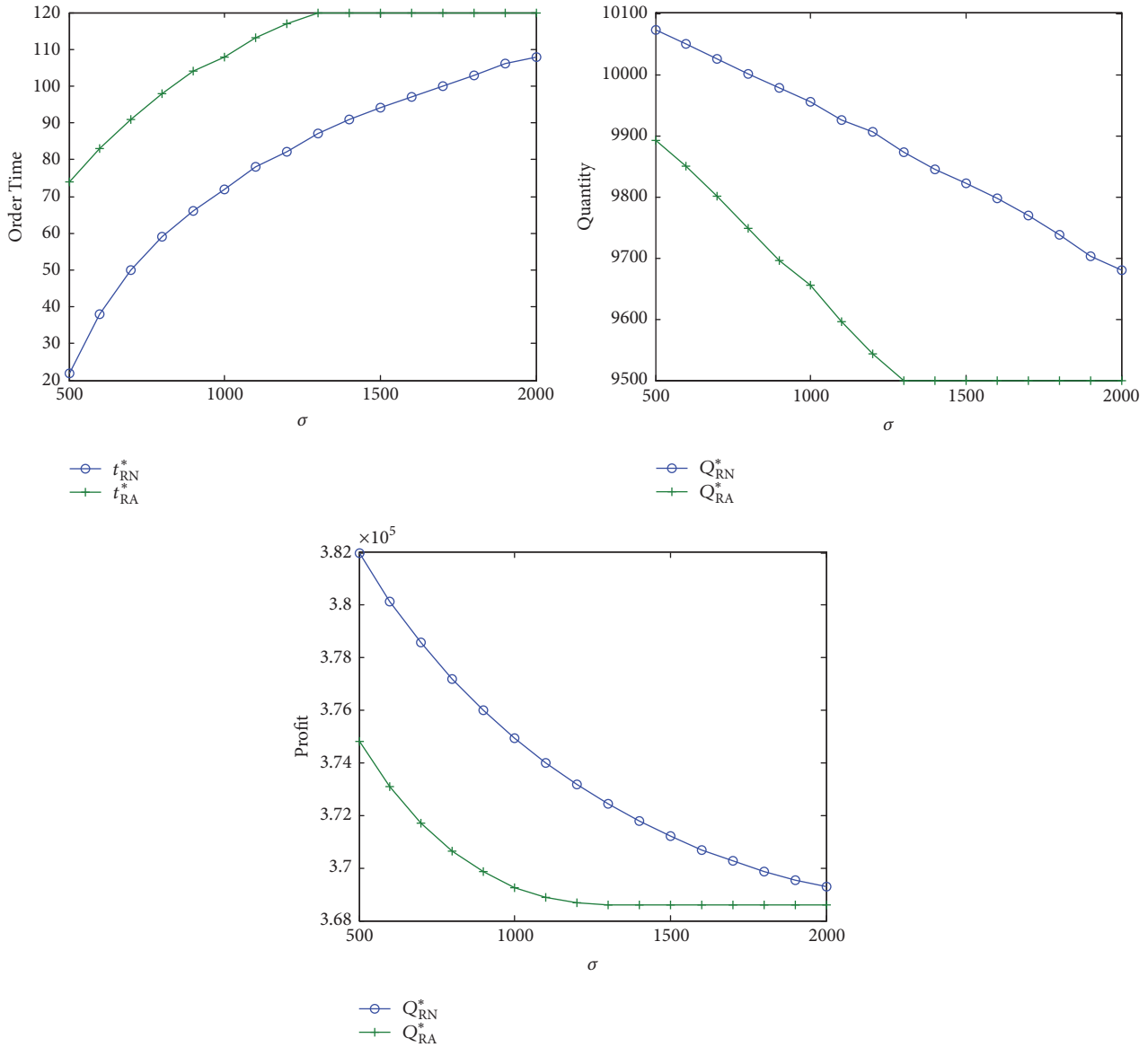

Figure 2: The effects of uncertainty of market demand σ with $\alpha = 500$, $\gamma = 0.025$, and $\eta = 0.8$.

in advance, even at the beginning stage. Although the risk-neutral merchant's order quantity increases due to the early purchase, the risk-averse merchant's order quantity first increases due to the early purchase but it then decreases with the increase of δ. This may happen because the increase of the purchase cost also means that the risk-averse merchant faces the risk of loss. Finally, the merchant's profit decreases with the increase of purchase cost. Overall, the time-sensitive purchase cost can indeed stimulate the risk-averse merchant to purchase more order in advance but this also increases their purchase cost and finally decreases their profit.

6.5. Effect of the Power of Retailer α. The power of merchant represented by α indicates the degree of market demand taken by the competition. Hence, when α is smaller, the merchant's power will be larger and less market demand will be taken. Figure 5 illustrates the merchant's market strategies with the increase of α. With the increase of α, the merchant's display time will be delayed, the order quantity will increase, and finally the profit will decrease. A merchant with smaller power in the market will consider avoiding competing with a strong competitor and will then opt to display the holiday merchandise earlier to capture the first-mover advantage. A monopolist will not be afraid to lose loyal customers and will delay the display time to enhance the forecast accuracy. Therefore, a risk-neutral merchant will order a higher quantity in advance to gain the advantage. However, the risk-averse merchant's order quantity does not always increase but instead it exhibits an approximate U-type fluctuation. The early display means that a risk-averse

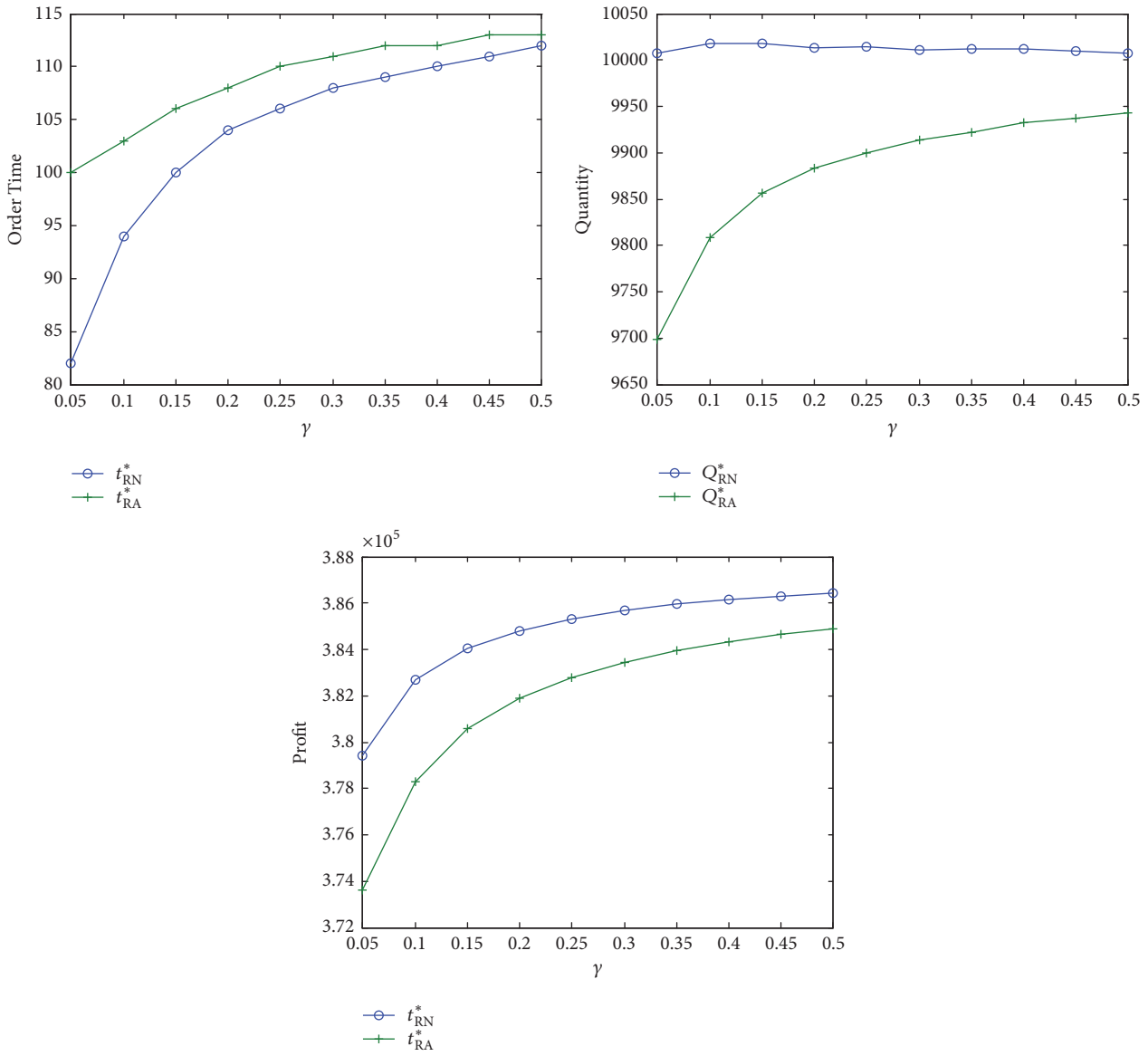

Figure 3: The effects of coefficient of elasticity of competitive γ with $\alpha = 500$, $\eta = 0.4$, and $\sigma = 1000$.

merchant must trade off the increased risk with the increased market power.

7. Conclusion

Holiday merchandise exhibits typical market characteristics due to its unofficial start date and limited life cycle. In this study, we have been able to capture the unique characteristics of holiday merchandise in the retail market by introducing the time-variant variance and time-variant expected market sales model. In particular, this study has investigated the market strategies that are used by merchants with different risk preferences to optimize the display time and inventory management of holiday merchandise in a competitive retail market. This work has enhanced the understanding of the phenomena of holiday goods, and it has provided management insight by conducting a numerical analysis. Our results suggest that the interactions of risk preference and the time-sensitive purchase cost have a significant effect on the merchant's market strategies. A risk-averse merchant will delay the holiday merchandise display time, decrease the order quantity, and finally miss the market opportunity. Meanwhile, the time-sensitive purchase cost can stimulate the merchant to purchase in advance, but this will also increase the merchant's order cost and will finally decrease the merchant's profit. The considerable uncertainty of the holiday market will cause the merchant to wait to avoid opportunity cost, and this pause allows them to enhance their forecast accuracy. A more risk-averse merchant may consider giving up the early-display advantage. All of the merchants, regardless of their risk preference, would prefer to enhance their forecast accuracy rather than capturing the

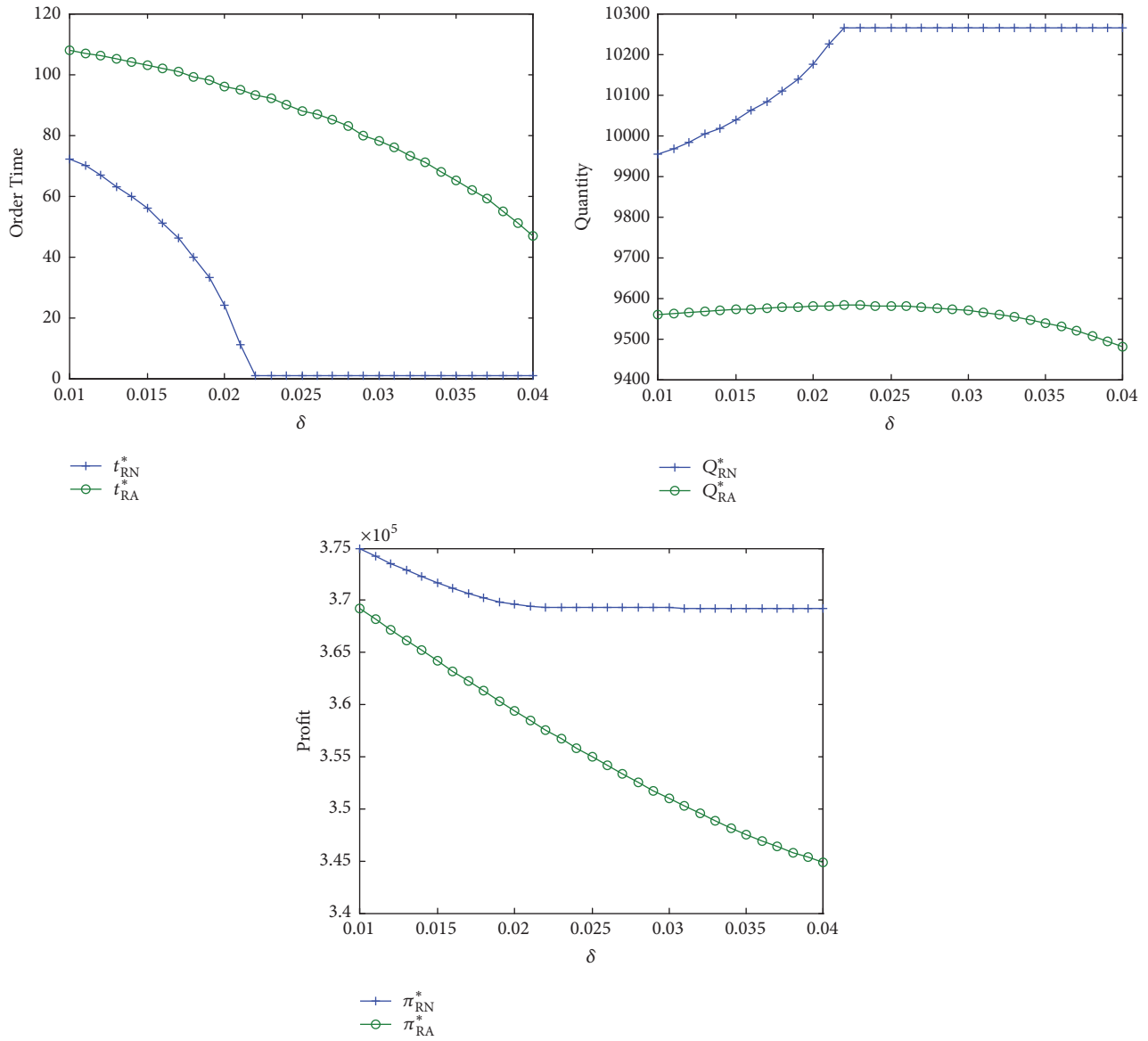

Figure 4: The effects of uncertainty of market demand σ with $\alpha = 500$, $\gamma = 0.025$, and $\eta = 0.4$.

early-display advantage if less of the market will be taken by the competition due to late display. A large market power merchant is not afraid to lose loyal customers due to late display. Generally, a merchant with larger market power will display their merchandise later and will make more profits. In comparison with the fixed purchase cost, a risk-averse merchant has to make a tradeoff between the challenge of making matched market strategies with the purchase cost, the advantage of early display, and the forecast error. While this study uses an extended newsvendor model, it goes further and investigates the display time and the traditional order quantity decision with time-sensitive purchase cost. This helps to offer a more detailed understanding of the interaction among these important parameters through numerical analysis.

It should be pointed out that the main limitation in the current study is that the optimal market strategies cannot be analytically derived from the decision-making equations. Therefore, we have numerically analyzed the impacts of these parameters on the risk reference merchants' market strategies. Several aspects of the present study warrant further research. For example, the scenarios that were used in this model can be extended to a supply chain context to consider the effects of the behavior of other players on the merchant's market strategies.

Conflicts of Interest

The authors declare that there are no conflicts of interest regarding the publication of this paper.

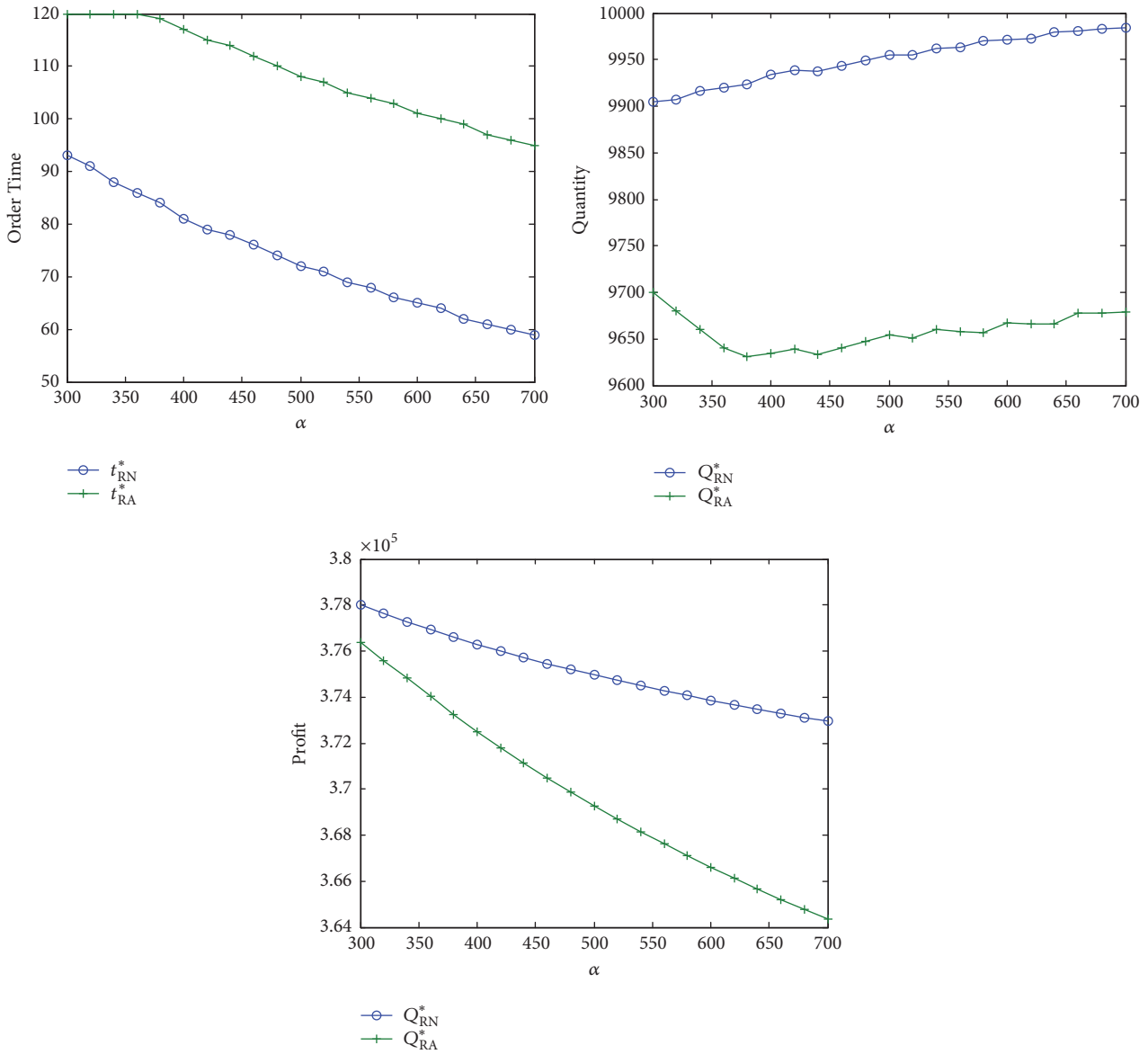

Figure 5: The effects of retailer's power α with $\sigma = 1000$, $\gamma = 0.025$, and $\eta = 0.4$.

Acknowledgments

This research was supported by the National Natural Science Foundation of China (71301054), the Fundamental Research Funds for the Central Universities (2015QNXM13, 2017X2D14), Provincial Natural Science Foundation of Guangdong (2015A030310271, 2015A030313679, and 2015A030313681), and Zhongshan City Science and Technology Bureau Project (no. 2017B1015).

References

[1] G. P. Soysal and L. Krishnamurthi, "Demand dynamics in the seasonal goods industry: An empirical analysis," *Marketing Science*, vol. 31, no. 2, pp. 293–316, 2012.

[2] R. Frank, *The Economic Naturalist: In Search of Explanations for Everyday Enigmas, Basic Book*, Basic Book, 2007.

[3] M. Fisher, "What is the right supply chain for your product?" *Harvard Business Review*, vol. 75, no. 2, pp. 105–116, 1997.

[4] A. V. Iyer and M. E. Bergen, "Quick response in manufacturer-retailer channels," *Management Science*, vol. 43, no. 4, pp. 559–570, 1997.

[5] Y. Li, F. Ye, and Q. Lin, "Optimal lead time policy for short life cycle products under Conditional Value-at-Risk criterion," *Computers & Industrial Engineering*, vol. 88, pp. 354–365, 2015.

[6] J. Wang, L. Wang, F. Ye, X. Xu, and J. Yu, "Order decision making based on different statement strategies under stochastic market demand," *Journal of Systems Science and Systems Engineering*, vol. 22, no. 2, pp. 171–190, 2013.

[7] J. Wang, Y. Li, F. Ye, and Q. Chen, "Optimal introduction time decision for holiday products with uncertain market demand," *International Journal of Production Research*, vol. 55, no. 1, pp. 161–175, 2017.

[8] J. D. Blackburn, *Time-based Competition: The Next Battleground in American Manufacturing*, Irwin Professional Pub, 1991.

[9] X. Gan, S. P. Sethi, and H. Yan, "Channel coordination with a risk-neutral supplier and a downside-risk-averse retailer," *Production Engineering Research and Development*, vol. 14, no. 1, pp. 80–89, 2005.

[10] L. Ma, F. Liu, S. Li, and H. Yan, "Channel bargaining with risk-averse retailer," *International Journal of Production Economics*, vol. 139, no. 1, pp. 155–167, 2012.

[11] Y. Li, Q. Lin, and F. Ye, "Pricing and promised delivery lead time decisions with a risk-averse agent," *International Journal of Production Research*, vol. 52, no. 12, pp. 3518–3537, 2014.

[12] J. M. Milner and M. J. Rosenblatt, "Flexible supply contracts for short life-cycle goods: the buyer's perspective," *Naval Research Logistics (NRL)*, vol. 49, no. 1, pp. 25–45, 2002.

[13] Z. K. Weng, "Coordinating order quantities between the manufacturer and the buyer: a generalized newsvendor model," *European Journal of Operational Research*, vol. 156, no. 1, pp. 148–161, 2004.

[14] Z. Hua, S. Li, and L. Liang, "Impact of demand uncertainty on supply chain cooperation of single-period products," *International Journal of Production Economics*, vol. 100, no. 2, pp. 268–284, 2006.

[15] N. C. Petruzzi and M. Dada, "Pricing and the newsvendor problem: a review with extensions," *Operations Research*, vol. 47, no. 2, pp. 183–194, 1999.

[16] L. Yao, Y. F. Chen, and H. Yan, "The newsvendor problem with pricing: Extensions," *International Journal of Management Science and Engineering Management*, vol. 1, no. 1, pp. 3–16, 2006.

[17] Z. Wu, W. Zhu, and P. Crama, "The newsvendor problem with advertising revenue," *Manufacturing and Service Operations Management*, vol. 13, no. 3, pp. 281–296, 2011.

[18] T.-M. Choi and C.-H. Chiu, *Risk Analysis in Stochastic Supply Chains*, vol. 41, Suppl 1, International, 2012.

[19] S. S. Sana and S. K. Goyal, "*(Q, r, L)* model for stochastic demand with lead-time dependent partial backlogging," *Annals of Operations Research*, vol. 233, pp. 401–410, 2015.

[20] M. Radhi and G. Zhang, "Optimal configuration of remanufacturing supply network with return quality decision," *International Journal of Production Research*, vol. 54, no. 5, pp. 1487–1502, 2016.

[21] F. Zhao, D. Wu, L. Liang, and A. Dolgui, "Lateral inventory transshipment problem in online-to-offline supply chain," *International Journal of Production Research*, vol. 54, no. 7, pp. 1951–1963, 2016.

[22] K. C. So and J.-S. Song, "Price, delivery time guarantees and capacity selection," *European Journal of Operational Research*, vol. 111, no. 1, pp. 28–49, 1998.

[23] K. Palaka, E. Erlebacher, and D. H. Kropp, "Lead-time setting, capacity utilization, and pricing decisions under lead-time dependent demand," *Institute of Industrial Engineers (IIE). IIE Transactions*, vol. 30, no. 2, pp. 151–163, 1998.

[24] T. Xiao, J. Jin, G. Chen, J. Shi, and M. Xie, "Ordering, wholesale pricing and lead-time decisions in a three-stage supply chain under demand uncertainty," *Computers & Industrial Engineering*, vol. 59, no. 4, pp. 840–852, 2010.

[25] S. S. Sana, "Optimal contract strategies for two stage supply chain," *Economic Modelling*, vol. 30, no. 1, pp. 253–260, 2013.

[26] M. S. Chen and C. C. Chuang, "Extended newsboy problem with shortage-level constraints," *International Journal of Production Economics*, vol. 67, no. 3, pp. 269–277, 2000.

[27] G. P. Cachon and R. Swinney, "The value of fast fashion: quick response, enhanced design, and strategic consumer behavior," *Management Science*, vol. 57, no. 4, pp. 778–795, 2011.

[28] Y. Tamura and S. Yamada, "Reliability computing and management considering the network traffic for a cloud computing," *Annals of Operations Research*, vol. 244, no. 1, pp. 163–176, 2016.

[29] C.-C. Chuang, "A distribution free newsboy problem under shortage-level constraints," *Journal of the Operations Research Society of Japan*, vol. 44, no. 4, pp. 301–312, 2001.

[30] Y. Qin, R. Wang, A. J. Vakharia, Y. Chen, and M. M. Seref, "The newsvendor problem: review and directions for future research," *European Journal of Operational Research*, vol. 213, no. 2, pp. 361–374, 2011.

[31] C. B. Weinberg, G. L. Lilien, and P. Kotler, "Marketing Decision Making: A Model Building Approach," *Journal of Marketing Research*, vol. 21, no. 3, p. 339, 1984.

[32] K. Tang and J. Tang, "Time-based pricing and lead time policies for a build-to-order manufacturer," *Production Operations Management*, vol. 11, no. 3, pp. 374–392, 2010.

[33] X. Wang and D. Li, "A dynamic product quality evaluation based pricing model for perishable food supply chains," *Omega* , vol. 40, no. 6, pp. 906–917, 2012.

[34] C.-H. Chiu, T.-M. Choi, and D. Li, "Price wall or war: The pricing strategies for retailers," *IEEE Transactions on Systems, Man, and Cybernetics: Systems*, vol. 39, no. 2, pp. 331–343, 2009.

[35] Y. Deng, Y. Liu, and D. Zhou, "An improved genetic algorithm with initial population strategy for symmetric TSP," *Mathematical Problems in Engineering*, vol. 2015, Article ID 212794, 6 pages, 2015.

[36] Q. Qu, K.-Y. Chen, Y.-M. Wei, Y. Liu, S.-B. Tsai, and W. Dong, "Using hybrid model to evaluate performance of innovation and technology professionals in marine logistics industry," *Mathematical Problems in Engineering*, vol. 2015, Article ID 361275, 8 pages, 2015.

[37] L. Eeckhoudt, C. Gollier, and H. Schlesinger, "The risk-averse (and prudent) newsboy," *Management Science*, vol. 41, no. 5, pp. 786–794, 1995.

[38] F. Chen and A. Federgruen, "Mean-Variance Analysis of Basic Inventory Models," *Financial Analyst Journal May*, vol. 9, no. 3, pp. 77–88, 2000.

[39] Y. Chen, M. Xu, and Z. G. Zhang, "A risk-averse newsvendor model under the CVaR criterion," *Operations Research*, vol. 57, no. 4, pp. 1040–1044, 2009.

[40] L. Yang, M. Xu, G. Yu, and H. Zhang, "Supply chain coordination with CVaR criterion," *Asia-Pacific Journal of Operational Research*, vol. 26, no. 1, pp. 135–160, 2009.

Hindawi
Mathematical Problems in Engineering
Volume 2018, Article ID 9874356, 10 pages
https://doi.org/10.1155/2018/9874356

Research Article

A New Plant Intelligent Behaviour Optimisation Algorithm for Solving Vehicle Routing Problem

Godfrey Chagwiza

Department of Applied Mathematics, National University of Science & Technology, P.O. Box AC939, Ascot, Bulawayo, Zimbabwe

Correspondence should be addressed to Godfrey Chagwiza; chagwizag@gmail.com

Received 20 June 2017; Revised 5 December 2017; Accepted 11 January 2018; Published 6 February 2018

Academic Editor: Leonilde Varela

A new plant intelligent behaviour optimisation algorithm is developed. The algorithm is motivated by intelligent behaviour of plants and is implemented to solve benchmark vehicle routing problems of all sizes, and results were compared to those in literature. The results show that the new algorithm outperforms most of algorithms it was compared to for very large and large vehicle routing problem instances. This is attributed to the ability of the plant to use previously stored memory to respond to new problems. Future research may focus on improving input parameters so as to achieve better results.

1. Introduction

A lot of research has been done and is ongoing on development of optimisation algorithms that are motivated by natural processes. In this research, an attempt to develop a new plant intelligence behaviour optimisation (PIBO) algorithm motivated by intelligent behaviour of plants to survive and avoid competition is presented. Natural processes such as how plants fight competition and change morphology in response to environmental changes make it worthwhile to develop an algorithm inspired by plant intelligence. Plant intelligence starts with cell molecular network. Molecular connections result in a living organism. It is believed that metabolic steps act like Boolean computer logic gates such as `Or`, `AND`, and `NOR` [1] and act like chemical neurones [2, 3].

Pattern recognition is achieved through assembling chemical neutron together [4]. Computational elements in plant intelligence are taken to be proteins [5]. Plants can forage for their food through changing their behaviour. This is achieved by changing physiology, phenotype, and architecture [6]. Plants make decisions as they grow, thereby placing roots, shoots, and leaves at optimal points or positions depending on availability or positions of perceived resources [7, 8].

Overgrown branches can trigger decision to seal the vascular connection system and redirect resources to the rest of the plant [9]. The plants have an ability to sense volume [10]. Plants can avoid competition and can respond to local opportunities that will be of use in future [11]. Roots plays a pivotal role in plant intelligence. The paper is highly motivated by adaptability of plants to severe conditions, ability to avoid competition, and ability to survive under dynamic conditions. Using this intelligence of plants to develop an optimisation algorithm can result in a better optimisation algorithm capable of adapting to conditions given. An optimisation algorithm that is flexible and adapting to different conditions is necessary with current advancement in technology. The proposed algorithm is different from other nature inspired algorithms in that it can redirect time resources to solutions that are feasible only. The remainder of the paper is arranged as follows. In Section 2, formulation of the new PIBO algorithm is presented. Computational experiments, results, and discussions are presented in Section 3, and conclusions are drawn in Section 4.

2. PIBO Algorithm Development

In this section an attempt to develop the new optimisation algorithm is presented. Basic steps of plant intelligence are used as steps of the new algorithm. Parameters and Variables section presents definitions of parameters and variables used.

2.1. Environmental Information. Environmental information comes in various forms that require different actions.

(1) START
(2) Objective function $O(x_i) = (x_1, x_2, \ldots, x_i)^T$
(3) Generate initial population of N environmental information x_i
(4) Define perception, F_i for x_i
(5) **while** $N <$ MaxGen **do**
(6) Get a plant randomly
(7) Initiate signal transduction creating response r_i
(8) Evaluate r_i appropriateness by finding $P(r_i)$
(9) Set up the initial adaptive network, G_0
(10) Get α, β, τ and η
(11) **if** $(\alpha x_i > 0 \wedge \beta x_i > 0 \wedge \tau x_i > 0) \wedge (\eta x_i > 0 \vee \eta x_i \leq 0)$ **then**
(12) Find $\max\{G(x_i)\}$
(13) Choose $(\alpha, \tau, \beta) > 0$ that produces the set $\max\{P(G)\}$
(14) **else if** $\alpha = \beta = \tau \leq 0$ **then**
(15) Set $P(G) = 0$
(16) Wait until $(\alpha > 0 \wedge \beta > 0 \wedge \tau > 0) \wedge (\eta > 0 \vee \eta \leq 0)$
(17) **end if**
(18) Construct the set $V = \{V_{1,1}^k, \ldots, V_{ji}^k\}$ of the response instances
(19) Generate the response tissue integration decision $M(x_i, t)$
(20) **if** $M(x_i, t+1) > M(x_i, t)$ **then**
(21) Choose the response $V_{(x_i,t+1)}$
(22) **else if** $M(x_i, t+1) < M(x_i, t)$ **then**
(23) Choose response $V_{(x_i,t)}$
(24) **else if** $V_{(x_i,t)} \notin V$ **then**
(25) Set $M(x_i, t) = 0$ and stop, abandon the response decision and make another decision
(26) **end if**
(27) Evaluate fitness, A_i
(28) **if** $A_i > A_i^*$ **then**
(29) Produce intelligent phenotype, C_i
(30) **else if** $A_i < A_i^*$ **then**
(31) Set $C_i = C_0$ and re-analyse F_i
(32) **end if**
(33) Determine compactness, $Z(x_i)$, of C_i
(34) **if** $Z(x_i) \geq Z(x_i^*)$ **then**
(35) Set $Z(x_i) = Z^*(x_i)$
(36) **else if** $Z(x_i) \leq Z(x_i^*)$ **then**
(37) Set $Z(x_i^*) = Z^*(x_i)$
(38) **end if**
(39) Find best current solution, $O(x_i^*)$
(40) **end while**
(41) Return the results
(42) STOP

Algorithm 1

A population, N, of environmental information, x_i, is generated by various plant parts such as roots, leaves, and trunk. A population $x_i \in N$ is generated first before anything else. Line (3) of Algorithm 1 defines environmental information.

2.2. Plant Perception. Plants perception, sometimes referred to as biocommunication, is a way how plants communicate. Plants have the ability to sense and respond to the environment. This can lead to adjustment in morphology, physiology, and phenotype. Reactions to chemicals, light, gravity, parasites, and many other factors have been noted in plants. Perception frequency, F_i, for environmental information, x_i, is defined. This will be used in future encounters with the same information. Equation (1) represents perception frequency where γ is drawn from a uniform distribution, $U[0, 1]$. In Algorithm 1, line (4) presents plant perception:

$$F_i = h\left(x_{i,\min}\right) + \gamma\left[h\left(x_{i,\max}\right) - h\left(x_{i,\min}\right)\right]. \quad (1)$$

2.3. Signal Transduction. Signal transduction occurs when the extracellular molecule activates a receptor that in turn triggers biochemical events resulting in a response. Signal transduction (line (7) of Algorithm 1), r_i, is affected by stimulus location, type, duration, and intensity. Equation (2) shows the signal transduction level of the environmental information by the plant:

$$r_i = \frac{1}{\left(s_{\text{type}} + s_{\text{loc}} + s_{\text{dur}} + s_{\text{int}}\right)} x_i \times 100\%. \quad (2)$$

2.4. Assessment. The plant will assess the information transmitted in order to make an informed decision. This is an important step of the algorithm because it is the one that affects the action to be taken. Assessment of x_i is carried out to determine the effect of the environmental information, and (3) presents assessment function. It is shown that $0 \leq P(r_i) \leq 1$ from (3). The smaller the value of $P(r_i)$ is, the greater the chance that the adaptive representational network, G, is formulated is. Research suggests that memory in plants cannot be constructed without first learning. Plants learn complex things such as stress, condition of drought, cold, heat, flooding, and many more through reinforcement [31–34], and this is the reason for using previous environmental information when carrying out current assessment.

$$P(r_i) = \frac{x_i^*}{x_i}, \quad x_i^* \leq x_i, \; x_i \neq 0. \tag{3}$$

2.5. Adaptive Representational Network. Adjustment in the morphology or physiology and phenotype may take place depending on the type of environmental information at hand. The network $G = (B, E)$ will be formulated where B is the set of components (morphology, phenotype, and physiology) and E are edges. This network presents what is to be done. Use of Boolean operators `AND`, `OR`, and `NOR` is carried out at this stage of the algorithm. To ensure that the adaptive representational network formulated is useful, set α, β, and τ to be nonnegative. The tolerance optimiser does not matter if it is negative.

2.6. Tissue Integration. The state of all nodes in the adaptive representational network can be modelled as follows:

$$\overline{Y}_i^{k+1} = Y_i\left(x_1^k, x_2^k, \ldots, x_I^k\right), \quad i \in I. \tag{4}$$

The variable $\overline{Y}_i^{[\cdot]}$ is updated according to

$$\overline{Y}_i^{k+1}\left(T_i^k\right) = Y_i\left(x_1^k\left[V_{1i}^k\right], x_2^k\left[V_{2i}^k\right], \ldots, x_I^k\left[V_{Ji}^k\right]\right), \quad k \in \mathbb{N}, \; j = 1, 2, \ldots, J, \tag{5}$$

where (6) and (7) represent T_i^k and V_{ji}^k, respectively.

$$T_i^k = \min_{jl}\left\{T_j^l \geq t\right\}, \quad \text{for some } k \tag{6}$$

$$V_{ji}^k = \max_l\left\{T_j^l : T_i^k > T_j^l\right\} = V. \tag{7}$$

The response tissue integration decision is then presented by

$$M(x_i, t) = \max\left\{\overline{Y}_i^1, \ldots, \overline{Y}_i^k\right\}. \tag{8}$$

2.7. Fitness and Intelligent Phenotype Production. In this step, the algorithm will evaluate the fitness of tissue integration decision. Information gathered from learning previous environmental information reinforces the evaluation criteria. This means that the previous environmental information intensity, x_i^*, leading to the optimal tissue integration decision, A_i^*, should be smaller than or equal to the current environmental information intensity, x_i, so that the current fitness, A_i, can lead to the intelligent phenotype production, C_i.

2.8. Compactness and the Solution. Compactness of the intelligent phenotype produced is important for the plant to achieve the goal. The algorithm ranks the current solution and the best solution is printed. This solution must be better than the previous solution produced for the same environmental information. The PIBO algorithm is presented as in Algorithm 1.

Figure 1 represents the algorithm flow chart of the new PIBO algorithm.

Relevance estimation and value calibration (REVAC) introduced by Nannen and Eiben [35] is used to assist tuning the control parameters. Racing of Maron and Moore [36] and sharpening used by Bartz-Beielstein et al. [37] are incorporated into the REVAC algorithm to fine-tune the parameters. Default values of the REVAC algorithm are used. The best values of tuning the tolerance optimiser are $\eta = -0.1$ and $\eta = 0.13$, throughput accelerator, $\tau = 0.077$, and filter parameter, $\alpha = 0.89$. These values of the input parameters are used to execute the PIBO algorithm using three sets of benchmark problems. Figures 2 and 3 show the graphical presentation of the tolerance optimiser of the best two values.

3. Computational Experiments

This section presents computational experiments of the PIBO algorithm and its results are compared to those available in literature. The algorithm is implemented to solve three sets of known benchmark vehicle routing problems, 12 very large-scale vehicle routing problems (VLVRP) in Li et al. (2005) [28], 20 large-scale vehicle routing problems (LVRP) in Golden et al. (1998) [38], and 14 small- or medium-sized vehicle routing problems (SVRP) in Christofides and Eilon (1969) [39]. Computational experiments are performed in MATLAB 7.0.4 on a PC with AMD E-300 APU with Radeon™ @1.30 GHz and 4.00 GB RAM. A total of 30 runs are performed for each set of benchmark problems. Table 1 presents information of the problem instances that are used in this paper.

Computational results of the PIBO algorithm are shown in Table 2. Two best values of tolerance optimiser, η, are used. The third column (avail sol) presents the available solution, time (m) is the time in minutes, and number of feasible solutions is presented in the succeeding column. The average solutions are presented by the column labeled "avg sol" and best solutions by the column titled "best sol," and D is the deviation. The results show that the PIBO algorithm performs better when $\eta = 0.13$ as compared to $\eta = -0.1$.

Table 3 show results of the PIBO algorithm compared to the best results available in the literature for the SVRP problems. The results show that PIBO algorithm is promising. The average deviation from the previous best solution obtained by executing the PIBO algorithm to achieve optimality is

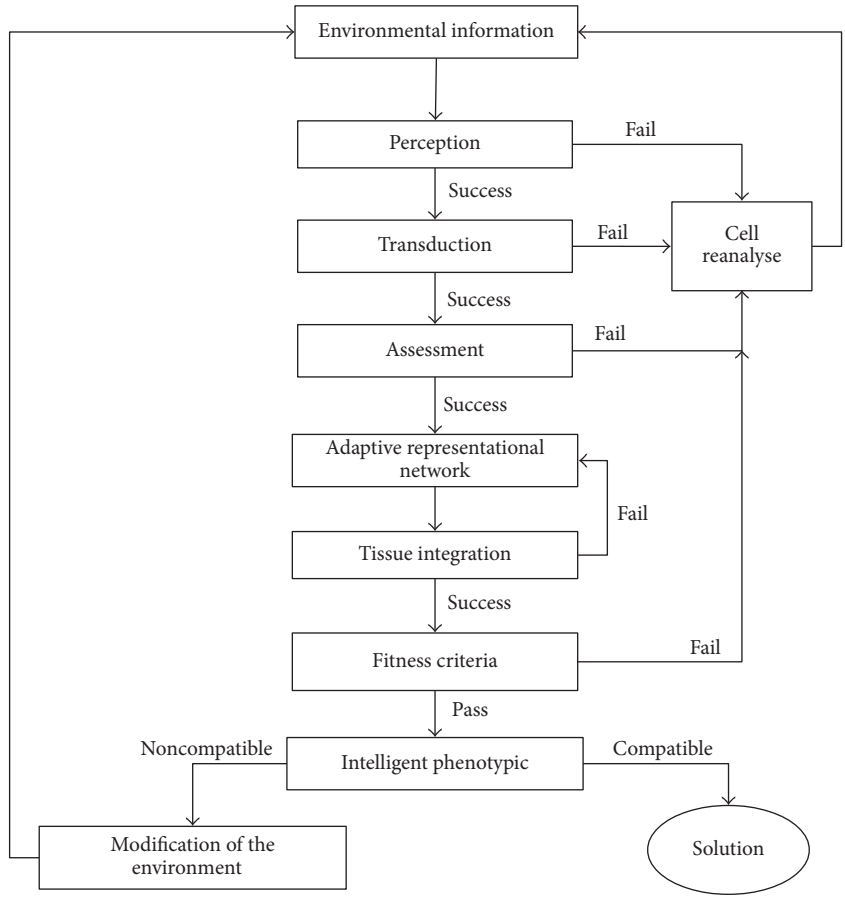

Figure 1: Algorithm flow chart.

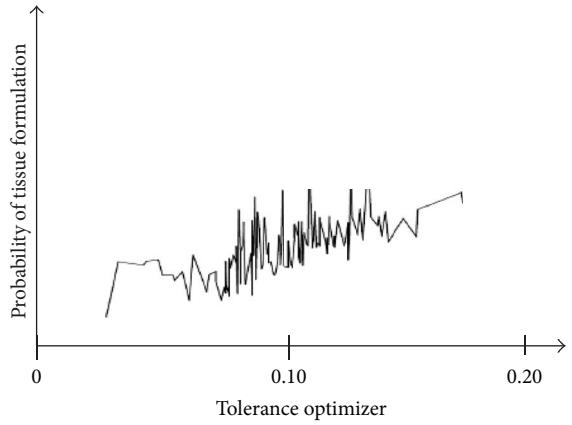

Figure 2: Graphical representation of $\eta = 0.13$.

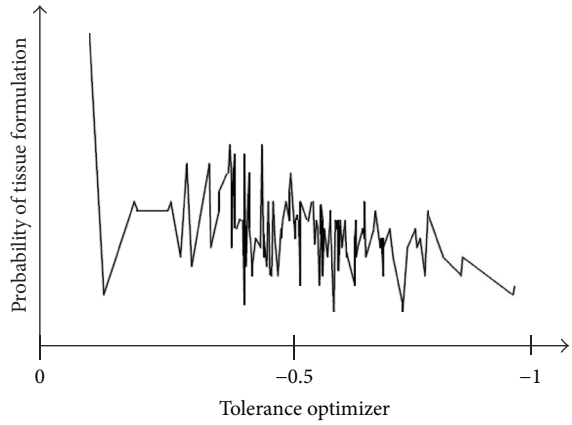

Figure 3: Graphical representation of $\eta = -0.1$.

0.07, while the best result so far is 0.00 seconds obtained by a computer with processor speed of 2 G. The algorithm outperformed most of the results in literature and might even perform better if it is executed on a PC with a faster processor.

In Table 4, PIBO algorithm with $\eta = 0.13$ is compared to the results available in literature for the LVRP set of benchmark problems. The best solutions obtained by the PIBO algorithm outperform all the other solutions they have been compared to for this set of benchmark problems. Finally, results obtained by executing PIBO to solve VLVRP are presented in Table 5. Again, the results show that PIBO algorithm outperforms all the other algorithms it has been compared with. The best average results deviation was obtained by Xiao et al. (2014) [26] as $D = 0.11$. There is a significant difference

Table 1: Information of the SVRP, LVRP and VLRP benchmark problems instance.

Type	Problem	Number of customers	Number of vehicles	Vehicles capacity	Maximum route length	Service time
SVRP	1	50	5	160		
	2	75	10	140		
	3	100	8	200		
	4	150	12	200		
	5	199	17	200		
	6	50	6	160	200	10
	7	75	11	140	160	10
	8	100	9	200	230	10
	9	150	14	200	200	10
	10	199	18	200	200	10
	11	120	7	200		
	12	100	10	200		
	13	120	11	200	720	50
	14	100	11	200	1040	90
LVRP	1	240		550	650	
	2	320		700	900	
	3	400		900	1200	
	4	480		1000	1600	
	5	200		900	1800	
	6	280		900	1500	
	7	360		900	1300	
	8	440		900	1200	
	9	255		1000	∞	
	10	323		1000	∞	
	11	399		1000	∞	
	12	483		1000	∞	
	13	252		1000	∞	
	14	320		1000	∞	
	15	396		1000	∞	
	16	480		1000	∞	
	17	240		200	∞	
	18	300		200	∞	
	19	360		200	∞	
	20	420		200	∞	
VLVRP	1	560	10			
	2	600	15			
	3	640	10			
	4	720	10			
	5	760	20			
	6	800	11			
	7	840	20			
	8	880	10			
	9	960	10			
	10	1040	10			
	11	1120	10			
	12	1200	11			

Table 2: Computational results of the SVRP, LVRP and VLVRP benchmark problems instance.

Type	Problem	Avail best	$\eta = -0.1$ Time (min)	No. feasible sol	Avg sol	Best sol	D% best	$\eta = 0.13$ Time (min)	No. feasible sol	Avg sol	Best sol	D%
SVRP	1	524.61	0.15*	30	524.61	524.6	0.00	0.15*	30	523.09	523.07	0.29
	2	835.26	0.32*	30	834.09	834.09	0.14	0.32*	30	834.01	834	0.00
	3	826.14	0.37*	29	825	824.9	0.15	0.35*	30	824.87	824.87	0.02
	4	1028.42	0.80*	30	1028.05	1028.05	0.04	0.78*	30	1028.04	1028.02	0.04
	5	1291.29	1.08*	27	1291.32	1291.31	0.00	1.07*	29	1292.01	1292.01	−0.06
	11	1042.11	0.48*	30	1042.06	1042.02	0.01	0.48*	30	1041.97	1041.97	0.01
	12	819.56	0.34*	30	819.6	819.56	0.00	0.33*	30	819.03	819.02	0.07
LVRP	1	5627.54	1.47	30	5554.01	5553.87	1.31	1.43	30	5551.98	5548.02	0.05
	2	8447.92	2.31	30	8447.92	8444.11	0.05	2.3	30	8440.99	8440.99	0.08
	3	11036.22	3.2	30	11025.10	11025.1	0.10	3.2	30	11022.01	11019.76	0.15
	4	13624.52	4.3	30	13602.34	13601.1	0.17	3.9	30	13548.9	13544.06	0.03
	5	6460.98	1.1	30	6459.07	6459.03	0.03	1	30	6458.63	6455.52	0.08
	6	8412.8	1.42	30	8409.30	8408.54	0.05	1.02	30	8402.33	8400.31	0.15
	7	10181.75	1.76	30	10177.98	10177.02	0.05	1.44	30	10167.71	10152.98	0.12
	8	11643.9	2.55	30	11638.02	11638.02	0.05	2.43	30	11635.7	11634.44	0.08
	9	580.48	4.02	30	580.02	580.02	0.08	3.91	30	567.2	565.75	0.00
	10	738.73	1.5	30	737.98	737.98	0.10	1.02	30	733.33	732.08	0.21
	11	914.75	3.72	30	912.22	912.04	0.30	3.22	30	909.14	909.14	0.31
	12	1106.33	4.2	30	1106.01	1106.01	0.03	3.78	30	1088.4	1088.4	0.02
	13	857.19	1.7	30	857.22	857.22	0.00	1.4	30	853.49	853.02	0.01
	14	1080.55	2.4	30	1080.03	1080.03	0.05	2.3	30	1077.54	1077.54	0.21
	15	1340.24	3	30	1338.11	1338.1	0.16	3	30	1333.61	1333.52	0.21
	16	1616.33	4.98	28	1614.20	1614.19	0.13	4.98	28	1614.2	1614.2	0.09
	17	707.76	1.1	30	702.82	702.8	0.70	0.9	30	702.66	701.76	0.00
	18	995.39	1.49	30	991.04	991.01	0.44	1.49	30	991.01	991.01	0.34
	19	1366.14	2.2	30	1364.90	1364.9	0.09	2.22	30	1355.82	1355.76	0.02
	20	1819.99	2.48	30	1815.81	1815.78	0.23	2.45	30	1811.11	1811.02	0.09
VLVRP	1	16212.74	5.90	30	16219.81	16219.81	−0.04	5.77	30	16211.81	16211.81	0.01
	2	14597.18	6.70	30	14567.09	14555.74	0.28	6.67	30	14553.78	14553.78	0.30
	3	18801.12	7.65	30	18889.05	18855.99	−0.29	7.56	30	18888.41	18888.41	−0.46
	4	21389.33	9.45	30	21373.91	21372.77	0.08	9.45	30	21370.99	21370.99	0.09
	5	16902.16	11.32	30	16880.01	16784.76	0.69	11.02	30	16878.05	16878.04	0.14
	6	23971.7	12.03	30	23965.70	23965.7	0.03	12.00	30	23964.17	23964.15	0.03
	7	17488.74	12.64	30	17473.11	17472.21	0.09	12.76	30	17467.63	17467.63	0.12
	8	26565.92	13.23	30	26566.38	26566.38	0.00	13.20	30	26565.04	26565.04	0.00
	9	29154.34	15.57	30	29144.93	29144.93	0.03	15.55	30	29141.09	29141.08	0.05
	10	31742.51	18.09	29	31746.72	31744.92	−0.01	18.66	30	31746.05	31746.03	−0.01
	11	34330.84	20.10	30	34335.01	34335	−0.01	20.11	30	34332.76	34332.76	−0.01
	12	36919.24	26.77	28	36912.51	36911.34	0.02	26.22	28	36912.03	36912.03	0.02

*Time recorded in seconds in order to show differences.

Table 3: Comparison of the results of different algorithms for the SVRP benchmark problem instances.

Problem	SA	SB	SC	SD	SE	SF	SG	SH	SI	SJ	SK	SL	SM	SN	SO	SP	PIBO
1	0.00	0.00	0.00	0.00	0.00	0.00	0.00	0.00	0.00	0.00	0.00	0.00	0.00	0.00	0.00	0.00	0.29
2	0.00	0.00	0.40	0.00	0.00	0.00	0.00	0.02	0.00	0.00	0.06	0.00	0.00	0.00	0.00	0.00	0.00
3	0.00	0.00	0.29	0.00	0.15	0.00	0.00	0.16	0.00	0.00	0.00	0.15	0.00	0.00	0.00	0.00	0.02
4	0.41	0.24	0.47	0.31	0.75	0.00	0.00	0.76	0.00	0.11	0.12	0.26	0.00	0.10	1.00	0.29	0.04
5	1.90	1.77	2.09	0.69	2.54	1.56	0.00	1.24	0.00	0.45	1.01	2.64	0.00	0.22	1.58	1.07	0.03
11	3.01	0.00	0.07	0.00	0.10	0.00	0.00	0.00	0.00	0.00	0.00	0.00	0.00	0.00	0.33	0.00	0.01
12	0.00	0.00	0.00	0.00	0.00	0.00	0.00	0.00	0.00	0.00	0.00	0.00	0.00	0.00	0.00	0.00	0.07
Avg	0.76	0.29	0.47	0.14	0.51	0.22	0.00	0.31	0.00	0.08	0.17	0.44	0.00	0.05	0.42	0.19	0.07
CPU	2 G	400 M	200 M	1 G	400 M	400 M	2 G	733 M	2.8 G	3 G	2.4 G	2.4 G	2.4 G	2.8 G	2.8 G	1.6 G	1.3 G
Time (min)	24.62	5.22	3.84	5.19	21.25	6.96	0.08	28.91	0.03	17.43	5.84	4.54	23.74	5.19	8.21	-	4.51

Notes. SA, Cordeau et al. (2001) [12]; SB, Tarantilis and Kiranoudis (2002) [13]; SC, Toth and Vigo (2003) [14]; SD, Prins (2004) [15]; SE, Berger and Barkaoui (2004) [16]; SF, Tarantilis (2005) [17]; SG, Mester and Braysy (2005) [18]; SH, Ergun et al. (2006) [19]; SI, Mester and Braysy (2007) [20]; SJ, Pisinger and Ropke (2007) [21]; SK, Derigs and Kaiser (2006) [22]; SL, Derigs and Kaiser (2006) [22]; SM, Nagata (2007) [23]; SN, Prins (2009) [24]; SO, Lin et al. (2009) [25]; SP, Xiao et al. (2014) [26].

Table 4: Comparison of the results of the LVRP benchmark problems instance.

Problem	LA	LB	LC	LD	LE	LF	LG	LH	LI	LJ	LK	LL	LM	PIBO
1	1.93	0.29	0.69	0.00	4.27	4.27	0.42	0.24	0.30	0.30	2.99	0.57	−0.01	0.05
2	1.24	0.01	0.25	0.00	0.34	0.34	0.25	0.18	0.03	0.00	0.64	0.20	0.06	0.08
3	3.32	0.00	0.99	0.00	0.07	0.07	0.10	0.04	0.51	0.00	2.98	0.21	0.00	0.15
4	9.44	0.55	0.98	0.00	0.10	0.05	0.08	0.83	0.80	0.00	3.76	0.00	0.02	0.03
5	3.66	0.00	0.26	0.00	0.00	0.00	0.09	0.00	0.00	0.00	0.79	0.00	0.00	0.08
6	6.54	0.00	1.51	0.00	0.03	0.03	0.04	0.01	0.00	0.00	1.67	0.00	0.00	0.15
7	3.59	0.14	1.06	0.14	1.14	1.14	0.00	0.84	0.14	0.14	2.37	0.84	0.14	0.12
8	3.37	1.59	2.38	0.17	1.99	1.96	0.60	1.95	1.98	0.00	2.94	0.97	0.17	0.08
9	2.22	1.10	1.34	0.50	6.92	6.92	0.80	0.80	1.44	0.99	1.07	0.80	0.00	0.00
10	1.75	1.63	1.46	0.38	8.42	6.23	1.38	0.97	1.20	0.76	1.38	0.90	0.04	0.21
11	2.33	1.37	1.22	0.40	9.44	7.88	0.87	0.89	1.65	0.84	1.09	0.65	0.17	0.31
12	3.69	3.12	1.96	0.08	10.34	9.28	1.15	1.12	1.08	0.88	1.75	0.97	0.25	0.02
13	1.35	0.92	0.93	0.22	10.28	8.01	0.87	0.97	0.92	0.60	1.18	0.52	0.24	0.01
14	1.45	1.22	1.59	0.07	9.52	6.91	1.37	1.43	1.41	0.81	1.69	0.77	0.00	0.21
15	2.18	1.34	1.58	0.37	10.17	9.05	1.47	1.11	1.22	0.91	1.22	1.20	0.36	0.21
16	2.23	1.16	1.19	0.39	8.62	7.83	1.41	1.56	1.89	1.11	1.64	0.89	0.35	0.09
17	0.47	0.14	0.56	0.00	5.09	2.58	0.16	0.25	0.27	0.15	0.64	0.16	0.17	0.00
18	2.15	0.35	1.50	0.34	11.05	8.25	0.71	0.73	0.95	0.68	2.26	1.52	0.52	0.34
19	2.55	0.08	1.20	0.05	6.53	5.74	0.59	1.26	1.12	0.40	1.38	1.21	0.24	0.02
20	5.27	0.16	1.70	0.01	9.32	6.49	0.59	1.65	1.46	0.60	1.97	1.09	0.21	0.09
Avg	3.04	0.76	1.22	0.16	5.68	4.65	0.65	0.84	0.92	0.46	1.77	0.67	0.15	0.11
CPU	200 M	900 M	1 G	2.8 G	3 G	3 G	3 G	2.4 G	2.4 G	2.8 G	2.8 G	2.93 G	1.6 G	1.3 G
Avg time (min)	17.55	49.3	1.33	24.35	0.18	1.01	107.61	109.63	111.10	66.9	118.98	284.4	-	2.65

Notes. LA, Toth and Vigo (2003) [14]; LB, Reimann et al. (2004) [27]; LC, Li et al. (2005) [28]; LD, Mester and Braysy (2007) [20]; LE, Kytöjoki et al. (2007) [29]; LF, Kytöjoki et al. (2007) [29]; LG, Pisinger and Ropke (2007) [21]; LH, Derigs and Kaiser (2006) [22]; LI, Derigs and Kaiser (2006) [22]; LJ, Prins (2009) [24]; LK, Lin et al. (2009) [25]; LL, Chen et al. (2010) [30]; LM, Xiao et al. (2014) [26].

between the result obtained by PIBO and the average best result in literature.

Statistical analysis of the results is done to establish significance differences between them, if any. Analysis of variance (ANOVA) is performed on the results obtained by the 30 runs performed. Results show that the results obtained by the PIBO algorithm are significantly different from those that are available in literature with the probability value $p = 0.02$ and $p = 0.00$ for the LVRP and VLVRP, respectively, but insignificantly different ($p = 0.65$) for the SVRP instances. Since the solution space is very large for these problems, memory of previous best solution is important. The ability of the plant to change morphology, physiology, and phenotype in response to the environment and conditions and storage

Table 5: Comparison of the results of the VLVRP benchmark problems instance.

Problem	VA	VB	VC	VD	VE	VF	PIBO
1	1.10	2.41	0.00	0.19	0.05	0.01	0.01
2	0.37	0.23	0.00	0.40	0.40	0.14	0.30
3	1.09	0.19	0.00	0.11	0.05	0.00	−0.46
4	1.85	0.62	0.00	0.06	0.06	0.01	0.09
5	1.47	0.00	1.14	3.72	2.7	0.65	0.14
6	0.91	0.18	0.00	0.36	0.1	0.04	0.03
7	1.91	0.71	0.00	4.34	4.26	−0.32	0.12
8	0.15	0.85	0.00	0.1	0.1	0.00	0.00
9	0.09	0.86	0.02	0.04	0.04	0.01	0.05
10	0.74	0.71	0.00	0.2	0.2	0.00	−0.01
11	3.02	1.28	0.00	0.06	0.06	0.00	−0.01
12	1.36	1.24	0.03	0.29	0.29	0.77	0.02
Average	1.28	0.58	0.10	0.82	0.69	0.11	0.02
CPU	1 G	3 G	2.8 G	3 G	3 G	1.6 G	1.3 G
Avg time (min)	2.72	7.7	8	0.04	0.13	-	5.03

Notes. VA, Li et al. (2005) [28]; VB, Pisinger and Ropke (2007) [21]; VC, Mester and Braysy (2007) [20]; VD, Kytöjoki et al. (2007) [29]; VE, Kytöjoki et al. (2007) [29]; VF, Xiao et al. (2014) [26].

of memory of previous experiences may have assisted the PIBO algorithm to be more efficient when solving these problems.

4. Conclusion

A new optimisation algorithm called PIBO is formulated and executed to solve some benchmark vehicle routing problems. The development of the algorithm is motivated by plant intelligence behaviour. Results show that the PIBO algorithm outperforms most of the results reported in literature for LVRP and VLVRP problem instances. The PIBO algorithm is a promising optimisation algorithm to solve large vehicle routing problems which have a very large solution space. The new algorithm has an ability to adjust to changing problem conditions. It is suggested that future research be directed towards improving input parameters and testing applicability of the algorithm to a wider range of problems.

Parameters and Variables

α: Filter parameter
β: Temporary pattern generator
τ: Throughput accelerator
η: Tolerance optimiser
γ: A random vector affecting decision making and $\gamma \sim U[0, 1]$
A_i: Fitness of the tissue integration decision
A_i^*: Previous fitness of tissue integration in response to the environmental information
B: Set of components
C_i: Intelligent phenotype
E: Edges
F_i: Perception
G: Adaptive representational network
h: Action taken in response to environmental information
$h(x_{i,\min})$: Minimum effect of action h responding to environmental information x_i
$h(x_{i,\max})$: Maximum effect of action h responding to environmental information x_i
i: Index identifying an instant, $i \in I$
k, l: Indexes identifying the protein
$M(x_i, t)$: Tissue integration decision
$O(x_i)$: Objective function
$P(r_i)$: Assessment function of the signal transduction
r_i: Signal transduction response level
s_{dur}: Stimulus duration expressed as a percentage
s_{int}: Stimulus intensity expressed as a percentage
s_{loc}: Stimulus location expressed as a percentage
s_{type}: Stimulus type expressed as a percentage
T_i^k: Updating time at node q
T_j^l: Updating time for the next node j
V: Set of response activities
V_{ji}^k: Most recent instant when node j is updated
x_i: Environmental information
x_i^*: Previous environmental information that triggered action
$Y(x_i^k)$: Regulating function with respect to environmental information x_i
$\overline{Y}_i^{[\cdot]}$: Protein
$Z(x_i)$: Compactness of the solution.

Conflicts of Interest

The author declares that there are no conflicts of interest regarding the publication of this paper.

References

[1] A. Arkin and J. Ross, "Computational functions in biochemical reaction networks," *Biophysical Journal*, vol. 67, no. 2, pp. 560–578, 1994.

[2] A. Hjelmfelt and J. Ross, "Chemical implementation and thermodynamics of collective neural networks.," *Proceedings of the National Acadamy of Sciences of the United States of America*, vol. 89, no. 1, pp. 388–391, 1992.

[3] M. Okamoto, T. Sakai, and K. Hayashi, "Switching mechanism of a cyclic enzyme system: role as a "chemical diode"," *BioSystems*, vol. 21, no. 1, pp. 1–11, 1987.

[4] A. Hjelmfelt, F. W. Schneider, and J. Ross, "Pattern recognition in coupled chemical kinetic systems," *Science*, vol. 260, no. 5106, pp. 335–337, 1993.

[5] D. Bray, "Protein molecules as computational elements in living cells," *Nature*, vol. 376, no. 6538, pp. 307–312, 1995.

[6] J. P. Grime and J. M. L. Mackey, "The role of plasticity in resource capture by plants," *Evolutionary Ecology*, vol. 16, no. 3, pp. 299–307, 2002.

[7] T. Yamada, T. Okuda, M. Abdullah, M. Awang, and A. Furukawa, "The leaf development process and its significance for reducing self-shading of a tropical pioneer tree species," *Oecologia*, vol. 125, no. 4, pp. 476–482, 2000.

[8] H. Honda and J. B. Fisher, "Tree branch angle: Maximizing effective leaf area," *Science*, vol. 199, no. 4331, pp. 888–890, 1978.

[9] J. Henriksson, "Differential shading of branches or whole trees: Survival, growth, and reproduction," *Oecologia*, vol. 126, no. 4, pp. 482–486, 2001.

[10] H. J. Schenk, R. M. Callaway, and B. E. Mahall, "Spatial Root Segregation: Are Plants Territorial?" *Advances in Ecological Research*, vol. 28, no. C, pp. 145–180, 1999.

[11] O. Falik, P. Reides, M. Gersani, and A. Novoplansky, "Self/non-self discrimination in roots," *Journal of Ecology*, vol. 91, no. 4, pp. 525–531, 2003.

[12] J.-F. Cordeau, G. Laporte, and A. Mercier, "A unified tabu search heuristic for vehicle routing problems with time windows," *Journal of the Operational Research Society*, vol. 52, no. 8, pp. 928–936, 2001.

[13] C. D. Tarantilis and C. T. Kiranoudis, "BoneRoute: an adaptive memory-based method for effective fleet management," *Annals of Operations Research*, vol. 115, pp. 227–241, 2002.

[14] P. Toth and D. Vigo, "The granular tabu search and its application to the vehicle-routing problem," *INFORMS Journal on Computing*, vol. 15, no. 4, pp. 333–346, 2003.

[15] C. Prins, "A simple and effective evolutionary algorithm for the vehicle routing problem," *Computers & Operations Research*, vol. 31, no. 12, pp. 1985–2002, 2004.

[16] J. Berger and M. Barkaoui, "A new hybrid genetic algorithm for the capacitated vehicle routing problem," *Journal of the Operational Research Society*, vol. 54, no. 12, pp. 1254–1262, 2004.

[17] C. D. Tarantilis, "Solving the vehicle routing problem with adaptive memory programming methodology," *Computers & Operations Research*, vol. 32, no. 9, pp. 2309–2327, 2005.

[18] D. Mester and O. Braysy, "Active guided evolution strategies for large-scale vehicle routing problems with time windows," *Computers & Operations Research*, vol. 32, no. 6, pp. 1593–1614, 2005.

[19] Ö. Ergun, J. B. Orlin, and A. Steele-Feldman, "Creating very large scale neighborhoods out of smaller ones by compounding moves," *Journal of Heuristics*, vol. 12, no. 1-2, pp. 115–140, 2006.

[20] D. Mester and O. Braysy, "Active-guided evolution strategies for large-scale capacitated vehicle routing problems," *Computers & Operations Research*, vol. 34, no. 10, pp. 2964–2975, 2007.

[21] D. Pisinger and S. Ropke, "A general heuristic for vehicle routing problems," *Computers & Operations Research*, vol. 34, no. 8, pp. 2403–2435, 2007.

[22] U. Derigs and R. Kaiser, "Applying the attribute based hill climber heuristic to the vehicle routing problem," *European Journal of Operational Research*, vol. 177, no. 2, pp. 719–732, 2006.

[23] Y. Nagata, "Edge assembly crossover for the capacitated vehicle routing problem," in *Evolutionary computation in combinatorial optimization*, vol. 4446 of *Lecture Notes in Comput. Sci.*, pp. 142–153, Springer, Berlin, 2007.

[24] C. Prins, "A grasp x evolutionary local search hybrid for the vehicle routing problem," in *Bio-inspired Algorithms for the Vehicle Routing Problem*, pp. 35–53, Springer, New York, NY, USA, 2009.

[25] S.-W. Lin, Z.-J. Lee, K.-C. Ying, and C.-Y. Lee, "Applying hybrid meta-heuristics for capacitated vehicle routing problem," *Expert Systems with Applications*, vol. 36, no. 2, pp. 1505–1512, 2009.

[26] Y. Xiao, Q. Zhao, I. Kaku, and N. Mladenovic, "Variable neighbourhood simulated annealing algorithm for capacitated vehicle routing problems," *Engineering Optimization*, vol. 46, no. 4, pp. 562–579, 2014.

[27] M. Reimann, K. Doerner, and R. F. Hartl, "D-ants: Savings based ants divide and conquer the vehicle routing problem," *Computers & Operations Research*, vol. 31, no. 4, pp. 563–591, 2004.

[28] F. Li, B. Golden, and E. Wasil, "Very large-scale vehicle routing: new test problems, algorithms, and results," *Computers & Operations Research*, vol. 32, no. 5, pp. 1165–1179, 2005.

[29] J. Kytöjoki, T. Nuortio, O. Bräysy, and M. Gendreau, "An efficient variable neighborhood search heuristic for very large scale vehicle routing problems," *Computers & Operations Research*, vol. 34, no. 9, pp. 2743–2757, 2007.

[30] P. Chen, H.-K. Huang, and X.-Y. Dong, "Iterated variable neighborhood descent algorithm for the capacitated vehicle routing problem," *Expert Systems with Applications*, vol. 37, no. 2, pp. 1620–1627, 2010.

[31] H. Bohnert, "Abiotic stress," in *Encyclopedia of Life Sciences*, pp. 1–9, John Wiley & Sons, Ltd, Chichester, UK, 2007.

[32] J. R. Dinneny, T. A. Long, J. Y. Wang et al., "Cell identity mediates the response of Arabidopsis roots to abiotic stress," *Science*, vol. 320, no. 5878, pp. 942–945, 2008.

[33] C. J. Frost, M. C. Mescher, J. E. Carlson, and C. M. De Moraes, "Plant defense priming against herbivores: Getting ready for a different battle," *Plant Physiology*, vol. 146, no. 3, pp. 818–824, 2008.

[34] L. A. C. J. Voesenek and R. Pierik, "Plant science: Plant stress profiles," *Science*, vol. 320, no. 5878, pp. 880-881, 2008.

[35] V. Nannen and A. E. Eiben, "A method for parameter calibration and relevance estimation in evolutionary algorithms," in *Proceedings of the 8th Annual Genetic and Evolutionary Computation Conference 2006*, pp. 183–190, usa, July 2006.

[36] O. Maron and A. W. Moore, "The Racing Algorithm: Model Selection for Lazy Learners," *Artificial Intelligence Review*, vol. 11, no. 1-5, pp. 193–225, 1997.

[37] T. Bartz-Beielstein, K. E. Parsopoulos, and M. . Vrahatis, "Design and analysis of optimization algorithms using computational statistics," *ANACM. Applied Numerical Analysis and Computational Mathematics*, vol. 1, no. 3, pp. 413–433, 2004.

[38] B. L. Golden, E. A. Wasil, J. P. Kelly, and I. Chao, "The impact of metaheuristics on solving the vehicle routing problem: Algorithms, problem sets, and computational results," in *Fleet Management and Logistics*, pp. 33–56, Kluwer, Boston, 1998.

[39] N. Christofides and S. Eilon, "An Algorithm for the Vehicle-Dispatching Problem," *Operational Research Quarterly*, vol. 20, no. 3, pp. 309–318, 1969.

Hindawi
Mathematical Problems in Engineering
Volume 2018, Article ID 9470236, 12 pages
https://doi.org/10.1155/2018/9470236

Research Article

Incorporation of Inefficiency Associated with Link Flows in Efficiency Measurement in Network DEA

Abolghasem Shamsijamkhaneh,[1] **Seyed Mohammad Hadjimolana**,[1] **Bijan Rahmani Parchicolaie**,[2] **and Farhad Hosseinzadehlotfi**[2]

[1]*Department of Industrial Engineering, Science and Research Branch, Islamic Azad University, Tehran, Iran*
[2]*Department of Mathematics, Science and Research Branch, Islamic Azad University, Tehran, Iran*

Correspondence should be addressed to Seyed Mohammad Hadjimolana; molana@srbiau.ac.ir

Received 11 June 2017; Revised 19 September 2017; Accepted 5 November 2017; Published 4 January 2018

Academic Editor: M. L. R. Varela

Data Envelopment Analysis (DEA) is a mathematical programming approach to measure the relative efficiency of peer decision making units (DMUs) which use multiple inputs to produce multiple outputs. One of the drawbacks of traditional DEA models is the neglect of internal structures of the DMUs. Network DEA models are able to overcome the shortcoming of the traditional DEA models. In network DEA a DMU is made up of some divisions linked together by intermediate products. An intermediate product has the dual role of output from one division and input to another one. Improving the efficiency of one process may reduce the efficiency of another process. To address the conflict caused by the dual role of intermediate measures, this paper presents a new approach which categorizes the intermediate measures into either input or output type endogenously, while keeping the continuity of link flows between divisions. This categorization allows us to measure the inefficiencies associated with intermediate measures and account their indirect effects on the objective function. In this paper we propose a new Slacks-based measure which includes any nonzero slacks identified by the model and inherits the properties of monotonicity in slacks and units invariance from the conventional SBM approach.

1. Introduction

Data Envelopment Analysis (DEA), developed by Charnes et al. [1] based on the seminal work of Farrell [2], is a mathematical programming approach to measure the relative performance of peer decision making units (DMUs) which use multiple inputs to produce multiple outputs. Conventional DEA models consider the DMUs as *black boxes* and neglect the operations and interrelations of the processes within the DMU. Recently, a number of studies have looked inside the *black box* and modeled it as a network of subtechnologies.

The simplest structure of network systems is a two-stage system composed of two processes connected in series. Besides inputs and outputs, there are a set of intermediate measures that link these two stages together. The intermediate measures play the role of outputs from the first stage and inputs to the second stage at the same time. Several models have been proposed to measure the efficiency of this type of system (see the review of Cook et al. [3]). The major problem in measuring efficiency of the DMUs with two-stage structure is that the outputs of the first stage are the inputs to the second, because improving the efficiency of the first stage by increasing its output may damage the efficiency of the second stage.

Many researchers propose solutions to address the potential conflict caused by the dual role of intermediate measures. There are four types of papers that use various approaches for measuring efficiency of DMUs with two-stage processes.

In the first type, two separate DEA runs are applied to the stages to measure the relative efficiency of each stage separately. [4–7]. Such an approach does not treat intermediate measures in an organized manner. Improving the efficiency of one division by controlling intermediate measures reduces the efficiency of the other one.

Another type of researches is called "Efficiency Decomposition Methodology," as in Kao and Hwang [8] who define

a two-stage efficiency score as the weighted sum of final outputs to the weighted sum of initial inputs. Their approach finds a set of multipliers that maximize either the first or the second stage efficiency score while maintaining the overall efficiency score [9, 10].

The third type of modeling called "Game theoretic approaches" originated from the work of Liang et al. [11]. They applied game theory to develop number of DEA models. They proposed a leader-follower model game and assumed the "same weights" for the intermediate products as outputs and inputs as a perfect coordination between the two subtechnologies.

In the case that there are additional independent inputs to second stage and the second stage has its own inputs not linked with the first stage, "Network DEA" approach is introduced to the literature of DEA. Färe and Grosskopf [12, 13] are pioneered in this line of research. They developed two-stage model into a general multistage model with intermediate products. Their representation of the flow of product is consistent with the industrial engineering and operations research literature on multistage systems (e.g., [14–17]).

Despotis et al. [18] presented a network DEA approach in the framework of multiobjective programming to assess the efficiency score of two-stage processes. They estimated efficiencies of the stages without a prior definition of the overall efficiency of the system. The overall efficiency is obtained by aggregating the stage efficiencies a posteriori.

Tone and Tsutsui [19] present a slacks-based NDEA model that measures the overall efficiency of the DMU and its components. The overall efficiency score is defined as the weighted average of the components that make up the DMU. The weight of each component is determined exogenously and represents the importance of that component. In their study they called the intermediate measures as links and define two possible cases for the linking constrains, the "fixed" link value case and the "free" link value case. In the latter case, the linking activities are freely determined and their target values can be smaller or greater than their observed values.

Tone and Tsutsui [20] propose slacks-based dynamic DEA model by extending their slacks-based NDEA model and taking carry-over activities into account. Network and dynamic model which is combination of the network structure by means of carry-over activities between two succeeding periods is also proposed in Tone and Tsutsui [21].

Lozano [22] proposes a slacks-based measure (SBM) model for general networks of processes that differs from the existing SBM Network Data Envelopment Analysis (NDEA) approaches. He enhances the discriminating power of his proposed model by relaxing the linking constraints proposed by Tone and Tsutsui [19]. Moreover, the model considers the exogenous inputs and outputs at the system level instead of at the process level.

F.-h. F. Liu and Y.-c. Liu [23] introduced a procedure to solve dynamic network DEA based on a Virtual Gap Measurement Model. They proposed a two-phase approach to resolve the problem of dual role of intermediate products and measure the nonzero slacks of intermediate measures.

As we discussed above the dual role of intermediate products is an issue that needs to be addressed in network DEA. In this paper we propose two new network DEA models in the slacks-based measure (SBM) framework, called Model (I) and Model (II), in which the intermediate products are categorized into either input or output type. The proposed models compute the input excesses and output shortfalls associated with intermediate measures and keep the continuity of link flows between divisions. Model (II) is able to take into account the inefficiency associated with the link variables.

The rest of this paper is structured as follows; Section 2 presents some preliminaries. In Section 3 we propose our new models and the new slack based measure. A numerical example is presented in Section 4 and to verify our proposed models we compare the results with the results of some existing approaches. Finally, Section 5 closes this paper with a few concluding remarks and some suggestions for further research.

2. Preliminaries

In this section the network SBM approaches of Tone and Tsutsui [19] and the separation approach are explained. All the preliminaries are taken from Cook et al. 2014.

2.1. Separation Approach. In this approach the divisional efficiency is evaluated individually. The weighted average of each division gives the overall efficiency of a DMU. In this case, for evaluating the efficiency of div k individually, we consider the all intermediate products consumed by div k as inputs and all intermediate products produced by div k as outputs and we evaluate the efficiency of div k with these inputs and outputs and the exogenous inputs used and outputs produced by div k. In this way, we can evaluate efficiency of each division of a company among the set of DMUs and can find benchmarks for each division. The separation model takes into account the inefficiency associated with the link variables. However, this approach does not account for the continuity of links between divisions.

2.2. NSBM Approach. Suppose that there are a set of n DMUs indexed by ($j = 1, \ldots, n$) consisting of K divisions ($k = 1, \ldots, K$)and that division k (div k) consumes m_k number of inputs denoted by x_{ij}^k ($i = 1, \ldots, m_k$) and produces r_k number of outputs denoted by y_{rj}^k ($r = 1, \ldots, r_k$). Intermediate products from div k to div h are also denoted by $z_{dj}^{(k,h)}$ ($d \in L_{(k,h)}$) where $L_{(k,h)}$ is the set of links between div k and div h and $l_{(k,h)}$ is the number of items in $L_{(k,h)}$.

Tone and Tsutsui [19] proposed the production possibility set $(x^k, y^k, z^{(k,h)})$ as follows:

$$\sum_{j=1}^{n} \lambda_j^k x_j^k \le x^k \quad (k = 1, \ldots, K)$$

$$\sum_{j=1}^{n} \lambda_j^k y_j^k \ge y^k \quad (k = 1, \ldots, K)$$

$$\sum_{j=1}^{n} \lambda_j^k z_j^{(k,h)} = z^{(k,h)} \quad (\forall (k,h)) \ \left(\text{as output from div } k\right)$$

$$\sum_{j=1}^{n} \lambda_j^h z_j^{(k,h)} = z^{(k,h)} \quad (\forall (k,h)) \ \left(\text{as input to div } h\right)$$

$$\sum_{j=1}^{n} \lambda_j^k = 1 \quad (\forall k), \ \lambda_j^k \geq 0 \ (\forall j,k), \tag{1}$$

where $\lambda^k \in R_+^n$ is the intensity vector corresponding to div k $(k = 1, \ldots, K)$.

It should be noted that the above model assumes the variable returns-to-scale (VRS) for production and by removing the last constraint $\sum_{j=1}^{n} \lambda_j^k = 1$ changes the assumption of VRS to the constant returns-to-scale (CRS) for production.

Regarding linking constraints, they proposed two possible cases called "*fixed link*" (2) and "*free link*" (3) formulated as follows:

$$\sum_{j=1}^{n} \lambda_j^k Z_j^{(k,h)} = Z_o^{(k,h)}$$

$$\sum_{j=1}^{n} \lambda_j^h Z_j^{(k,h)} = Z_o^{(k,h)} \tag{2}$$

$$\sum_{j=1}^{n} \lambda_j^k Z_j^{(k,h)} = \sum_{j=1}^{n} \lambda_j^h Z_j^{(k,h)}. \tag{3}$$

When linking activities are beyond the control of DMUs (nondiscretionary) they are kept unchanged by applying *fixed link* case (2) and in the case that the linking activities are freely determined (discretionary) the *free link* case (3) needs to be used. Note that in both cases the continuity of link values between divisions is assured.

In the next section we propose our new network models.

3. Proposing New Network SBM Model

As we discussed in previous section the linking constraints proposed by Tone and Tsutsui [19] do not consider the slacks of the intermediate measures unless they are exogenously categorized into either input type or output type. In this section we propose new network DEA models based on SBM framework which categorize the intermediate measures into input or output type endogenously. To incorporate the inefficiency associated with intermediate measures in efficiency measurement we propose two models referred to as Model (I) and Model (II). These models have only different objective functions. In Model (I) the slacks of intermediate products do not appear in the objective function while in Model (II) they do.

Incorporation of the slacks of intermediate measures in objective function allows us to incorporate the inefficiency associated with intermediate measures in efficiency measurement directly.

3.1. Model (I). We present Model (I) as follows:

$$\tau_p^* = \min \quad \frac{\sum_{k=1}^{K} w_k \left[1 - (1/m_k)\left(\sum_{i=1}^{m_k} \left(s_{ip}^{k-}/x_{ip}^k\right)\right)\right]}{\sum_{k=1}^{K} w_k \left[1 + (1/r_k)\left(\sum_{r=1}^{r_k} \left(s_{rp}^{k+}/y_{rp}^k\right)\right)\right]} \tag{4}$$

$$\text{s.t.} \quad \sum_{j=1}^{n} \lambda_j^k x_{ij}^k + s_{ip}^{k-} = x_{ip}^k \quad (k = 1, \ldots, K), \ (i = 1, \ldots, m_k) \tag{5}$$

$$\sum_{j=1}^{n} \lambda_j^k y_{rj}^k - s_{rp}^{k+} = y_{rp}^k \quad (k = 1, \ldots, K), \ (r = 1, \ldots, r_k) \tag{6}$$

$$\sum_{j=1}^{n} \lambda_j^h z_{dj}^{(k,h)} + s_{dp}^{(k,h)-} = z_d^{(k,h)} \quad \left(d = 1, \ldots, l_{(k,h)}\right), \ \forall (k,h) \tag{7}$$

$$\sum_{j=1}^{n} \lambda_j^k z_{dj}^{(k,h)} - s_{dp}^{(k,h)+} = z_d^{\prime(k,h)} \quad \left(d = 1, \ldots, l_{(k,h)}\right), \ \forall (k,h) \tag{8}$$

$$\sum_{j=1}^{n} \lambda_j^k z_{dj}^{(k,h)} = \sum_{j=1}^{n} \lambda_j^h z_{dj}^{(k,h)} \quad \left(d = 1, \ldots, l_{(k,h)}\right), \ \forall (k,h) \tag{9}$$

$$0 \leq s_{dp}^{(k,h)-} \leq M y_d^{(k,h)} \quad \left(d = 1, \ldots, l_{(k,h)}\right), \ \forall (k,h) \tag{10}$$

$$0 \leq s_{dp}^{(k,h)+} \leq M\left(1 - y_d^{(k,h)}\right) \quad \left(d = 1, \ldots, l_{(k,h)}\right), \ \forall (k,h) \tag{11}$$

$$z_{dp}^{(k,h)} - M y_{dp}^{(k,h)} \leq z_d^{\prime(k,h)} \leq z_{dp}^{(k,h)} + M y_{dp}^{(k,h)} \quad \left(d = 1, \ldots, l_{(k,h)}\right), \ \forall (k,h) \tag{12}$$

$$z_{dp}^{(k,h)} - M\left(1 - y_d^{(k,h)}\right) \leq z_d^{(k,h)} \leq z_{dp}^{(k,h)} + M\left(1 - y_d^{(k,h)}\right) \quad \left(d = 1, \ldots, l_{(k,h)}\right), \ \forall (k,h) \tag{13}$$

$$\sum_{j=1}^{n} \lambda_j^k = 1 \quad (k = 1, \ldots, K) \tag{14}$$

$$y_d^{(k,h)} = \{0, 1\};$$

$$z_d^{(k,h)}, z_d^{\prime(k,h)} : \text{free},$$

$$\lambda_j^k \geq 0,$$

$$s_{rp}^{k+} \geq 0, \tag{15}$$

$$s_{ip}^{k-} \geq 0,$$

where M is a large positive number. $\sum_{k=1}^{K} w_k = 1$ and $w_k \geq 0$ is the relative weight of div k which is determined

corresponding to its importance. The proposed model is a mixed integer programming and we can solve this problem by transforming into a mixed integer linear programming using Charnes and Cooper transformation (see Appendix). The model presented above assumes the condition of variable returns-to-scale (VRS) for production and the production frontiers are spanned by the convex hull of the existing DMUs. If we neglect the last constraints (14) we can deal with the constant returns-to scale (CRS) case as well.

Note that if $y_d^{(k,h)} = 1$, then the utilization intermediate product $z_d^{(k,h)}$ is under the control of div h and $z_d^{(k,h)}$ is considered as an input to div h. We denote the set of those intermediate measures by $L_{(k,h)}^{\text{in}}$. In a similar manner, if $y_d^{(k,h)} = 0$, then the production of intermediate measure $z_d^{(k,h)}$ is under the control of div k and $z_d^{(k,h)}$ is considered as an output from div k. We denote the set of those intermediate measures by $L_{(k,h)}^{\text{out}}$. It is clear that

$$\begin{aligned} L_{(k,h)}^{\text{out}} \cup L_{(k,h)}^{\text{in}} &= L_{(k,h)}, \\ L_{(k,h)}^{\text{out}} \cap L_{(k,h)}^{\text{in}} &= \phi. \end{aligned} \tag{16}$$

In other words the proposed model classifies the intermediate measures into input or output type. The proposed model also identifies nonzero slacks and uncovers the sources of inefficiency associated with intermediate measures. Since the optimal values of intermediate measures can be equal, above, or below the observed value the proposed model corresponds to the free link case.

Set of constraints (9) allows model to keep the continuity of link flows between divisions and lets the shadow prices for the corresponding intermediate products be free. If we relax the constraints (9) by changing them to the constraints (17) we will enlarge the production possibility set and therefore increase the discriminating power of the approach. It also guarantees that no more intermediate products are consumed than are produced.

$$\sum_{j=1}^{n} \lambda_j^k z_{dj}^{(k,h)} \geq \sum_{j=1}^{n} \lambda_j^h z_{dj}^{(k,h)}. \tag{17}$$

The objective function of Model (I) is similar to that of NSBM model of Tone and Tsutsui [19]; hence we can define the overall and divisional input or output-oriented efficiency score similar to NSBM.

The output-oriented efficiency of DMU p can be evaluated by solving mixed integer linear programming below:

$$\frac{1}{\pi_p^*} = \max \quad \sum_{k=1}^{K} w_k \left[1 + \frac{1}{r_k} \left(\sum_{r=1}^{r_k} \frac{s_{rp}^{k+}}{y^k{}_{rp}} \right) \right] \tag{18}$$

subject to (5)–(15).

And the output-oriented divisional efficiency for div k of DMUp can be calculated as follows:

$$\frac{1}{\pi_p^{k*}} = \left[1 + \frac{1}{r_k} \left(\sum_{r=1}^{r_k} \frac{s_{rp}^{*k+}}{y^k{}_{rp}} \right) \right], \tag{19}$$

where s_{rp}^{*k+} is the optimal output-slacks obtained by minimizing (18) subject to (5)–(15).

Similarly the input-oriented efficiency of DMU p can be evaluated by solving mixed integer linear programming below:

$$\rho_p^* = \min \quad \sum_{k=1}^{K} w_k \left[1 - \frac{1}{m_k} \left(\sum_{i=1}^{m_k} \frac{s_{ip}^{k-}}{x_{ip}^k} \right) \right], \tag{20}$$

subject to (5)–(15).

And the input-oriented divisional efficiency for div k of DMUp can be calculated as follows:

$$\rho_p^{*k} = 1 - \frac{1}{m_k} \left(\sum_{i=1}^{m_k} \frac{s_{ip}^{*k-}}{x_{ip}^k} \right), \tag{21}$$

where s_{ip}^{*k-} denote the optimal output-slacks obtained by minimizing (20) subject to (5)–(15).

3.1.1. Efficiency of the Projected DMU

Projection. Let an optimal solution to our proposed model be $(\lambda_j^{*k}, s_p^{*k-}, s_p^{*k+}, s_p^{*(k,h)+}, s_p^{*(k,h)-}, y_d^{*(k,h)}, z_d^{*(k,h)}, z_d^{\prime(k,h)})$ $\forall j$, $\forall k$, $\forall (k,h) \in l_{(k,h)}$. Then we have the projection onto the frontier as follows:

$$x_{ip}^{*k} = x_{ip}^k - s_{ip}^{*k-} \quad (k = 1, \ldots, K), \ (i = 1, \ldots, m_k) \tag{22}$$

$$y_{rp}^{*k} = y_{rp}^k + s_{rp}^{*k+} \quad (k = 1, \ldots, K), \ (r = 1, \ldots, r_k) \tag{23}$$

$$z_{dp}^{*(k,h)} = z_{dp}^{(k,h)} - s_{dp}^{*(k,h)-} \quad \forall d \in L_{(k,h)}^{\text{in}} \tag{24}$$

$$z_{dp}^{*(k,h)} = z_{dp}^{(k,h)} + s_{dp}^{*(k,h)+} \quad \forall d \in L_{(k,h)}^{\text{out}}. \tag{25}$$

Theorem 1. *The projected DMU in Model (I) is overall efficient.*

Proof. We prove the theorem in the nonoriented case.

Let τ_p^* be the efficiency of the projected DMU $(X_p^{*k}, Y_p^{*k}, Z_p^{*k})$.

And let $(\widehat{\lambda}_j^k, \widehat{s}_p^{k-}, \widehat{s}_p^{k+}, \widehat{s}_p^{(k,h)+}, \widehat{s}_p^{(k,h)-}, \widehat{y}_p^{(k,h)}, \widehat{z}_d^{(k,h)}, \widehat{z}_d^{\prime(k,h)})$ $\forall j$, $\forall k$, $\forall d \in L_{(k,h)}$, $\forall (k,h)$ be an optimal solution to the proposed model. Then

$$\begin{aligned} \sum_{j=1}^{n} \widehat{\lambda}_j^k x_{ij}^k + \widehat{s}_{ip}^{k-} &= x_{ip}^{*k}, \\ \sum_{j=1}^{n} \widehat{\lambda}_j^k y_{rj}^k - \widehat{s}_{rp}^{k+} &= y_{rp}^{*k}, \\ \sum_{j=1}^{n} \widehat{\lambda}_j^h z_{dj}^{(k,h)} + \widehat{s}_{dp}^{(k,h)-} &= z_{dp}^{*(k,h)} \quad \forall d \in L_{(k,h)}^{\text{in}} \\ \sum_{j=1}^{n} \widehat{\lambda}_j^k z_{dj}^{(k,h)} - \widehat{s}_{dp}^{(k,h)+} &= z_{dp}^{*(k,h)} \quad \forall d \in L_{(k,h)}^{\text{out}}. \end{aligned} \tag{26}$$

Replacing x_{ip}^{*k} and y_{rp}^{*k} by (22) and (23) we have

$$\sum_{j=1}^{n} \widehat{\lambda}_j^k x_{ij}^k + \widehat{s}_{ip}^{k-} + s_{ip}^{*k-} = x_{ip}^k,$$
$$\sum_{j=1}^{n} \widehat{\lambda}_j^k y_{rj}^k - \widehat{s}_{rp}^{k+} - s_{rp}^{*k+} = y_{rp}^{*k}. \tag{27}$$

Hence we have the overall efficiency as follows:

$$\widehat{\tau}_p = \min \quad \frac{\sum_{k=1}^{K} w_k \left[1 - (1/m_k)\left(\sum_{i=1}^{m_k}\left(\left(s_{ip}^{*k-} + \widehat{s}_{ip}^{k-}\right)/x_{ip}\right)\right)\right]}{\sum_{k=1}^{K} w_k \left[1 + (1/r_k)\left(\sum_{r=1}^{r_k}\left(\left(s_{rp}^{*k+} + \widehat{s}_{rp}^{k+}\right)/y_{rp}\right)\right)\right]}. \tag{28}$$

If only one of $\widehat{s}_{rp}^{k+}$ $(\forall k, \forall r)$ or $\widehat{s}_{ip}^{k-}$ $(\forall k, \forall i)$ is positive then we have

$$\widehat{\tau}_p < \tau_p^*. \tag{29}$$

And it contradicts the optimality of τ_p^*. Thus, we have $\widehat{s}_{rp}^{k+} = 0$ $(\forall k, \forall r)$ and $\widehat{s}_{ip}^{k-} = 0$ $(\forall k, \forall i)$. Therefore, the projected DMU is overall efficient. □

3.2. Incorporation of Inefficiency Corresponding to Intermediate Measures in the Objective Function (Model (II)). Although the slacks of intermediate products in Model (I) are not included in the objective function, their indirect effect on the objective function incorporates inefficiency corresponding to intermediate measures in efficiency measurement. In order to include the inefficiency associated with intermediate measure in the objective function directly, we propose Model (II) that minimizes the objective function (30) subject to (5)–(15).

$$\eta_p^* = \min \quad \frac{\sum_{k=1}^{K} w_k \left[1 - \left(1/\left(m_k + \sum_{d=1}^{l_{(k,h)}} y_d^{(k,h)}\right)\right)\left(\sum_{i=1}^{m_k}\left(s_{ip}^{k-}/x_{ip}\right) + \sum_{d=1}^{l_{(k,h)}}\left(s_{dp}^{(k,h)-}/z_{dp}^{(k,h)}\right)\right)\right]}{\sum_{k=1}^{K} w_k \left[1 + \left(1/\left(r_k + l_{(k,h)} - \sum_{d=1}^{l_{(k,h)}} y_d^{(k,h)}\right)\right)\left(\sum_{r=1}^{r_k}\left(s_{rp}^{k+}/y_{rp}\right) + \sum_{d=1}^{l_{(k,h)}}\left(s_{dp}^{(k,h)+}/z_{dp}^{(k,h)}\right)\right)\right]}. \tag{30}$$

The term $l_{(k,h)} - \sum_{d=1}^{l_{(k,h)}} y_d^{*(k,h)}$ represents the number of those intermediate measures that are considered as the output from div k (i.e., the cardinal number of set $L_{(k,h)}^{\text{out}}$). Similarly the term $\sum_{d=1}^{l_{(k,h)}} y_d^{(k,h)}$ represents the number of those intermediate measures that are considered as the input to div h (i.e., the cardinal number of set $L_{(k,h)}^{\text{in}}$).

Neglecting the constraints (9) in solving Model (II) causes links to be treated as ordinary (discretionary) inputs or outputs and reduces the model structurally to the separation model. We can solve this case separately division by division and it assures the existence of at least one divisionally efficient DMU for every division.

The slack based measure (30) is invariant with respect to the unit of measurement of each input output and intermediate measure item (Units invariant). It is also monotone decreasing with respect to each input, output, and intermediate product slack. It represents the ratios of average input, output mix inefficiencies with the upper limit of 1.

To measure the nonoriented divisional efficiency score applying the direct effect of intermediate slacks on efficiency score we use the following formula:

$${\eta_p}^{*k} = \frac{1 - \left(1/\left(m_k + \sum_{d=1}^{l_{(f,k)}} y_d^{*(f,k)}\right)\right)\left(\sum_{i=1}^{m_k}\left(s_{ip}^{*k-}/x_{ip}\right) + \sum_{d=1}^{l_{(f,k)}}\left(s_{dp}^{*(f,k)-}/z_{dp}^{(f,k)}\right)\right)}{1 + \left(1/\left(r_k + l_{(k,h)} - \sum_{d=1}^{l_{(k,h)}} y_d^{*(k,h)}\right)\right)\left(\sum_{r=1}^{r_k}\left(s_{rp}^{*k+}/y_{rp}\right) + \sum_{d=1}^{l_{(k,h)}}\left(s_{dp}^{*(k,h)+}/z_{dp}^{(k,h)}\right)\right)}, \tag{31}$$

where $y_d^{*(k,h)}$, $y_d^{*(f,k)}$, s_{ip}^{*k-}, $s_{dp}^{*(f,k)-}$, $s_{dp}^{*(k,h)+}$, and s_{rp}^{*k+} are optimal values for the variables obtained from solution of Model (II). Note that the overall nonoriented efficiency score is a weighted mean of the divisional efficiency scores in which the weights are set exogenously and denote the importance of divisions.

To evaluate the input-oriented efficiency score of DMU$_p$ we can solve the following model.

$$\varphi_p^* = \min \quad \sum_{k=1}^{K} w_k \left[1 - \frac{1}{m_k + \sum_{d=1}^{l_{(k,h)}} y_d^{(k,h)}}\left(\sum_{i=1}^{m_k} \frac{s_{ip}^{k-}}{x_{ip}} + \sum_{d=1}^{l_{(k,h)}} \frac{s_{dp}^{(k,h)-}}{z_{dp}^{(k,h)}}\right)\right] \tag{32}$$

subject to (5)–(15).

The efficiency score in the output-oriented case for DMU$_p$ can be evaluated from following model.

$$\psi_p^* = \text{Max} \quad \sum_{k=1}^{K} w_k \left[1 + \frac{1}{r_k + l_{(k,h)} - \sum_{d=1}^{l_{(k,h)}} y_d^{*(k,h)}}\left(\sum_{r=1}^{r_k} \frac{s_{rp}^{*k+}}{y_{rp}} + \sum_{d=1}^{l_{(k,h)}} \frac{s_{dp}^{*(k,h)+}}{z_{dp}^{(k,h)}}\right)\right] \tag{33}$$

subject to (5)–(15).

Theorem 2. *The projected DMU in Model (II) is overall efficient.*

Proof. We prove the theorem in the nonoriented case.

Let η_p^* be the efficiency of the projected DMU $(X_p^{*k}, Y_p^{*k}, Z_p^{*k})$.

And let $(\widehat{\lambda}_j^k, \widehat{s}_p^{k-}, \widehat{s}_p^{k+}, \widehat{s}_p^{(k,h)+}, \widehat{s}_p^{(k,h)-}, \widehat{y}_p^{(k,h)}, \widehat{z}_d^{(k,h)}, \widehat{z}_d^{\prime(k,h)})$ $\forall j$, $\forall k$, $\forall d \in L_{(k,h)}$, $\forall (k,h)$ be an optimal solution to the proposed model. Then

$$\begin{aligned}
\sum_{j=1}^{n} \widehat{\lambda}_j^k x_{ij}^k + \widehat{s}_{ip}^{k-} &= x_{ip}^{*k},\\
\sum_{j=1}^{n} \widehat{\lambda}_j^k y_{rj}^k - \widehat{s}_{rp}^{k+} &= y_{rp}^{*k},\\
\sum_{j=1}^{n} \widehat{\lambda}_j^h z_{dj}^{(k,h)} + \widehat{s}_{dp}^{(k,h)-} &= z_{dp}^{*(k,h)} \quad \forall d \in \widehat{L}_{(k,h)}^{\text{in}}\\
\sum_{j=1}^{n} \widehat{\lambda}_j^k z_{dj}^{(k,h)} - \widehat{s}_{dp}^{(k,h)+} &= z_{dp}^{*(k,h)} \quad \forall d \in \widehat{L}_{(k,h)}^{\text{out}}.
\end{aligned} \tag{34}$$

Suppose $L_{(k,h)}^{\text{in}} = \widehat{L}_{(k,h)}^{\text{in}}$. By replacing x_{ip}^{*k}, y_{rp}^{*k}, and $z_{dp}^{*(k,h)}$ by (22), (23), (24), or (25) we have

$$\begin{aligned}
\sum_{j=1}^{n} \widehat{\lambda}_j^k x_{ij}^k + \widehat{s}_{ip}^{k-} + s_{ip}^{*k-} &= x_{ip}^k,\\
\sum_{j=1}^{n} \widehat{\lambda}_j^k y_{rj}^k - \widehat{s}_{rp}^{k+} - s_{rp}^{*k+} &= y_{rp}^{*k},\\
\sum_{j=1}^{n} \widehat{\lambda}_j^h z_{dj}^{(k,h)} + \widehat{s}_{dp}^{(k,h)-} + s_{dp}^{*(k,h)-} &= z_{dp}^{(k,h)} \quad \forall d \in \widehat{L}_{(k,h)}^{\text{in}}\\
\sum_{j=1}^{n} \widehat{\lambda}_j^k z_{dj}^{(k,h)} - \widehat{s}_{dp}^{(k,h)+} - s_{dp}^{*(k,h)+} &= z_{dp}^{(k,h)} \quad \forall d \in \widehat{L}_{(k,h)}^{\text{out}}.
\end{aligned} \tag{35}$$

Hence we have the overall efficiency as follows:

$$\widehat{\eta}_p = \frac{\sum_{k=1}^{K} w_k \left[1 - \left(1/\left(m_k + \sum_{d=1}^{l_{(k,h)}} y_d^{*(k,h)}\right)\right)\left(\sum_{i=1}^{m_k}\left(\left(s_{ip}^{*k-} + \widehat{s}_{ip}^{k-}\right)/x_{ip}\right) + \sum_{d=1}^{l_{(k,h)}}\left(\left(s_{dp}^{*(k,h)-} + \widehat{s}_{dp}^{(k,h)-}\right)/z_{dp}^{(k,h)}\right)\right)\right]}{\sum_{k=1}^{K} w_k \left[1 + \left(1/\left(r_k + l_{(k,h)} - \sum_{d=1}^{l_{(k,h)}} y_d^{*(k,h)}\right)\right)\left(\sum_{r=1}^{r_k}\left(\left(s_{rp}^{*k+} + \widehat{s}_{rp}^{k+}\right)/y_{rp}\right) + \sum_{d=1}^{l_{(k,h)}}\left(\left(s_{dp}^{*(k,h)+} + \widehat{s}_{dp}^{*(k,h)+}\right)/z_{dp}^{(k,h)}\right)\right)\right]}. \tag{36}$$

If only one of $\widehat{s}_{rp}^{k+}$ $(\forall k, \forall r)$, $\widehat{s}_{ip}^{k-}$ $(\forall k, \forall i)$ $\widehat{s}_{dp}^{(k,h)-}$ or $\widehat{s}_{dp}^{(k,h)+}$ $\forall (k, h)$, $\forall d \in L_{(k,h)}$, is positive then we have

$$\widehat{\eta}_p < \eta_p^* \tag{37}$$

and it contradicts the optimality of η_p^*. Thus, we have $\widehat{s}_{rp}^{k+} = 0$ $(\forall k, \forall r)$, $\widehat{s}_{ip}^{k-} = 0$ $(\forall k, \forall i)$, $\widehat{s}_{dp}^{(k,h)-} = 0$ $\forall d \in \widehat{L}_{(k,h)}^{\text{in}}$ and $\widehat{s}_{dp}^{(k,h)+} = 0$ $\forall d \in \widehat{L}_{(k,h)}^{\text{out}}$. Therefore, the projected DMU is overall efficient. □

It should be noted that, in the case $L_{(k,h)}^{\text{in}} \neq \widehat{L}_{(k,h)}^{\text{in}}$, there exists $d \in \widehat{L}_{(k,h)}^{\text{in}}$ that $d \notin L_{(k,h)}^{\text{in}}$. Therefore $d \in L_{(k,h)}^{\text{out}}$, and this means that the link value is free to be greater than or equal to (but not lower than) the observed one in production possibility set. On the other hand $d \in \widehat{L}_{(k,h)}^{\text{in}}$ means that the link value is free to be smaller than or equal to (but not greater than) the observed one in production possibility set and it is not possible unless the link target value of both solutions is equal to the observed value. Therefore, $\widehat{s}_{dp}^{(k,h)-}$ and $s^{*(k,h)-}_{dp}$ should be equal to zero.

4. Numerical Example

In this section to illustrate our proposed models, we will use a numerical example and compare the results of our proposed models with some existing approaches in SBM framework. Table 1 exhibits the data of our numerical example.

Consider the dataset provided by Tone and Tsutsui [19]. It consists of 10 DMUs, corresponding to vertically integrated electric power companies. They illustrated the vertically integrated electric power companies as three divisions of generation, transmission, and distribution that are linked together via intermediate products as shown in Figure 1. Each division has a single exogenous input: *Labor*. The *Electric Power Sold* to large customers and to small customers are, respectively, the output of *Transmission* and *Distribution* divisions. *Electric Power Generated* by *Generation* division is consumed by *Transmission* Division therefore *Electric Power Generated* is an intermediate measure which links the *Generation* Division to *Transmission* Division. *Electric Power Sent* produced by *Transmission* Division and consumed by *Distribution* Division is used as an intermediate measure which links *Transmission* Division to *Distribution* Division.

4.1. Black Box and Proposed Model. In this section first, we solved the black box model using Inputs 1, 2, and 3 and Outputs 2 and 3 where links were neglected. The column "black box" in Table 2 exhibits the results.

Next, we solved the two proposed models explained in Sections 3.1 and 3.2. The numbers 0.4, 0.2, and 0.4 are weights to div 1, div 2, and div 3, respectively. This weight selection is just for illustrative purpose. Table 2 reports the results where "Overall score" indicates the weighted average scores of divisions.

Throughout this section, we used the input-oriented SBM (slacks-based measure) under the variable returns-to-scale (VRS) assumption for efficiency evaluation.

Figure 2 clearly illustrates that the black box model has lower discriminate power than those of our proposed

Table 1: Exhibits data for inputs, outputs, and links of the ten DMUs in their numerical example; data for inputs, outputs, and links of the ten DMUs presented by Tone and Tsutsui [19].

DMU	Generation process (div 1)	Transmission process (div 2)		Distribution process (div 3)		links	
	Input 1 (x_1)	Input 2 (x_2)	Output 2 (y_2)	Input 3 (x_3)	Output 3 (y_3)	Link 12 (z_1)	Link 23 (z_2)
DMU1	0.838	0.277	0.879	0.962	0.337	0.894	0.362
DMU2	1.233	0.132	0.538	0.443	0.180	0.678	0.188
DMU3	0.321	0.045	0.911	0.482	0.198	0.836	0.207
DMU4	1.483	0.111	0.570	0.467	0.491	0.869	0.516
DMU5	1.592	0.208	1.086	1.073	0.372	0.693	0.407
DMU6	0.790	0.139	0.722	0.545	0.253	0.966	0.269
DMU7	0.451	0.075	0.509	0.366	0.241	0.647	0.257
DMU8	0.408	0.074	0.619	0.229	0.097	0.756	0.103
DMU9	1.864	0.061	1.023	0.691	0.380	1.191	0.402
DMU10	1.222	0.149	0.769	0.337	0.178	0.792	0.187

Table 2: SBM scores for black box and proposed models.

DMU	Black Box	Model (I)				Model (II)		
	Overall efficiency score	Overall efficiency score	div 1 (0.4)	div 2 (0.2)	div 3 (0.4)	ρ^*	div 1 (0.4)	div 2 (0.2)	div 3 (0.4)
DMU1	1.00	0.385	0.383	0.383	0.389	0.441	0.383	0.659	0.389
DMU2	0.54	0.433	0.260	0.341	0.652	0.433	0.26	0.341	0.652
DMU3	1.00	0.968	1.00	1.00	0.919	0.968	1	1	0.919
DMU4	1.00	0.719	0.297	1.00	1.00	0.719	0.297	1	1
DMU5	1.00	0.456	0.263	1	0.377	0.456	0.263	1	0.377
DMU6	0.681	0.484	0.406	0.420	0.593	0.608	0.406	0.643	0.792
DMU7	1.00	0.778	0.712	0.740	0.863	0.778	0.712	0.74	0.863
DMU8	1.00	0.969	0.922	1.00	1.00	0.969	0.922	1	1
DMU9	1.00	0.832	1.00	1.00	0.581	0.832	1	1	0.581
DMU10	1.00	0.506	0.271	0.338	0.825	0.506	0.271	0.338	0.825
Average	0.9221	0.602	0.524	0.688	0.637	0.620	0.524	0.738	0.657

network models. The scores of black box are greater than the overall scores obtained by proposed models and the rank of scores of the DMUs is not corresponding. For example DMU5 is scored worse in the proposed models while best in black box model. This means that there is no significant correlation between the scores of network models and black box. There is also a sharp contrast between the trends of black box and proposed models. This is quite natural since we ignored the internal linking activities in black box model.

4.2. Separation Approach and Proposed Models. In this section we compare our proposed model with separation model.

In order to take into account the inefficiency associated with link flows, there is another approach to evaluate divisional efficiency individually called *separation* approach (see Cook et al. 2014, p. 233). In this approach we evaluate the efficiency of div 1 of our numerical example using Input 1 as input and Link 12 as output. Similarly we evaluate the efficiency of div 2 of each DMU using *Link 12* and *Input 2* as inputs and Link 23 and Output 2 as outputs. In the same way we evaluate the efficiency of div 3 using *Link 23* and *Input 3* as inputs and *Output 3* as output.

Table 3 reports the overall and divisional efficiency scores obtained by separation approach where the overall scores are the weighted sum of the divisional scores. We utilized the numbers 0.4, 0.2, and 0.4 as the weights to div 1, div 2, and, div 3, respectively.

Table 3: SBM scores for separation model.

DMU	Separation model			
	Overall score	div 1 (0.4)	div 2 (0.2)	div 3 (0.4)
DMU1	0.659	0.633	0.662	0.684
DMU2	0.657	0.26	0.763	1.00
DMU3	0.984	1.00	1.00	0.959
DMU4	0.719	0.297	1.00	1.00
DMU5	0.547	0.202	1.00	0.665
DMU6	0.844	1.00	0.635	0.792
DMU7	0.855	0.712	1.00	0.926
DMU8	0.893	0.787	0.890	1.00
DMU9	0.915	1	1	0.786
DMU10	0.640	0.263	0.672	1

Model (II) and separation model both take into the account the inefficiency associated with link flows. In proposed models the continuity of link values between divisions is assured whereas in separation model it is not. Figure 3

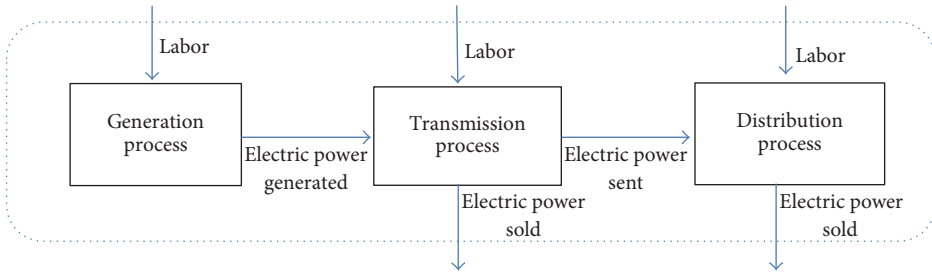

Figure 1: Network structure of vertically integrated electric power companies.

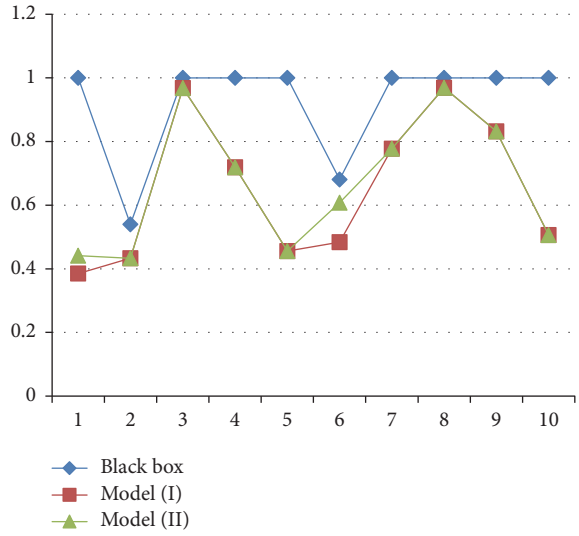

Figure 2: Comparisons of scores between black box and proposed models.

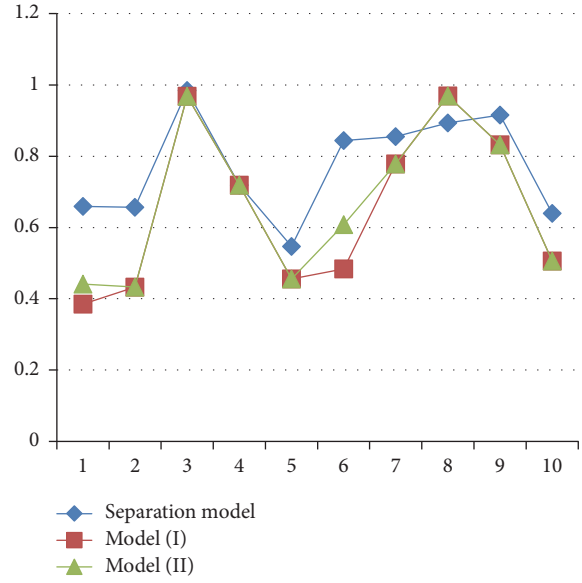

Figure 3: Comparisons of scores between proposed models and separation approach.

compares the overall efficiency scores of the separate model and proposed models. It can be seen from Figure 3 that the trends of the three models are close together. The gaps between proposed models and separation model must be caused by the difference of assumption on the links among divisions.

4.3. NSBM and Proposed Models. In this section we aim to compare the scores given by Slacks-Based Network DEA Models (proposed by Tone and Tsutsui [19]) and our proposed models. The overall and divisional SBM scores given by free link and fixed link case NSBM are tabulated in Table 4.

Based on the results shown in Table 4, Model (I) yields the same results as applying free link NDEA model. It was not unexpected because the projected values of the intermediate products in both models are free to be greater or lower than their observed values; both models have the same objective function and the continuity of links between divisions is assured in both models.

The advantage of applying Model (I) instead of free link case is that we can find out the intermediate products are being viewed as inputs or outputs in the system.

The linking constraints in fixed link case are tighter than free link case and the proposed models; hence the overall

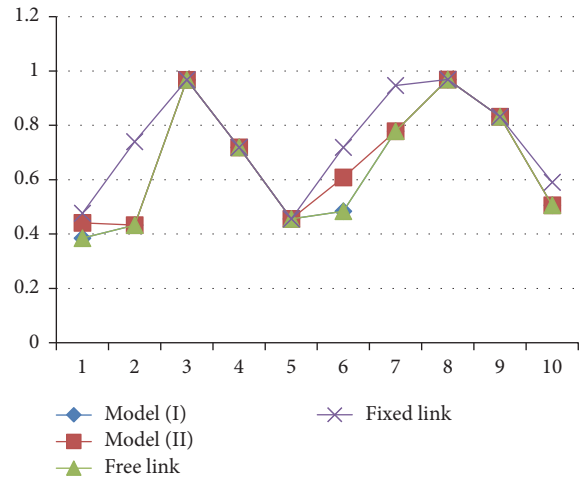

Figure 4: Comparisons of scores between proposed network models and NSBM models proposed by Tone and Tsutsui.

scores of the fixed link case exceed or are equal to those of the free case and Model (I) for every DMU. Figure 4 compares scores of the proposed models and network models (fixed and free link cases).

Table 4: Slacks-based network DEA.

DMU	Free link case				Fixed link case			
	ρ_0^*	div 1 (0.4)	div 2 (0.2)	div 3 (0.4)	ρ^*	div 1 (0.4)	div 2 (0.2)	div 3 (0.4)
DMU1	0.385	0.383	0.383	0.389	0.477	0.633	0.339	0.393
DMU2	0.433	0.260	0.341	0.652	0.740	0. 349	1.000	1.000
DMU3	0.968	1.000	1.000	0.919	0.968	1.000	1.000	0.919
DMU4	0.719	0.297	1.000	1.000	0.719	0.297	1.000	1.000
DMU5	0.456	0.263	1.000	0.377	0.456	0.263	1.000	0.377
DMU6	0.484	0.406	0.420	0.593	0.719	1.000	0.403	0.596
DMU7	0.778	0.712	0.740	0.863	0.947	1.000	1.000	0.868
DMU8	0.969	0.922	1.000	1.000	0.969	0.922	1.000	1.000
DMU9	0.832	1.000	1.000	0.581	0.832	1.000	1.000	0.581
DMU10	0.506	0.271	0.338	0.825	0.590	0.287	0.376	1.000
Avarage	0.653	0.551	0.722	0.720	0.742	0.675	0.812	0.773

Table 5: Exhibition of the role of intermediate measures in proposed models.

DMU	Model (I)		Model (II)	
	$Z1$	$Z2$	$Z1$	$Z2$
DMU1	Input to div 2	Input to div 3	Input to div 2	Output from div 2
DMU2	Output from div 1	Output from div 2	Output from div 1	Output from div 2
DMU3	Input to div 2	Input to div 3	Input to div 2	Output from div 2
DMU4	Input to div 2	Input to div 3	Input to div 2	Input to div 3
DMU5	Input to div 2	Input to div 3	Input to div 2	Output from div 2
DMU6	Input to div 2	Input to div 3	Input to div 2	Input to div 3
DMU7	Output from div 1	Input to div 3	Output from div 1	Output from div 2
DMU8	Input to div 2	Input to div 3	Input to div 2	Output from div 2
DMU9	Input to div 2	Input to div 3	Output from div 1	Output from div 2
DMU10	Output from div 1	Output from div 2	Output from div 1	Output from div 2

Model (II) takes into account the inefficiency associated with the link variables, whereas the NSBM does not.

4.4. Model (I) and Model (II). Comparing the SBM scores obtained by Model (I) and Model (II) shows that incorporation of intermediate product slacks in efficiency measurement may increase or decrease the divisional or overall efficiency (see Figure 2). To explain more, let us see how the categorization of intermediate measures into input or output type will change when we change the objective function (4) to (30).

As it can be seen from Table 4 changing the objective function (4) to (30) categorizes the intermediate measures into input or output type in a different way. For example in the optimal solution of Model (I) for DMU9 the intermediate measure z_1 is considered as an input to div 2, while in Model (II) it is considered as the outputs from div 1. It means that the target value of z_1 which links div 1 to div 2 in Model (I) is greater and in Model (II) is smaller than its observed value.

Table 5 exhibits the optimal role of intermediate measures obtained from Model (I) and Model(II). In optimal solutions of both models for DMU6 z_1, which links div 1 to div 2, is considered as input to div 2 while there are significant difference between the divisional efficiency scores of ρ_6^{*2} and φ_6^{*2}. Calculation below reveals the reason (see Appendix Tables 6 and 7):

$$\begin{aligned}
\rho_6^{*2} &= 1 - \frac{1}{m_2}\left(\sum_{i=1}^{m_2}\frac{s_{i6}^{*k-}}{x_{i6}}\right) = 1 - \frac{1}{1}\left(\frac{0.081}{0.139}\right) = 0.420,\\
\varphi_6^{*2} &= 1\\
&\quad - \frac{1}{m_k + \sum_{d=1}^{l_{(f,k)}} y_d^{*(f,k)}}\left(\sum_{i=1}^{m_k}\frac{s_{i6}^{*k-}}{x_{i6}} + \sum_{d=1}^{l_{(f,k)}}\frac{s_{d6}^{*(f,k)-}}{z_{d6}^{(f,k)}}\right)\\
&= 1 - \frac{1}{1+1}\left(\frac{0.081}{0.139} + \frac{0.130}{0.966}\right) = 0.643.
\end{aligned} \tag{38}$$

We can also show the efficiency calculations for div 2 of DMU1.

$$\begin{aligned}
\rho_1^{*2} &= 1 - \frac{1}{m_2}\left(\sum_{i=1}^{m_2}\frac{s_{i1}^{*k-}}{x_{i1}}\right) = 1 - \frac{1}{1}\left(\frac{0.171}{0.277}\right) = 0.383,\\
\varphi_1^{*2} &= 1\\
&\quad - \frac{1}{m_k + \sum_{d=1}^{l_{(f,k)}} y_d^{*(f,k)}}\left(\sum_{i=1}^{m_k}\frac{s_{i1}^{*k-}}{x_{i1}} + \sum_{d=1}^{l_{(f,k)}}\frac{s_{d1}^{*(f,k)-}}{z_{d1}^{(f,k)}}\right)\\
&= 1 - \frac{1}{1+1}\left(\frac{0.171}{0.277} + \frac{0.058}{0.894}\right) = 0.659.
\end{aligned} \tag{39}$$

Table 6: Optimum slack variables in Model (I).

	s_1^{*1-}	s_1^{*2-}	s_1^{*3-}	s_1^{*2+}	s_1^{*3+}	$s_1^{*(1,2)+}$	$s_1^{*(1,2)-}$	$s_1^{*(2,3)-}$	$s_1^{*(2,3)+}$
DMU1	0.517	0.171	0.588	0.000	0.000	0.000	0.058	0.000	0.007
DMU2	0.912	0.087	0.154	0.373	0.016	0.158	0.000	0.019	0.000
DMU3	0.00	0.000	0.039	0.000	0.000	0.000	0.000	0.000	0.000
DMU4	1.043	0.000	0.00	0.000	0.000	0.000	0.000	0.000	0.000
DMU5	1.173	0.000	0.669	0.000	0.015	0.000	0.000	0.000	0.002
DMU6	0.469	0.081	0.222	0.112	0.000	0.000	0.130	0.000	0.003
DMU7	0.130	0.019	0.050	0.341	0.000	0.189	0.000	0.000	0.000
DMU8	0.032	0.000	0.00	0.000	0.000	0.000	0.000	0.000	0.000
DMU9	0.00	0.000	0.290	0.000	0.002	0.000	0.000	0.000	0.000
DMU10	0.891	0.099	0.059	0.088	0.000	0.029	0.000	0.001	0.000

Table 7: Optimum slack variables in Model (II).

	s_1^{*1-}	s_1^{*2-}	s_1^{*3-}	s_1^{*2+}	s_1^{*3+}	$s_1^{*(1,2)+}$	$s_1^{*(1,2)-}$	$s_1^{*(2,3)-}$	$s_1^{*(2,3)+}$
DMU1	0.517	0.171	0.588	0.000	0.000	0.000	0.058	0.000	0.000
DMU2	0.912	0.087	0.154	0.373	0.016	0.158	0.000	0.019	0.000
DMU3	0.000	0.000	0.039	0.000	0.000	0.000	0.000	0.000	0.000
DMU4	1.043	0.000	0.000	0.000	0.000	0.000	0.130	0.000	0.000
DMU5	1.173	0.000	0.669	0.000	0.015	0.000	0.000	0.000	0.000
DMU6	0.469	0.081	0.222	0.112	0.000	0.000	0.000	0.000	0.002
DMU7	0.130	0.019	0.050	0.341	0.000	0.189	0.000	0.000	0.000
DMU8	0.032	0.000	0.000	0.000	0.000	0.000	0.000	0.000	0.000
DMU9	0.000	0.000	0.290	0.000	0.002	0.000	0.000	0.000	0.000
DMU10	0.891	0.099	0.059	0.088	0.000	0.029	0.000	0.001	0.000

Calculations above show the impact of inefficiency associated with link flows on efficiency score.

5. Conclusion

In this paper in order to address the conflict caused by the dual role of intermediate measures we proposed two alternative slacks-based measure models, called Model (I) and Model (II). To resolve this conflict the intermediate measures are categorized into input or output type endogenously. These categorizations allow models to identify nonzero slacks and uncover the sources of inefficiency associated with intermediate measures. In Model (I) the excesses or shortfalls corresponding to intermediate measures are contributed to the optimum objective indirectly. In order to incorporate the direct effect of inefficiency associated with intermediate measures, we proposed Model (II) in which the average reduction or expansion rate of intermediate products has been taken into the account in the objective function. Keeping continuity of link flows between divisions and incorporation of link flows in efficiency measurements at the same time is the clear advantage of our proposed model over other approaches.

To verify our proposed models we provided a numerical example and we compared the results with black box model, separation model, and Slacks-based network DEA (free link and fixed link case). In comparing the scores obtained by proposed network models and black box model, no significant correlation between the efficiency scores was found and the trends of network models were in sharp contrast to that of black box model. It was not unexpected because the internal linking activities in black box approach were neglected.

Overall and divisional efficiency scores obtained by Model (I) in the numerical example are equal to those of free link case. It is quite natural because in both models the continuity of link values between divisions is assured and the target values of the intermediate products are free to be above or below their observed values. A clear advantage of using Model (I) is revealing the role of intermediate product in the system. Since the linking constraints of the fixed link case are tighter than that of Model (I), the scores of the fixed link case tend to be higher than those of Model (I) for every DMU.

The scores of separate model follow a roughly similar trend to those of the proposed network models. However there are some differences between network models and separate model that must be caused by different assumption on the linking activities. The proposed network models keep the continuity of link flows among divisions whereas the separate model does not.

Separate model and Model (II) both take into account the inefficiency associated with the link variables.

Comparing the results of Model (I) and Model (II), we can see how the inclusion of intermediate product slacks in the objective function may change the categorization of the intermediate products and exert influence over the efficiency of each division.

For further research we can suggest the following issues.

The proposed approach can be easily extended to the dynamic network models.

LP formulation of Model (II) could be analyzed and interpreted. The proposed models can be extended to the situation in which some input/output data are fuzzy numbers. Another possible line of research is to include undesirable (or bad) outputs.

Appendix

See Tables 6 and 7.

ILP Formulation of Model (I)

In Model (I) the objective function is clearly nonlinear. The objective function can be easily transformed to linear form by Charnes-Cooper transformations.

By introducing a positive scalar variable t we change the objective function 1 as follows:

$$\rho = \min \quad \sum_{k=1}^{K} w_k \left[t - \frac{1}{m_k} \left(\sum_{i=1}^{m_k} \frac{t s_{pi}^{k-}}{x_{ip}} \right) \right]$$
$$\sum_{k=1}^{K} w_k \left[1 + \frac{1}{r_k} \left(\sum_{r=1}^{r_k} \frac{s_{rp}^{k+}}{y_{rp}} \right) \right] = t. \tag{A.1}$$

Now let us define
$t\lambda_j^k = \Lambda_j^k$, $S_{ip}^{k-} = t s_{ip}^{k-}$, $S_{rp}^{k+} = t s_{ip}^{k+}$, $S_{dp}^{(k,h)+} = t s_{dp}^{(k,h)+}$, $S_{dp}^{(k,h)-} = t s_{dp}^{(k,h)-}$, $Z_d^{(k,h)} = t z_d^{(k,h)}$, $Z_d'^{(k,h)} = t z_d'^{(k,h)}$, and $M' = Mt$.

Then the model becomes as follows:

$$\rho = \min \quad \sum_{k=1}^{K} w_k \left[t - \frac{1}{m_k} \left(\sum_{i=1}^{m_k} \frac{S_{ip}^{k-}}{x_{ip}^k} \right) \right]$$

$$\text{s.t.} \quad \sum_{k=1}^{K} w_k \left[t + \frac{1}{r_k} \left(\sum_{r=1}^{r_k} \frac{S_{rp}^{k+}}{y_{rp}} \right) \right] = 1$$

$$(k = 1, \ldots, K), \ (r = 1, \ldots, r_k)$$

$$\sum_{j=1}^{n} \Lambda^k{}_j x_{ij}^k + S_{ip}^{k-} = t x_{ip}^k$$

$$(k = 1, \ldots, K), \ (i = 1, \ldots, m_k)$$

$$\sum_{j=1}^{n} \Lambda^k{}_j y_{rj}^k - S_{rp}^{k+} = t y_{rp}^k$$

$$(k = 1, \ldots, K), \ (r = 1, \ldots, r_k)$$

$$\sum_{j=1}^{n} \Lambda^h{}_j z_{dj}^{(k,h)} + S_{dp}^{(k,h)-} = Z_d'^{(k,h)}$$

$$\left(d = 1, \ldots, l_{(k,h)}\right), \ \forall (k,h)$$

$$\sum_{j=1}^{n} \Lambda^k{}_j z_{dj}^{(k,h)} - S_{dp}^{(k,h)-} = Z_d^{(k,h)}$$

$$\left(d = 1, \ldots, l_{(k,h)}\right), \ \forall (k,h)$$

$$\sum_{j=1}^{n} \Lambda^k{}_j z_{dj}^{(k,h)} = \sum_{j=1}^{n} \Lambda^h{}_j z_{dj}^{(k,h)}$$

$$\left(d = 1, \ldots, l_{(k,h)}\right), \ \forall (k,h)$$

$$0 \le S_{dp}^{(k,h)-} \le M' y_d^{(k,h)}$$

$$\left(d = 1, \ldots, l_{(k,h)}\right), \ \forall (k,h)$$

$$0 \le S_{dp}^{(k,h)+} \le M' \left(1 - y_d^{(k,h)}\right)$$

$$\left(d = 1, \ldots, l_{(k,h)}\right), \ \forall (k,h)$$

$$t z_{dp}^{(k,h)} - M' y_{dp}^{(k,h)} \le Z'^{(k,h)}_d$$

$$\le t z_{dp}^{(k,h)} + M' y_{dp}^{(k,h)}$$

$$\left(d = 1, \ldots, l_{(k,h)}\right), \ \forall (k,h)$$

$$t z_{dp}^{(k,h)} - M t' \left(1 - y_d^{(k,h)}\right) \le Z_d^{(k,h)}$$

$$\le t z_{dp}^{(k,h)} + M' \left(1 - y_d^{(k,h)}\right)$$

$$\left(d = 1, \ldots, l_{(k,h)}\right), \ \forall (k,h)$$

$$\sum_{j=1}^{n} \Lambda^k{}_j = t \quad (k = 1, \ldots, K)$$

$$y_d^{(k,h)} = \{0, 1\}; \tag{A.2}$$

$$Z_d^{(k,h)}, \ Z_d'^{(k,h)} : \text{free},$$

$$\Lambda^k{}_j \ge 0, \tag{A.3}$$

$$S_{rp}^{k+} \ge 0,$$

$$S_{ip}^{k-} \ge 0.$$

Conflicts of Interest

The authors declare that they have no conflicts of interest.

References

[1] A. Charnes, W. W. Cooper, and E. Rhodes, "Measuring the efficiency of decision making units," *European Journal of Operational Research*, vol. 2, no. 6, pp. 429–444, 1978.

[2] M. J. Farrell, "The measurement of productive efficiency," *Journal of the Royal Statistical Society: Series A (Statistics in Society)*, vol. 120, pp. 253–290, 1957.

[3] W. D. Cook, L. Liang, and J. Zhu, "Measuring performance of two-stage network structures by DEA: a review and future perspective," *Omega*, vol. 38, no. 6, pp. 423–430, 2010.

[4] J. Chilingerian and H. D. Sherman, "Health care applications: from hospitals to physician, from productive efficiency to quality frontiers," in *Handbook on Data Envelopment Analysis*, W. W. Cooper, L. M. Seiford, and J. Zhu, Eds., Springer, Boston, Mass, USA, 2004.

[5] L. M. Seiford and J. Zhu, "Profitability and marketability of the top 55 U.S. commercial banks," *Management Science*, vol. 45, no. 9, pp. 1270–1288, 1999.

[6] J. Zhu, "Multi-factor performance measure model with an application to fortune 500 companies," *European Journal of Operational Research*, vol. 123, no. 1, pp. 105–124, 2000.

[7] T. R. Sexton and H. F. Lewis, "Two-stage DEA: an application to major league baseball," *Journal of Productivity Analysis*, vol. 19, no. 2-3, pp. 227–249, 2003.

[8] C. Kao and S.-N. Hwang, "Efficiency decomposition in two-stage data envelopment analysis: an application to non-life insurance companies in Taiwan," *European Journal of Operational Research*, vol. 185, no. 1, pp. 418–429, 2008.

[9] H. Fukuyama and W. L. Weber, "A slacks-based inefficiency measure for a two-stage system with bad outputs," *Omega International Journal of Management Science*, vol. 38, no. 5, pp. 398–409, 2010.

[10] C.-M. Chen, "A network-DEA model with new efficiency measures to incorporate the dynamic effect in production networks," *European Journal of Operational Research*, vol. 194, no. 3, pp. 687–699, 2009.

[11] L. Liang, F. Yang, W. D. Cook, and J. Zhu, "DEA models for supply chain efficiency evaluation," *Annals of Operations Research*, vol. 145, pp. 35–49, 2006.

[12] R. Färe and S. Grosskopf, "Productivity and intermediate products: a frontier approach," *Economics Letters*, vol. 50, no. 1, pp. 65–70, 1996.

[13] R. Färe and S. Grosskopf, "Network DEA," *Socio-Economic Planning Sciences*, vol. 34, no. 1, pp. 35–49, 2000.

[14] S. C. Graves, A. H. G. Rinnoy Kan, and P. H. Zipkin, *Logistics of Production and Inventory*, North-Holland, The Netherlands, 1993.

[15] S. T. Hackman and R. C. Leachman, "A general framework for modeling production," *Management Science*, vol. 35, pp. 478–495, 1989.

[16] L. A. Johnson and D. C. Montgomery, *Operations Research in Production Planning, Scheduling and Inventory Control*, Wiley, New York, NY, USA, 1974.

[17] M. D. Troutt, P. J. Ambrose, and C. K. Chan, "Optimal throughput for multistage input-output processes," *International Journal of Operations and Production Management*, vol. 21, no. 1-2, pp. 148–158, 2001.

[18] D. K. Despotis, G. Koronakos, and D. Sotiros, "A multi-objective programming approach to network DEA with an application to the assessment of the academic research activity," in *Proceedings of the 3rd International Conference on Information Technology and Quantitative Management, ITQM 2015*, pp. 370–379, July 2015.

[19] K. Tone and M. Tsutsui, "Network DEA: a slacks-based measure approach," *European Journal of Operational Research*, vol. 197, no. 1, pp. 243–252, 2009.

[20] K. Tone and M. Tsutsui, "Dynamic DEA: a slacks-based measure approach," *Omega– International Journal of Management Science*, vol. 38, no. 3-4, pp. 145–156, 2010.

[21] K. Tone and M. Tsutsui, "Dynamic DEA with network structure: a slacks-based measure approach," *Omega–International Journal of Management Science*, vol. 42, no. 1, pp. 124–131.

[22] S. Lozano, "Alternative SBM model for network DEA," *Computers & Industrial Engineering*, vol. 82, pp. 33–40, 2015.

[23] F.-h. F. Liu and Y.-c. Liu, "Procedure to solve network DEA based on a virtual gap measurement model," *Mathematical Problems in Engineering*, vol. 2017, Article ID 3060342, 13 pages, 2017.

Hindawi
Mathematical Problems in Engineering
Volume 2017, Article ID 8109730, 15 pages
https://doi.org/10.1155/2017/8109730

Research Article

Secure *kNN* Computation and Integrity Assurance of Data Outsourcing in the Cloud

Jun Hong,[1,2] Tao Wen,[1] Quan Guo,[3] and Zhengwang Ye[1]

[1]*School of Computer Science and Engineering, Northeastern University, Shenyang, Liaoning 110819, China*
[2]*School of Software, North University of China, Taiyuan, Shanxi 030051, China*
[3]*Department of Computer Science and Technology, Dalian Neusoft University, Dalian, Liaoning 116023, China*

Correspondence should be addressed to Jun Hong; hongjun@nuc.edu.cn

Received 20 May 2017; Revised 1 October 2017; Accepted 5 November 2017; Published 13 December 2017

Academic Editor: M. L. R. Varela

As cloud computing has been popularized massively and rapidly, individuals and enterprises prefer outsourcing their databases to the cloud service provider (CSP) to save the expenditure for managing and maintaining the data. The outsourced databases are hosted, and query services are offered to clients by the CSP, whereas the CSP is not fully trusted. Consequently, the security shall be violated by multiple factors. Data privacy and query integrity are perceived as two major factors obstructing enterprises from outsourcing their databases. A novel scheme is proposed in this paper to effectuate k-nearest neighbors *(kNN)* query and *kNN* query authentication on an encrypted outsourced spatial database. An asymmetric scalar-product-preserving encryption scheme is elucidated, in which data points and query points are encrypted with diverse encryption keys, and the CSP can determine the distance relation between encrypted data points and query points. Furthermore, the similarity search tree is extended to build a novel verifiable SS-tree that supports efficient *kNN* query and *kNN* query verification. It is indicated from the security analysis and experiment results that our scheme not only maintains the confidentiality of outsourced confidential data and query points but also has a lower *kNN* query processing and verification overhead than the MR-tree.

1. Introduction

As the spatial data resources have been developed by leaps and bounds, to be well geared into such transition, the enterprises are required to proliferate the resources of both the hardware and software resources and to recruit professionals to manage and maintain data. Accordingly, the data maintenance has been boomed overhead. On the other hand, cloud computing has become progressively popularized in recent years. This arises from their capability to offer scores of benefits, such as quick deployment, on-demand service, high scalability and cost reduction [1–4]. A growing number of companies are currently being motivated to outsource their daily business, even their core business, to the cloud service provider to eliminate the investment in hardware and software and to reduce the costs to maintain data. Moreover, using the advantages of cloud computing, the end users can use on-line software applications and access the service at any time and any place [5]. Outsourcing spatial database is progressively reflecting the trend of reality. Spatial data has scores of practical applications, such as environmental monitor, location-based services, flow control, etc. In the data outsourcing model, the cloud service provider (CSP) hosts the outsourced databases and provides query services for the clients, and the data owner loses the management and control of the outsourced data. Consequently, the confidentiality and security of data shall be violated. Data privacy and security problems count as the major factors obstructing the data owners from outsourcing their databases to the CSP [6, 7].

Data encryption is perceived as the most frequently adopted approach to maintain data confidentiality. Merely the authorized parties can conduct decryption. It is noteworthy that the destination of outsourcing data is to draw on the strong computing power and high bandwidth of the cloud service provider to offer the rapid and efficient services to users. Yet, the traditional encryption approaches, such as DES and RSA, are primarily designed to encrypt the confidential data, the encrypted data cannot support efficient query and

analysis as well as the original data. Many effective schemes [8–11] have been proposed to support how to execute queries on encrypted data.

With the exception of data privacy, query integrity, also known as query authentication, is deemed as another critical problem to be solved in the domain of data outsourcing. Since the CSP is not fully trusted, it can return incorrect or incomplete query results. Extra authentication information shall be offered to the client to ensure the correctness and completeness of query results without having to trust the CSP. Correctness bespeaks that the records in the results really exist in the owner's database and are not modified by any user. Completeness bespeaks that all the records that satisfy the query condition are included in the results. Query integrity, in particular, is crucial in the case of the results laying the foundation for critical decisions.

The k-nearest neighbors *(kNN)* query is deemed as a crucial data analysis operation which can be used as an independent query or as a core module of data mining and has been applied in many practical applications, such as geospatial technology, location-based services, and pattern recognition. Recent studies [12–16] have proposed various techniques to support either *kNN* queries on encrypted data or *kNN* query authentication. However, both privacy protection and query authentication should be provided in an insecure cloud computing environment. Thus, we focus on the *kNN* query processing and *kNN* query authentication on an encrypted spatial dataset. In this paper, we introduce an asymmetric scalar-product-preserving encryption to encrypt confidential data points and query points, and then we propose an authenticated spatial index structure based on the SS-tree [17], called verifiable SS-tree (VSS-tree), for secure *kNN* query processing and *kNN* query authentication. Our main contributions are illuminated as follows:

(1) We introduce an asymmetric scalar-product-preserving encryption through which the data owner encrypts confidential data and query points with diverse encryption keys. The cloud server can perform a *kNN* query on encrypted outsourced spatial database.

(2) We extend SS-tree [17] and propose a novel verifiable SS-tree (VSS-tree) for the *kNN* query processing and *kNN* query authentication.

(3) We perform a detailed security analysis and performance evaluation of our scheme.

The rest of this paper is organized as follows. The relevant work is reviewed in Section 2. The system model is proposed in Section 3. Section 4 specifies the encryption scheme. Section 5 elaborates on the VSS-tree. In Section 6, we perform security analysis of our scheme. In Section 7, the performance and experimental results are presented. Eventually, we conclude this paper in Section 8.

2. Related Work

The encryption approach, called "bucket-based," is proposed in [8, 9]. The domain of private data is subdivided into multiple disjoint ranges and each range is identified by a unique identifier. The cloud server performs a range query in the light of the identifiers and returns a super set of real result set. The client has to do extra processing to get the real results. Agrawal et al. [10] proposed an order-preserving encryption to support one-dimensional range query on encrypted data. The input data distribution is accordingly transformed into a user-specified target distribution. The encrypted data is kept in the same order as the original data, which simplifies the course to effectuate encrypted range query. Nevertheless, this scheme fails to resist known-plaintext attack [18]. Oliveira and Zaiane [11] proposed a distance-preserving transformation (DPT) approach. DPT transforms an original data point x into a new point $Nx + t$, where N is a $d \times d$ matrix and t is a d-dimensional vector. DPT ensures that the Euclidean distance between any two encrypted data points is equal to that between the corresponding original data points; that is, $d(x, y) = d(E(x), E(y))$. However, DPT cannot resist level 2 and level 3 attacks [19]. Man et al. [20] proposed a data transformation approach to maintain data confidentiality. Using the transforming function, the data owner and user transform their original spatial data and query ranges into encrypted ones. The cloud server performs range queries on encrypted data. Chen et al. [21] proposed a random space encryption approach to support range query on encrypted data. The outsourced data and queries are encrypted on the trust agent. The cloud server indexes the encrypted data and executes queries on it. And yet, the trust agent may become the single point of failure and network bottleneck of the system. Kalnis et al. [22] adopted k anonymity to the outsourced data. The cloud server cannot distinguish a record from at least $k - 1$ records. Obviously, the cloud server fails to perform exact query in line with this scheme. Similarly, Chow et al. [23] adopted location anonymity to hide the real location of query points. Asymmetric scalar-product-preserving encryption (ASPE) is proposed in [12] for secure *kNN* query on encrypted data. The outsourced data and query points are encrypted with diverse encryption keys, and the cloud server can execute a *kNN* query on encrypted data. However, ASPE assumes that the clients are fully trusted, which is unrealistic in real applications. The client can easily obtain the encryption key from his legal inputs and outputs. Optimized ASPE is proposed in [13, 14] in which the clients are not trusted and only the data owner knows the encryption key. Data points and query points are extended to $(2d + 2)$-dimensional points in [13], which requires more than double computation overhead than that of computing original data. Paillier homomorphic encryption is used in [14] to keep the query points confidential to the data owner. Thus, the client has to provide more computing resources to encrypt and decrypt the query points.

Digital signature chain mechanism is adopted in [24–27] for query authentication. Each record is signed with its immediate predecessor or successor record (attribute). The records and their corresponding signatures are stored together on CSP. When answering a query, the CSP returns the matched records along with their corresponding signatures to the client, and thereupon the client verifies the correctness and completeness of query results according to

the corresponding signatures. However, the computational complexity of digital signature is too high. Even though using signature aggregation [28], the client has to provide more computing power for signature verification and modular multiplications.

Being different from the signature chain, Merkle [29] first proposed Merkle Hash Tree (MHT), a memory-based binary tree with authentication information, for one-dimensional equality query. The digest rather than signature, computed by a one-way and collision-resistant hash function, is associated with each node. Only one signature is computed on the top of MHT. Devanbu et al. [30] extended MHT to support one-dimensional range query. Pang and Tan [31] extended MHT and proposed a verifiable B-tree (VB-tree). Data owner has to sign each record and node in the VB-tree, which results in high signature computation overhead. The VB-tree only guarantees the correctness of the query results. Li et al. [32] proposed Merkle B-Tree (MBT) to support disk-based query authentication. To response a range query, the CSP performs two depth-first traversals to find the leftmost and rightmost records of query results and build the verification object (VO). The VO includes the following information: the digests of entries contained in each visited internal node that do not overlap with the range; the query results along with the digests of the residual entries in the corresponding leaves; the leftmost and rightmost records of the query results for completeness verification.

In multidimensional database outsourcing, Cheng et al. [33] proposed verifiable KD-tree (VKD-tree) and verifiable R-tree (VR-tree), applying signature chain to the KD-tree and the R-tree to ensure the integrity of query results, respectively. Yang et al. [34] proposed Merkle R-tree (MR-tree) and Merkle R*-tree (MR*-tree) for query verification of spatial data. MR*-tree combines the concepts from MBT and R*-tree. The authentication information is combined with the R*-tree. Range query is performed by a depth-first traversal of MR*-tree. The VO comprises all the data entries in the visited leaf nodes and the MBRs along with the corresponding digests of the sibling nodes pruned in the visited internal nodes. Yiu et al. [15] presented a framework for authenticating moving kNN queries using the safe region approach.

In other query authentication approaches, Xie et al. [35] proposed a probabilistic query integrity authentication scheme. The data owner inserts some fabricated records into the database and outsources them together to the CSP. The CSP cannot distinguish the fabricated records from the real ones. In response to a query, the CSP returns the query results (including the real and fabricated records) to the client. The client verifies the correctness and completeness of query results by verifying whether all the qualified fabricated records are included in the results.

Both privacy protection and query authentication are realized in [36–38]. Wang et al. [36] applied duplicated encryption for query verification. Part of the original data are encrypted with two diverse encryption keys. The user transforms a query into two different queries according to the encryption schemes and probabilistically verifies the query integrity by checking the two query result sets. Shamir secret sharing is used in [37] for privacy protection and multiparty computation. k service providers collaboratively compute the aggregation results without gaining knowledge of intermediate results. The integrity of aggregate results is guaranteed by MHT. Pedersen commitment protocol and MHT are used in [38] for aggregation computation and query verification.

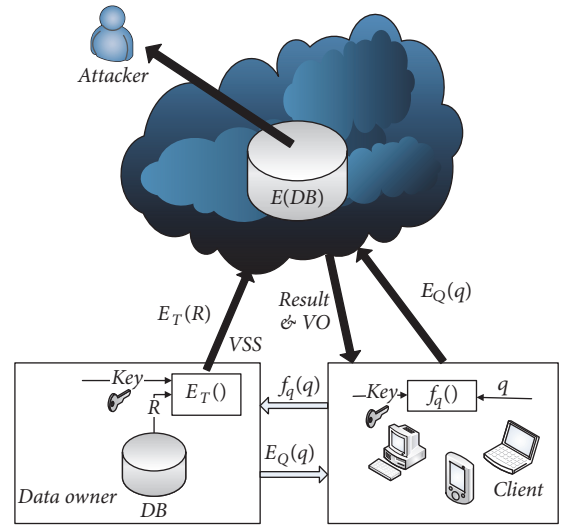

Figure 1: System model.

3. System Framework and Assumption

3.1. System Model. Figure 1 illustrates our system framework. It consists of three parts: data owner *(DO)*, client, and cloud service provider *(CSP)*. The data owner possesses two encryption keys. One is obtained from a trusted key distribution center, encompassing a private and a public key for signature. The other is generated by *DO* himself for encrypting sensitive data and query points. *DO* outsources the encrypted database D' to the *CSP*. Whenever updates occur, the corresponding encrypted data and the new signature are forwarded to *CSP*. The *CSP* hosts the outsourced database D' and provides query services for the client. To process spatial query efficiently, *CSP* maintains an authenticated spatial index structure. For each incoming query, it initiates the search algorithm to find a *kNN* query results and builds the corresponding *VO* for query authentication. To maintain the confidentiality of query points, a client transmits the processed query points to *DO* for encryption. After receiving an encrypted query point, the client transmits it to *CSP* for a *kNN* query. Once receiving *VO*, the client extracts the query results and performs query authentication. In general, the clients are located at the edge of networks and possess low network bandwidth and computing power. The clients only trust the signature information that the *DO* published.

3.2. System Assumption. We assume that the privacy data are numeric and denoted by real numbers, like the position coordinates of navigation, minimum, maximum and amount, etc. Each multidimensional piece of data is denoted as a

column vector. The *CSP* is semitrusted; thus, it can directly access the outsourced database D', fabricate or tamper with the data, and return a subset of real result set to save the computation power for providing paid services for more users. Simultaneously, *CSP* performs our scheme honestly. To maintain the confidentiality of query points, the client first transmits a processed query point to DO for encryption and thereupon extracts the encrypted query point and transmits it to *CSP* for a *kNN* query processing. The client verifies a *kNN* query results through *VO* and the public key *DO* published. Furthermore, the client is semitrusted, which may collude with *CSP* or other clients to recover the original data. Therefore, the encryption key owned by *DO* should not be revealed to the client and the CSP.

In summary, the attacks can be divided into three levels based on the knowledge the attackers can learn.

Level 1. The attacker only observes encrypted database and encrypted query points. This is known as ciphertext-only attack proposed in [18].

Level 2. With the exception of encrypted data, the attacker also knows part of the original plain data and some encryption information, such as the maximum, minimum, and data distribution of encrypted data. However, the attacker does not know the corresponding encrypted values of those plain data. This corresponds to known-sample attack [39].

Level 3. In addition to the knowledge obtained in level 2, the attacker observes a set of plain data and knows the corresponding ciphertext, and this is known as known-plaintext attack in cryptography [18].

It turns out to be evident that the knowledge of lower level that the attacker learns is a subset of what a higher-level attacker learns. If an encryption scheme can resist higher-level attacks, it can also resist lower-level attacks. Since we usually capture known-sample attack in practical applications, we design our encryption scheme against known-sample attacks.

Based on these assumptions, we should preserve the confidentiality of outsourced sensitive data and query points and provide query integrity authentication for *kNN* queries. The details are as follows:

(1) Data privacy: the confidential data should not be revealed to anyone else. Only encrypted data is outsourced to the CSP.

(2) Query privacy: query privacy bespeaks that a client's query points should be kept private to himself. Neither *DO* nor *CSP* can obtain the plain query points.

(3) Key privacy: the existing research usually shares the key with the clients. The *CSP* can easily obtain the key from the colluded or compromised client to recover the original data. Therefore, these schemes have to assume the clients are fully trusted. In our system assumption, each part of our system is semitrusted, the encryption key owned by *DO* should not be disclosed to anyone else.

Table 1: Symbol list.

Symbols	Description
p_i	A multidimensional point in the database
p_i'	The encrypted query point of p_i
q	A query point
q'	The encrypted query point of q
d	The dimensionality of spatial data
D	The private database of DO
M	A $d \times d$ matrix
M^{-1}, M^T	Inverse and transpose of matrix M
$d(p_i, q)$	The distance between p_i and q
$d(p_i', q')$	The distance between p_i' and q'
p^T, p'^T	Transposition of p, p'
$\|p\|$	Euclidean norm of point p
$E(p, Key)$	Encryption function: *Key* is the encryption key
$p_i \cdot p_j$	Scalar product of p_i *and* p_j

(4) Query authentication: based on the SS-tree, we propose a novel authenticated spatial index structure for *kNN* queries and *kNN* query authentication.

The main symbols used are listed in Table 1.

4. EASPE

4.1. Preliminary of ASPE. The basic idea of ASPE [12] is the observation that the distance between database points is not necessary for a *kNN* query. According to (1), ASPE can determine the distance relation between any two data points p_i, p_j and query point q.

$$\begin{aligned} & d(p_i, q) \le d(p_j, q) \\ & \sqrt{\|p_i\|^2 - 2p_i \cdot q + \|q\|^2} \le \sqrt{\|p_j\|^2 - 2p_j \cdot q + \|q\|^2} \\ & \Updownarrow \\ & \|p_i\|^2 - \|p_j\|^2 + 2(p_j - p_i) \cdot q \le 0, \end{aligned} \tag{1}$$

where $\|p_i\|^2$ is the scalar product of point p_i with itself, which can be computed in advance and stored with the corresponding data together for *kNN* queries. Then, ASPE does not need to preserve $\|p\|^2$. For any two encrypted points p_i', p_j', $p_i' \cdot p_j' = E(p_i, key) \cdot E(p_j, key)$. The distance between them can be computed by

$$d(p_i', p_j') = \sqrt{p_i' \cdot p_i' - 2(p_i' \cdot p_j') + p_j' \cdot p_j'}. \tag{2}$$

It is easy to see from (1) and (2) that ASPE does not keep the scalar product $p_i \cdot p_j$ to ensure that the CSP cannot compute the distance between any database points through (2). Moreover, the CSP is able to determine which data point is nearer to the query point q through (1).

Definition 1 (asymmetric scalar-product-preserving encryption (ASPE)). An encryption function E is an ASPE if and only if it satisfies the following two conditions:

(1) For any point p_i and any query point q, $p_i \cdot q = E(p_i, K) \cdot E(q, K)$.

(2) For any p_i and p_j in D, $p_i \cdot p_j \neq E(p_i, K) \cdot E(p_j, K)$.

As can be seen from Definition 1, data point and query point must be encrypted with diverse encryption keys to ensure that the encrypted value of any query point q is different from that of any data point p in D, even if $p = q$.

When encrypting a data point, ASPE randomly generates a $(d+1) \times (d+1)$ invertible matrix M_k as the encryption key and extends every data point p to a new $(d+1)$-dimensional point $\widehat{p} = (p^T, -0.5\|p\|^2)^T$ which is encrypted into $p' = M_k^T \cdot \widehat{p}$. When encrypting a query point q, the client randomly selects a positive random number r and extends the query point q to a new $(d+1)$-dimensional point $\widehat{q} = r(q^T, 1)^T$, and then he encrypts $\widehat{q}$ into $q' = M_k^{-1} \cdot \widehat{q}$, where M_k^{-1} is the encryption key of query points. To determine whether an encrypted data point p_i' is nearer to a query point q' than p_j' is, the *kNN* search algorithm checks whether $(p_i' - p_j') \cdot q' > 0$:

$$\begin{aligned}
\left(p_i' - p_j'\right) \cdot q' &= \left(p_i' - p_j'\right)^T q' = \left(M_k^T \widehat{p}_i - M_k^T \widehat{p}_j\right)^T \\
&\cdot M_k^{-1} \widehat{q} = \left(\widehat{p}_i - \widehat{p}_j\right)^T \widehat{q} \\
&= \left(\left(p_i^T, -0.5\left\|p_i\right\|^2\right)^T - \left(p_j^T, -0.5\left\|p_j\right\|^2\right)^T\right)^T \\
&\cdot r\left(q^T, 1\right)^T \\
&= \left(\left(p_i - p_j\right)^T, \left(-0.5\left\|p_i\right\|^2 + 0.5\left\|p_j\right\|^2\right)\right)(rq, r) \\
&= \left(p_i - p_j\right)^T (rq) + \left(0.5\left\|p_j\right\|^2 - 0.5\left\|p_i\right\|^2\right) r \\
&= 0.5r\left(\left\|p_j\right\|^2 - \left\|p_i\right\|^2 + 2\left(p_i - p_j\right)^T q\right) \\
&= 0.5r\left(d\left(p_j, q\right) - d\left(p_i, q\right)\right).
\end{aligned} \tag{3}$$

Since r is a positive random number, we can determine that

$$d\left(p_j, q\right) - d\left(p_i, q\right) > 0 \Longleftrightarrow d\left(p_j, q\right) > d\left(p_i, q\right). \tag{4}$$

4.2. kNN Query on ASPE. As described in Section 4.1, the client is assumed to be fully trusted by the data owner, and the encryption key and configuration information are shared with the client. However, in a more practical scenario, a client may be compromised or colludes with the CSP so that the CSP can easily obtain the key and the private configuration to decrypt the encrypted data. One plausible approach is that the DO keeps the encryption key privately and performs a secure two-party computation protocol [29, 30] with the clients. DO encrypts a processed query point $\widehat{q}$ and only transmits the encrypted query point q' to the client without disclosing the encryption key M. However, the combination of ASPE and secure two-party computation remains unable to maintain the key confidentially [14]. The encryption key shall be leaked to the others from legal outputs. The client can adequately choose enough query points $Q = (q_1, q_2, \ldots, q_{d+1})$ and obtain the corresponding encrypted query points $Q' = (q'_1, q'_2, \ldots, q'_{d+1})$, and then the client obtains $Q' = M^{-1}Q$. Obviously, if Q is an invertible matrix, the client can obtain $M^{-1} = Q'Q^{-1}$, by which the client can encrypt a new query point $q' = Q'Q^{-1}(q_{\text{new}}, 1)^T$. Therefore, the encryption key and sensitive data are exposed to the attackers.

4.3. Enhanced ASPE. We propose an enhanced ASPE (EASPE) that keeps the encryption key confidential to the clients. Being different from ASPE, it is hypothesized in this paper that the three parties in our system model are not trusted by each other. Therefore, the DO must keep the encryption key confidentially and the key cannot be obtained by anyone, while the client should keep the query points secret to the DO and the CSP. Our encryption scheme is similar to the approach proposed in [14]. However, the scheme in [14] adopted Paillier homomorphic encryption to encrypt query points which burdened the client with more computation overhead. In our scheme, we apply a 1-out-of-N oblivious transfer protocol [40] for query processing. A 1-out-of-N oblivious transfer protocol [40] is a protocol such that one party, Bob, has N inputs $X_1, \ldots, X_n$ and the other party, Alice, learns one of the inputs X_i for some $1 \leq i \leq n$ of her choice, without learning anything about the other inputs and without allowing Bob to learn anything about i. A random matrix encompassing the processed inquiry point is generated by the client and is sent to the DO for encryption.

Before encrypting data points, several artificial columns are introduced to the data points and are associated with some nonce random numbers generated independently which allows the same points to be encrypted into diverse points. Likewise, the client adds the same number of artificial columns to a query point and then perturbs the query point with some random numbers generated independently. The client sends a mixed matrix Q, encompassing the extended query point and some random vectors generated randomly, to the DO for encryption. Eventually, DO perturbs Q before matrix transformation so that the encrypted query points cannot reveal the key.

The outputs of p_i, q in the data process stage are denoted by $\widehat{p}_i$, $\widehat{q}$, respectively. *DO* finishes the encryption of $\widehat{p}_i$ and $\widehat{q}$ and outputs the ciphertexts p_i' and q' in the data encryption stage. It is noteworthy that *DO* cannot directly compute $\widehat{q}$ while encrypting the query point; nobody except the client knows the original query point. To simplify the description, $\widehat{q}$ is adopted to state our scheme in the first phase. Next, the two phases are elaborated on.

Data Processing. For each data point p, *DO* first selects a positive integer c as system security parameter in advance. In point perturbation, two random vectors ω of $(d+1)$ dimensions and χ of c dimensions are generated by *DO*, taking up the encryption key and shared by all points in the

database. The permutation function f_p changes the sequence of the extended vector randomly. As the foregoing processing is effectuated, (5) is acquired.

$$\widehat{p_i} = f_p\left(\omega_j - 2p_i, \omega_{(d+1)} + \|p_i\|^2, \chi\right), \tag{5}$$

where ω_j $(1 \le j \le d)$ indicates the jth dimension of ω.

For each query point q, firstly a positive random r is selected, and a random vector δ of c dimensions is created by the client, followed by the client's extension of q to $\dot{q} = (r(q^T, 1), \delta)$ and transmitting $\dot{q}$ to the *DO*. *DO* generates a random vector R of c dimensions to perturb the last c dimensions of $\dot{q}$. Accordingly (6) is acquired.

$$\widehat{q} = f_p\left(r\left(q, 1\right), R + \delta\right). \tag{6}$$

Since the permutation function f_p does not change the scalar product between data point and query point, then, $\widehat{p_i}\widehat{q}^T = (\omega_j - 2p_i)rq^T + (\omega_{(d+1)} + \|p_i\|^2)r + \chi(R+\delta)^T$. For any two data points p_i, p_j and a query point q, we have

$$\begin{aligned}\widehat{p_i}\widehat{q}^T - \widehat{p_j}\widehat{q}^T &= \|p_i\|^2 r - 2p_i r q^T - \|p_j\|^2 r + 2p_j r q^T \\ &= r\left(\left(\|p_i\|^2 - 2p_i q^T\right) - \left(\|p_j\|^2 - 2p_j q^T\right)\right) \\ &= r\left(d\left(p_i, q\right) - d\left(p_j, q\right)\right).\end{aligned} \tag{7}$$

Since random number r is positive, it does not affect the comparative result of (7); that is,

$$d\left(p_i, q\right) - d\left(p_j, q\right) > 0 \Longleftrightarrow d\left(p_i, q\right) > d\left(p_j, q\right). \tag{8}$$

Encryption Phase. *DO* generates an invertible matrix M as the encryption key to encrypt $\widehat{p_i}$, such that $p_i' = \widehat{p_i}M$. For each query point q, *DO* randomly generates a positive random number α to compute $q' = \alpha M^{-1}\widehat{q}^T$.

The details of encryption process are as follows.

KeyGen( ). Let $l = (d + 1 + c)$. *DO* generates a $(d + 1)$-dimensional vector ω, a c-dimensional vector χ, a $l \times l$ invertible matrix M, and a permutation function $f_p(\cdot)$ of l numbers. DO sets the quadruple $\{f_p, \omega, \chi, M\}$ as the encryption key and keeps it privately.

EncDB(D, Key). Once obtaining $\widehat{p_i} = f_p(\omega_j - 2p_i, \omega_{(d+1)} + \|p_i\|^2, \chi)^T$, *DO* computes the encrypted point $p_i' = \widehat{p_i}M$. The encrypted database is denoted as $D' = \{p_i' \mid p_i \in D\}$.

EncQuery (q, Key)

(1) After obtaining the extended $(d + 1 + c)$-dimensional point $\dot{q} = (r(q, 1), \delta)$, the client uses the 1-out-of-N oblivious transfer protocol [40] to generate a $l \times l$ matrix M_q encompassing $\dot{q}$ and other $(l - 1)$ vectors. The first d columns of the other $(l-1)$ column vectors in M_q are generated randomly and are extended to $(d + 1 + c)$-dimensional column vectors the same as the query point. The position i of column vector $\dot{q}$ is randomly selected from 1 to l and is only known to the client himself. The client transmits M_q to *DO* for encryption.

(2) For each query point q, *DO* randomly generates a random vector R of c dimensions to confuse the last c dimensions of $\dot{q}$, and then he applies the permutation function f_p to obtain $f_p(M_q)$. *DO* randomly selects a random positive number α and computes matrix $Q = \alpha M^{-1} f_p(M_q)$.

(3) After obtaining Q, the client extracts the encrypted query point q', that is, the ith column vector of matrix Q.

kNNQuery(q). To determine whether $d(p_i', q') < d(p_j', q')$, the *kNN* algorithm checks whether $(p_i' - p_j')\cdot q' < 0$ according to

$$\begin{aligned}p_i'q' - p_j'q' &= \left(p_i' - p_j'\right)q' = \left(\widehat{p_i} - \widehat{p_j}\right)M\alpha M^{-1}\widehat{q}^T \\ &= \alpha\left(\widehat{p_i} - \widehat{p_j}\right)\widehat{q}^T \\ &= \alpha r\left(\left(\|p_i\|^2 - 2p_i q^T\right) - \left(\|p_j\|^2 - 2p_j q^T\right)\right) \\ &= \alpha r\left(d\left(p_i, q\right) - d\left(p_j, q\right)\right).\end{aligned} \tag{9}$$

5. VSS-Tree

The simplest approach to find the results of a *kNN* query is to scan the entire database space. Yet, the query time and complexity are proportional to the data size and disk accesses, which usually cannot meet the needs of users. To improve the efficiency of spatial query, researchers build diverse spatial index structures, like R-tree [41], SS-tree [17], etc. In this section, we extend the SS-tree [17] with authentication information and build a verifiable SS-tree (VSS-tree) for *kNN* query processing and *kNN* query authentication.

5.1. VSS-Tree. Being different from the R-tree and the R*-tree, the similarity search tree (SS-tree) [17] applies bounding sphere rather than bounding rectangle for region shape. The SS-tree divides multidimensional points into isotropic neighbors. Due to the use of bounding sphere, the overlap area between regions is reduced, thereby improving *kNN* query efficiency. The structure of SS-tree is shown in Figure 2. A verifiable SS-tree (VSS-tree) is built by extending the SS-tree with authentication information, and its structure is shown in Figure 3. The center of a bounding sphere is the centroid of the underlying points of its children. Compared with the R-tree, the SS-tree only spends nearly half storage. Because a bounding sphere can be denoted by a center and a radius, its storage cost is a multidimensional point plus an integer, while a rectangle is determined by the two points at the lower left and upper right corner, its storage is twice that of dimensions. This determines that the SS-tree has more fanout and lower height.

The structure of leaf nodes is defined as follows:

$$\begin{aligned}&Leaf: \left(E_1, \ldots, E_f\right) \quad (m \le f \le M), \\ &E_i : (p, I, H),\end{aligned} \tag{10}$$

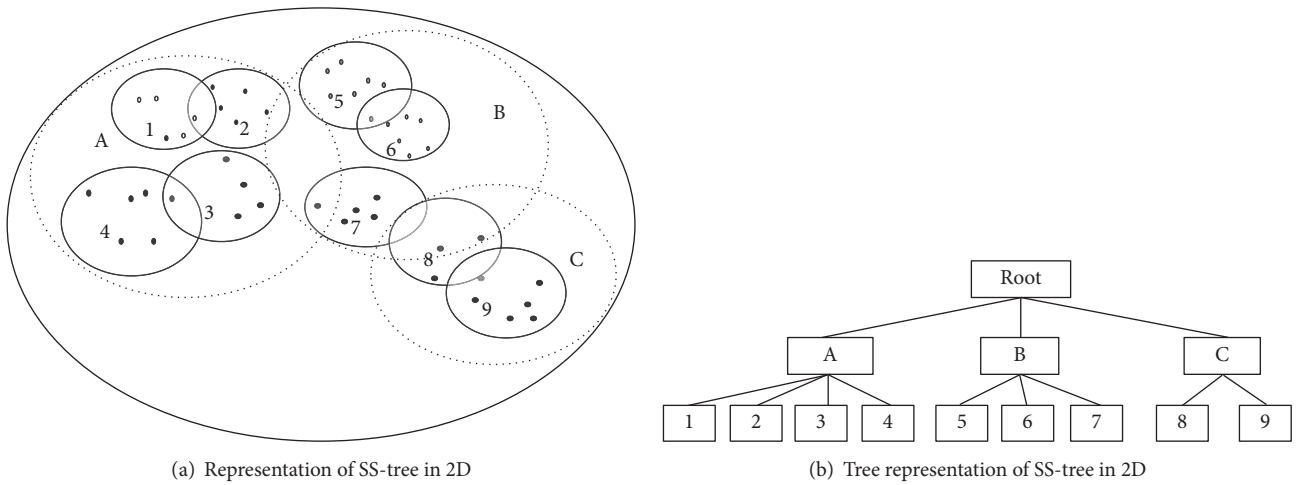

(a) Representation of SS-tree in 2D (b) Tree representation of SS-tree in 2D

Figure 2: Structure of SS-tree.

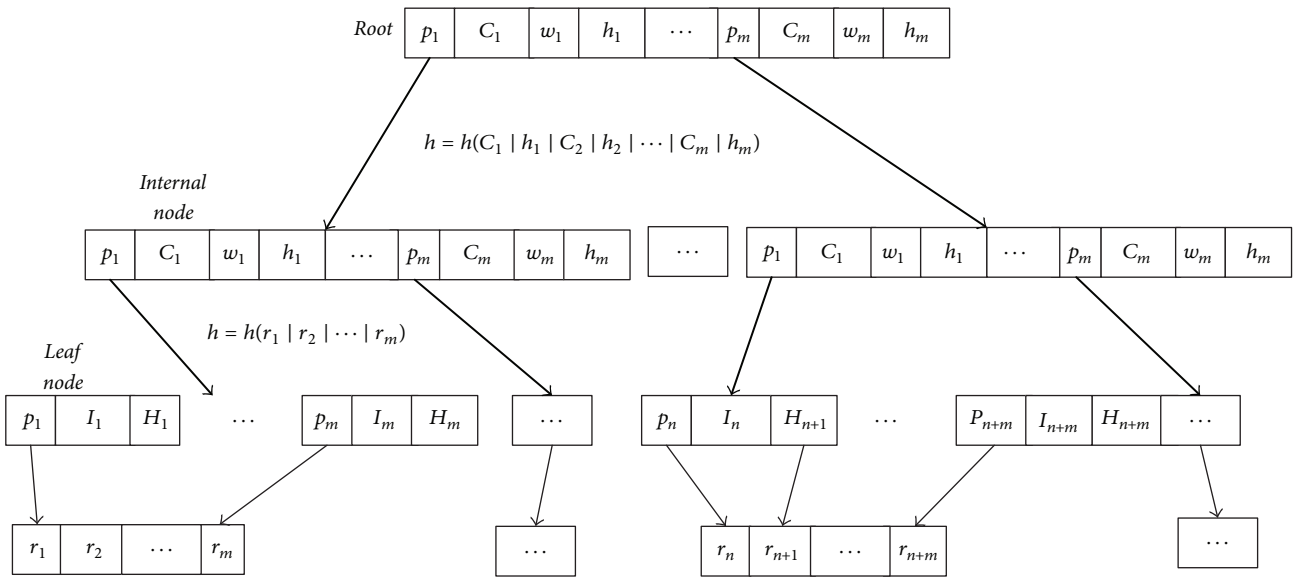

Figure 3: Structure of VSS-tree.

where m and M denote the minimum and maximum values of the entries in the leaf node, respectively. An entry of the leaf node is denoted as a triple (p, I, H), where p is a data point in database, I is the enclosing sphere of p, and H is the hash value computed on the record that p points to. An internal node of VSS-tree is elucidated as follows:

$$\begin{aligned} Node &: \left(E_1, \ldots, E_f\right) \quad (m \le f \le M), \\ E_i &: (c, p, w, h), \end{aligned} \tag{11}$$

where c indicates the minimum bounding sphere that encompasses all the regions of the ith children, consisting of a center and a radius. The pointer p points to the ith child. The variable w indicates the number of points contained in the subtree whose top is the child E_i. The hash value h summarizes all the bounding spheres and their digests of the ith child, that is, $h = h(c_1|h_1|\cdots|c_f|h_f)$. The center of a bounding sphere $x(x_1, x_2, \ldots, x_d)$ is computed according to

$$x_i = \frac{\sum_{j=1}^{n} c_j.x_i \times c_j.w}{\sum_{j=1}^{n} c_j.w} \quad (1 \le i \le d), \tag{12}$$

where j $(1 \le j \le d)$ is an index of its children, i is an index to the dimensions, $c_j.x_i$ indicates the ith dimensional coordinate of $c_j.x$, and $c_j.w$ indicates the number of its children of E_j. The radius of a bounding sphere is computed according to

$$r = \max_{1 \le j \le f} \left(\left\| c.x - c_j.x \right\| + c_j.r \right), \tag{13}$$

where $c.x$ indicates the center of the current node itself, $c_j.x$ and $c_j.r$ indicate the center and radius of the jth child node, respectively, and $\|c - c_j.x\|$ indicates the distance between the centers $c.x$ and $c_j.x$.

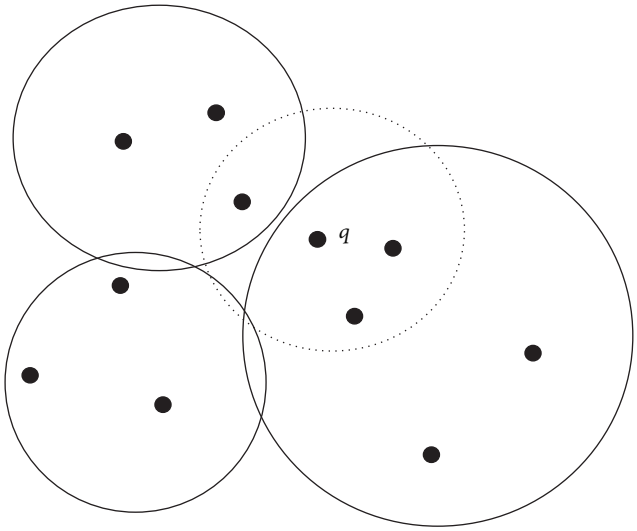

Figure 4: kNN search.

VSS-tree is built from bottom to top. All the leaf nodes are on the same level. Finally, the digest of root node is signed and published to *CSP*.

Approaching the MR*-tree, the VSS-tree also supports dynamic operations, including insertion, update, and deletion. An update can be perceived as a combination of a deletion and an insertion. The insertion adopts enforced reinsert; that is, we first add a new data object to the reinsert list and then perform insertion for the entries in the reinsert list until the list is empty. The deletion is the same as the other query authentication approaches. In our scheme, scalar product comparison rather than Euclidean distance comparison is adopted to determine where to insert a data point. When a node overflows, the split algorithm shall be revoked. Accordingly, its coordinate variance on each dimension from the centroids of its children shall be computed, and the dimension will be selected with the highest variance for splitting it.

5.2. kNN Query on VSS-Tree. Figure 4 shows a *kNN* query ($k = 3$) based on the VSS-tree. Given a query point q, *kNN* search algorithm gradually increases the search distance with the query point q as the center until the search area just encompasses three data points. We perform the *kNN* search algorithm and build the *VO* based on VSS-tree on the cloud server side. Diverse from other distance-based comparison methods, we determine the distance relationship by comparing the scalar products between the data points and the query points. The *kNN* search algorithm is shown in Algorithm 1. According to (9), we can compare the distances between any two encrypted data points and encrypted query point to determine which point is closer to a given query point. Furthermore, we introduce a sorted list *BranchList*, storing the entries of a visited internal node, to avoid unnecessary access. *KnnRes* comprises candidate *kNN* results, *KnnRes.MaxDist* denotes the maximum value in the *KnnRes*, and if *KnnRes* comprises less than k objects, *KnnRes.MaxDist* is elucidated as $+\infty$. The results shall be searched via the *kNN* search algorithm from top to bottom, and if the current visited node is an internal node, all the entries and their corresponding scalar products shall be inserted into the list *BranchList*. On that basis, the CSP shall iterate through the ordered list *BranchList* and recursively invokes the search algorithm on its visited child nodes. Once a scalar product is greater than *KnnRes.MaxDist*, the remaining entries in the *BranchList* are ignored, bespeaking that the results shall impossibly exist in the remaining entries. Thus, the minimum bounding spheres and digests of the remaining unvisited entries in the *BranchList* are inserted into *VO*. If the current visited node is a leaf node and the length of *KnnRes* is less than k, the visited entry and its scalar product will be inserted into list *KnnRes*; otherwise, whether to insert the entry into list *KnnRes* shall be determined by judging whether its scalar product is less than *KnnRes.MaxDist*. The *VO* is constructed in the search process, which consists of all the multidimensional encrypted data points in the visited leaf nodes, and the boundary spheres and their corresponding digests of the child nodes pruned of the visited internal nodes. Eventually, Algorithm 1 outputs list *KnnRes* and *VO*.

Require:
node *Node*, query point p, k
Ensure:
VO; *KnnRes*
(1) Append [to *VO*
(2) **if** *Node* is a leaf node **then**
(3) **for** each entry E in *Node* **do**
(4) VO.append(E)
(5) $dist = E.getProduct(p)$
(6) **if** $KnnRes.size() < k$ **then**
(7) $KnnRes.add(E, dist)$
(8) **else**
(9) Sort *KnnRes* in ascending order
(10) **if** $dist < KnnRes.MaxDist$ **then**
(11) $KnnRes.remove(k)$
(12) $KnnRes.add(E, dist)$
(13) **end if**
(14) **end if**
(15) **end for**
(16) **else**
(17) **for** each entry E in *Node* **do**
(18) $dist = E.getProduct(p)$
(19) $BranchList.add(E, dist)$
(20) **end for**
(21) Sort *BranchList* in ascending order
(22) **for** each entry E in *BranchList* **do**
(23) **if** $dist < KnnRes.MaxDist$ **then**
(24) $KnnSearch(E.p, q, k)$
(25) **else**
(26) $VO.append(E.C, E.h)$
(27) **end if**
(28) **end for**
(29) **end if**
(30) Append] to *VO*

Algorithm 1: *KnnSearch*.

```
Require:
    VO, q, KnnRes
Ensure:
    C, hash, result
(1)  dist = KnnRes.MaxDist
(2)  for each entry E in VO do
(3)     if E is a data object then
(4)        str = str | E
           //Enlarge the C to encompass E
(5)        C.Enlarge(E)
(6)     end if
(7)     if E.getProduct(q) ≤ KnnRes.MaxDist and
        E.id in KnnRes then
(8)        result.add(q)
(9)     end if
(10)    if E.getProduct(p) ≤ KnnRes.MaxDist
        and E.id not in KnnRes then
(11)       Alarm the client
(12)    end if
(13)    if E is a symbol [ then
(14)       (C, hash) = KnnVerify(VO, q, KnnRes)
(15)    end if
(16)    if E is a pair (C, hash) then
(17)       if C.getProduct(p) ≤ KnnRes.MaxDist
           then
(18)          Alarm the client
(19)       end if
(20)       C.Enlarge(C)
(21)       str = str|C|hash
(22)    end if
(23)    if E is a symbol ] then
(24)       Return(C, hash(str))
(25)    end if
(26) end for
```

Algorithm 2: *KnnVerify*.

Once receiving the *VO* and *KnnRes*, the client extracts the encrypted *kNN* query results from the *VO* and performs query verification. Diverse from other approaches, the client obtains the maximum *KnnRes.MaxDist* and verifies whether it is less than the other scalar products not in the list *KnnRes* to check the completeness of the *kNN* results. The verification process is as follows:

(1) The client obtains *KnnRes.MaxDist* from the list *KnnRes* and verifies that any scalar product in the *KnnRes* is less than or equal to *KnnRes.MaxDist*, while the other scalar products are greater than *KnnRes.MaxDist*.

(2) The client verifies that any scalar product between the bounding sphere in the pair *(Circle, hash)* and the query point q is greater than *KnnRes.MaxDist*.

(3) The client checks whether the reconstructed hash h_{root} agrees with s_{root}.

The *kNN* verification algorithm is shown in Algorithm 2.

The essence of the *kNN* verification algorithm is to reconstruct the VSS-tree by scanning *VO*. During the process of verification, the bounding sphere is enlarged gradually by encompassing the objects read from *VO*. Eventually, the algorithm reconstructs the bounding sphere and digest of root node, and the client validates whether the reconstructed h_{root} agrees with s_{root} for query verification.

6. Security Analysis and Integrity Verification

6.1. Security Analysis. As described in Section 3, three parties are all semitrusted. In our scheme, the privacy issues of outsourced database D', query points, and encryption key are deliberated. *CSP* can directly access the outsourced database. We need to ensure their confidentiality against *CSP*. We consider data privacy together with query privacy against *CSP* under level-2 attack.

Theorem 2. *EASPE is not distance-recoverable.*

Proof. EASPE is an enhanced ASPE, its encryption key is $\{f_p, S, \chi, M\}$, where the role of the invertible matrix M is applicable to the encryption key of ASPE. M and M^{-1} are adopted by EASPE to encrypt data points in D and query points, respectively. As ASPE proves, our EASPE is also not distance-recoverable. □

Theorem 3. *EASPE is secure against level 2 attacks.*

Proof. There are scores of types of level 2 attacks. According to the system security assumption, the following attacks are deliberated: distance-based inference attack, PCA, duplicate analysis, distribution analysis attack, and ICA-based attack. According to Theorem 2, EASPE is not distance-recoverable. Distance-based inference attack is obviously not feasible to our scheme.

Principal component analysis (PCA) has been proposed in [19] to match the correlations in the known data and the correlations in the encrypted data. Using the matched data, the attacker endeavors to reconstruct the entire original database. However, in EASPE, the values on each dimension of $E(DB)$ are a linear combination of the values on all dimensions in the original database. EASPE adds c artificial columns and generates a random vector ω to confuse the original data. Furthermore, *DO* uses permutation function f_p to change the sequence of the extended data point randomly. It turns out to be evident that EASPE does not preserve the correlations among the original dimensions in the transformed space, and thus PCA is not applicable to EASPE.

Duplicate analysis [10] is applicable to the attribute whose domain is small, such as the day of the week or the day of the month. Through the analysis of observations on encrypted data, the attacker may determine the domain of original attribute. Duplicate analysis is value-based encryption, that is, the values in each dimension are encrypted individually. However, EASPE is a tuple-based encryption, and duplicate analysis is not applicable to EASPE. Similarly, distribution analysis attack exists for estimating from Y. Observations on the encrypted database may help an attacker to determine the plain data fall into intervals $I_1, I_2, \ldots, I_n$. This attack is value-based encryption and is not applicable to EASPE.

ICA-based attack [18, 19] tries to recover the plain data X from the transformed data Y. The approach is based on the observation that the eigenvectors of Y are computed by X left-multiplied by M. Therefore, by estimating $\sum y$ and $\sum x$ and matching their eigenvectors, the attacker can produce $\widehat{M}$, an estimation of M, and then data record x_i is estimated as $\widehat{x_i} = \widehat{M^T} y_i$. This attack is on the assumption that the known samples follow the same distribution with the original data. The matrix M must be orthogonal or full rank. However, we introduce one-time random vectors χ and R for each data point and query point, respectively. Random vectors χ and R are generated independently and privately kept by *DO*, and matrix M can be generated as an invertible but nonorthogonal matrix. Hence, EASPE can impede both ICA and deriving the transformation matrix M. EASPE is therefore resilient to ICA-based Attacks.

To keep the query points confidential to *DO*, a positive number r is randomly selected and a random vector δ of c dimensions is generated to extend a query point q to a $(d + 1 + c)$-dimensional point $\dot{q} = (r(q, 1), \delta)$. And, then, 1-out-of-$N$ oblivious transfer protocol is used to generate a $l \times l$ matrix M_q including the processed query point $\dot{q}$ and other $(l - 1)$ random column vectors. The position i of column vector $\dot{q}$ is randomly selected in range from 1 to l and is only known to the client himself. *DO* cannot learn which one the client has chosen. □

Theorem 4. *The encryption key is kept confidentially against CSP and clients.*

Suppose that a client can transmit a few number of query points to *DO* for encryption, and then the encryption key is derived from the correlation between plaintext and corresponding ciphertext. If we can keep the encryption key confidential to the clients. It turns out to be evident that the key is confidential to *CSP*. Thus, we only need to prove that the encryption key is confidential to the clients.

Proof. A client transmits processed query points to *DO* and interacts with the *DO* during the query encryption stage. The encryption of query points is considered without applying permutation function in the first place. *DO* encrypts a processed query point $\widehat{q} = (r(q^T, 1), R + \delta)^T$ into $q' = \alpha M^{-1} \widehat{q}$. The ith dimension of q' is $q'_i = \alpha M^{-1}_{i*} \widehat{q}$; concretely,

$$q'_i = \alpha \left(r \sum_{j=1}^{d} M^{-1}_{ij} q_j \right) + \left(\alpha r M^{-1}_{i,d+1} + \alpha \sum_{j=d+2}^{d+1+c} M^{-1}_{ij} (\chi + R)_{j-d-1} \right). \tag{14}$$

In (14), all the values of $\{\alpha, M^{-1}_{ij}, R\}$ are kept confidential to the client. The client only knows the original query point q and its corresponding encrypted query point q'. Let $X^i_q = r \sum_{j=1}^{d} M^{-1}_{ij} q_j$, and $\varphi^i_q = (\alpha r M^{-1}_{i,d+1} + \alpha \sum_{j=d+2}^{d+1+c} M^{-1}_{ij} (\chi + R)_{j-d-1})$. The client can set up an equation $q'_i = \alpha X^i_q + \varphi^i_q$. The client can obtain enough encrypted query points by his legal input or collusion with other clients. However, the invertible matrix M is generated randomly and $\{\alpha, R\}$ are one-time random parameters selected independently for each query point. φ^i_q is entirely random to the client. Moreover, the client can learn nothing about M_{ij} $(1 \le j \le d)$ from X^i_q. Furthermore, EASPE applies permutation function f_p to the query points. The client cannot learn the correspondence of the dimensions of $\widehat{q}$ and M_{i*}. In addition, the permutation can prevent the client from setting up equation (14). Obviously, it enhances the security of our scheme. In conclusion, the encryption key is kept private against *CSP* and the clients. □

6.2. Integrity Verification. Our scheme provides correctness and completeness verification for *kNN* queries.

Theorem 5. *The correctness of kNN query results can be ensured by our scheme.*

Proof. Suppose that there is one or more falsified or modified data points in the results. We note that VSS-tree is built from bottom to top. All data points in the database are involved in the construction of the root hash. As we know that the hash function is one-way and collision-resistant. The digest of any falsified or modified data must be different from the original one, and this change propagates from the leaf node to the root node which makes the reconstructed root digest h_{root} different from the original one and thus does not agree with s_{root}. Therefore, the client can detect any falsified or modified data in the results. □

Theorem 6. *The completeness of kNN query results is ensured by our scheme.*

Proof. Suppose that a data point p in a leaf node L_n is one of a *kNN* query results, but p is not involved in the results. To make the reconstructed root hash h_{root} match s_{root}, *VO* either comprises all the data entries in L_n or comprises the pair $(C, hash)$ of L_n. For the former, the client can determine that p is one of a *kNN* query results according to the verification algorithm and there exists at least one point in the results whose distance to q is farther than that of p. For the latter, the client can detect that the scalar product between L_n and q is less than *KnnRes.MaxDist*, which means that L_n comprises one or more data points that are closer to the query result q, but L_n is not visited by the search algorithm which can be detected during the verification process. □

7. Experiment Evaluation

In this section, we mainly evaluate and compare the performance between DPT and our scheme. All programs are implemented in Java. Experiments are performed on an Intel Core i7-4790 3.6 GHz computer with 8 GB RAM running Windows 7. The block size is set as 2048 KB and the default value of security parameter c as 1. The experiments are conducted on both synthetic and real datasets. The random points generated in the synthetic database are uniformly distributed in a d-dimensional space. The real dataset adopted

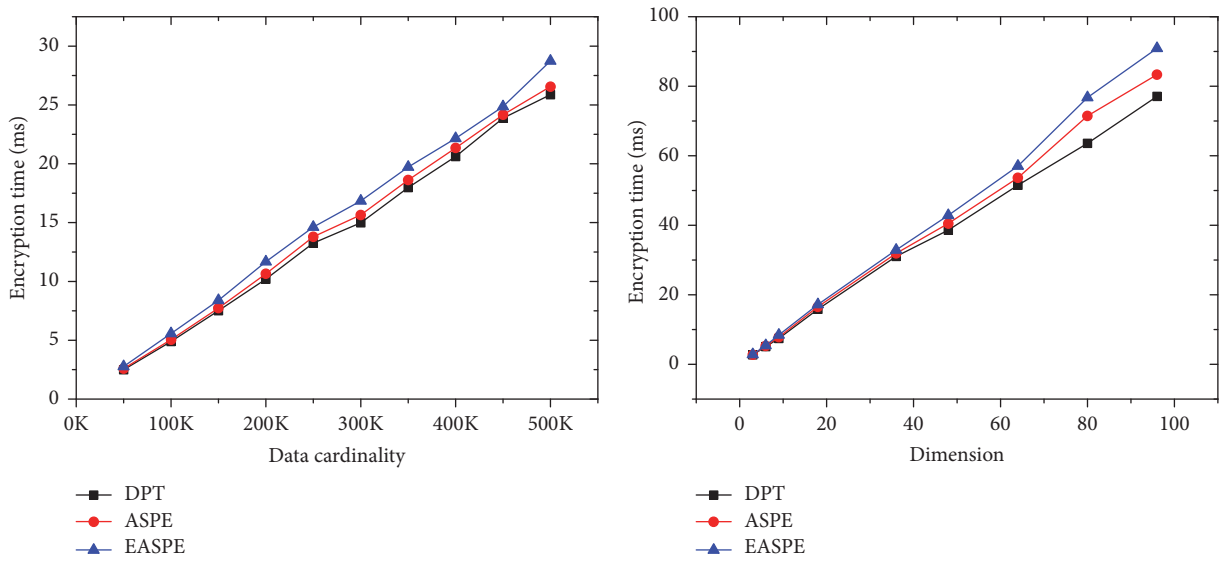

(a) Encryption time versus data cardinality ($d = 6$)

(b) Encryption time versus dimension ($n = 100$ K)

Figure 5: Encryption time.

Table 2: Symbol list.

	DPT	EASPE
Encryption time (ms)	2.712	2.718

is the dataset "Shuttle" from the UCI repository, which comprises 58 K points and 9 dimensions. We run each experiment 100 times and take the average to show the performance of diverse schemes. We effectuate two experiments under diverse data cardinalities and dimensions in the synthetic database. In the first experiment, data cardinality is changed from 50 K to 500 K with a fixed dimension $d = 6$. In the second experiment, the dimensions are changed from 3 to 100 with a fixed data cardinality $n = 100$ K. The performance is evaluated from the following aspects: (1) data encryption; (2) construction and storage of the VSS-tree; (3) *kNN* query; (4) query verification.

7.1. Key Generation and Data Encryption. As described in Section 4, the transition matrix used in EASPE is a $(d + 1 + c) \times (d + 1 + c)$ invertible matrix. In practical applications, the dimension d of spatial data is usually less than 100. In our experiments, we generate the encryption key only once, which takes less than 1 ms for diverse dimensions ranging from 3 to 100. Figure 5 illustrates the data encryption time on diverse data cardinalities. The encryption time includes: generating the encryption key and encrypting all the data points. The encryption time of the Shuttle dataset is shown in Table 2.

As can be seen from Figure 5, data encryption time is proportional to both data dimension and data cardinality. The encryption time of DPT is slightly shorter than that of EASPE in that EASPE performs $(d + 1 + c) \times (d + 1 + c)$ multiplications and $(d + c)$ additions, while DPT performs $(d \times d)$ multiplications and $(2d - 1)$ additions. As EASPE has c more dimensions than ASPE, the encryption time of EASPE is slightly larger than that of ASPE.

7.2. Construction and Storage Cost of VSS-Tree. The storage cost of VSS-tree is indicated from Figure 6. The storage costs under all schemes are proportional to data dimension and data cardinality. Due to the added $(c + 1)$ dimensions of EASPE, the storage cost of EASPE is larger than that of DPT and ASPE. Furthermore, the SS-tree only spends nearly half storage of that of the MR-tree as described in Section 5.1, the storage cost of the MR-tree is lager than that of the VSS-tree.

The build time of the VSS-tree is illuminated from Figure 7. The build time of the VSS-tree under both encryption schemes is proportional to both data cardinality and dimension. The build time of VSS-tree under EASPE is longer than that under DPT, this is because a d-dimensional data point is extended to a $(d + 1 + c)$-dimensional data point in EASPE which makes the computation overhead greater than that under DPT. Eventually, it should be noted that the larger the parameter c we set, the longer the time required to build the VSS-tree. The build time under the MR-tree is shorter than that under the VSS-tree, the reason is that bounding rectangle requires only comparison operations between each dimension of point, while bounding sphere needs to compute the center and radius.

The fanouts of internal node are exhibited in Figure 8 under diverse encryption schemes. Since we add $(c + 1)$ dimensions to each data point in EASPE, the fanout of VSS-tree based on it is slightly less than that based on DPT and ASPE. The fanouts under all schemes decrease with the increase of the dimensions. This is because the storage cost of a record increases as the dimension increases. Furthermore, bounding rectangle is used in MR-tree whose storage is twice

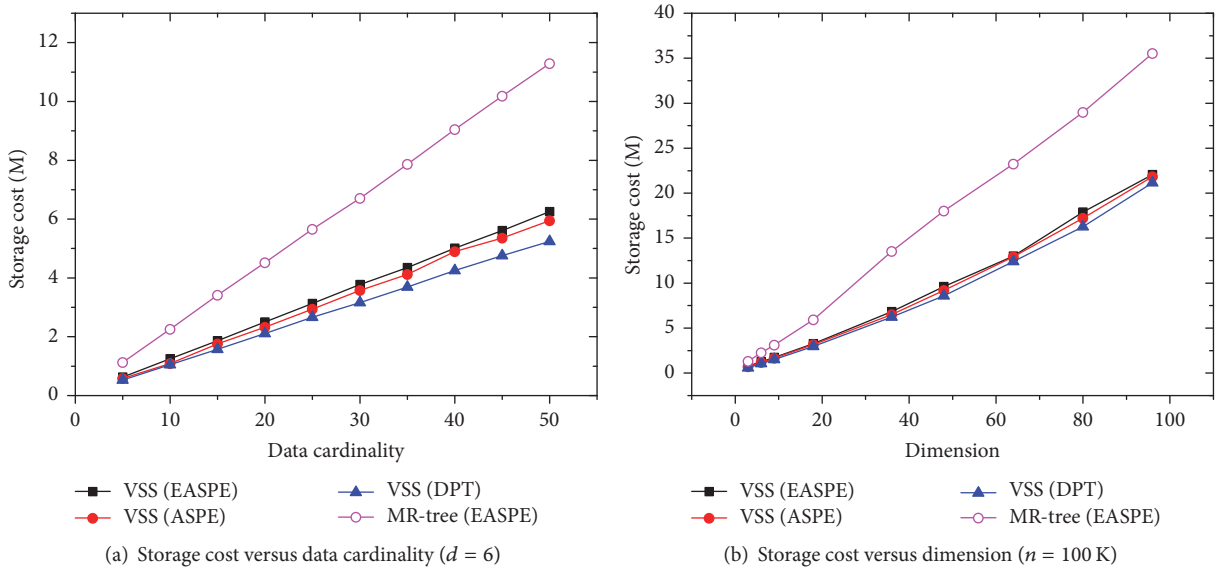

(a) Storage cost versus data cardinality ($d = 6$) (b) Storage cost versus dimension ($n = 100$ K)

Figure 6: Storage cost of VSS-tree.

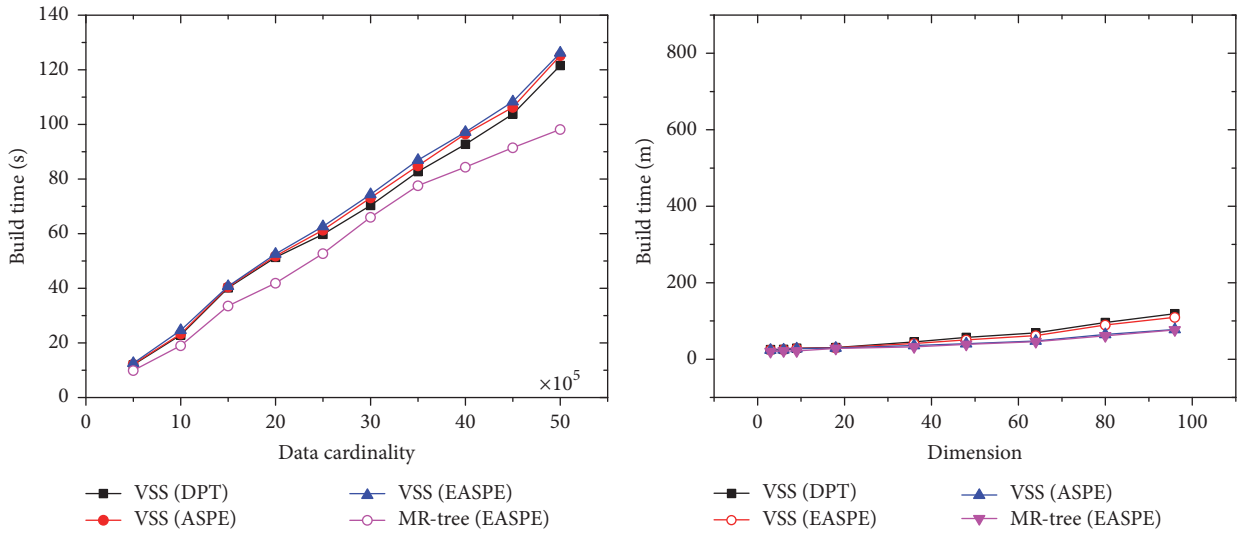

(a) Build time versus data cardinality ($d = 6$) (b) Build time versus dimension ($n = 100$ K)

Figure 7: Build time of VSS-tree.

that of dimensions, the fanout of the MR-tree is less than that of the VSS-tree.

7.3. kNN Query Cost. We perform a *kNN* query on the VSS-tree and set $k = 3$. Figure 9 shows that the query processing time is proportional to both data dimension and data cardinality. The query efficiency under EASPE is higher than that under DPT. This is because the *kNN* search algorithm performs $(d + 1 + c)$ multiplications and $(d + c)$ additions to compute $p' \cdot q'$ for each visited entry under EASPE, while Euclidean distance $dist(p, q)$ is computed in DPT, the *kNN* search algorithm performs d multiplications, d subtractions and $(d - 1)$ additions for each visited entry. As described in Section 5.1, the overlap area and regions in the MR-tree are larger than those in the VSS-tree, and more nodes need to be accessed for a query. Thus, the query processing time based on the MR-tree is longer than that based on the VSS-tree.

The size of *VO* directly affects the server's response speed and network bandwidth resources. In our experiment, *VO* contains multidimensional data points of the visited leaf nodes, the bounding spheres, and corresponding digests of nodes pruned. Figure 10 illustrates that the *VO* size increases with data cardinality. Due to the use of bounding rectangle in the MR-tree, its *VO* size is larger than that under the VSS-tree.

Once receiving *VO*, the client extracts the query results from it and validates the correctness and completeness of the *kNN* query results. The verification cost includes the

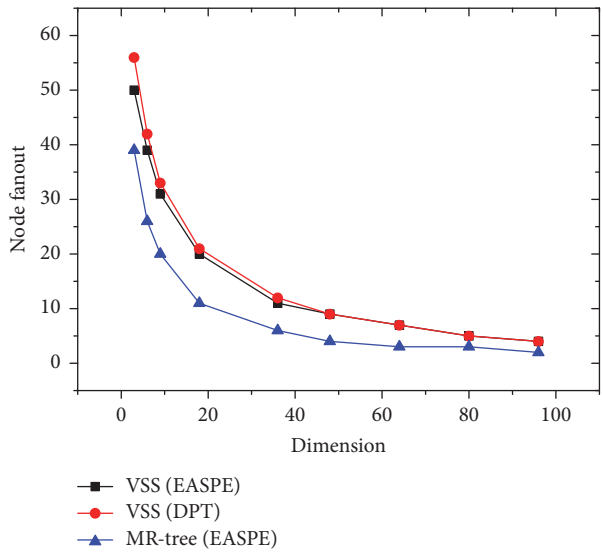

Figure 8: Fanout of internal node.

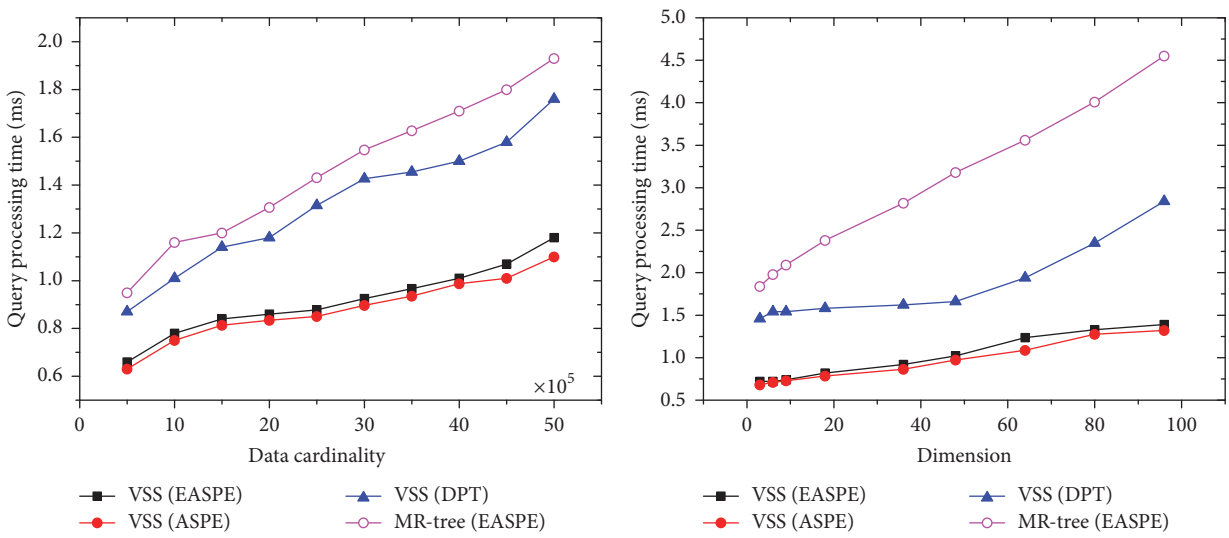

(a) Query time versus cardinality ($d = 6$)

(b) Query time versus dimension ($n = 100$ K)

Figure 9: kNN query processing time.

following: scanning *VO*, hash computation, scalar product computation and comparison, and signature verification.

The verification time is shown in Figure 11. We can see that the verification time is proportional to the data cardinality. The verification time under EASPE is shorter than that under DPT. The reason is that *kNN* verification algorithm computes $p' \cdot q'$ under EASPE, while it computes $dist(p, q)$ under DPT.

8. Conclusion

In this paper, EASPE is firstly introduced to support secure *kNN* query. EASPE is not distance-recoverable and only preserves the scalar products between data points in database and query points. In addition, we proposed a verifiable spatial data index structure VSS-tree to improve *kNN* query efficiency and provide *kNN* query verification. The security analysis and experiment results show that EASPE can resist level 2 attacks; the cloud server can efficiently perform a *kNN* query on encrypted data points and query points. The encryption cost, *kNN* query cost, and verification cost can meet the practical requirement.

In the future, the actual application scenarios shall be considered that there are more than one data source or the outsourced databases distributed on diverse cloud service providers. The VSS-tree shall be extended to support query authentication with multiple data sources or distributed databases.

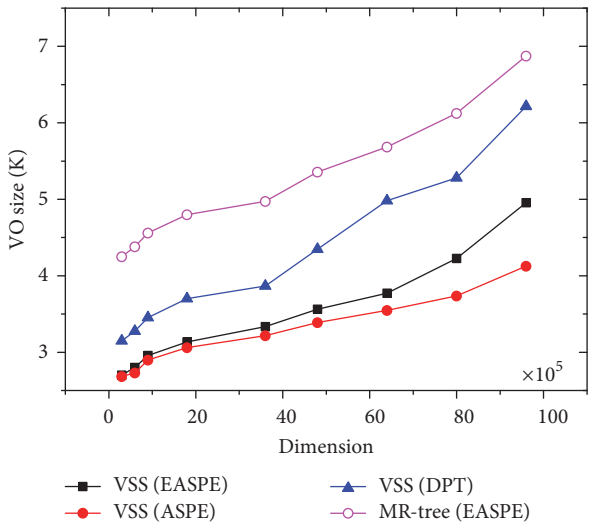

Figure 10: VO size versus data cardinality ($d = 6$).

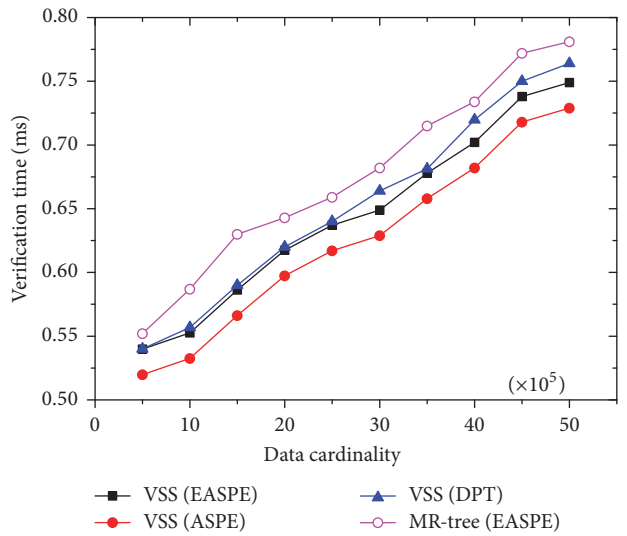

Figure 11: Verification time versus cardinality ($d = 6$).

Conflicts of Interest

The authors declare that there are no conflicts of interest regarding the publication of this paper.

Acknowledgments

This research is supported by the National Nature Science Foundation of China (nos. 61772101, 61170169, 61170168, and 61602075).

References

[1] M. Armbrust, F. Armando, R. Griffith, D. A. Joseph, and R. H. Katz, "Technical Report UCB/EECS-2009-28," Tech. Rep., Eecs Department, University of California, Berkeley, 2009.

[2] M. Armbrust, A. Fox, R. Griffith et al., "A view of cloud computing," *Communications of The ACM*, vol. 53, no. 4, pp. 50–58, 2010.

[3] M. Whaiduzzaman, M. Sookhak, A. Gani, and R. Buyya, "A survey on vehicular cloud computing," *Journal of Network and Computer Applications*, vol. 40, no. 1, pp. 325–344, 2014.

[4] P. M. Mell and T. Grance, "The NIST Definition of Cloud Computing," Tech. Rep. SP 800-145, National Institute of Standards & Technology, 2011.

[5] I. Emanuel Baciu, "Advantages and disadvantages of cloud computing services," *from the employees point of view*, 2015.

[6] S. Subashini and V. Kavitha, "A survey on security issues in service delivery models of cloud computing," *Journal of Network and Computer Applications*, vol. 34, no. 1, pp. 1–11, 2011.

[7] H. Takabi, J. B. D. Joshi, and G.-J. Ahn, "Security and privacy challenges in cloud computing environments," *IEEE Security & Privacy*, vol. 8, no. 6, pp. 24–31, 2010.

[8] E. Mykletun and G. Tsudik, "Aggregation queries in the database-as-a-service model," *Lecture Notes in Computer Science (including subseries Lecture Notes in Artificial Intelligence and Lecture Notes in Bioinformatics): Preface*, vol. 4127, pp. 89–103, 2006.

[9] H. Hacigümüş, B. Iyer, C. Li, and S. Mehrotra, "Executing SQL over encrypted data in the database-service-provider model," in *Proceedings of the ACM SIGMOD International Conference on Management of Data (SIGMOD '02)*, pp. 216–227, Madison, Wis, USA, June 2002.

[10] R. Agrawal, J. Kiernan, R. Srikant, and Y. R. Xu, "Order preserving encryption for numeric data," in *Proceedings of the ACM SIGMOD International Conference on Management of Data (SIGMOD '04)*, pp. 563–574, ACM, Paris, France, June 2004.

[11] S. R. M. Oliveira and O. R. Zaiane, "Privacy preserving clustering by data transformation," *Journal of Information and Data Management*, vol. 1, no. 1, p. 37, 2010.

[12] W. K. Wong, D. W. Cheung, B. Kao, and N. Mamoulis, "Secure kNN computation on encrypted databases," in *Proceedings of the International Conference on Management of Data and 28th Symposium on Principles of Database Systems (SIGMOD-PODS '09)*, pp. 139–152, Providence, RI, USA, July 2009.

[13] Y. Zhu, R. Xu, and T. Takagi, "Secure k-NN computation on encrypted cloud data without sharing key with query users," in *Proceedings of the 2013 1st International Workshop on Security in Cloud Computing, Cloud Computing 2013*, pp. 55–60, China, May 2013.

[14] Y. Zhu, Z. Huang, and T. Takagi, "Secure and controllable k-NN query over encrypted cloud data with key confidentiality," *Journal of Parallel and Distributed Computing*, vol. 89, pp. 1–12, 2016.

[15] M. L. Yiu, E. Lo, and D. Yung, "Authentication of moving kNN queries," in *Proceedings of the 2011 IEEE 27th International Conference on Data Engineering, ICDE 2011*, pp. 565–576, April 2011.

[16] Y. Jing, L. Hu, W.-S. Ku, and C. Shahabi, "Authentication of k nearest neighbor query on road networks," *IEEE Transactions on Knowledge and Data Engineering*, vol. 26, no. 6, pp. 1494–1506, 2014.

[17] D. A. White and R. Jain, "Similarity indexing with the SS-tree," in *Proceedings of the 1996 IEEE 12th International Conference on Data Engineering*, pp. 516–523, March 1996.

[18] H. Delfs and H. Knebl, *Introduction to cryptography*, Information Security and Cryptography, Springer, Berlin, Second edition, 2007.

[19] K. Liu, C. Giannella, and H. Kargupta, "An attacker's view of distance preserving maps for privacy preserving data mining," in *Knowledge Discovery in Databases: PKDD 2006*, vol. 4213 of *Lecture Notes in Computer Science*, pp. 297–308, Springer, Berlin, Germany, 2006.

[20] L. Y. Man, G. Ghinita, C. S. Jensen, and P. Kalnis, "Outsourcing search services on private spatial data," in *Proceedings of the 25th IEEE International Conference on Data Engineering, ICDE 2009*, pp. 1140–1143, China, April 2009.

[21] K. Chen, R. Kavuluru, and S. Guo, "RASP: Efficient multidimensional range query on attack-resilient encrypted databases," in *Proceedings of the 1st ACM Conference on Data and Application Security and Privacy, CODASPY'11*, pp. 249–260, USA, February 2011.

[22] P. Kalnis, G. Ghinita, K. Mouratidis, and D. Papadias, "Preventing location-based identity inference in anonymous spatial queries," *IEEE Transactions on Knowledge and Data Engineering*, vol. 19, no. 12, pp. 1719–1733, 2007.

[23] C.-Y. Chow, M. F. Mokbel, and W. G. Aref, "Casper*: query processing for location services without compromising privacy," *ACM Transactions on Database Systems (TODS)*, vol. 34, no. 4, article 24, 2009.

[24] H. Pang, A. Jain, K. Ramamritham, and K.-L. Tan, "Verifying completeness of relational query results in data publishing," in *Proceedings of the SIGMOD 2005: ACM SIGMOD International Conference on Management of Data*, pp. 407–418, USA, June 2005.

[25] M. Narasimha and G. Tsudik, "DSAC: Integrity for outsourced databases with signature aggregation and chaining," in *Proceedings of the CIKM'05 - Proceedings of the 14th ACM International Conference on Information and Knowledge Management*, pp. 235-236, Germany, November 2005.

[26] M. Zhang, C. Hong, and C. Chen, "Server transparent query authentication of outsourced database," *Journal of Computer Research and Development*, vol. 1, no. 28, pp. 182–190, 2010.

[27] J. Hong, T. Wen, Q. Gu, and G. Sheng, "Query integrity verification based-on MAC chain in cloud storage," in *Proceedings of the 2014 13th IEEE/ACIS International Conference on Computer and Information Science, ICIS 2014 - Proceedings*, pp. 125–129, China, June 2014.

[28] D. Boneh, C. Gentry, B. Lynn, and H. Shacham, "Aggregate and verifiably encrypted signatures from bilinear maps," in *Cryptology — EUROCRYPT 2003*, vol. 2656 of *Lecture Notes in Computer Science*, pp. 416–432, Springer, Berlin, Heidelberg, 2003.

[29] R. C. Merkle, "A certified digital signature. in advances in cryptology," in *Proceedings of the International Cryptology Conference, CRYPTO 89*, pp. 218–238, Santa Barbara, Calif, Usa, 1989.

[30] P. Devanbu, M. Gertz, C. Martel, and S. G. Stubblebine, "Authentic data publication over the internet," *Journal of Computer Security*, vol. 11, no. 3, pp. 291–314, 2003.

[31] H. H. Pang and K. L. Tan, "Authenticating query results in edge computing," in *Proceedings of the Proceedings - 20th International Conference on Data Engineering - ICDE 2004*, pp. 560–571, USA, April 2004.

[32] F. Li, M. Hadjieftheriou, G. Kollios, and L. Reyzin, "Authenticated index structures for outsourced databases," *Handbook of Database Security: Applications and Trends*, pp. 115–136, 2008.

[33] W. Cheng, H. H. Pang, and K. L. Tan, "Authenticating multidimensional query results in data publishing," in *Lecture Notes in Computer Science*, vol. 4127, pp. 60–73, 2006.

[34] Y. Yang, S. Papadopoulos, D. Papadias, and G. Kollios, "Spatial outsourcing for location-based services," in *Proceedings of the 2008 IEEE 24th International Conference on Data Engineering, ICDE'08*, pp. 1082–1091, April 2008.

[35] M. Xie, H. Wang, J. Yin, and X. Meng, "Integrity auditing of outsourced data," in *Proceedings of the 33rd International Conference on Very Large Data Bases, VLDB 2007*, pp. 782–793, aut, September 2007.

[36] H. Wang, J. Yin, C.-S. Perng, and P. S. Yu, "Dual encryption for query integrity assurance," in *Proceedings of the 17th ACM Conference on Information and Knowledge Management, CIKM'08*, pp. 863–872, USA, October 2008.

[37] B. Thompson, S. Haber, W. G. Horne, T. Sander, and D. Yao, "Privacy-preserving computation and verification of aggregate queries on outsourced databases," *Lecture Notes in Computer Science (including subseries Lecture Notes in Artificial Intelligence and Lecture Notes in Bioinformatics): Preface*, vol. 5672, pp. 185–201, 2009.

[38] B. Thompson, S. Haber, W. G. Horne, T. Sander, and D. Yao, "Privacy-aware verification of aggregate queries on outsourced databases with applications to historic data integrity," *In Privacy Enhancing Technologies*, 2009.

[39] B. Goethals, S. Laur, H. Lipmaa, and T. Mielikäinen, "On private scalar product computation for privacy-preserving data mining," in *Information Security and Cryptology – ICISC 2004*, vol. 3506 of *Lecture Notes in Computer science*, pp. 104–120, Springer, 2005.

[40] C. Cachin, S. Micali, and M. Stadler, "Computationally private information retrieval with polylogarithmic communication," *Lecture Notes in Computer Science (including subseries Lecture Notes in Artificial Intelligence and Lecture Notes in Bioinformatics): Preface*, vol. 1592, pp. 402–414, 1999.

[41] A. Guttman, "R-trees: a dynamic index structure for spatial searching," in *Proceedings of the ACM SIGMOD International Conference on Management of Data (SIGMOD '84)*, pp. 47–57, ACM, 1984.

Hindawi
Mathematical Problems in Engineering
Volume 2017, Article ID 7274565, 14 pages
https://doi.org/10.1155/2017/7274565

Research Article

Analysis of Success Factors to Implement Sustainable Supply Chain Management Using Interpretive Structural Modeling Technique: A Real Case Perspective

Mengke Yang,[1] Mahmood Movahedipour,[2,3] Jianqiu Zeng,[2] Zhou Xiaoguang,[1] and Ludi Wang[1]

[1]*School of Automation, Beijing University of Posts and Telecommunications, Beijing 100876, China*
[2]*School of Economic and Management, Beijing University Posts and Telecommunications, Beijing 100876, China*
[3]*Academic Center for Education, Culture and Research (ACECR), Tehran 14155-4364, Iran*

Correspondence should be addressed to Mahmood Movahedipour; mahmood.movahedipour@yahoo.com

Received 11 May 2017; Revised 12 July 2017; Accepted 29 August 2017; Published 10 December 2017

Academic Editor: M. L. R. Varela

Sustainability draws increased supply chain management (SCM) attention. This article analyzes critical success to the assessment, evaluation, and attainment of sustainable supply chain management (SSCM), assessed through critical-success identification and qualitative data analysis. Namely, a literature review selected of 188 articles, published between January 1994 and November 2016, helps identify the most influential success factors. The qualitative data analysis pertains to fifteen such successes, identified in the literature review and through our collaboration with other academic researchers and industrial specialists. Notably, the study's qualitative data analysis, interpretive structural modeling (ISM), unconceals the mutual impact among the most prominent SSCM success factors. The economic benefits and environmental awareness of suppliers are recognized as the most significant success factors, which could allow business enterprises and other organizations to implement a SSCM framework, with intentionality and the sustainability in their business. The article concludes with suggestions for future research directions.

1. Introduction

Nowadays, with people's higher and higher consideration about environmental protection, many companies have shifted their focus to SCM to achieve a sustainable competitive gain [1, 2]. Supply managing in a sustainable behavior becomes an increasing awareness for organizations in different sizes and wide scope of industries [3].

There are a number of serious, social, economic, and environmental issues that are highly interconnected which need higher attention from industrial executives [4, 5]. Besides, human population is also rising exponentially and it seems that there may be an increase in the natural resources consumption by nearly 170% of the earth's capacity by 2020 [6]. Also from the perspective of a developing and emerging nation, one of the major problems is the high level of carbon emissions (CO_2). It is an interesting fact that more than 20% of global greenhouse gases emissions are made by about 2500 largest global companies, and their supply chains take the main responsibility for emissions resulting from corporate operations [7]. Moreover, developing nations generally lack an implementation of technologies that promote lower pollution as well as measures to cut down emission resulting from industrial activities [8]. Concerning social and environmental impacts, along with all stages, easier reactive approach can seem to have more responsibility for external pressure from nongovernmental organizations, consumers, and governments [9]. This study was conducted in electrical power supply manufacturing that is located in the northern part of Iran.

However, one of the most critical issues for industries of different types in recent global market is the increasing requirement for integrating eco-friendly practices into sustainable supply chain [10, 11]. But the main point is to

familiarize the concept of knowledge on the management point of view and make participations in the industries' sustainable supply chain network more cost effective, environmentally friendly, and socially practical [12]. For this order, it calls for the need to identify different types of success to implement SSCM and to extend a hierarchy of ISM to apply SSCM to sustainable practices.

Purposes and Forms of This Study. This study has some purposes, shown as follows:

(i) To undertake a systematic literature review to distinguish key critical success factors in SSCM practices to implement SSCM towards sustainable practices from industrial point of view

(ii) To identify the mutual relationships between identified success factors of SSCM practices by ISM and MICMAC analysis

(iii) To confer the research managerial implications.

The rest of the research is arranged as follows: in the second chapter we outline our systematic literature review. In the third part we show the theoretical framework for the solution method of this research. Section 4 presents the outline of our SSCM theoretical framework as the outcome of the MICMAC analysis. Then we relate this to literature in the discussion, Section 5, and in Section 6, we conclude our research and provide suggestions for further research directions.

2. Literature Review

2.1. Initial Data Statistics. The concepts of supply chain management and environmental management as strategic organizational practices to gain competitive advantage have been receiving increased attention especially during the period of the late 1980s and early 1990s [13]. Identifying the appropriate search terms and keyword structure was completed through several trial and error attempts.

We used the following iterative multistep process to design an effective keyword structure:

(i) Defining initial set of keywords and search structure

(ii) Checking the resulting articles and journals to ensure the appropriate coverage (whether key articles and major journals are appearing in search results) and updating the keywords accordingly

(iii) Looking for irrelevant articles and research areas, identifying the "exclusion keywords," and updating the keyword structure accordingly

(iv) Looking for irrelevant subject areas to narrow down the search space and updating the keyword structure accordingly.

The following subject areas were found to be irrelevant to our review scope: (1) sustainable, (2) sustainability environmental, (3) sustainability environmentally, sustainable environmentally, (4) sustainable supply chain managements, (5) green, (6) green supply chain management, (7) ecological sustainable, (8) ecological economics, (9) gas emission, (10) environmental resources management, and (11) sustainable development. This reduced the number of relevant articles to 1,780. The search results were stored in RIS4 format to include all the essential article information such as article title, authors' names and affiliations, abstract, keywords, and references.

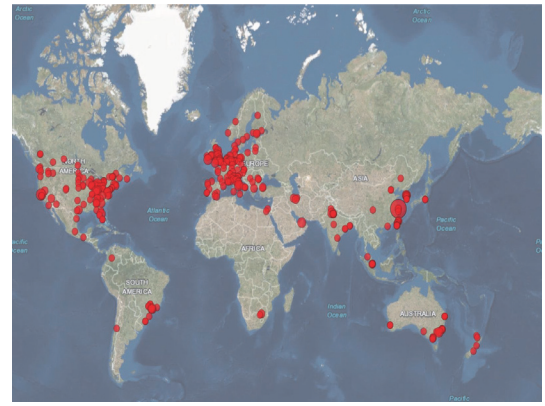

Figure 1: Geographical locations of all contributing organizations.

2.2. Refinement of the Search Results. BibExcel allows modifying and/or adjusting the data imported from various databases including Scopus and Web of Science. The data output can be exported to Excel or any program that takes tabbed data records. This high degree of flexibility makes BibExcel a powerful tool, yet relatively difficult to work with especially in performing the initial setups. We use BibExcel to perform some initial bibliometric and statistical analysis and to prepare the input data for additional network analysis in Gephi. The data source that we use as input into BibExcel is in RIS format (Scopus output) containing the bibliographic information of the articles. Our analysis focuses on the following data fields: authors, title, journal, publication year, keywords, abstract, affiliations, and references. These analyses require reformatting of the RIS file into a number of different formats and hence producing several file types.

Now, the data transfer to Bib Excel software is possible for future process. After this stage the analyzed data conduct to Global Positioning System (GPS) visualizer web site for building multiple geocodes. For this purpose we used the "http://www.gpsvisualizer.com" web site. It is a free GPS visualizer online to make maps from geographic data. There is some limitation to draw a map for multiple geocodes but with asking keyword mapping from *"Google Map"* or *"Bing Map"* website we could create our geographical map with large numbers of cities. Figure 1 shows the map which is created by *"GPS visualizer"* [15] (GPS 2003–2016 Visualizer) online website. It shows the institutions' location which works on different branches of sustainable supply chain network. The large numbers of literatures are located in some western countries in Europe and then west states in USA. Also the number of publications in western Asia is impressive. In Figure 1 the diameter of each circle expresses the relative degree of each institution to the contribution. In general view, in the map, the geographical distribution of these institutions

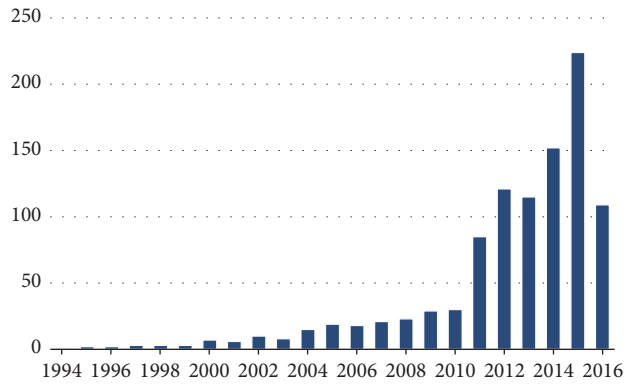

Figure 2: Publication trend in the area of SSCM.

expresses that sustainable supply chain network has attracted many researchers around the world.

Our map on the national collaborations statistics shows that the United States holds the highest national collaboration rate. There are 229 affiliations belonging to USA, followed by 70 affiliations with UK. This could be most likely encouraged by the many top authors and organizations within the United States. While still in its early growth and expansion period, the area of sustainable supply chain managements is attracting a geometric growth in the number of academic publications. This significant growth is more noticeable after 2010. The details of a number of publications are illustrated in Figure 2.

2.3. Sustainable Supply Chain and Success Factors. Sustainable supply chain concerns the management of material, information, and capital flows as well as cooperation among companies along the supply chain while taking goals from all three dimensions of sustainable development, that is, economic, environmental, and social, into account which are derived from customer and stakeholder requirements. Therefore, SSCM can be understood as SCM focusing on maintaining environmental, economic, and social stability for long-term sustainable growth. We focused on 188 articles which are more compatible with our topic. From these literatures we classified the key success of SSCM. Fifteen themes arose, as explained in the following subsections.

2.3.1. Initiation and Commitment of Top Management (S1). Top management commitment and support is a fundamental requirement for a company to manufacture environmentally friendly products, and a primary decision rests on which supplier will enhance the green supply chain of a company [16]. Initiation and commitment of top management are necessary for any organization to allocate adequate technological, financial, and human resources for adopting SSCM concepts, ideas, and strategy development. Top management commitment helps in achieving resources for effective implementation of organizational sustainable supply chain management initiatives.

2.3.2. Strategic Planning (S2). Domestic government legislations and environmental regulations are of the major drivers affecting strategic planning in SSCM practices adoption in any country [17, 18]. Organizations need to respond to the government policies and regulations of the concerned countries towards greening the firms.

2.3.3. State Government Legalizations (S3). The authors in [19] believe that state regulatory framework plays significant importance in promotion environmental sustainability [20]. Again there are several cells, boards, and units under them to look after the issues. In state level, there are similar "bodies" for promoting green practices. State government regulation has been identified as an important success factor to implement SSCM practices.

2.3.4. Societal Issues (S4). Societal issues are product/process related aspects of operations that influence human safety, welfare, and community development [21–23]. Strong business ethics is an essential factor for the success of sustainability initiatives in an organization. Some subthemes are important in this section: rights, ethics, poverty, and increasing sustainable development to consider major contributions and promise fields to further the area. References [24, 25] examined briefly the conceptualizations of SSM and of social responsibility, to show the understanding of topics.

2.3.5. Encouragement from Customers (S5). Organizations should design and manufacture products by considering environment properties of products/services which must meet customers' requirements and expectations to obtain most sustainable solution [23]. The customer is the essence of any business. Businesses must design and manufacture products and provide services that meet customers' needs and expectations. Environmental consciousness of consumers is one of the most significant driving forces for companies to engage in environmental management [26, 27].

2.3.6. Motivation of Suppliers and Vendors towards Green Practices (S6). Perception of an organization of taking steps towards environmental good-will is not their responsibility. Lack of appropriate organizational structures and widespread ignorance of supply chain philosophy are also success factors identified for implementation of GSCM [28]. Companies could find they are not fully familiar with the real risks and costs and connected to their investments over time.

2.3.7. Economic Benefits (S7). There is a lack of funds for environmental projects or the consideration that Return on Investment (ROI) period after implementing green supply chain management is very long. Taking over GSCM initiatives needs additional endeavors and also higher cost and it has less visible economic benefits from these initiatives [29, 30]. In this situation, the value of national money will decrease and prices will increase, which empowers hesitation between customers and investors. Reference [31] explained that weak economic performance could lead to government collapse and diplomatic unrest.

2.3.8. Scarcity of Natural Resources (S8). Industrial professionals need training to adopt SSCM system in their

industries and need training to maintain and monitor growth [32]. The growth of gross domestic product has been raised. Effective employees' training offers several potential advantages in real life. Most social benefits, derived from the accumulation of human skills, such as good health, more urban employment, reduction of crime, and increase in social correlation, will affect the economic growth in the long term.

2.3.9. Firm's Competitiveness (S9). Organizations implementing green innovation can enjoy the first mover advantage and, at the same time, improve their corporate images, develop new markets, and gain competitive advantages [33]. Supplying must pay high attention to supply chain sustainability issues, while the environmental benefits may hold them responsible for unsustainable supply chain behaviors. Mostly, unsustainability obstacles occur upstream at the different subsupplier stages [34].

2.3.10. Information Quality and Sharing (S10). An efficient interorganizations/intraorganization communication, sharing of innovative ideas, and developing healthy organizational culture in implementing of SSC activities can be achieved through information sharing among industries [35, 36]. Sustainable technologies are cleaner and reconfigurable and even recyclable, which do not harm the nature but need high investment [37, 38]; also waste treatment is another important area that needs attention in the sustainable development strategy. Thus, we argue that enabling advanced technologies and information should be taken into consideration as an enabler in the strategic framework formulation of sustainable supply chain.

2.3.11. State Government Legalizations (S11). There is a lack of number of laborers in the organization and/or the quality of the employees. Basically, a fundamental obstacle to improving environmental performance of the SME sector is a lack of state government legalizations [39]. But among the item mentioned above, the task of developing human resources in both developed and developing industries is accepted as a vital need in the societies [40].

2.3.12. Fearlessness of Failure (S12). The fear of failure is involved while adopting sustainable supply chain which could lead to monetary losses for the firm or the fear of failure of the product, hence leading to losing the competitive advantage [41]. Sustainable development approach reflects on the role of information as a strategic resource in supply chain [42]. Reference [43] further emphasized the need to develop reverse logistics networks, to increase the utilization of resources and for the reuse and recycling of the product.

2.3.13. Pressure from Non-Government Organizations (NGOs) Lobby (S13). Legislation and regulation are the instruments very much necessary for the proper governance of business enterprises including the environment in which they operate. Environmental laws and regulations are an important framework, within which the companies must operate [44]. In the large scale, environmental pollution caused by factory production processes in the other side costs of production conducts to be lower than related community costs [45]. Due to high attention to the environmental protection and sustainable development, such as pressures from NGOs and stakeholder groups, organizations are being pushed to effectively incorporate sustainability issues into their supply chain network managing program [46].

2.3.14. Measure and Monitor the Environmental Practice of Suppliers (S14). Metrics misalignment is thought to be a primary source of inefficiency and disruption in supply chain interactions [47]. It means sustainability practice or environmental protection is one of the goals that exist in organization. The good summary of the aims with a sustainability keeps focusing the organizations on track during adverse times and leads to fighting the inner battle among commercialization and esteemed values.

2.3.15. Maintaining the Environmental Awareness of Suppliers (S15). Industries are unable to maintain the environmental conscious suppliers and suppliers also are concerned to maintain the environmental concepts in their industries [48]. The growing recognition of the contribution of local areas to energy and environmental policies has led to important initiatives for the reallocation of planning actions [49].

3. Research Gap

Adopting sustainable concepts in traditional supply chain management is very difficult, and there are many obstacles to integrating environmental consciousness in traditional SCM. Based on our systematic literature, it is found that in this field many researchers worked on performance and enablers for the adopting of SSCM in different branches [50–52] and that only a handful of researchers address the analysis among the critical success for implementation of SSCM in organizations [14, 53]. One serious issue in industries is environmental contamination. The manufacturing industries have started to adopt sustainable concepts in their SCM in order to retain their customers. This study is helpful for industries to analyze the success for SSCM and to find the key success; industries will also be able to improve their sustainable performance by identifying the leading or dominant success for adopting sustainable supply chain management. It is difficult for industries to eradicate all the success in the initial stage of adopting sustainable concepts in traditional SCM.

4. Solution Methodology

4.1. Interpretive Structural Modeling. The ISM is a qualitative data analysis which was proposed by [54]. Firstly it was used as a solving method to basically understand and identify the interrelationships of the components in sophisticated systems or condition [55]. Also ISM is based on group decision-making, social sciences, discrete mathematics, graph theory, and computer assistance [56]. The ISM methodology is started by separately or group mental types in order to calculate binary matrices, to explain the individual/mutual relations of the elements. In some references this matrix is nominated as relation matrix too [38].

The relation matrix may be shaped by considering this question "regarding this feature will e_i effect e_j?" Following the reply, if it is "no" then $\pi_{ij} = 0$; otherwise $\pi_{ij} = 1$. The relation matrix, in general form, is shown as follows:

$$D = \begin{matrix} e_1 \\ e_2 \\ \vdots \\ e_m \end{matrix} \begin{pmatrix} 0 & \pi_{12} & \cdots & \pi_{1n} \\ \pi_{21} & 0 & \cdots & \pi_{2n} \\ \vdots & \vdots & \ddots & \vdots \\ \pi_{m1} & \pi_{m2} & \cdots & 0 \end{pmatrix}. \quad (1)$$

Here "e_i" is the same as "ith" variable in the framework. "π_{ij}" also reveals the connection among "ith" and "jth" variables. D is the relation matrix.

$$M = D + I, \quad (2)$$

$$M^* = M^K = M^{K+1}, \quad K \geq 0. \quad (3)$$

In (2), "I" is nominated as the unit matrix, and in (3) "K" express the powers. Also in (3) M^* presented the reachability matrix. Keep in mind that this matrix runs under the "Boolean operation" (e.g., $1 \times 1 = 1$ and $0 \times 0 = 0$; see as follows)

$$M = \begin{pmatrix} 1 & 0 \\ 1 & 1 \end{pmatrix}, \qquad M^2 = \begin{pmatrix} 1 & 0 \\ 1 & 1 \end{pmatrix}. \quad (4)$$

Now, we are ready to calculate the reachability matrix and priority matrix, respectively, as follows:

$$R(t_i) = \left\{ e_i \mid m^*_{ji} = 1 \right\}, \quad (5)$$

$$A(t_i) = \left\{ e_i \mid m^*_{ij} = 1 \right\}. \quad (6)$$

"m_{ij}" explains the value of the "ith" and "jth" in row and column, respectively.

Now, based on (7), the interrelationships among the elements could be discovered and the arrangement of the relationship of elements could be explained by the graph

$$R(t_i) \cap A(t_i) = R(t_i). \quad (7)$$

4.2. The Main ISM Steps. The various steps involved in the ISM methodology are described as follows.

Step 1. Variables (criteria) considered for the system under consideration are listed.

Step 2. From the variables identified in Step 1, a contextual relationship is established among the variables in order to identify which pairs of variables should be examined.

Step 3. A structural self-interaction matrix (SSIM) is developed for variables, which indicates pairwise relationships among variables of the system under consideration.

Step 4. Reachability matrix is developed from the SSIM and the matrix is checked for transitivity. The transitivity of the contextual relation is a basic assumption made in ISM. It states that if a variable A is related to B and B is related to C, then A is necessarily related to C.

Step 5. The reachability matrix obtained in Step 4 is partitioned into different levels.

Step 6. Based on the relationships given above in the reachability matrix, a directed graph is drawn and the transitive links are removed.

Step 7. The resultant digraph is converted into an ISM, by replacing variable nodes with statements.

Step 8. The ISM model developed in Step 7 is reviewed to check for conceptual inconsistency and necessary modifications are made. The above steps and necessary modifications are made [18] which are indicated in Figure 3.

4.3. Interpretive Structural Modeling. The ISM technique is a well-known methodology for identifying and summarizing relationships between specific elements. In the first step to develop the theoretical framework, we use ISM to recognize the mentioned fifteen successes of SSM based on our systematic literature review in the previous sections. This methodology allows an interactive learning practice and helps to understand the complex relationships among variables of systems. To find experts we identified practitioners who have implemented sustainability initiatives within their supply chains. They have suitable experience and are working at tactical operation in different levels of supply chain. The experts were consulted to verify the drivers that were stemmed from the literature review in the context of manufacturing. The wording of the variables was verified but we did not drop or add new variables.

4.4. Sampling Design and Data Collection. In our study, 12 manufacturing firms were identified from various sectors including electrical power supply, UPSs and battery charger consumer goods, and batteries. The targeted experts have twenty plus years of experience and were working in the tactic level of supply chain operations. Ten academics from reputable engineering and management institutes were also consulted for the survey of the SSCM drivers. The use of professional networking sites made our efforts much easier. The questionnaire was emailed to a total of 24 experts out of which 32 exploitable responses were considered for the study. Thus, we achieved a response rate of 75%. The flow chart or our research is illustrated in Figure 4.

4.5. Structural Interpretive Matrix. As per ISM technique, we used the survey to establish the contextual relationships between the drivers identified earlier, and the structural self-interaction matrix (SSIM) emerged [14, 57]. The relationship among the variables in the survey is denoted by V, A, X,

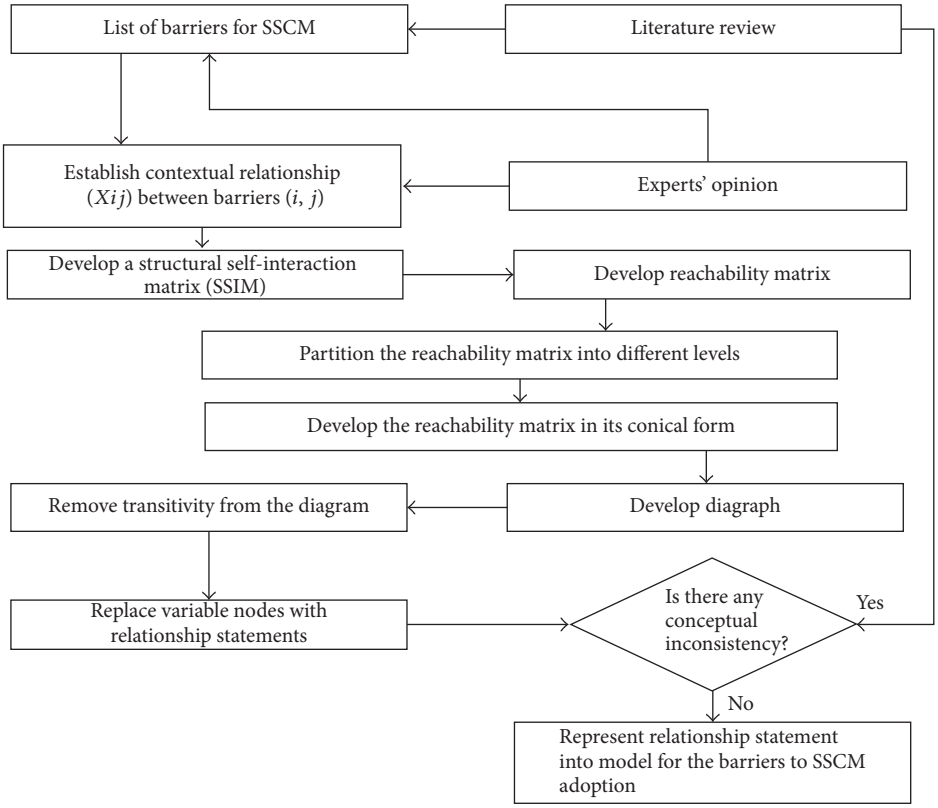

Figure 3: ISM diagram modified from [14].

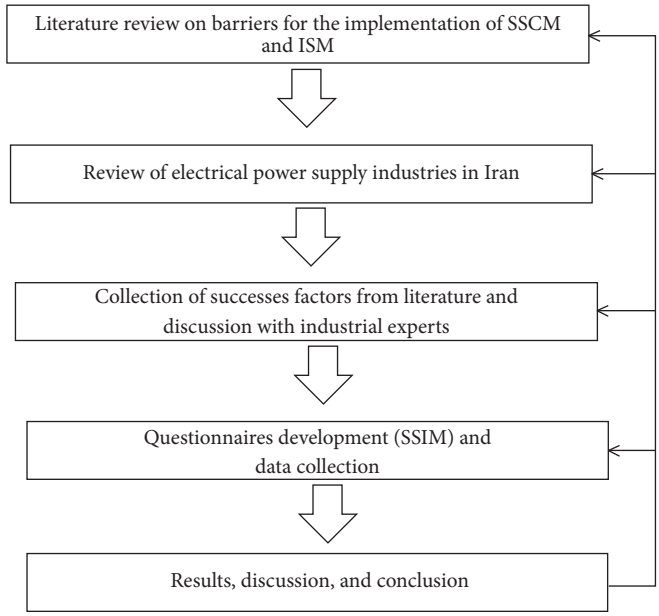

Figure 4: Flow chart of the research work.

and O. Using the symbols i and j to denote columns and rows, the relationships between nodes are shown as follows:

V: if i leads to j but j does not lead to i

A: if i does not lead to j but j leads to i

X: if i and j lead to each other

O: if i and j are not related each other.

In Table 1, structural self-interaction matrix is shown.

4.6. Structural Model. The SSIM (Table 1) is further converted into initial and final reachability matrices (see Tables

Table 1: Structural self-interaction matrix (SSIM).

Success factor	S15	S14	S13	S12	S11	S10	S9	S8	S7	S6	S5	S4	S3	S2
S1	*X*	*V*	*V*	*A*	*A*	*X*	*V*	*A*	*A*	*A*	*A*	*V*	*A*	*A*
S2	*A*	*A*	*O*	*O*	*X*	*O*	*O*	*A*	*A*	*V*	*X*	*V*	*X*	
S3	*O*	*A*	*O*	*X*	*A*	*A*	*A*	*A*	*X*	*O*	*X*	*A*		
S4	*O*	*X*	*V*	*V*	*X*	*V*	*O*	*V*	*V*	*X*	*V*			
S5	*A*	*A*	*O*	*V*	*X*	*A*	*A*	*A*	*A*	*O*				
S6	*X*	*X*	*O*	*O*	*O*	*O*	*O*	*O*	*V*					
S7	*X*	*A*	*O*	*O*	*V*	*A*	*O*	*X*						
S8	*V*	*O*	*V*	*V*	*V*	*A*	*A*							
S9	*O*	*A*	*X*	*V*	*O*	*X*								
S10	*V*	*V*	*V*	*V*	*V*									
S11	*A*	*A*	*O*	*O*										
S12	*O*	*A*	*X*											
S13	*A*	*V*												
S14	**O**													

Table 2: Initial reachability matrix.

Success factor	S1	S2	S3	S4	S5	S6	S7	S8	S9	S10	S11	S12	S13	S14	S15
S1	0	0	0	0	0	0	0	0	0	0	0	0	0	0	0
S2	0	0	0	0	0	0	0	0	0	0	0	0	0	0	0
S3	0	0	0	0	1	0	0	0	0	0	0	0	0	0	1
S4	1	1	1	0	1	0	1	1	0	0	1	1	1	0	0
S5	1	1	1	0	1	0	0	0	0	0	1	1	1	0	0
S6	0	0	0	0	0	1	0	0	0	0	0	0	0	0	0
S7	0	0	0	0	1	0	0	0	0	0	0	0	0	0	1
S8	1	1	1	0	1	0	1	1	0	0	1	1	1	0	0
S9	1	1	1	0	1	0	0	0	0	0	1	1	1	0	0
S10	0	0	0	0	0	1	0	0	0	0	0	0	0	0	0
S11	1	0	0	0	1	0	1	0	0	0	1	0	0	0	0
S12	1	1	1	0	1	0	1	1	1	0	1	1	1	0	1
S13	1	1	1	0	1	0	0	0	1	0	1	1	1	0	1
S14	0	0	0	0	1	0	0	0	0	0	0	0	0	0	1
S15	**1**	**1**	**1**	**0**	**1**	**0**	**1**	**1**	**0**	**0**	**1**	**1**	**1**	**0**	**0**

2 and 3). The initial reachability matrix emerged when we converted the SSIM by substituting *V*, *A*, *X*, and *O* by 1 and 0; as per the following rules SSIM becomes binary format, for example, 0 or 1; the instruction for substitution is mentioned as follows based on [58].

(i) If the (i, j) relationship in SSIM is *V*, the corresponding binary relationship is 1 for (i, j) and is 0 for (j, i).

(ii) If the (i, j) relationship in SSIM is *A*, the corresponding binary relationship is 0 for (i, j) and is 1 for (j, i).

(iii) If the (i, j) relationship in SSIM is *X*, the corresponding binary relationship is 1 for both (j, i) and (i, j).

(iv) If the (i, j) relationship in SSIM is *O*, the corresponding binary relationship is 0 for both (j, i) and (i, j).

As the above rules, the initial reachability matrix is shown in Table 2.

4.7. Structural Final Reachability Matrix. The transitivity principle can be explained with an illustrative example: if *a* leads to *b* and *b* leads to *c*, the transitivity property implies that *a* leads to *c*. The transitivity property helps to remove the gaps among the variables if any. By adopting the above criteria, the final reachability matrix is prepared and is shown in Table 3 based on [14].

4.8. Level Partitioning. The fifth step involves extracting of a hierarchical ordering from the reachability matrix by level partitioning [59]. The reason for this step is to make easy construction of the digraph from the reachability matrix. From the final reachability matrix, the reachability and antecedent sets for each success factor are established. The level partition related to this research is shown in Table 4.

4.9. ISM Model. Based on final reachability matrix, the structural model is introduced as follows.

Table 3: Final reachability matrix.

Success factor	S1	S2	S3	S4	S5	S6	S7	S8	S9	S10	S11	S12	S13	S14	S15
S1	0	0	0	0	0	0	0	0	0	0	0	0	0	0	0
B2	0	0	0	0	0	0	0	0	0	0	0	0	0	0	0
S3	1*	1*	0	0	1*	1*	1*	1*	0	0	1*	1*	1*	0	1
S4	0	0	0	0	0	0	0	0	0	0	0	0	0	0	0
S5	0	0	0	0	0	0	0	0	0	0	0	0	0	0	0
S6	1*	1*	0	0	1*	1*	1*	1*	0	0	1*	1*	1*	0	1
S7	1	1	1*	0	1	1	1	1	1*	0	1	1	1	0	1*
S8	1	1	0	0	1	1	1	1	0	0	1	1	1	0	1*
S9	0	0	0	0	0	0	0	0	0	0	0	0	0	0	0
S10	1*	1*	0	0	1*	1*	1*	1*	0	0	1*	1*	1*	0	1
S11	1	1	1*	0	1	1	1	1	1*	0	1	1	1	0	1*
S12	1	1	0	0	1	1	1	1	0	0	1	1	1	0	1*
S13	0	0	0	0	0	0	0	0	0	0	0	0	0	0	0
S14	0	1*	0	0	1	0	0	1*	0	0	1	0	1*	0	1*
S15	**0**	**0**	**0**	**0**	**0**	**0**	**0**	**0**	**0**	**0**	**0**	**0**	**0**	**0**	**0**

* Entries are included to incorporate transitivity.

Table 4: Level partition.

Success factor	Reachability set	Antecedent set	Intersection set	Level
S10	7	1, 2, 3, 4, 5, 6, 7, 8, 9, 10, 11, 14, 15	1	I
S14	9	3, 4, 5, 7, 8, 9, 10, 11, 12, 13, 14, 15	13	II
S13	8	2, 3, 4, 5, 7, 8, 9, 10, 11, 14, 15	2	II
S2	14	5, 7, 8, 9, 10	6	II
S12	4	1, 2, 3, 4, 5, 6, 7, 8, 9, 10, 14, 15	12	II
S3	4, 7, 8, 10, 14	3, 4, 5, 7, 8, 9, 10, 11, 14, 15	3, 5, 11, 15	III
S9	4, 8, 9, 10, 14	3, 4, 5, 7, 8, 9, 10, 11, 14, 15	3, 5, 11, 15	III
S8	4, 8, 10	3, 4, 5, 7, 8, 9, 10, 11, 15	3, 5, 11, 15	III
S4	4, 7, 8, 10, 14	3, 4, 5, 7, 8, 9, 10, 11, 15	3, 5, 15	III
S5	1	3, 5, 11, 15	7	IV
S11	13	3, 5, 11, 15	9	IV
S1	2	3, 5, 11, 15	8	IV
S6	6	3, 5, 11, 15	14	V
S7	12	3, 5, 11, 15	4	VI
S15	10	3, 5, 11, 15	10	VI

If there is any interrelationship among the successes j and i, an arrow is used to show this relationship. The output result is named as "digraph." With the replacing of nodes, the "digraph" will convert to an ISM model. In Figure 3, we illustrated ISM model structure. As this ISM model, the 15 success factors are categorized in six levels. In the top level, two successes appear, which are "information quality and sharing (S10)" in minimum level, and economic benefits (S7) and "maintaining the environmental awareness of suppliers (S15)" are found as maximum level illustrated in Figure 6.

4.10. MICMAC Analysis. Based on dependence power and driving power matrix (Table 5), it is desirable to seek a method by which we can draw up the hierarchical relationship among them and also establish which of the myriad indicators are "stand-alone" ones in their impacts, which ones do not hold true, and which ones generate secondary and higher order impacts. Cross impact matrix multiplication applied to classification (MICMAC) can be used as the best tool to meet the purpose. Based on this research, all successes are categorized into four modules: independent, autonomous, linkage, and dependent. Also it is divided into two main parts: dependence power and driver power, which are given in Figure 5:

(i) Success factors in autonomous quadrant: in this section, successes do not have strong driving power and also weak dependence. Usually they keep disconnected from the system life cycle, but in some parts they have a few connections, which could be strong. These types of success are appointed in quadrant I.

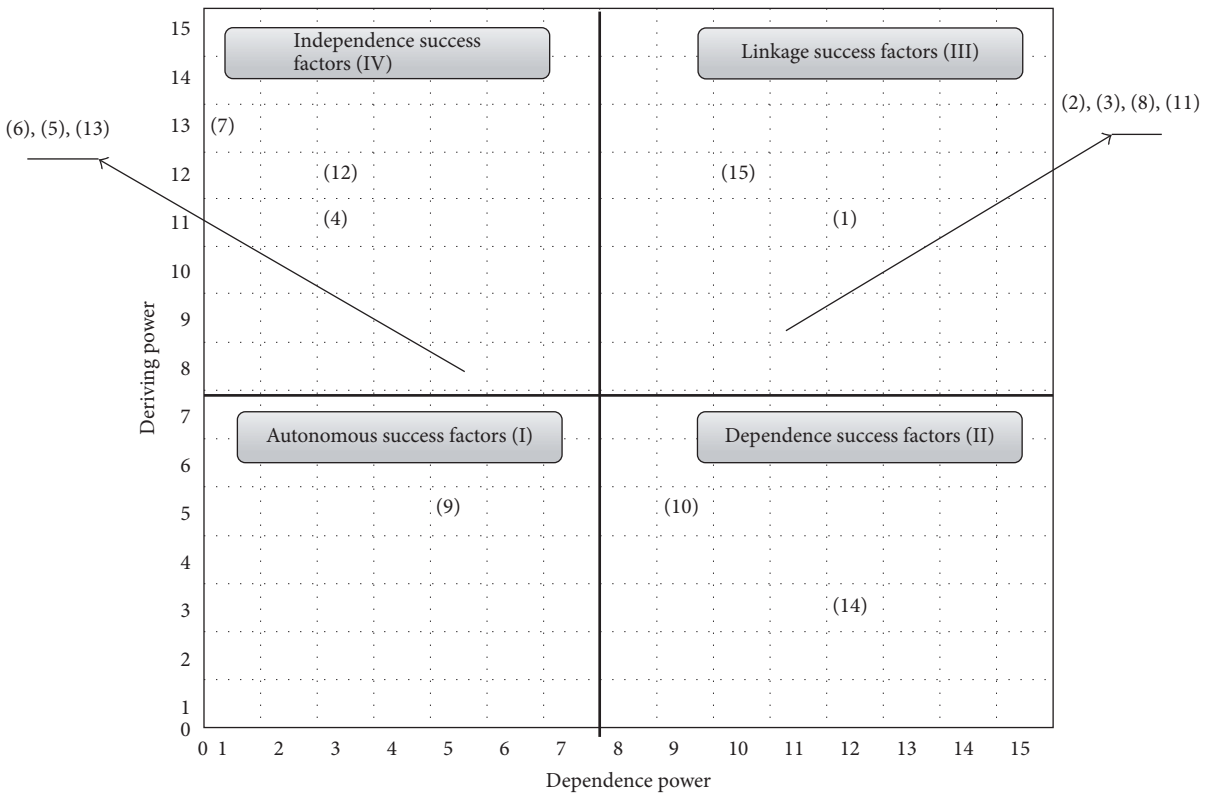

Figure 5: MICMAC analysis towards implementing SSM, a case industry under study.

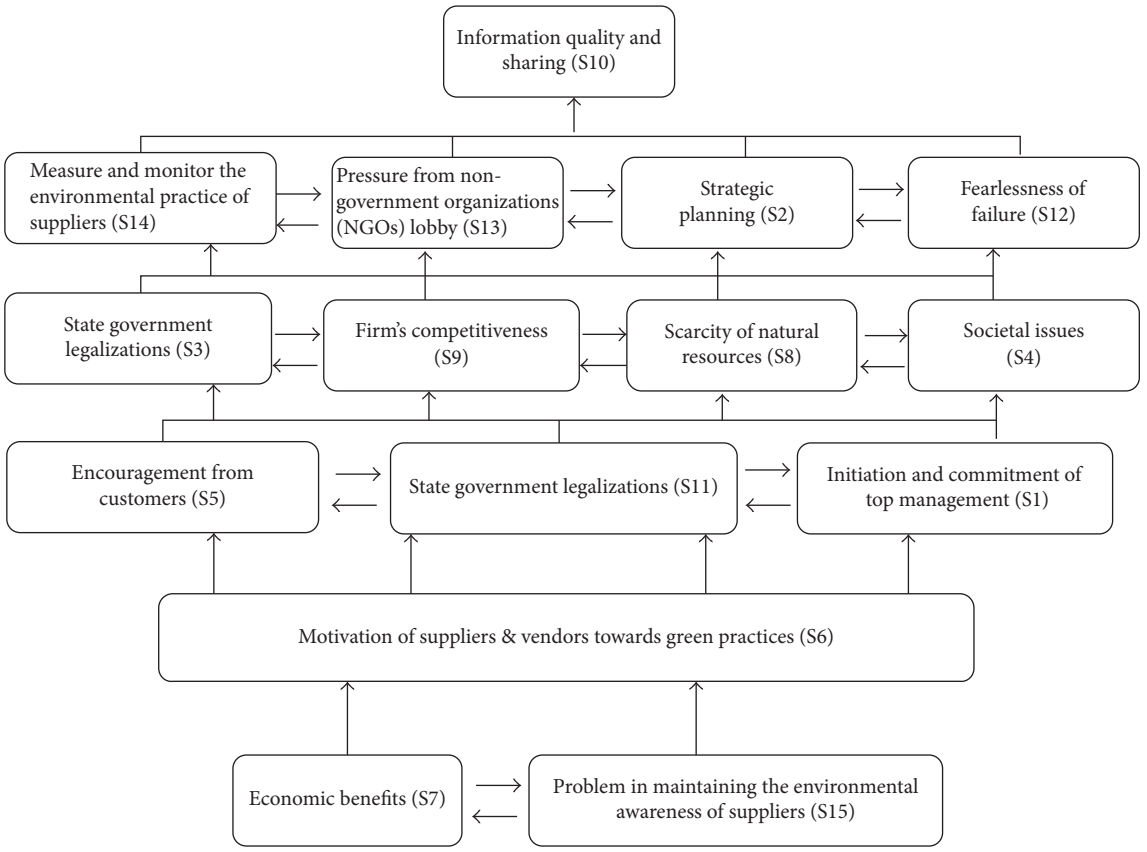

Figure 6: ISM based model for success factors.

Table 5: Dependence power and driving power.

Success factor	S4	S3	S5	S6	S11	S9	S13	S12	S15	S2	S8	S7	S14	S1	S10	Driver power
S1	0	0	0	0	0	0	0	0	1	0	0	0	0	0	0	1
S11	0	0	0	0	0	0	0	0	0	0	0	1	0	0	0	1
S2	0	0	0	1	0	1	0	0	0	0	0	0	0	0	0	2
S5	0	0	0	0	0	0	0	0	0	0	0	0	0	0	0	2
S12	0	0	0	0	0	0	0	1	0	0	1	0	0	0	0	2
S3	0	1	1	0	1	1	1	1	1	0	0	0	1	0	0	8
S6	0	1	1	0	1	1	1	1	1	0	0	0	0	0	1	8
S13	0	1	1	0	1	1	1	1	1	0	1	0	0	0	0	8
S4	0	1	1	0	1	1	1	1	1	0	0	0	0	1	0	8
S9	0	1	1	1	1	1	1	1	1	1	0	0	0	0	0	8
S10	0	1	1	0	1	1	1	1	1	0	1	0	0	0	0	8
S8	0	1	1	1	1	1	1	1	1	1	1	1	0	0	0	11
S14	1	1	1	1	1	1	1	0	1	1	1	0	1	0	0	11
S15	1	1	1	1	1	0	1	1	1	1	1	0	1	0	0	11
S7	1	1	1	1	1	1	1	1	1	1	1	1	1	0	1	14
Dependence power	3	10	10	6	10	10	10	10	11	5	7	3	4	1	2	

(ii) Success factors in dependent quadrant: this quadrant includes the success which has weak driving power but in the other side has strong dependence power and is represented in Section 2.

(iii) Success factors in linkage quadrant: in this section, the successes at the same time have strong driving power and strong dependence. They are represented in Section 3. These successes are unstable and any reaction on them will make an impression on the other successes.

(iv) Success factors in independent quadrant: in this section, the successes have enough strong driving power but very weak dependence power. These are placed in Section 4.

5. Discussions of Findings

Our study has implications for SSCM managerial practice, in terms of offering guidelines on those factors that managers should pay attention to in order to adopt SSCM practices in their organizations and supply chains. In particular, our study underlines the role of institutional pressures on internal pressures and commitment. Therefore, managers should be aware on how to "translate" these pressures into appropriate strategies and strategic collaboration with suppliers in order to achieve sustainability. The role of green product design as enabled by continuous improvement is important, and information needed for this purpose could be provided by appropriate information technologies. Logistics and warehousing should be also improved, and particular changes in these operations will enable organizations and supply chains to become more environmentally friendly and will also help them become economically viable and stable. Paying attention to these drivers means acquiring and cultivating particular employee skills; hence, this study proposes that managers should also attend to the different skills and capabilities needed to achieve SSCM, as determined by the proposed drivers. During the production, customer service, consumption, post-disposal disposition, and entire supply chain, the local optimization of environmental factors will be considered [60].

Although industrial development in Iran is acceptable, the consequences of this growth towards ecology should also be considered. Environmental issues are vital for industries, and for both managers and executive engineers, implementation of SSCM is challenging. However, the establishment of SSCM is not a simple job and it needs accurate analysis. The output of this research demonstrates that Iranian industrial top level managers have begun to arrange sustainability concerns in sustainable development and environmental science. But the point is not only that they are in the initial phase but also that they have to get rid of the barriers step by step.

The dependence and driving power demonstrate the 15 success positions in 4 sections (Figure 5). The outcome of this research of success analysis with the ISM approach is presented as the following clarification:

(i) In autonomous success factors, just one success factor S(9) appears in this section. Generally, autonomous successes are not strong drivers but are weak dependent and these success factors do not have much effect on the approach. This graph shows that nearly all successes play a significant role in the match on the SSCM in electrical power supply industries.

(ii) In dependent success factors area, there are two success factors S(10) and S(14). This section is mentioned as dependent quadrant, and the success in this section does not have strong driving power and also high dependence power. Considering the information quality and sharing in industries will drive power for these success factors [56] and also

high dependence power is indicated as the absence of corporative social obligation as a significant barrier to the implementation of SSCM approach. These point out that those industries are giving minimum attention to social issue and governmental regulation. So, in our research case, we need the government to build proper framework to draw special attention to social responsibility for Iranian industries. Following these points, the Iranian industries are not specially motivated to social responsibility participation without outside pressure [61].

(iii) Six success factors, S(1), S(2), S(3), S(8), S(11), and B(15), fall in linkage success factors section. These success factors are organized into one group. Maintaining the environmental awareness of suppliers is the main issue in this quadrant. The success factors which are placed in this section have both strong driving and at the same time strong dependence power and they are unstable too. Any reaction on these successes will have an action on the other success and will also provide feedback. Also they might agitate all system specifications [58, 62].

(iv) S(4), S(5), S(6), S(7), S(12), and S(13) are given in dependent success factors in section. These success factors have a strong driving power but weak dependence power and this may be known as "key successes." Among these success factors S(12) "fearlessness of failure" and S(7) "economic benefits" are in top levels. The suppliers always are fighting to avoid recession in their workplace and practice to implement the appropriate sustainability model, because they are faced with high investments and low profit. Supply chain management contributes to the overall accomplishment of a supply chain, and one poor supplier activity affects very quickly the performance of the whole chain [61]. S(5), S(6), and S(13), "encouragement from customers," "motivation of suppliers and vendors towards green practices," and "pressure from non-government organizations (NGOs) lobby," are also in the same layers. Growing human skill in a company will supply goal attainment, being employee-oriented, and quality in productivity [59].

6. Conclusion

In the era of globalization, industries are facing pressure to greening their supply chain from intentional and domestic levels. It is because the environmental concerns have been gaining more attentions recently among organizations, and an adequately significant number of factors related to environmental and sustainable issues still need to be recognized from industrial viewpoints. In present work, we make an attempt to recognize the major critical success factors that facilitate successful implementation of SSCM practices towards sustainable development. At first, based on systematic review (Section 2) we focused on some high prestige scientific journals to investigate dominant success in SSCM practices. In second stage, we applied ISM and MICMAC analysis to understand the relationships of 15 success factors in the implementation of sustainable supply chain management. It is impossible to reach all kinds of success; therefore, companies need to know the most obtained success factors based on their policy. This research summarizes the data analysis of success factors and categorizes success factors with ISM and MICMAC support.

In Figure 6, ISM diagram indicates the connection between the success factors. There are six levels in this diagram. One success factor drops in the first level, which is "information quality and sharing" (S10). This success factor is less influential for the implementation of sustainable supply chain management in electrical power supply industries. In the middle levels, the four success factors appeared. In the end, (S10) and (S15) that occur in the lower level play an influential role in adopting sustainable supply chain management. Industries need to give more attention to these success factors. The ISM outcome identifies the most significant success in electrical power supply industries which can easily help to process for the implementation of sustainable supply chain management.

Based on MICMAC analysis (Figure 5), one barrier (S6) has been reported as autonomous. The success factor "firm's competitiveness" has little link to the system, with low driving power and minimum dependency. It mentions that key variables are nominated as the success factor with a very strong driving power. They are independent or linkage criteria. We can call (S15) "problem in maintaining the environmental awareness of suppliers" the high impact key barrier, which also is dominated by (S1), (S2), (S3), (S8), and (S11), respectively.

In this study we have not used a structured questionnaire to further test the framework. Instead we relied completely on a survey of the perceptions of experts for developing the theoretical model, which alone may not be sufficient to statistically test the framework, and this is a limitation of the ISM method. For future research, a structured questionnaire could be prepared and a survey must be conducted by targeting highly experienced supply chain professionals, who embrace sustainability thinking in their operations to test the framework. We believe that our study provides useful thoughts for those who would like to further engage in theory building on the drivers of SSCM. In addition, Fuzzy ISM (FISM) [63, 64], which could be a progress over normal ISM, has been advised to expand ISM in fuzzy environment. It could specify the several network structures in the principles and practices.

Conflicts of Interest

The authors declare that they have no conflicts of interest.

Authors' Contributions

Professor Jianqiu Zeng made precious editorial contributions to improving the presentation of this paper.

Acknowledgments

This work is supported by China National Key Research and Development Program under Grant no. 2016YFC0803206.

References

[1] Y. Y. Yusuf, A. Gunasekaran, A. Musa, M. Dauda, N. M. El-Berishy, and S. Cang, "A relational study of supply chain agility, competitiveness and business performance in the oil and gas industry," *International Journal of Production Economics*, vol. 147, pp. 531–543, 2014.

[2] H. Ding, Q. Zhao, Z. An, and O. Tang, "Collaborative mechanism of a sustainable supply chain with environmental constraints and carbon caps," *International Journal of Production Economics*, 2014.

[3] S. Luthra, K. Govindan, D. Kannan, S. K. Mangla, and C. P. Garg, "An integrated framework for sustainable supplier selection and evaluation in supply chains," *Journal of Cleaner Production*, vol. 140, pp. 1686–1698, 2017.

[4] Z. Wu and M. Pagell, "Balancing priorities: Decision-making in sustainable supply chain management," *Journal of Operations Management*, vol. 29, no. 6, pp. 577–590, 2011.

[5] W. Qian, "Environmental management accounting and supply chain management," *Journal of Cleaner Production*, vol. 20, no. 1, pp. 186-187, 2012.

[6] WBCSD, "World Business Council for Sustainable Development," in *Sustainable Production Consumption from a Business Perspective. A status report by WBCSD*, 2008.

[7] Carbon Disclosure Projec, *Carbon Disclosure Project Supply Chain Report. Migrating to a Low Carbon Economy through Leadership and Collaboration*, London, UK.

[8] F. Li, S. Dong, Z. Li, Y. Li, S. Li, and Y. Wan, "The improvement of CO_2 emission reduction policies based on system dynamics method in traditional industrial region with large CO_2 emission," *Energy Policy*, vol. 51, pp. 683–695, 2012.

[9] R. Mungkung, J. Aubin, T. H. Prihadi, J. Slembrouck, H. M. G. Van Der Werf, and M. Legendre, "Life cycle assessment for environmentally sustainable aquaculture management: a case study of combined aquaculture systems for carp and tilapia," *Journal of Cleaner Production*, vol. 57, pp. 249–256, 2013.

[10] C. S. Tang and S. Zhou, "Research advances in environmentally and socially sustainable operations," *European Journal of Operational Research*, vol. 223, no. 3, pp. 585–594, 2012.

[11] L. Luo, L. Qin, Y. Wang, and Q. Wang, "Environmentally-friendly agricultural practices and their acceptance by smallholder farmers in China—a case study in Xinxiang County, Henan Province," *Science of the Total Environment*, vol. 571, pp. 737–743, 2016.

[12] B. Fahimnia, J. Sarkis, and H. Davarzani, "Green supply chain management: a review and bibliometric analysis," *International Journal of Production Economics*, vol. 162, pp. 101–114, 2015.

[13] GPS 2003-2016 Visualizer, http://www.gpsvisualizer.com/map_input.

[14] J.-J. Huang, G.-H. Tzeng, and C.-S. Ong, "Multidimensional data in multidimensional scaling using the analytic network process," *Pattern Recognition Letters*, vol. 26, no. 6, pp. 755–767, 2005.

[15] Z. Wang, K. Mathiyazhagan, L. Xu, and A. Diabat, "A decision making trial and evaluation laboratory approach to analyze the barriers to green supply chain management adoption in a food packaging company," *Journal of Cleaner Production*, 2015.

[16] N. Subramanian and R. Ramanathan, "A review of applications of analytic hierarchy process in operations management," *International Journal of Production Economics*, vol. 138, no. 2, pp. 215–241, 2012.

[17] W. F. Lam, "Institutional design of public agencies and coproduction: a study of irrigation associations in Taiwan," *World Development*, vol. 24, no. 6, pp. 1039–1054, 1996.

[18] F. Knobloch and J.-F. Mercure, "The behavioural aspect of green technology investments: A general positive model in the context of heterogeneous agents," *Environmental Innovation and Societal Transitions*, vol. 21, pp. 39–55, 2016.

[19] P. Waide and C. Brunner, "Energy-efficiency policy opportunities for electric motor-driven systems. Energy efficiency series working paper," *International Energy Agency*, 2011.

[20] A. Kolk, "The social responsibility of international business: from ethics and the environment to CSR and sustainable development," *Journal of World Business*, 2015.

[21] V. Mani, R. Agarwal, A. Gunasekaran, T. Papadopoulos, R. Dubey, and S. J. Childe, "Social sustainability in the supply chain: construct development and measurement validation," *Ecological Indicators*, vol. 71, pp. 270–279, 2016.

[22] K. H. Brunk, "Exploring origins of ethical company/brand perceptions - a consumer perspective of corporate ethics," *Journal of Business Research*, vol. 63, no. 3, pp. 255–262, 2010.

[23] A. Sallez, "Sous-traitance, productivité économique et croissance régionale," *Appliquée*, vol. 2/3, pp. 459–496, 1975.

[24] J. Fisher, "Business marketing and the ethics of gift giving," *Industrial Marketing Management*, vol. 36, no. 1, pp. 99–108, 2007.

[25] J. A. Wade, "Chapter 6 - Stakeholders, ethics and social responsibility in the food supply chain," in *Food Supply Chain Management*, Chapter 6, pp. 111–124, Oxford, UK, 2001.

[26] R. Imrie and J. Morris, A review of recent changes in buyer-supplier relations, 1992.

[27] W. J. Yoon and K. S. Park, "A study on the market instability index and risk warning levels in early warning system for economic crisis," *Digital Signal Processing*, vol. 29, pp. 35–44, 2014.

[28] R. Cerchione and E. Esposito, "A systematic review of supply chain knowledge management research: State of the art and research opportunities," *International Journal of Production Economics*, vol. 182, pp. 276–292, 2016.

[29] A. H. Tabassam, S. H. Hashmi, and F. U. Rehman, "Nexus between political instability and economic growth in pakistan," *Procedia - Social and Behavioral Sciences*, vol. 230, pp. 325–334, 2016.

[30] A. Alesina, S. Ozler, N. Roubini, and P. Swagel, "Political instability and economic growth," National Bureau of Economic Research, Cambridge, UK, 1992.

[31] M. Pasban and S. H. Nojedeh, "A review of the role of human capital in the organization," in *Proceedings of the 3rd International Conference on New Challenges in Management and Organization*, vol. 230, pp. 249–253, Organization and Leadership, 2016.

[32] J. H. Grimm, J. S. Hofstetter, and J. Sarkis, "Exploring sub-suppliers' compliance with corporate sustainability standards," *Journal of Cleaner Production*, vol. 112, pp. 1971–1984, 2016.

[33] M. Wilhelm, C. Blome, E. Wieck, and C. Y. Xiao, "Implementing sustainability in multi-tier supply chains: strategies and contingencies in managing sub-suppliers," *International Journal of Production Economics*, vol. 182, pp. 196–212, 2016.

[34] J. O. Okeniyi, O. A. Omotosho, O. O. Ogunlana et al., "Investigating prospects of phyllanthus muellerianus as eco-friendly/sustainable material for reducing concrete steel-reinforcement corrosion in industrial/microbial environment," *Energy Procedia*, vol. 74, pp. 1274–1281, 2015.

[35] S. Kerdsuwan, K. Laohalidanond, and W. Jangsawang, "Sustainable development and eco-friendly waste disposal technology for the local community," *Energy Procedia*, vol. 79, pp. 119–124, 2015.

[36] M. Kishna, E. Niesten, S. Negro, and M. P. Hekkert, "The role of alliances in creating legitimacy of sustainable technologies: a study on the field of bio-plastics," *Journal of Cleaner Production*, vol. 155, pp. 7–16, 2017.

[37] S. Luthra, S. Kumar, D. Garg, and A. Haleem, "Barriers to renewable/sustainable energy technologies adoption: Indian perspective," *Renewable & Sustainable Energy Reviews*, vol. 41, pp. 762–776, 2015.

[38] R. Dubey, A. Gunasekaran, T. Papadopoulos, S. J. Childe, K. Shibin, and S. F. Wamba, "Sustainable supply chain management: framework and further research directions," *Journal of Cleaner Production*, vol. 142, pp. 1119–1130, 2017.

[39] K. Govindan and H. Soleimani, "A review of reverse logistics and closed-loop supply chains: a journal of cleaner production focus," *Journal of Cleaner Production*, vol. 142, no. 1, pp. 371–384, 2017.

[40] Y. Wang, J. R. Huscroft, B. T. Hazen, and M. Zhang, "Green information, green certification and consumer perceptions of remanufctured automobile parts," *Resources, Conservation & Recycling*, 2016.

[41] M. Levy and P. Powell, "Information systems strategy for small and medium sized enterprises: An organisational perspective," *The Journal of Strategic Information Systems*, vol. 9, no. 1, pp. 63–84, 2000.

[42] S. Dowlatshahi, "Developing a theory of reverse logistics," *Interfaces*, vol. 30, no. 3, pp. 143–155, 2000.

[43] Y. Zhang, L. Yin, and X. Li, "A decision study on river carrying capacity of changsha-zhu-tan region," *Systems Engineering Procedia*, vol. 1, pp. 422–431, 2011.

[44] H. Ding, Q. Liu, and L. Zheng, "Assessing the economic performance of an environmental sustainable supply chain in reducing environmental externalities," *European Journal of Operational Research*, vol. 255, no. 2, pp. 463–480, 2016.

[45] S. Gold, S. Seuring, and P. Beske, "Sustainable supply chain management and inter-organizational resources: a literature review," *Corporate Social Responsibility and Environmental Management*, vol. 17, no. 4, pp. 230–245, 2010.

[46] E. Chardine-Baumann and V. Botta-Genoulaz, "A framework for sustainable performance assessment of supply chain management practices," *Computers & Industrial Engineering*, vol. 76, no. 1, pp. 138–147, 2014.

[47] F. Taillandier, L. Mora, and D. Breysse, "Decision support to choose renovation actions in order to reduce house energy consumption – An applied approach," *Building and Environment*, vol. 109, pp. 121–134, 2016.

[48] A. Diabat, D. Kannan, and K. Mathiyazhagan, "Analysis of enablers for implementation of sustainable supply chain management - a textile case," *Journal of Cleaner Production*, vol. 83, pp. 391–403, 2014.

[49] M. D. P. Pablo-Romero, R. Pozo-Barajas, and A. Sánchez-Braza, "Analyzing the effects of energy action plans on electricity consumption in covenant of mayors signatory municipalities in Andalusia," *Energy Policy*, vol. 99, pp. 12–26, 2016.

[50] P. Ahi and C. Searcy, "An analysis of metrics used to measure performance in green and sustainable supply chains," *Journal of Cleaner Production*, vol. 86, pp. 360–377, 2015.

[51] K. Mathiyazhagan, K. Govindan, A. NoorulHaq, and Y. Geng, "An ISM approach for the barrier analysis in implementing green supply chain management," *Journal of Cleaner Production*, vol. 47, pp. 283–297, 2013.

[52] J. N. Warfield, "Toward interpretation of complex structural models," *IEEE Transactions on Systems, Man, and Cybernetics*, vol. 4, no. 5, pp. 405–417, 1974.

[53] S. Luthra, D. Garg, and A. Haleem, "Critical success factors of green supply chain management for achieving sustainability in Indian automobile industry," *Production Planning and Control*, vol. 26, no. 5, pp. 339–362, 2015.

[54] J. N. Warfield, "Developing interconnection matrices in structural modeling," *IEEE Transactions on Systems, Man, and Cybernetics*, vol. SMC-4, no. 1, pp. 81–87, 1974.

[55] J. Hörisch, E. Ortas, S. Schaltegger, and I. Álvarez, "Environmental effects of sustainability management tools: an empirical analysis of large companies," *Ecological Economics*, vol. 120, pp. 241–249, 2015.

[56] V. Narayanaswamy and L. Stone, "From cleaner production to sustainable production and consumption in Australia and New Zealand: achievements, challenges, and opportunities," *Journal of Cleaner Production*, vol. 15, no. 8-9, pp. 711–715, 2007.

[57] S. Sindhu, V. Nehra, and S. Luthra, "Identification and analysis of barriers in implementation of solar energy in Indian rural sector using integrated ISM and fuzzy MICMAC approach," *Renewable & Sustainable Energy Reviews*, vol. 62, pp. 70–88, 2016.

[58] E. A. Adegbola, "Corporate social responsibility as a marketing strategy for enhanced performance in the nigerian banking industry: a granger causality approach," *Procedia - Social and Behavioral Sciences*, vol. 164, pp. 141–149, 2014.

[59] A. Jayant and M. Azhar, "Analysis of the barriers for implementing green supply chain management (GSCM) practices: an interpretive structural modeling (ISM) approach," in *Proceedings of the 12th Global Congress on Manufacturing and Management, GCMM 2014*, pp. 2157–2166, India, December 2014.

[60] D. Kannan, R. Khodaverdi, L. Olfat, A. Jafarian, and A. Diabat, "Integrated fuzzy multi criteria decision making method and multi-objective programming approach for supplier selection and order allocation in a green supply chain," *Journal of Cleaner Production*, vol. 47, pp. 355–367, 2013.

[61] A. Ohuchi and I. Kaji, "Correction Procedures for Flexible Interpretive Structural Modeling," *IEEE Transactions on Systems, Man, and Cybernetics*, vol. 19, no. 1, pp. 85–94, 1989.

[62] P. Seri and A. Zanfei, "The co-evolution of ICT, skills and organization in public administrations: Evidence from new European country-level data," *Structural Change and Economic Dynamics*, vol. 27, pp. 160–176, 2013.

[63] T. Wakabayashi, L. Itoh, and A. Ohuchi, "A method for constructing system models by fuzzy flexible interpretive structural modeling," in *Proceedings of the 1995 IEEE International Conference on Fuzzy Systems. The International Joint Conference of the Fourth IEEE International Conference on Fuzzy Systems and The Second International Fuzzy Engineering Symposium*, pp. 913–918, Yokohama, Japan, 1995.

[64] A. Ohuchi, S. Kase, and I. Kaji, "MINDS: a flexible interpretive structural modeling system," in *Proceedings of the 1988 IEEE International Conference on Systems, Man, and Cybernetics*, pp. 1326–1329, Beijing, China.

Hindawi
Mathematical Problems in Engineering
Volume 2017, Article ID 9549323, 7 pages
https://doi.org/10.1155/2017/9549323

Research Article

A Cycle Deep Belief Network Model for Multivariate Time Series Classification

Shuqin Wang,[1,2] Gang Hua,[1] Guosheng Hao,[2] and Chunli Xie[2]

[1]*School of Information and Electrical Engineering, China University of Mining and Technology, Xuzhou, Jiangsu 221116, China*
[2]*School of Computer Science and Technology, Jiangsu Normal University, Xuzhou, Jiangsu 221116, China*

Correspondence should be addressed to Gang Hua; ghua@cumt.edu.cn

Received 27 May 2017; Revised 11 July 2017; Accepted 24 August 2017; Published 4 October 2017

Academic Editor: M. L. R. Varela

Multivariate time series (MTS) data is an important class of temporal data objects and it can be easily obtained. However, the MTS classification is a very difficult process because of the complexity of the data type. In this paper, we proposed a Cycle Deep Belief Network model to classify MTS and compared its performance with DBN and KNN. This model utilizes the presentation learning ability of DBN and the correlation between the time series data. The experimental results showed that this model outperforms other four algorithms: DBN, KNN_ED, KNN_DTW, and RNN.

1. Introduction

Time series data are sequences of real-valued signals that are measured at successive time intervals. They can be divided into two kinds: univariate time series and multivariate time series (MTS). Univariate time series contain one variable, while MTS have two or more variables. MTS is a more important data type of time series because it is widely used in many areas such as speech recognition, medicine and biology measurement, financial and market data analysis, telecommunication and telemetry, sensor networking, motion tracking, and meteorology.

As the availability of MTS data increases, the problem of MTS classification attracts great interest recently in the literature [1]. MTS classification is a supervised learning procedure aimed for labeling a new multivariate series instance according to the classification function learned from the training set [2]. However, the features in traditional classification problems are independent of their relative positions, while the features in time series are highly correlated. That resulted in the loss of some important information if the traditional classification algorithms are used for MTS, since they treat each feature as an independent attribute. Many techniques have been proposed for time series classification. A method based on boosting are presented for multivariate time series classification [3]. In [4], the authors proposed a DTW based decision tree to classify time series and the error rate is 4.9%. In [5], the authors utilize a multilayer perceptron neural network on the control chart problem and the best performance achieved is 1.9% error rate. Hidden Markov Models are used on the PCV-ECG classification problem and achieve 98% accuracy [6]. Support vector machine combined with Gaussian Elastic Metric Kernel is used for time series classification [7]. The dynamics of recurrent neural networks (RNNs) for the classification of time series are presented in [8]. However, simple combination of one-nearest-neighbor with DTW distance is claimed to be exceptionally difficult to beat [9].

Deep Belief Network is a type of deep neural network with multiple hidden layers, introduced by Hinton et al. [10] along with a greedy layer-wise learning algorithm. Restricted Boltzmann Machine (RBM), a probabilistic model, is the building block of DBN. DBN and RBM have witnessed increased attention from researchers. They have already been applied in many problems and gained excellent performance, such as classification [11], dimensionality-reduction [12], and information retrieval [13]. Taylor et al. [14] proposed conditional RBM, an extension of the RBM, which is applied to human notion sequences. Chao et al. [15] evaluated the DBN performance as a forecasting tool on predicting exchange rate. Längkvist et al. [16] applied DBN for sleep stage classification and evaluated the performance. The result illustrated that DBN either with features (feat-DBN) or using the raw

data (raw-DBN) performed better than the feat-GOHMM. The feat-DBN achieved 72.2% and the raw-DBN achieved 67.4%, while the feat-GOHMM achieved only 63.9%.

Raw-DBN do not need to extract feature before classifying the sleep data and this algorithm is easy to implement. However, it neglects the important information in time series data and its performance is not satisfactory. This paper proposed a Cycle DBN model for time series classification. This model possesses the ability of feature learning since it is developed on the basis of DBN. Meanwhile, the characters of time series data are taken into consideration in the model.

The remainder of the paper is organized as follows. Next section reviews the background material. In Section 3, we detail the Cycle DBN model for multivariate time series. Section 4 evaluates the performance of our Cycle DBN on two real data sets. Section 5 concludes the work of this paper.

2. Background Material

A time series is a sequence of observations over a period of time. Formally, a univariate time series $x = \{x(i) \in R : i = 1, 2, \ldots, n\}$ is an ordered set of n real-valued numbers, and n is called the length of the time series x. Multivariate time series is more common in real life and it is more complex since it has two or more variables. A MTS is defined as a finite sequence of univariate time series

$$X = (x_1, x_2, \ldots, x_m). \quad (1)$$

The MTS X has m variables and the corresponding component of the jth variable x_j is a univariate time series of length n:

$$x = \{x_j(i) \in R : i = 1, 2, \ldots, n\} \quad (j = 1, 2, \ldots, m). \quad (2)$$

In this paper, we use bold face characters for MTS and regular fonts for univariate time series.

The time series classification problem is a supervised learning procedure. First we should learn a function $f : X \to y$ according to the given training set $A = \{(X^{(i)}, y^{(i)})\}$ $i = 1, 2, \ldots, k$. The training set A includes k samples and each sample consists of an input $X^{(i)}$ paired with its corresponding label $y^{(i)}$. Then we can assign a label to a new time series instance based on the function we learned from the training set.

A Deep Belief Network (DBN) consists of an input layer, a number of hidden layers, and finally an output layer. The top two layers have undirected, symmetric connections between them. The lower layers receive top-down, directed connections from the layer above.

The process of training DBNs includes two phases. Each two consecutive layers in DBN are treated as a Restricted Boltzmann Machine with visible units v and hidden units h. There are full connections between visible layer and hidden layer, but no visible-to-visible or hidden-to-hidden connections (see Figure 1). The visible and hidden units are connected with a weight matrix, W, and have a visible bias vector b and a hidden bias vector c, respectively. We need to train each RBM independently one after another and then stack them on top of each other in the first phase. This procedure is also called pretraining. In the second phase, the BP network is set up at the last level of the DBN, and the output of the highest RBM is received as its input. Then we can perform a supervised learning in this phase. This procedure is called fine-tuning since the parameters in the DBN are tuned using error back propagation algorithm in this phase.

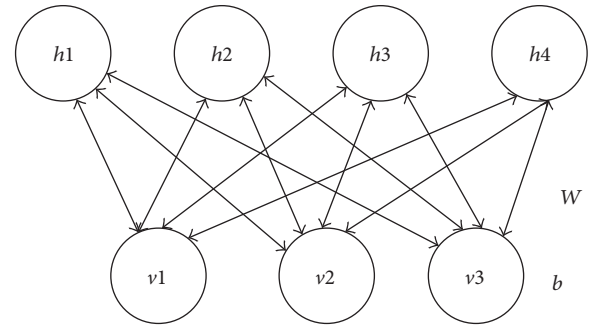

Figure 1: Graphical depiction of RBM.

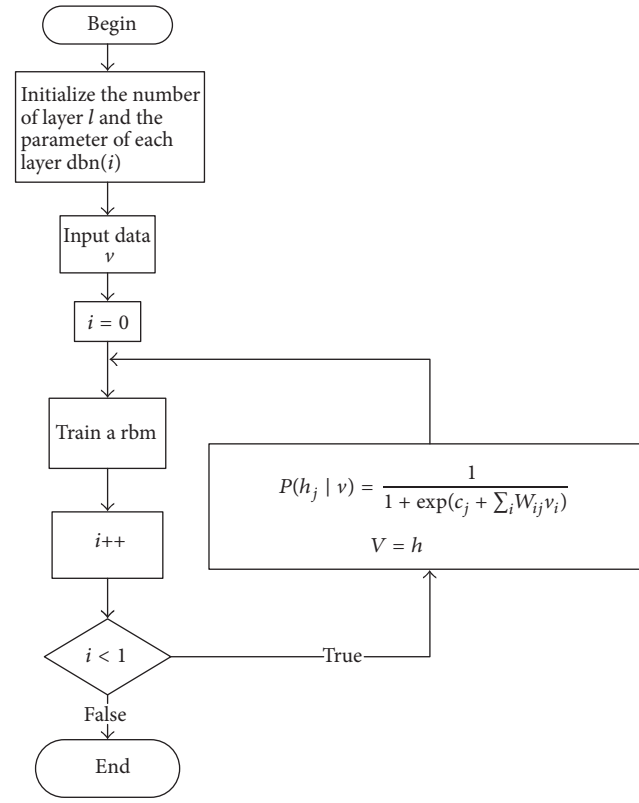

Figure 2: The flowchart of DBN training.

The procedure of training DBN is shown by Algorithm 1 and the corresponding flowchart is given by Figure 2.

From the above analysis, we can conclude that the most important of DBN is the training of each RBM.

Since there are no hidden-hidden or visible-visible connections in the RBM, the probability that hidden unit h_j is activated by visible vector $P(h_j|v)$ and the probability that

Begin
Initialize α (the learning rate), l (the number of DBN layers), m_k (the number of hidden unites in k layer and $k = 1, 2, \ldots, l$), epochs, DBN(k).parameters (the parameters of each layer and $k = 1, 2, \ldots, l$).
Input data X;
$V1 = X$;
$k = 1$;
do
trainRBM($V1$, DBN(k).parameters);
k++;
compute h according to Equation (3)
$V1 = h$;
while ($k < l$)
End.

Algorithm 1: DBN train algorithm.

visible unit v_i is activated by given hidden vector $P(v_i|h)$ is given by

$$P\left(h_j \mid v\right) = \frac{1}{1 + \exp\left(c_j + \sum_i w_{ij} v_i\right)}, \tag{3}$$

$$P\left(v_i \mid h\right) = \frac{1}{1 + \exp\left(b_i + \sum_j w_{ji} h_j\right)}. \tag{4}$$

Contrastive Divergence (CD) approximation is used to train the parameters by minimizing the reconstruction error and the learning rule is given by

$$\frac{\partial \log P(v)}{\partial W_{ij}} \approx \left\langle v_i h_j \right\rangle_{\text{data}} - \left\langle v_i h_j \right\rangle_{\text{recon}}. \tag{5}$$

$\langle v_i h_j \rangle_{\text{data}}$ is expectation of the training set and $\langle v_i h_j \rangle_{\text{recon}}$ represents the expectation of the distribution of reconstructions.

The procedure of training RBM is shown as Algorithm 2 and the corresponding flowchart is given by Figure 3.

3. Cycle_DBN for Time Series Classification

Längkvist et al. [16] applied DBN in time series classification and obtained a remarkable result. The standard DBN optimizes the posterior probability $p(y_t \mid x_t)$ of the class labels given the current input xt. However, time series data are different from other kinds of data and there are correlations between time series data. It is unsuitable to apply DBN for time series classification without any modification because it neglects the important information in time series data.

Based on the above discussion, this paper proposed a Cycle DBN model for time series classification just as Figure 4. The model inherits the powerful feature representation of DBN and utilizes the data correlation of the time series. Thus, this model is quite suitable for time series classification.

In this model, X_t is the input at time step t and O_t is the corresponding output of DBN. Since our purpose is classification, we add a softmax function on the top layer and y_t is the corresponding label. After training DBN and getting the

Begin
m = 1;
while (m < epoch)
for all hidden units j
$P\left(h1_j \mid v1\right) = \frac{1}{1 + \exp\left(c_j + \sum_i W_{ij} v1_i\right)}$
Sample $h1_i \in \{0, 1\}$ from $P(h1_j|v1)$
End for
For all visible units i do
$P\left(v2_i \mid h1_j\right) = \frac{1}{1 + \exp\left(b_i + \sum_j W_{ij} h1_j\right)}$
Sample $v2_i \in \{0, 1\}$ from $P(v2_j \mid h1)$
End for
For all hidden units j do
$P\left(h2_j \mid v2\right) = \frac{1}{1 + \exp\left(c_j + \sum_i W_{ij} v2_i\right)}$
$h2_j = P\left(h2_j \mid v2\right)$
end for
$w = w + \alpha * \left(h1 * v1' - h2 * v2'\right)$
$b = b + \alpha * (v1 - v2)$
$c = c + \alpha * (h1 - h2)$
End while
End.

Algorithm 2: The algorithm for RBM train.

label y_t, y_t is then treated as one item input of DBN. At time t, the inputs of DBN not only include X_t but also include y_{t-1}, the output of DBN at time $t - 1$.

The training procedure of this Cycle_DBN, which is similar to the traditional DBN, includes two procedures. The only difference is that the output at time $t - 1$ is feedback to Cycle_DBN as one of the inputs at time t. The first procedure is unsupervised training to initiate the parameters of DBN. After unsupervised learning, we add a softmax function on the top layer and do a supervised training procedure.

4. Experimental Evaluation

In this section, we conduct extensive experiments to evaluate the classification performance of the proposed model Cycle_DBN and compare it against traditional DBN, KNN_ED, KNN_DTW, and recurrent neural networks (RNN).

The k-NN is one of the most well-known classification algorithms that are very simple to understand but performs well in practice. An object in the testing set is classified according to the distances of the object to the objects in the training set and the object is assigned to the class its k nearest neighbors belongs to. We will choose $k = 1$ in our experiment and the algorithm is simply called the nearest neighbor algorithm. In KNN_ED, we use Euclidean Distance to measure the similarity between two instances.

Dynamic Time Warping (DTW) [17] is another distance measure for time series and it was originally and typically designed for univariate time series. However, the time series handled in this paper is multidimensional and a multidimensional version of DTW is needed. Fortunately, ten

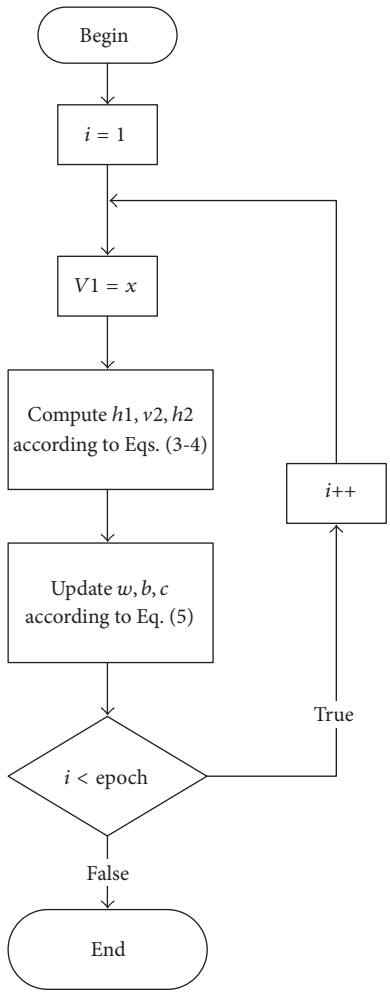

Figure 3: The flowchart of RBM training.

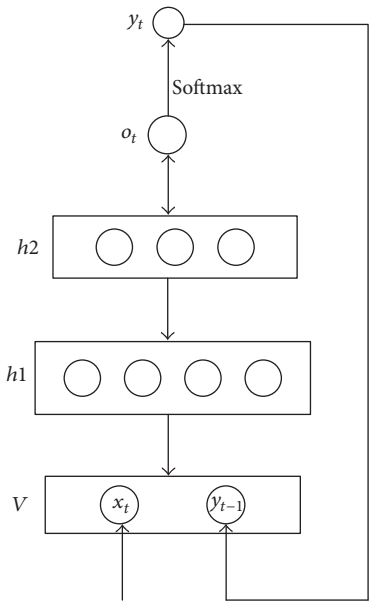

Figure 4: The architecture of Cycle DBN.

Holt et al. [18] proposed a multidimensional DTW and it utilizes all dimensions to find the best synchronization. In standard DTW, the distance is usually calculated by taking the squared distance between the feature values of each combination of points: $d(q_i, c_j) = (q_i - c_j)^2$. But in multidimensional DTW, a distance measure for two K-dimensional points must be calculated: $d(q_i, c_j) = \sum_{k=1}^{K} (q_{ik} - c_{j_k})^2$. In KNN_DTW, we use multidimensional DTW distance to measure the similarity between two instances.

RNN allows the identification of dynamic system with an explicit model of time and memory, which makes it ideal for time series classification. In this paper, we choose Elman's architecture, which consist of a context layer, an input layer, one hidden layer, and an output layer.

To evaluate the performance of these methods, we test them on real-world time series datasets, including sleeping dataset, PAMAP2 dataset, and UCR Time Series Classification Archive.

The performance of the classifier is reported using error rate and the error rate of classifiers is defined as shown in

$$\text{error\_rate} = \frac{\text{total number of misclassification data}}{\text{total number of testing data}}. \quad (6)$$

4.1. Sleep Stage Classification. We first consider the problem of sleep stage classification. The data used in the paper is provided by St. Vincent's University Hospital and University College Dublin and can be downloaded from http://www.physionet.org/pn3/ucddb/ PhysioNet.

4.1.1. Dataset. The recordings of this data set have been obtained from 25 adult subjects with suspected sleep-disordered breathing. Each recording consists of 2 EEG channels (C3-A2 and C4-A1), 2 EOG channels, and 1 EMG channel. We only use one of the EEG signals (C3-A2) in our study

$$X_t = \left(\text{EEG}_t \quad \text{EOG1}_t \quad \text{EOG2}_t \quad \text{EMG}_t\right). \quad (7)$$

According to Rechtschaffen and Kales (R&K) [19], sleep recordings can be divided into the following five stages: awake, rapid eye movement (REM), stage 1, stage 2, and slow wave sleep (SWS). Our goal is to find a map function f that correctly predicts the corresponding sleep stage according to the $\mathbf{X}_t$: $y_t = f(X_t)$.

4.1.2. Experiment Setup. The raw signals of all subjects are slightly preprocessed by notch filtering at 50 Hz to cancel out power line disturbances and then are prefiltered with a bandpass filter of 0.3 to 32 Hz for EEG and EOG and 10 to 32 Hz for EMG. After that they are downsampled to 64 Hz.

Since the sample rate is 64 samples per second and we set window width w to be 1 second of data, our time series become

$$X_i = \left(\text{EEG}_{1+i}^{64+i}, \text{EOG1}_{1+i}^{64+i}, \text{EOG2}_{1+i}^{64+i}, \text{EMG}_{1+i}^{64+i}\right). \quad (8)$$

Table 1: Distribution of five classes in the data set.

Subject	Total	Awake	REM	Stage 1	Stage 2	SWS
trainSamples	25000	5017	5005	4993	4986	4999
Val Samples	5000	983	995	1007	1014	1001
Ucdbb009	20000	4230	3720	6420	740	4890
Ucdbb010	20000	1980	11040	2610	2480	1890
Ucdbb011	20000	3270	6170	2430	390	7740
Ucdbb012	20000	4380	7710	930	3660	3320
Ucdbb013	20000	2670	4040	3660	2010	7620
Ucdbb014	20000	0	6780	7380	1190	4650

Table 2: Classification error rate of five models on sleep datasets.

Subject	Cycle_DBN	DBN	*K*NN_ED	*K*NN_DTW	RNN
Ucdbb009	**0.0061**	0.27619	0.3572	0.3359	0.432568
Ucdbb010	**0.0112**	0.19108	0.45832	0.3971	0.5609
Ucdbb011	**0.0044**	0.10805	0.58243	0.57314	054586
Ucdbb012	**0.0098**	0.04804	0.41244	0.3379	0.45141
Ucdbb013	**0.0068**	0.19709	0.4964	0.4857	0.65820
Ucdbb014	**0.0077**	0.26535	0.47192	0.36183	0.58422

Since the length of $\mathbf{X}_t$ is 64, we have corresponding 64 labels. The last label is selected as the label of the time series $\mathbf{X}_t$.

In our study, we use five people recordings as the training set. In order to balance the samples, we select 6000 records every category random. So we have 30000 recordings and we divide 25000 into train samples and 5000 into validation samples. The other six people recordings are used for test data. The distribution of dataset is listed in Table 1.

4.1.3. Experiment Result. Our goal is to compare the performance of IDBNs with original DBN, *k*NN_ED, *K*NN_DTW, and RNN for time series classification. We illustrate the error rate of each model in Table 2. The best results are recorded in boldface in Table 2.

Compared with other four algorithms, the proposed algorithm has best performance. The classification accuracies of Cycle_DBN on all the test data are up to 90% and especially most of them are more than 99%. Standard DBN has a higher rate of correct classification than *K*NN_ED, *K*NN_DTW, and RNN. RNN shows quite poor performance and the error rate is about 50%.

4.2. Activity Classification. Our second experiment is on the PAMAP2 dataset for activity classification. This dataset can be downloaded at http://archive.ics.uci.edu/ml/datasets/PAMAP2+Physical+Activity+Monitoring.

4.2.1. Dataset. This data set records 18 activities performed by 9 subjects wearing 3 IMUs and a HR-monitor. Each of data contains 54 columns per row and the columns contain the following data: timestamp (1), activityID (2), heart rate (3), IMU hand (4–20), IMU chest (21–37), and IMU ankle (38–54). In our experiment, we only select 7 activities which are "lying (1)," "sitting (2)," "standing (3)," "walking (4)," "running (5)," "cycling (6)," "Nordic walking (7)." Since the records of subject103 and subject109 do not have all the above seven activities and we discard these two subjects. That is to say, we select subject 101~subject 102 and subject 104~subject 108, seven subjects to classify seven activities. Furthermore, the record of heart rate is not used in our experiment.

4.2.2. Experiment Setup. To improve the performance of the proposed approach, we need to carry out a data preprocessing process at the beginning of the experiment. Each dimension of time series is normalized through

$$x = \frac{x - \text{mean}(x)}{\text{std}(x)}, \tag{9}$$

where mean(x) and std(x) are the mean and standard deviation of the variable for samples belonging to the same column, not all samples.

For each subject of seven subjects, we randomly select 1/2 as training set, 1/6 as validation set, and the rest as test set.

4.2.3. Experiment Result. We evaluate classification accuracies of each model on these seven subjects. Table 3 shows the detailed error rates comparison of each subject. From Table 3 we can see that the classification accuracies of the five models on the seven datasets are more than 90%. However, our Cycle_DBN model is either the lowest error rate one or very close to the lowest error rate one for each subject. *K*NN_ED also shows quite excellent performance and we should note that *K*NN is feature-based model.

It is well known that feature-based models have an advantage over lazy classification models such as *K*NN in efficiency. Although *K*NN has high classification accuracy, the prediction time of *K*NN will increase dramatically when the size of training data set grows. The prediction time of DBN and Cycle_DBN will not increase no matter how large the training data is. Therefore, Cycle_DBN shows excellent

Table 3: Classification error rate of five models on PAMAP2.

Subject	Cycle_DBN	DBN	*K*NN_ED	*K*NN_DTW	RNN
Subject 101	**5.70E − 05**	0.01208	0.000171	0.03	0167081
Subject 102	$1.82E-05$	0.000675	**0**	0.034	0.036484
Subject 104	**0**	0.000197	$3.93E-05$	0.006	0.000995
Subject 105	$3.38E-05$	0.004746	**0**	0.024	0.101161
Subject 106	**1.82E − 05**	0.001546	$3.64E-05$	0.018	0
Subject 107	**0**	0.000438	$3.99E-05$	0.024	0.062604
Subject 108	$3.48E-05$	0.000869	**1.74E − 05**	0.018	0.0833

Table 4: Classification error rate of five models on ten UCR time series datasets.

Dataset	Cycle_DBN	DBN	*K*NN_ED	*K*NN_DTW	RNN
uWaveGestureLibrary_Z	**0.333333**	**0.330656**	0.350363	0.35	0.419598
UWaveGestureLibraryAll	0.095047	0.07095	**0.051926**	0.052	0.100503
FordA	0.489647	0.487211	**0.341016**	0.341	0.484865
Two Patterns	0.044365	**0.032374**	0.09325	0.090	0.10775
ECG5000	**0.049161**	0.051559	0.075111	0.075	0.072889
Wafer	**0.000838**	0.002513	0.004543	0.005	0.006976
StarLightCurves	**0.069481**	0.070779	0.151166	0.151	0.326979
ElectricDevices	**0.029931**	0.338983	0.449228	0.376	0.9135
InsectWingbeatSound	0.39782	**0.384196**	0.438384	0.438	0.408081
Face (all)	**0.101333**	0.106667	0.286391	0.286	0.193491

performance in terms of classification accuracy and time consuming.

4.3. UCR Time Series Classification. Besides the above two data sets, we also test our Cycle_DBN on the ten distinct time series datasets from UCR time series [20]. All the dataset has been split into training and testing by default. The only preprocessing in our experiment is normalization and divides them into training, validating, and testing set.

Table 4 shows the test error rate and a comprehensive comparison with *K*NN_ED, *K*NN_DTW, RNN, DBN, and Cycle_DBN.

Cycle_DBN outperforms other four methods on five datasets of ten datasets; *K*NN_ED and *K*NN_DTW achieve best performance on the same two datasets. DBN achieves best performance on two datasets. Although the performance of RNN is not prominent, the effect is also acceptable.

5. Conclusion

Time series classification is becoming more and more important in a broad range of real-world applications. However, most existing methods have lower classification accuracy or need domain knowledge to identify representative features in data. In this paper, we proposed a Cycle_DBN for classification of multivariate time series data in general. Like DBN, Cycle_DBN is an unsupervised learning algorithm which can discover the structure hidden in the data and learn representations that are more suitable as input to a supervised machine than the raw input. Comparing with DBN, the new model Cycle_DBN predicts the label of time t y_t not only based on the current input x_t but also based on the label of previous time y_{t-1}. We evaluated our Cycle_DBN model on twelve real-world datasets and experimental results show that our model outperforms DBN, *K*NN_ED, *K*NN_DTW, and RNN on most datasets.

Conflicts of Interest

The authors declare that there are no conflicts of interest regarding the publication of this paper.

Acknowledgments

This work was supported by the National Natural Science Foundation of China (nos. 51574232, 61379100, 61673196, and 61502212).

References

[1] L. Chen and M. S. Kamel, "Design of multiple classifier systems for time series data," *Lecture Notes in Computer Science*, pp. 216–225, 2005.

[2] I. Batal et al., "Multivariate time series classification with temporal abstractions," *The Florida Ai Research Society*, vol. 22, 344 pages, 2009.

[3] J. J. Rodriguez, C. J. Alonso, and H. Bostrom, "Boosting interval based literals," *Intelligent Data Analysis*, vol. 5, no. 2, pp. 245–262, 2001.

[4] J. J. Rodríguez and C. J. Alonso, *Interval and Dynamic Time Warping-Based Decision Trees*, p. 548, 2004.

[5] A. Nanopoulos, R. Alcock, and Y. Manolopoulos, "Feature-based classification of time-series data," in *Information Processing and Technology*, M. Nikos and D. N. Stavros, Eds., pp. 49–61, Nova Science Publishers, Inc., New York, USA, 2001.

[6] S. Kim, P. Smyth, and S. Luther, "Modeling waveform shapes with random effects segmental hidden Markov models," in *Proceedings of the 20th Conference on Uncertainty in Artificial Intelligence*, pp. 309–316, AUAI Press, Banff, Canada, July 2004.

[7] D. Zhang, W. Zuo, D. Zhang, and H. Zhang, "Time series classification using support vector machine with Gaussian elastic metric kernel," in *Proceedings of the 2010 20th International Conference on Pattern Recognition (ICPR '10)*, IEEE, Istanbul, Turkey, August 2010.

[8] M. Hüsken and P. Stagge, "Recurrent neural networks for time series classification," *Neurocomputing*, vol. 50, pp. 223–235, 2003.

[9] X. Xi, E. Keogh, C. Shelton, L. Wei, and C. A. Ratanamahatana, "Fast time series classification using numerosity reduction," in *Proceedings of the the 23rd International Conference on Machine learning (ICML '06)*, pp. 1033–1040, ACM, Pittsburgh, Pennsylvania, USA, June 2006.

[10] G. E. Hinton, S. Osindero, and Y.-W. Teh, "A fast learning algorithm for deep belief nets," *Neural Computation*, vol. 18, no. 7, pp. 1527–1554, 2006.

[11] H. Lee, R. Grosse, R. Ranganath, and A. Y. Ng, "Convolutional deep belief networks for scalable unsupervised learning of hierarchical representations," in *Proceedings of the 26th Annual International Conference on Machine Learning (ICML '09)*, pp. 609–616, ACM, Montreal, Quebec, Canada, June 2009.

[12] G. E. Hinton and R. Salakhutdinov, "Reducing the dimensionality of data with neural networks," *Science*, vol. 313, no. 5786, pp. 504–507, 2006.

[13] M. W. Amp, M. Rosenzvi, and G. E. Hinton, "Exponential family harmoniums with an application to information retrieval," in *Proceedings of the 18th Annual Conference on Neural Information Processing Systems (NIPS '04)*, 2004.

[14] G. W. Taylor, G. E. Hinton, and S. T. Roweis, "Modeling human motion using binary latent variables," in *Proceedings of the International Conference on Neural Information Processing*, 2006.

[15] J. Chao, F. Shen, and J. Zhao, "Forecasting exchange rate with deep belief networks," in *Proceedings of the 2011 International Joint Conference on Neural Network (IJCNN '11)*, IEEE, San Jose, CA, USA, August 2011.

[16] M. Längkvist, L. Karlsson, and A. Loutfi, "Sleep stage classification using unsupervised feature learning," *Advances in Artificial Neural Systems*, vol. 2012, Article ID 107046, 9 pages, 2012.

[17] J. Kruskall and M. Liberman, "Thesymmetric time warping problem: from continuous to discrete," in *Time Warps, String Edits and Macromolecules: The Theory and Practice of Sequence-Comparison*, Addison-Wesley, 1983.

[18] G. A. ten Holt, M. J. Reinders, and E. Hendriks, "Multi-dimensional dynamic time warping for gesture recognition," in *Proceedings of the Thirteenth annual conference of the Advanced School for Computing and Imaging*, 2007.

[19] A. Rechtschaffen and A. Kales, *A Manual of Standardized Terminology, Techniques, and Scoring Systems for Sleep Stages of Human Subjects*, 1968.

[20] Y. Chen et al., The ucr time series classification archive, http://www.cs.ucr.edu/~eamonn/time_series_data/, 2015.

Hindawi
Mathematical Problems in Engineering
Volume 2017, Article ID 6916575, 17 pages
https://doi.org/10.1155/2017/6916575

Research Article

Simulated Annealing Genetic Algorithm Based Schedule Risk Management of IT Outsourcing Project

Fuqiang Lu, Hualing Bi, Min Huang, and Shupeng Duan

College of Information Science and Engineering, Northeastern University, Shenyang 110819, China

Correspondence should be addressed to Hualing Bi; bihualing081@126.com

Received 10 April 2017; Revised 20 July 2017; Accepted 3 August 2017; Published 28 September 2017

Academic Editor: M. L. R. Varela

IT outsourcing is an effective way to enhance the core competitiveness for many enterprises. But the schedule risk of IT outsourcing project may cause enormous economic loss to enterprise. In this paper, the Distributed Decision Making (DDM) theory and the principal-agent theory are used to build a model for schedule risk management of IT outsourcing project. In addition, a hybrid algorithm combining simulated annealing (SA) and genetic algorithm (GA) is designed, namely, simulated annealing genetic algorithm (SAGA). The effect of the proposed model on the schedule risk management problem is analyzed in the simulation experiment. Meanwhile, the simulation results of the three algorithms GA, SA, and SAGA show that SAGA is the most superior one to the other two algorithms in terms of stability and convergence. Consequently, this paper provides the scientific quantitative proposal for the decision maker who needs to manage the schedule risk of IT outsourcing project.

1. Introduction

With the increasing development of information technology, IT outsourcing has been developing rapidly. It is currently being used as an important strategy by many companies to focus on the core competency, reduce cost, and increase profit. In Europe and other developed countries, either small businesses or large multinational companies always give the noncore business to external professional company [1–4]. According to Gartner, one of the leading information technology research firms, global spending for IT services was approximately $932 billion in 2013 and is expected to grow to $967 billion in 2014, a growth of 3.8% from 2013 [5].

Although IT outsourcing has many advantages including reducing cost and enhancing the core competence, there also exist some problems that need to be solved urgently, especially the problem of managing the schedule risk of IT outsourcing, which may bring about huge loss to company. Consequently, it is very vital to research how to manage the schedule risk of IT outsourcing.

Researchers have done a lot of related research [6–12]. But most methods and models proposed in the literature only discuss the risk management issues on project itself and ignore the cooperation between principal and agent and the distribution characteristics of the IT outsourcing activities. In recent years, principal-agent theory has been widely employed to solve the problem of risk management of IT outsourcing and good results have been achieved through these studies.

Earl et al. concluded some adverse consequences of IT outsourcing based on existing literatures [13–16]. Then, he argued that the risk of IT outsourcing came from enterprises, agents, and the process of IT activities and proposed corresponding risk management measures based on principal-agent theory [17–19]. Bahli and Rivard proposed a scenario-based conceptualization of the IT outsourcing risk and applied it to the specific context of IT outsourcing using transaction cost and agency theory [20]. Osei-Bryson and Ngwenyama offered a method and some mathematical models for analyzing risks and constructing incentive contracts for information system outsourcing [21]. Sanfa et al. analyzed risk factors of producer services outsourcing from the perspective of engineering and afforded managers a theoretic method to manage outsourcing risks by designing the incentive and monitoring mechanism of the producer services outsourcing contract [22]. Xianli et al. present the idea of applying DDM (distributed decision making) to the

risk management of virtual enterprises and design incentive and punishment mechanism in the principal-agent model [23].

In this paper, we build a two-level principal-agent model combined with reward and punishment mechanism for schedule risk management of IT outsourcing project based on the Distributed Decision Making (DDM) theory and principal-agent theory [24–26]. According to the feature of problem, the SAGA is designed to solve the proposed model and the optimal plan of managing schedule risk is given based on the simulation analysis. The purpose of this paper is to provide crucial decision support for the people who need to manage the schedule risk of IT outsourcing project.

The remainder of this paper is structured as follows. Section 1 presents the schedule risk management model of IT outsourcing project. In Section 2, the design of algorithm is given. In addition, numerical examples and results analyzed are depicted in Section 3. Finally, conclusion is given in Section 4.

2. Schedule Risk Management Model of IT Outsourcing Project

2.1. Problem Description. For IT outsourcing, principal divides a whole project into some serial subprojects in the IT developing process, as shown in Figure 1. The definition of serial subprojects is that subproject i ($i = 2, \ldots, I$) is performed after completion of subproject $i-1$.

The schedule risk is reflected in two aspects of duration and risk loss. Each subproject has an initial duration and initial risk loss. In order to effectively manage the schedule risk, the reward and punishment mechanism is added in outsourcing contract; that is, if the project is completed in advance, the agent is rewarded; otherwise the agent is punished. Each subproject will be contracted with different agents, and a typical principal-agent relationship between principal and agent will be generated. For the relationship between principal and agents, see Figure 2.

The optimal solution of top-level model is the optimal combination of risk management capital, and the optimal solution of base-level model is the optimal combination of risk management measure of subproject. In the decision making process, the principal transfers risk management capital to the predicted base-level model. The optimal solution of top-level model is obtained based on the goal of maximizing the profit of the principal and the information returned from the predicted base-level model. Then, the optimal solution of top-level model is transferred to the real base-level model. Under the constraint of risk management capital, the agents obtain the best control measure combination of the subproject according to the goal of maximizing the profit. The information exchange process between the principal and the agents is shown in Figure 3.

For the IT development, the duration of the subproject is determined by the duration of the activities on the critical path. Hence we only consider the schedule of the activities on the critical path. Figure 4 shows the network diagram of subproject I, in which the critical path is 1–3-4–6-7-8. So agent i only allocates risk management capital to activities 1, 2, 3, 6, 8, and 9.

2.2. Assumptions

(1) Subprojects are serial relation in the IT developing process.

(2) The change of completion probability or duration of subproject will not have an effect on other subprojects; that is, subprojects are independent of each other.

(3) The critical path of subproject will not become noncritical path under the influence of risk management capital.

(4) The duration and risk loss of project only are affected by risk management capital.

(5) Due to the information asymmetry, the risk loss per unit of subproject is clear to the agents, but the principal only masters its distribution function.

2.3. The Two-Level Principal-Agent Model. Based on the DDM theory and principal-agent theory, a two-level schedule risk management model of IT outsourcing project is built [27, 28]. In the top-level, the decision maker is the principal who determines how to allocate the risk management capital among agents. The objective of top-level is to maximize the profit of principal, and the reward and punishment mechanism is introduced into the model. In the base-level, the decision maker is the agents who determine the best combination of risk management measure of subproject. The objective of base-level is to maximize the agent's benefit.

2.3.1. Top-Level

Variable Definition

x_i: risk management capital of subproject i

$\widehat{y}_i$: the predicted combination of risk management measure of subproject i

b_i: the agent's profit sharing coefficient of subproject i

I: the number of agents or subprojects

$t_i(\widehat{y}_i)$: predicted duration of subproject i

T_i^0: planned duration of subproject i

$\Delta L_i(\widehat{y}_i)$: predicted saved risk loss of subproject i

$B_i(x_i, \widehat{y}_i)$: predicted profit of agent i

$X^{\max}$: risk management capital budget

$h_i(\widehat{y}_i)$: predicted reward and punishment function of subproject i

AL_i: the aspiration level of agent i

e_i: additional profit per time unit of subproject i.

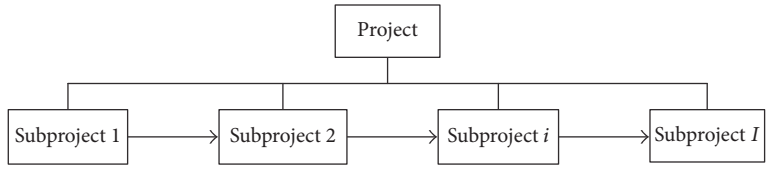

Figure 1: The diagram of project construction.

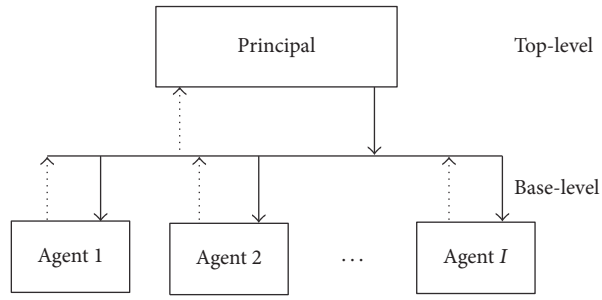

Figure 2: The relationship between principal and agents.

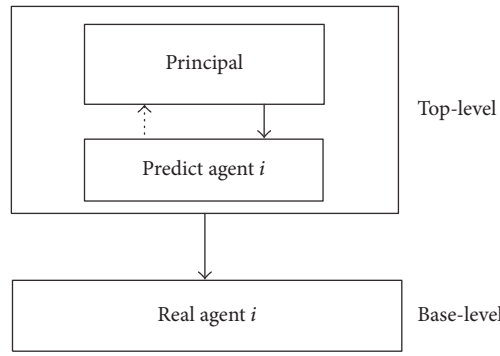

Figure 3: The information exchange process between the principal and the agents.

$$\max \quad \sum_{i=1}^{I} b_i \Delta L_i\left(\widehat{y}_i\right) - x_i + h_i\left(\widehat{y}_i\right) - e_i\left(t_i\left(\widehat{y}_i\right) - T_i^0\right)^- \tag{1}$$

$$\text{s.t.} \quad B_i\left(x_i, \widehat{y}_i\right) \geq \mathrm{AL}_i \tag{2}$$

$$B_i\left(x_i, \widehat{y}_i^*\right) \geq B_i\left(x_i, \widehat{y}_i\right) \tag{3}$$

$$\sum_{i=1}^{I} x_i \leq X^{\max} \tag{4}$$

$$x_i \in N^+. \tag{5}$$

The objective of top-level shown in formula (1) is to maximize the profit of principal; the reward and punishment mechanism is fulfilled by item $h_i(\widehat{y}_i)$. The operation $(x)^-$ is defined as

$$(x)^- = \begin{cases} x, & x < 0, \\ 0, & \text{else.} \end{cases} \tag{6}$$

Formula (2) indicates participation constraint; formula (3) indicates incentive compatibility constraint; formula (4) indicates risk management capital constraint; formula (5) indicates that the risk management capital x_i is a natural integer, which is the decision variable in the top-level model.

2.3.2. Predicted Base-Level. In the predicted base-level, the decision makers are the agents, and there are I agents. Take agent i, for example.

Variable Definition

Y_{ij}: the number of management measures of activity j

J_i: the number of activities of subproject i

L_i: initial risk loss of subproject i

ξ_i: predicted risk loss per unit of subproject i

q_i: reward and punishment standard of subproject i

$c_i(t_i(\widehat{y}_i))$: predicted cost of subproject i

$d_i(\widehat{y}_i)$: predicted invested risk management capital of subproject i

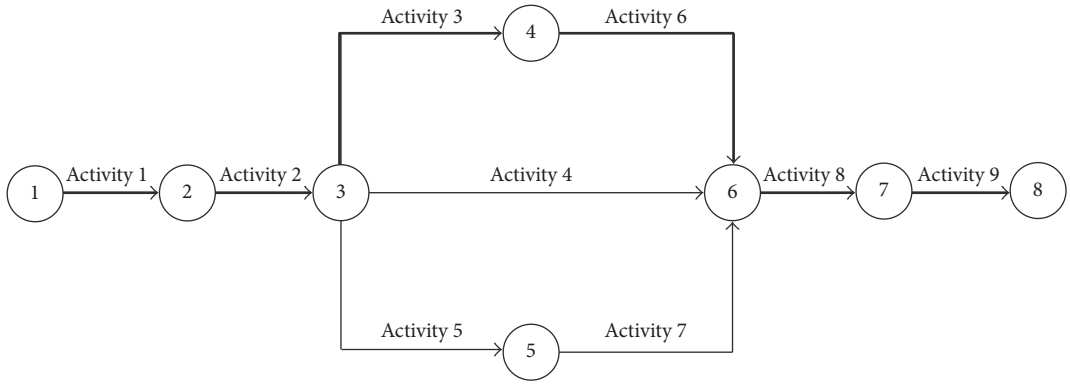

Figure 4: The network diagram of subproject i.

α_i: confidence level

$C_i^{\max}$: the upper bound of cost of subproject i.

$$B_i(x_i, \hat{y}_i) = \max \quad B_i \tag{7}$$

$$\text{s.t.} \quad \text{pr}\{b_i \Delta L_i(\hat{y}_i) - c_i(t_i(\hat{y}_i)) + x_i - d_i(\hat{y}_i) - h_i(\hat{y}_i) \geq B_i\} \geq \alpha_i \tag{8}$$

$$h_i(\hat{y}_i) = q_i\left(t_i(\hat{y}_i) - T_i^0\right) \tag{9}$$

$$\Delta L_i(\hat{y}_i) = L_i - a_i\left(t_i(\hat{y}_i) - T_i^0\right)^+ \tag{10}$$

$$d_i(\hat{y}_i) \leq x_i \tag{11}$$

$$c_i(t_i(\hat{y}_i)) \leq C_i^{\max} \tag{12}$$

$$\hat{y}_i = \left(\hat{y}_{i1}, \hat{y}_{i2}, \ldots, \hat{y}_{iJ_i}\right) \tag{13}$$

$$\hat{y}_{ij} \in \left\{1, 2, \ldots, Y_{ij}\right\}. \tag{14}$$

Formula (7) indicates that the objective of predicted base-level is to maximize agent's benefit. Formula (8) indicates chance constraint. Formula (9) indicates the reward and penalty function based on the duration. Formula (10) indicates the saved risk loss of subproject; the operation $(x)^+$ is defined as

$$(x)^+ = \begin{cases} x, & x > 0, \\ 0, & \text{else}. \end{cases} \tag{15}$$

Formula (11) indicates that the sum of used risk management capital is not greater than the risk management capital which is allocated to subproject; formula (13) represents a set of the predicted base-level variables; formula (14) represents the value range of $\hat{y}_{ij}$ that is the decision variable in the predicted base-level model.

2.3.3. Real Base-Level. In the real base-level, the decision makers are the agents, and there are I agents. Take agent i, for example.

Variable Definition

y_i: the actual combination of risk management measure of subproject i

a_i: risk loss per unit of subproject i

$\Delta L_i(y_i)$: actual saved risk loss of subproject i

$t_i(y_i)$: actual duration of subproject i

$h_i(y_i)$: actual reward and penalty function of subproject i

$d_i(y_i)$: actual invested risk management capital of subproject i

$c_i(t_i(y_i))$: actual cost of subproject i.

$$B_i\left(x_i^*, y_i\right) = \max \quad b_i \Delta L_i\left(y_i\right) - c_i\left(t_i\left(y_i\right)\right) x_i^* - d_i\left(y_i\right) - h_i\left(y_i\right) \tag{16}$$

$$\text{s.t.} \quad h_i\left(y_i\right) = q_i\left(t_i\left(y_i\right) - T_i^0\right) \tag{17}$$

$$\Delta L_i\left(y_i\right) = L_i - a_i\left(t_i\left(y_i\right) - T_i^0\right)^+ \tag{18}$$

$$d_i\left(y_i\right) \le x_i^* \tag{19}$$

$$c_i\left(t_i\left(y_i\right)\right) \le C_i^{\max} \tag{20}$$

$$y_i = \left(y_{i1}, y_{i2}, \ldots, y_{iJ_i}\right) \tag{21}$$

$$y_{ij} \in \left\{1, 2, \ldots, Y_{ij}\right\}. \tag{22}$$

Formula (16) indicates that the objective of real base-level is to maximize agent's benefit; formula (17) indicates the reward and penalty function based on the duration; formula (18) indicates the saved risk loss of subproject; formula (19) indicates that the sum of used risk management capital is not greater than the risk management capital which is allocated to subproject; formula (20) represents the cost that should not be beyond the upper bound of cost for subproject i; formula (21) represents a set of the real base-level variables; formula (22) represents the value range of y_{ij} that is the decision variable in the real base-level model.

3. Algorithm Design

The top-level model is an integer programming problem, and the base-level model (including the predicted base-level model) is a combinatorial optimization problem. The whole problem is a NP hard problem, because the base-level is embedded in the top-level. So, we use genetic algorithm (GA) to solve the problem in this paper. It is well known that GA that was first introduced by Holland is very effective for solving combinatorial optimization problems. For example, GA has been successfully applied in solving traveling salesman problem, knapsack problem, bin packing problem, and so on. However, the disadvantage of GA is that the local search capability is not strong [29–33]. Simulated annealing (SA) is a general random search algorithm, which is an extension of the local search algorithm [34–37]. Considering the strong local search capability of SA, we designed a hybrid algorithm named simulated annealing genetic algorithm (SAGA) by combining simulated SA with GA.

The overall thought of SAGA is simple. Firstly, some initial solutions of GA are generated randomly. After a period of iteration, some superior solutions are produced. Then, sort the corresponding fitness value of these superior solutions in descending order. And then select the solutions in top 10% as the initial solutions of SA. We try to find the best solution of the proposed problem around these superior solutions. For the random variables of the predicted base-level model, we embed Monte Carlo Simulation in SAGA.

3.1. Encoding Scheme. In top-level, each chromosome represented by real number is a combination of risk management capital and the length of chromosome represents the number of agents. The top-level encoding scheme of SAGA is shown in Figure 5. We can see that there are 4 agents, and \$580.2 is allocated to agent 1; \$600.9 is allocated to agent 2; the rest can be done in the same manner.

In base-level, each chromosome represented by real number is a combination of risk management capital and the length of chromosome represents the number of the activities on the critical path. Take the base-level encoding scheme shown in Figure 6 as example; it can be seen that there are 5 activities on the critical path, and measure 2 is used to manage the risk of activity 1, measure 4 is used to manage the risk of activity 2, and so on.

3.2. Population Initialization. Initial population is generated randomly. Punishment strategy is adopted to deal with the constraints, so we do not have to judge whether the initial solution meets the constraint conditions.

3.3. Fitness Function. Considering the proposed optimization problems with constraints, we set up a fitness function with punishment term to evaluate individuals. The top-level fitness function is given as

$$F_T = f_T - \sum_{i=1}^{I}\left(\alpha_i\left(B_i\left(x_i, \widehat{y}_i\right) - \mathrm{AL}_i\right)\right) - \beta\left(\sum_{i=1}^{I} x_i - X^{\max}\right), \tag{23}$$

where

$$f_T = \sum_{i=1}^{I} b_i \Delta L_i\left(\widehat{y}_i\right) - x_i + h_i\left(\widehat{y}_i\right) - e_i\left(t_i\left(\widehat{y}_i\right) - T_i^0\right)^-. \tag{24}$$

Function (24) is top-level objective function; α_i and β are punishment coefficients, respectively.

Agent	1	2	3	4
Capital	580.2	600.9	643.7	576

Figure 5: The top-level encoding scheme of SAGA.

Activity	1	2	3	4	5
Measure	2	4	2	3	1

Figure 6: The base-level encoding scheme of SAGA.

The base-level fitness function is given as

$$F_{Bi} = f_{Bi} - \gamma_i \left(d_i\left(y_i\right) - x_i^*\right)^+ - \delta_i \left(c_i\left(t_i\left(y_i\right)\right) - C_i^{\max}\right)^+, \quad (25)$$

where

$$f_{Bi} = b_i \Delta L_i\left(y_i\right) - c_i\left(t_i\left(y_i\right)\right) + x_i^* - d_i\left(y_i\right) - h_i\left(y_i\right). \quad (26)$$

Function (25) is base-level objective function; γ_i and δ_i are punishment coefficients, respectively.

The Monte Carlo Simulation method is used to deal with the random variable [37–40]. The process of calculating the fitness of the predicted base-level model by Monte Carlo Simulation is shown as follows.

Step 1. Set Q' is equal to $[\alpha_i Q]$; Q is sampling number.

Step 2. Samples $\xi_i^1, \xi_i^2, \ldots, \xi_i^Q$ are generated by normal distribution function $N(a_i, 0.01)$.

Step 3. Calculate F_{Bi}^t that is the fitness value of the predicted base-level model by formula (26), $t = 1, 2, \ldots, Q$.

Step 4. The Q'th biggest element of $\{F_{Bi}^t, F_{Bi}^t, \ldots, F_{Bi}^t\}$ can be used as the fitness value of the ith predicted base-level model, which can be seen by the law of large numbers.

3.4. Selection. This paper takes proportional selection strategy [41, 42]. For each individual, the probability of being selected is the proportion of its fitness to the sum of all individuals' fitness. Then, the probability of selected individual I is given by

$$P_i = \frac{F_i}{\sum_{i=1}^{NP} F_i}, \quad (27)$$

where F_i is the fitness of individual i and NP is the population size. Here, we adopt well-known Roulette Wheel scheme. In order to prevent the best individual in each generation from being destroyed, elite-preservation strategy is also used. That is to say, the best individual of each generation directly becomes one of individuals in the next generation without crossover and mutation operation.

3.5. Crossover. Double-point crossover is adopted in this paper, which is beneficial for keeping excellent individual. Figure 7 shows the example of the double-point crossover operator, where $P_1 = (1, 3, 3, 2, 4)$ and $P_2 = (2, 2, 5, 1, 3)$ are parent chromosomes. So, the generated children chromosomes are $C_1 = (1, 2, 5, 1, 4)$ and $C_2 = (2, 3, 3, 2, 3)$.

3.6. Mutation. Reversal mutation is adopted in this paper [35]. Under the condition of satisfying the mutation rate, randomly select two points in the parent and sort the genes between these two points in reverse order. The reversal mutation operator of SAGA is shown in Figure 8. Parent chromosome $P = (1, 4, 2, 3, 1)$ is selected for mutation operation. And the generated children chromosome is $P' = (1, 2, 4, 3, 1)$.

3.7. Neighborhood Definition. The bit x_i is selected from the current state $x = [x_1, x_2, \ldots, x_m]$, and the value of x_i is changed in the range of its value. So, a neighborhood solution is generated.

3.8. Neighborhood Movement. The Metropolis criterion is adopted in this paper. If the objective value of neighborhood solution is smaller than the current solution's objective value, the current solution is replaced by the neighborhood solution. Otherwise, the current solution moves according to a certain probability.

3.9. Thermal Equilibrium. Thermal equilibrium is achieved when the preset number of internal loop is reached.

3.10. Cooling Rule. Reduce T_k by multiplying a number r, which is in the range $[0, 1]$ and close to 1. Cooling rule is shown as

$$T_{k+1} = T_k, \quad (28)$$

where T_k is the current temperature, T_0 is initial temperature, k is the iterative index, and $r \in (0.95, 0.99)$.

3.11. Procedure of SAGA. The flow chart of SAGA is shown in Figure 9. The process of the SAGA is made up of two parts, GA and SA. In Figure 9, the left part is the process of GA; GA

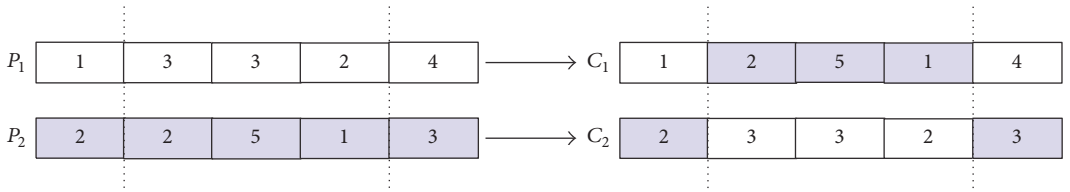

Figure 7: The double-point crossover operator of SAGA.

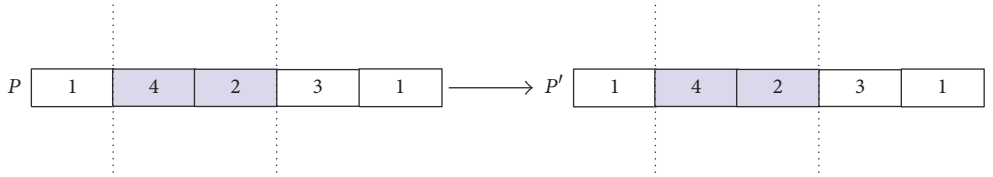

Figure 8: The reversal variation operator of SAGA.

is used firstly to find a good solution of the problem. To cover the defect of GA on the local area search, SA is used to find an optimal solution around the "good solution" find by GA. The process of SA is shown on the right part of the figure. After the local search of SA, the proposed algorithm ended.

4. Numerical Examples

4.1. Example 1. Take the IT outsourcing project including 1 principal and 1 agent ($I = 1$) for an example. The principal outsources the whole project to the agent. Schedule risk is reflected by duration and risk loss of project. It is assumed that if the project is completed before planned duration, there will be no risk loss. On the contrary, the project will lose \$80 per day; namely, $a_1 = 80$. Due to the information asymmetry, the agent is clear for parameter a_1, but the principal only knows its distribution function, which is approximated as $N(80, 0.01)$. The planned duration of project T_1^0 is 400, the initial duration of project T_1 is 500, and the initial duration of activities t_{1j}^0 is $\{55, 60, 65, 70, 75, 80, 95\}$. The profit sharing coefficient of principal b_1 is 0.51, the expected profit of agent AL_1 is 2000, and confidence level α is 0.9.

There is an initial schedule risk, which can be seen from the parameters of duration. The principal prepares \$900 to manage schedule risk, $X^{\max} = 900$. The project consists of 7 activities, $J_1 = 7$. There are 10 available risk management measures for each activity, $Y_{1j} = 10$, $j \in \{1, 2, \ldots, 7\}$. It is assumed that the agent must choose a numbered measure for each activity and that the selected numbered measure can be selected multiple times.

Risk management measure is the only variable that affects the duration and risk loss of project, which can be seen from the proposed model. It is assumed that the impact of risk management measure on the project is enhanced with the increase of the number of measures. For example, for an activity, the implementation of measure 7 will result in a shorter duration and a smaller risk loss than the implementation of measure 2. So, the monotonic decreasing function is used to represent the duration function that is shown in formula (29), and risk loss function is shown in formula (30), respectively,

$$t_1(y_1) = \sum_{j=1}^{J_1} t_{1j}^0 \exp\left(-y_{1j}\sigma_{1j}\right), \tag{29}$$

$$L_1(y_1) = a_1\left(t_1(\widehat{y}_1) - T_1^0\right)^+, \tag{30}$$

where σ_{1j} is control parameter, which is used to represent that a management measure has different effects on different activities. The saved risk loss of project is shown as follows:

$$\Delta L_1(y_1) = a_1\left(T_1 - T_1^0\right) - L_1(y_1). \tag{31}$$

If the project can be completed before the planned duration, the principal will obtain additional profit. It is assumed that the additional profit e_1 is \$25 per time unit. So, the reward and punishment function about duration is shown in formula (32), which is designed by the principal

$$h_1(y_1) = q_1\left(t_1(y_1) - T_1^0\right). \tag{32}$$

It is assumed that the reward and punishment parameter q_1 is \$21. If the subproject is completed in advance, the agent can get \$21 per day; otherwise, he will lose \$21 per day.

4.1.1. The Parameters of SAGA. The parameters of SAGA mainly include population size (NP), maximum generations (NG), crossover rate (Pc), mutation rate (Pm), initial temperature (Ti), termination temperature (Ts), and internal loop number (Ni). The parameters have a significant impact on the performance of algorithm. For example, big population size may lead to slower convergence speed but can avoid suboptimal solution. Small population size may lead to premature but can ensure the quick speed of convergence.

In this paper, NG is determined by

$$NG = \frac{1500}{NP}. \tag{33}$$

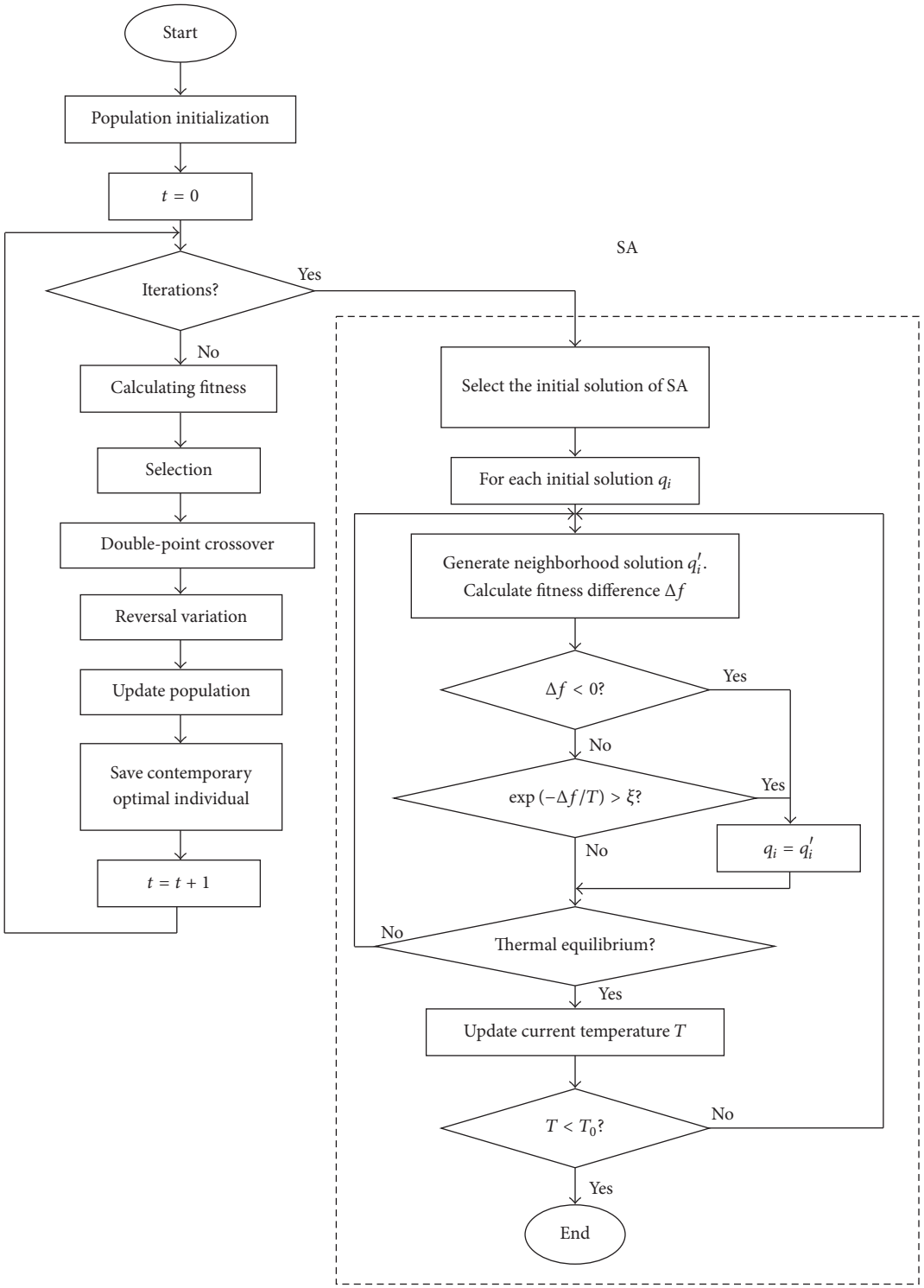

Figure 9: The flow chart of SAGA.

Generally, Ts is a smaller positive number; let $Ts = 1$ here. So, we only need to test the other 5 parameters with the following method.

(1) Provide two values for each parameter. One is relatively small, and the other is relatively big.

(2) For each combination of parameter, run algorithm 20 times. There are 2^5 combinations.

(3) The final parameter combination is the one with best average fitness value.

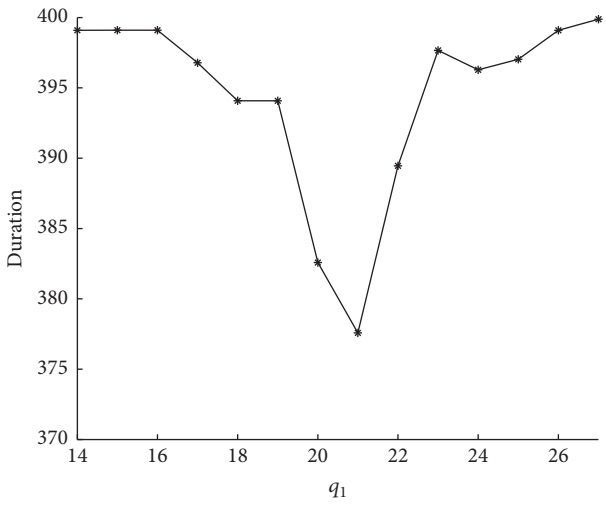

Figure 10: The influence of q_1 on duration.

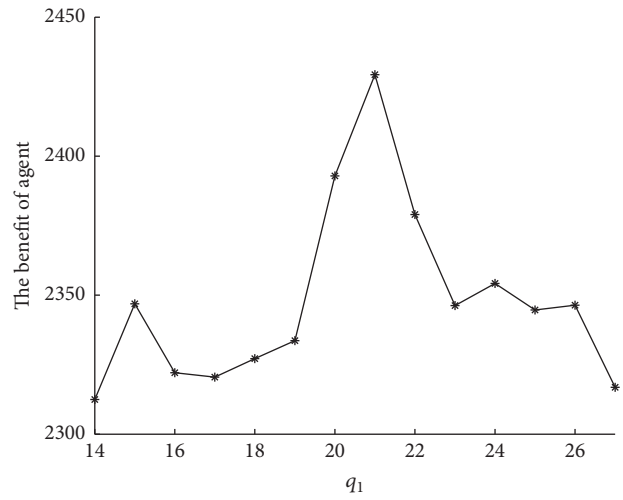

Figure 11: The influence of q_1 on the profit of agent.

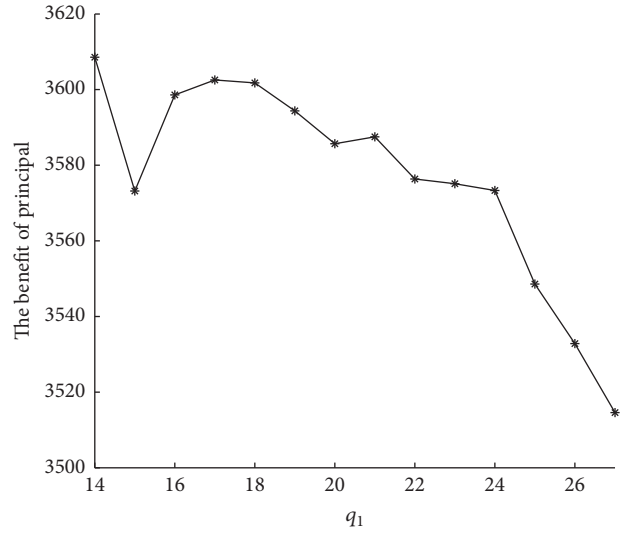

Figure 12: The influence of q_1 on the profit of principal.

The testing process is shown in Table 1. The final combination is {30, 50, 0.6, 0.1, 100, 10}.

4.1.2. Simulation Results. The simulation results of example 1 are shown in Table 2. For real results, agent is allocated \$597 and he selects measures 2 1 10 1 10 10 10 to manage risk. After that, the duration of project is reduced from 500 days to 377.41 days; that is to say, the project is completed in advance. For index duration and risk loss, the schedule risk of IT outsourcing project has been well managed.

It can be seen that the predicted results and real results are different, such as profit of principal, because there is information asymmetry between principal and agent, and the principal's prediction is not completely correct in the real situation, which always plays an important role in the process of schedule risk management. If there is no prediction, the whole project would be completely out of control; the effect of schedule risk management will be worse than it is now.

4.1.3. Model Comparison. Model I refers to the proposed model in Section 2.3; Model II is the one in which there is no reward and punishment item. Model I is Model II, when the parameter $q_1 = 0$. For the simulation results in Table 3, from index 3 to 8, Model I is better than Model II. Therefore, it is significant to join the reward and punishment mechanism in the model.

4.1.4. The Parameter of Reward and Punishment Mechanism. If parameter q_1 is not set reasonably, the reward and punishment will not really play its role. Therefore, the effect of the parameter q_1 is tested on the proposed model. The test results are shown in Table 4. The influence of q_1 on the duration, the profit of agent, and the profit of principal are shown in Figures 10–12, respectively.

We can get some information from Table 4 and Figures 10–12. When $q_1 \leq c_1 = 16$ where c_1 is additional cost per day due to duration reduction, total risk loss is saved, but duration is not significantly reduced compared to the planned duration. The reason for the above phenomenon is that the agent will not make efforts to shorten duration, if the reward is not greater than the cost because of duration reduction. When $q_1 \geq e_1 = 25$, the reward of agent is greater than the additional profit of principal due to shorting duration, resulting in the decline of principal's profit. Obviously, this is not acceptable to the principal. So, we must determine the specific value of q_1 in the interval (c_1, e_1) based on the 4 indexes: duration, saved risk loss, profit of agent, and profit of principal. Considering managing the schedule risk of IT outsourcing project, we set q_1 to be 21. Finally, the way for setting the reward and punishment mechanism's parameter is summarized as follows.

(1) Set the two values c and e, $c < e$.

(2) Determine the specific value of q_1 in the interval $[c, e]$ based on the 4 indexes: duration, recovered risk loss, profit of agent, and profit of principal.

Table 1: The parameters of SAGA.

NP	*NG*	*Pc*	*Pm*	*Ti*	*Ni*	Fitness
30	50	0.9	0.1	130	20	2417.8
30	50	0.9	0.1	130	10	2352.3
30	50	0.9	0.1	100	20	2344.9
30	50	0.9	0.1	100	10	2327.5
30	50	0.9	0.01	130	20	2417.3
30	50	0.9	0.01	130	10	2407.6
30	50	0.9	0.01	100	20	2327.9
30	50	0.9	0.01	100	10	2423.4
30	50	0.6	0.1	130	20	2334.8
30	50	0.6	0.1	130	10	2338.3
30	50	0.6	0.1	100	20	2348.7
30	**50**	**0.6**	**0.1**	**100**	**10**	**2441.1**
30	50	0.6	0.01	130	20	2417.4
30	50	0.6	0.01	130	10	2339.2
30	50	0.6	0.01	100	20	2326.3
30	50	0.6	0.01	100	10	2404.1
50	30	0.9	0.1	130	20	2319.5
50	30	0.9	0.1	130	10	2408.2
50	30	0.9	0.1	100	20	2328.6
50	30	0.9	0.1	100	10	2328.2
50	30	0.9	0.01	130	20	2402.0
50	30	0.9	0.01	130	10	2316.8
50	30	0.9	0.01	100	20	2322.8
50	30	0.9	0.01	100	10	2317.0
50	30	0.6	0.1	130	20	2394.7
50	30	0.6	0.1	130	10	2396.3
50	30	0.6	0.1	100	20	2324.5
50	30	0.6	0.1	100	10	2326.3
50	30	0.6	0.01	130	20	2361.7
50	30	0.6	0.01	130	10	2319.3
50	30	0.6	0.01	100	20	2367.9
50	30	0.6	0.01	100	10	2321.6

Table 2: The simulation results of example 1.

Index	Predicted results	Real results
Allocated capital	597	597
Measure combination	1 10 1 1 9 10 10	2 1 10 1 10 10 10
Duration	380.52	377.41
Finish the project before planned duration	Y	Y
Saved risk loss	7985.6	8000
Save total risk loss?	Y	Y
Profit of agent	2430.69	2440.50
Profit of principal	3565.15	3564.98

4.1.5. Performance Comparison of Algorithms. In this paper, we use three algorithms, SA, GA, and SAGA to carry out the simulation calculation for the proposed model. The simulation results are compared in Table 5. Focusing on indexes, duration, finishing the project before planned duration, saved risk loss, total risk loss saved, profit of agent, and profit of principal, the conclusion can be drawn that SAGA is better than GA and SA

The convergence process of 3 algorithms in example 1 is shown in Figure 13. For convergent speed, SA achieves its

Table 3: The model comparison of example 1.

Index	Mode I	Model II
Allocated capital	597	502
Measure combination	2 1 10 1 10 10 10	2 1 1 9 1 10 10
Duration	377.41	400.98
Finish the project before planned duration	Y	N
Saved risk loss	8000	7921.60
Save total risk loss?	Y	N
Profit of agent	2440.50	2306.76
Profit of principal	3564.98	3532.84

Table 4: The effect of q_1 on the model.

q_1	Duration	Saved risk loss	Profit of agent	Profit of principal
14	399.09	8000	2312.44	3608.55
15	399.10	8000	2346.89	3573.18
16	399.10	8000	2322.08	3598.58
17	396.78	8000	2320.52	3602.54
18	394.08	8000	2327.17	3601.78
19	394.08	8000	2333.63	3594.37
20	382.58	8000	2392.89	3585.67
21	**377.58**	**8000**	**2429.31**	**3587.50**
22	389.46	8000	2379.02	3576.35
23	397.96	8000	2346.25	3575.10
24	396.28	8000	2354.21	3573.32
25	397.03	8000	2344.66	3548.59
26	399.09	8000	2346.40	3532.84
27	399.88	8000	2316.86	3514.58

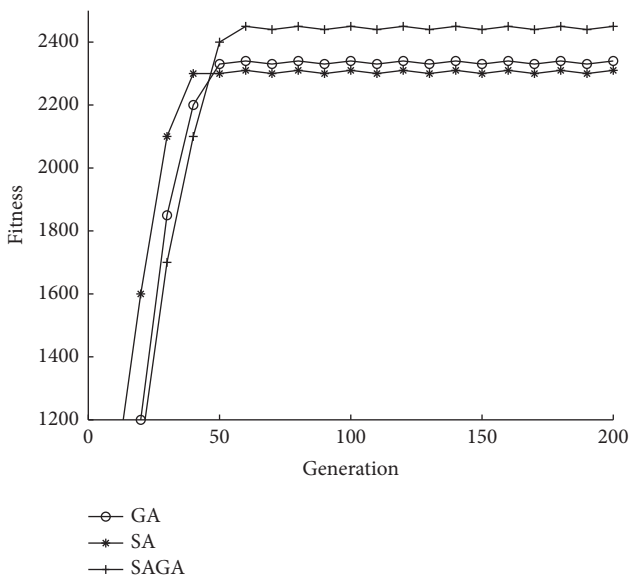

Figure 13: The convergence process of the three algorithms in example 1.

convergence after about 40 iterations; GA and SAGA need about 50 iterations. So, the convergence speed of the three algorithms is near. However, considering the fitness from the three algorithms, it is easy to see that SAGA finds the best solution, among the three algorithms. Therefore, SAGA is the best choice for the problem in example 1.

4.2. Example 2, 3, and 4. In this section, further examples 2, 3, and 4 are given in this section to test the performance of SAGA. The values of the main parameters for models in the three examples are shown in Table 6, and the values of others parameters are the same to example 1.

4.2.1. The Parameters of SAGA. According to the method of parameters setting in example 1, the parameters combination of SAGA for example 2, 3, and 4 is shown in Table 7.

4.2.2. Simulation Results. The simulation results of examples 2 and 3 are shown in Tables 8 and 9, respectively. The comprehensive results of example 4 are not shown in this section, for its large amount of data, but a part of selected results is used to analyze the algorithm in the next section.

For real results of example 3, the principal allocates \$682, \$579, \$579, \$649, \$609, \$579, \$689, \$689, \$617, and \$646 to 10 agents, respectively. The agents select the measure combination shown in table to manage risk. After that, the duration of projects is reduced from 500 days to 391.4, 400.1,

Table 5: The comparison of three algorithms.

Index	GA	SA	SAGA
Allocated capital	542	556	597
Measure combination	1 2 9 1 5 10 7	1 2 1 1 9 10 10	2 1 10 1 10 10 10
Duration	399.76	400.07	377.41
Finish the project before planned duration?	Y	N	Y
Saved risk loss	8000	7943.24	8000
Save total risk loss?	Y	N	Y
Profit of agent	2325.04	2313.29	2440.50
Profit of principal	3540.89	3515.23	3564.98

Table 6: The model parameters of examples 2, 3, and 4.

Example	Principal's number	Agent's number	Activity's number	Measure's number	Risk management capital
2	1	5	7	10	3500
3	1	10	7	10	7000
4	1	25	7	10	17500

400.1, 384.7, 397.1, 397.1, 384.7, 368.5, 386.4, and 379. days, and total risk loss is saved except for subprojects 2 and 3. For the two indexes of duration and risk loss, the schedule risk of IT outsourcing project has been well managed.

We can see that the predicted results and real results are different, such as profit of agent, because there is information asymmetry between principal and agent, and the principal's prediction is not completely correct in the real situation, which always plays an important role in the process of schedule risk management. But if there is no prediction, the whole project would be completely out of control; the effect of schedule risk management will be worse than it is now.

4.2.3. Performance Comparison of Algorithms. Examples 2, 3, and 4 are solved by GA, SA, and the SAGA designed in this paper to give a further test of the performance of SAGA. The convergence process of three algorithms in examples 2, 3, and 4 is shown in Figures 14–16, respectively. In these three examples, SAGA performs better than the other two algorithms in terms of convergent speed and the best fitness value. Therefore, SAGA is the best choice for the problem in examples 2, 3, and 4.

In addition, for each example, run the 3 algorithms 20 times to collect some statistics information, including maximum fitness (Max), minimum fitness (Min), average fitness (Aver), and fitness variance (Var), which is processed using the normalization method. The statistics information is shown in Table 10, where Na represents the number of agents, B represents risk management capital, A represents algorithms, ΔA represents the average fitness increasing ratio of SAGA relative to other two algorithms, and ΔV represents the difference of fitness variance between SAGA and two other algorithms.

The convergent degree of algorithm is shown by the average fitness, and the reliability of algorithm is shown by the fitness variance. The conclusion that the SAGA designed in this paper shows a certain advantages in each example can be seen from the table. With the increase of the problem scale, the convergence and reliability of SAGA are also compared with GA and SA in Figures 17 and 18, respectively. It can be seen that SAGA performs better than GA and SA on convergence and reliability, especially for the large scale problem.

Besides convergence and reliability, the running time of the algorithm is also an important index to measure the performance of the algorithm. Running time is greatly influenced by the experimental environment. The experimental environment in this experiment: software conditions: Windows 7, hardware conditions: DELL Optiplex 9020 +i7 Core, and development tools: Eclipse. Figure 19 shows the running time of the three algorithms for the four examples. From the Figure 19, it can be seen that when the problem scale is relatively small, the running time of the three algorithms is almost equal. When the scale of the problem is larger, for examples 3 and 4, the running time of SAGA is significantly longer than that of GA and SA, because SAGA takes more time to operate its complex searching process. It also can be seen that the running time of the three algorithms is always in the same order of magnitude for each case. Therefore, the running time of SAGA is acceptable.

5. Conclusion

This paper focuses on the schedule risk of IT outsourcing project, the DDM theory and principal-agent theory are applied to build a two-level principal-agent schedule risk management model for IT outsourcing project, and the SAGA is also designed to solve the resulting optimization problem. The simulation results illustrate that the model

Table 7: Parameters setting of SAGA for examples 2, 3, and 4.

Example	*NP*	*NG*	*Pc*	*Pm*	*Ti*	*Ni*
2	40	80	0.9	0.1	150	10
3	50	100	0.9	0.1	150	20
4	50	120	0.9	0.01	200	10

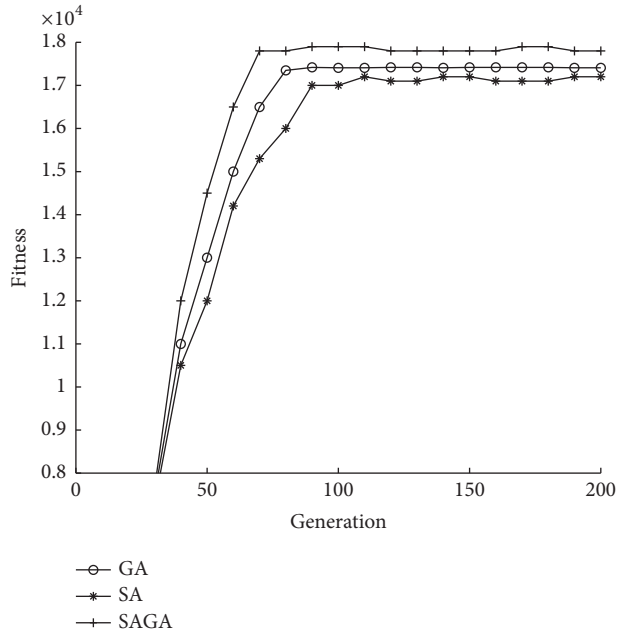

Figure 14: The convergence process of the three algorithms in example 2.

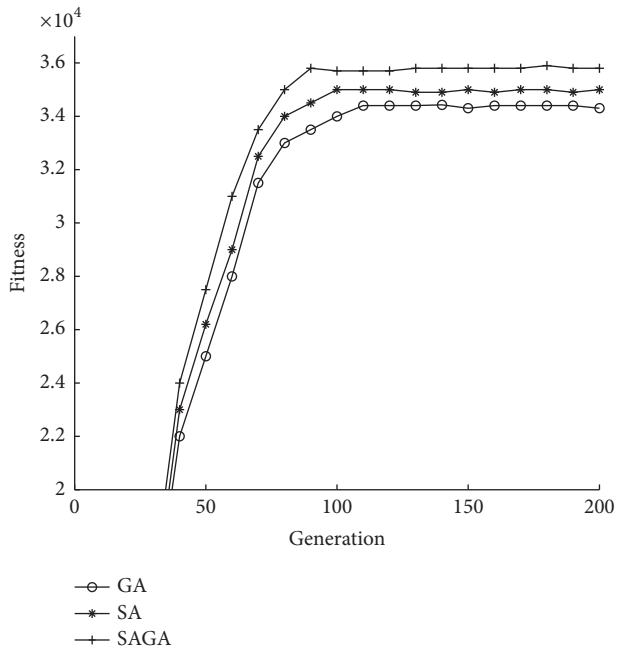

Figure 15: The convergence process of the three algorithms in example 3.

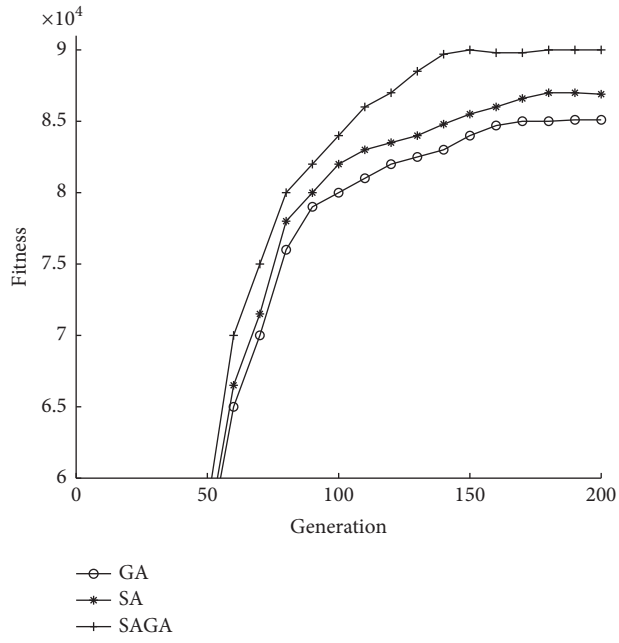

Figure 16: The convergence process of the three algorithms in example 4.

Table 8: The simulation results of example 2.

Index	Predicted results	Real results
Allocated capital	696 625 693 679 686	696 625 693 679 686
Measure combination	4 5 2 10 10 8 10 4 5 2 9 6 2 10 3 8 10 1 10 9 8 9 1 10 1 1 10 10 2 1 10 9 8 9 10	1 2 6 10 6 9 9 9 3 7 3 9 3 3 7 3 7 7 9 7 3 7 3 7 7 9 3 7 3 3 7 7 9 7 3
Duration	365.1 393.7 369.2 388.5 364.7	377.9 404.5 386.5 384.1 393.7
Finish the project before planned duration?	Y YYYY	Y N Y YY
Saved risk loss	7990.4 7988.4 7986.8 7987.5 7984.9	8000 7637.9 8000 8000 8000
Save total risk loss?	Y YYYY	Y N Y YY
Profit of agent	2494.6 2376.5 2482.9 2488.6 2505.2	2494.6 2150.6 2411.7 2409.7 2411.0
Profit of principal	17864.6	17762.6

Table 9: The simulation results of example 3.

Index	Predicted results	Real results
Allocated capital	682 579 579 646 609 579 689 689 617 646	682 579 579 646 609 579 689 689 617 646
Measure combination	9 1 9 2 10 10 10 10 2 1 9 1 7 9 1 2 6 7 9 3 8 5 10 2 5 10 2 10 2 6 2 2 9 9 9 1 3 6 1 8 9 9 8 4 1 10 7 10 10 1 10 10 1 10 8 9 1 3 7 1 10 10 8 8 2 1 8 10 9 7	3 1 6 3 10 8 7 4 3 10 4 1 5 9 1 3 10 4 9 5 4 1 3 10 4 9 5 9 1 3 10 4 4 5 9 1 3 10 4 4 5 9 1 3 10 4 9 5 9 1 3 10 10 9 5 10 1 1 10 4 9 5 10 1 3 10 4 10 5 10
Duration	364.0 394.9 396.6 382.5 388.3 392.4 364.8 369.3 386.5 377.7	391.4 400.1 400.1 384.7 397.1 397.1 384.7 368.5 386.4 379.7
Finish the project before planned duration?	Y YYYY Y YYYY	Y N N Y Y Y YYYY
Saved risk loss	7986.9 7988.9 7983.4 7989.5 7985.6 7988.7 7989.0 7988.0 7984.2 7986.2	8000 7998.5 7925.1 8000 8000 8000 8000 8000 8000 8000
Save total risk loss?	Y YYYY Y YYYY	Y N N Y Y Y YYYY
Profit of agent	2497.9 2355.7 2333.5 2413.4 2389.2 2367.6 2490.7 2502.1 2415.9 2424.9	2451.1 2327.9 2279.9 2424.7 2366.7 2336.7 2467.7 2498.7 2418.4 2441.3
Profit of principal	35750.6	35707.7

Table 10: The comparison of algorithms' performance.

Example	Na	B	A	Max	Min	Aver	ΔA (%)	Var	ΔV
1	1	700	GA	2350.2	2300.8	2328.6	3.7	0.562	−0.39
1	1	700	SA	2380.7	2315.6	2344.0	2.9	0.264	−0.09
1	1	700	SAGA	2465.5	2400.2	2413.6	0	0.174	0
2	5	3500	GA	17726.1	17001.3	17419.6	2.1	0.657	−0.51
2	5	3500	SA	17466.0	17180.7	17353.8	2.5	0.196	−0.05
2	5	3500	SAGA	17911.0	17637.0	17787.3	0	0.147	0
3	10	7000	GA	35012.0	33567.9	34347.1	4.0	0.869	−0.85
3	10	7000	SA	35230.5	34616.1	35048.2	2.0	0.109	−0.09
3	10	7000	SAGA	35828.3	35546.4	35713.9	0	0.022	0
4	25	17500	GA	85000.4	84250.2	84706.0	6.1	0.399	−0.31
4	25	17500	SA	87526.4	86815.3	87236.5	2.7	0.509	−0.42
4	25	17500	SAGA	90006.3	89639.1	89860.5	0	0.092	0

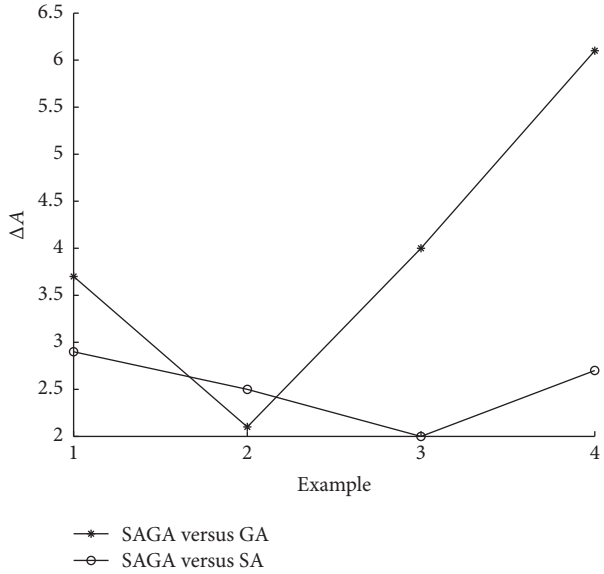

Figure 17: The convergence advantage change graph of SAGA.

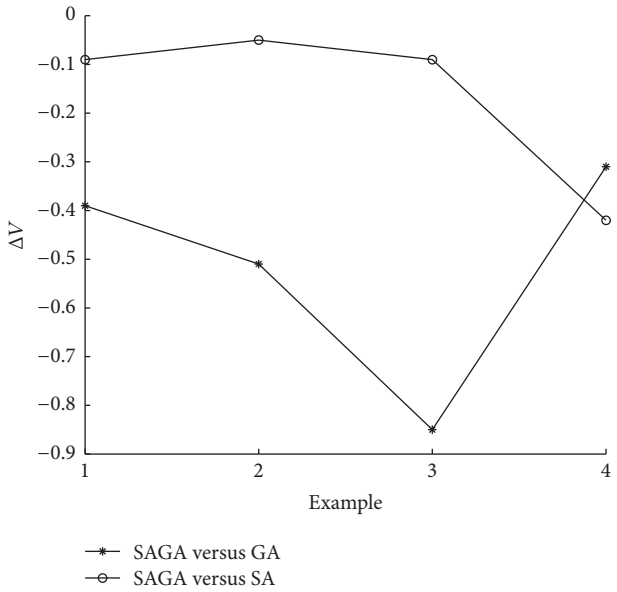

Figure 18: The stability advantage change graph of SAGA.

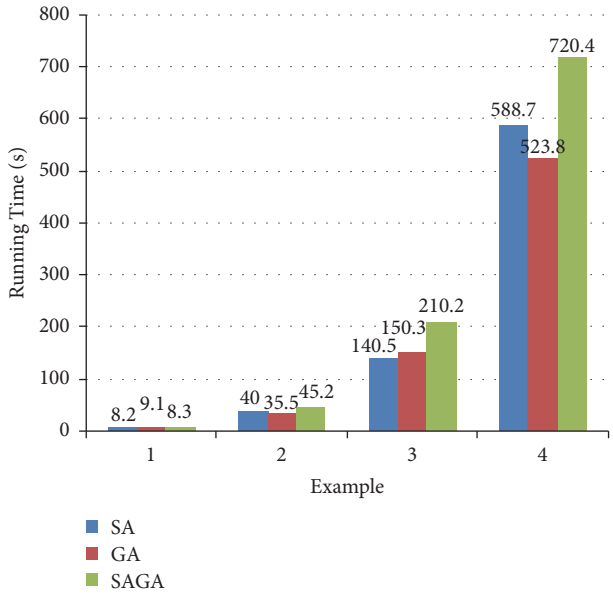

Figure 19: The running time comparison of the three algorithms.

can greatly reduce the risk loss and the duration of IT outsourcing project, which achieves the goal of managing the schedule risk effectively. In addition, the proposed SAGA is a greatly improved method, which can effectively solve the described problem comparing with the other two algorithms. Consequently, the above model and algorithm can provide important decision support for managing the schedule risk of IT outsourcing project.

Conflicts of Interest

The authors declare that the funding in Acknowledgments did not lead to any conflicts of interest regarding the publication of this manuscript.

Acknowledgments

This work is supported by the National Science Foundation for Distinguished Young Scholars of China under Grant no. 71325002; Major International Joint Research Project of NSFC under Grant no. 71620107003; the National Natural Science Foundation of China under Grant no. 71401027; Natural Science Foundation of Hebei Province under Grant no. G2016501086; Key Project of Science and Technology Research of Higher Education in Hebei Province under Grant no. ZD2016202.

References

[1] M. C. Lacity, S. A. Khan, and L. P. Willcocks, "A review of the IT outsourcing literature: Insights for practice," *Journal of Strategic Information Systems*, vol. 18, no. 3, pp. 130–146, 2009.

[2] Z. P. Fan, W. Suo, and B. Feng, "Identifying risk factors of IT outsourcing using interdependent information: an extended DEMATEL method," *Expert Systems with Applications*, vol. 39, no. 3, pp. 3832–3840, 2012.

[3] B. Bahli and S. Rivard, "Validating measures of information technology outsourcing risk factors," *Omega*, vol. 33, no. 2, pp. 175–187, 2005.

[4] K. Huang, "Research on risk early-warning of information technology outsoucing project based on neural network," *Applied Mechanics and Materials*, vol. 411-414, pp. 2400–2405, 2013.

[5] Gartner, *Gartner says worldwide IT spending on pace to grow 2.1 percent in 2014*, Press release, Stamford, CT, USA, 2014.

[6] R. Kliem, "Managing the risks of offshore It development projects," *Information Systems Management*, vol. 21, no. 3, pp. 22–27, 2004.

[7] L. M. Abdullah and J. M. Verner, "Analysis and application of an outsourcing risk framework," *Journal of Systems and Software*, vol. 85, no. 8, pp. 1930–1952, 2012.

[8] M. Alexandrova, "Risk Factors in IT Outsourcing Partnerships: Vendors' Perspective," *Global Business Review*, vol. 16, no. 5, pp. 747–759, 2015.

[9] C. Samantra, S. Datta, and S. S. Mahapatra, "Risk assessment in IT outsourcing using fuzzy decision-making approach: An Indian perspective," *Expert Systems with Applications*, vol. 41, no. 8, pp. 4010–4022, 2014.

[10] H. Samadi, S. Nazari-Shirkouhi, and A. Keramati, "Identifying and analyzing risks and responses for risk management in information technology outsourcing projects under fuzzy environment," *International Journal of Information Technology and Decision Making*, vol. 13, no. 6, pp. 1283–1323, 2014.

[11] L. Qin, H. Wu, N. Zhang, and X. Li, "Risk identification and conduction model for financial institution IT outsourcing in China," *Information Technology and Management*, vol. 13, no. 4, pp. 429–443, 2012.

[12] X. Huang, T. Zhao, and S. Kudratova, "Uncertain mean-variance and mean-semivariance models for optimal project selection and scheduling," *Knowledge-Based Systems*, vol. 93, pp. 1–11, 2016.

[13] M. Earl, "The risks of outsourcing IT [J]," *Sloan Management Review*, vol. 37, no. 3, pp. 26–32, 1996.

[14] B. W. Boehm, "Software Risk Management: Principles and Practices," *IEEE Software*, vol. 8, no. 1, pp. 32–41, 1991.

[15] L. Wang, C. Fang, C.-D. Mu, and M. Liu, "A pareto-archived estimation-of-distribution algorithm for multiobjective resource-constrained project scheduling problem," *IEEE Transactions on Engineering Management*, vol. 60, no. 3, pp. 617–626, 2013.

[16] B. W. Boehm, "Software risk management," *IEEE Software*, vol. 14, no. 3, pp. 1–19, 1989.

[17] B. Aubert, S. Dussault, M. Patry, and S. Rivard, "Managing the risk of IT outsourcing," in *Proceedings of the HICSS 32 - 32nd Annual Hawaii International Conference on System Sciences*, p. 10, Maui, HI, USA.

[18] B. A. Aubert, S. Dussault et al., "Assessing IT outsourcing risk," in *Proceedings of the 31nd Hawaii International Conference on System Sciences*, Maui, HI, USA, 1998.

[19] B. A. Aubert, S. Dussault, M. Patry et al., "outsourcing risk management at British Petroleum," in *Proceedings of the 34nd Hawaii International Conference on System Science*, Maui, HI, USA, 2001.

[20] B. Bahli and S. Rivard, "The information technology outsourcing risk: a transaction cost and agency theory-based perspective," *Journal of Information Technology*, vol. 18, no. 3, pp. 211–221, 2003.

[21] K. Osei-Bryson and O. K. Ngwenyama, "Managing risks in information systems outsourcing: an approach to analyzing outsourcing risks and structuring incentive contracts," *European Journal of Operational Research*, vol. 174, no. 1, pp. 245–264, 2006.

[22] C. Sanfa, C. Kai, and Z. Bin, "Producer Services Outsourcing Risk Control Based on Outsourcing Contract Design: Industrial Engineering Perspective," *Systems Engineering Procedia*, vol. 2, pp. 308–315, 2011.

[23] S. Xianli, H. Min, and W. Xingwei, "Distributed decision-making risk management of virtual enterprises with principal agent characteristics," *Journal of System Engineering*, vol. 25, no. 3, 2010.

[24] S. Christoph, *Distributed Decision Making*, Springer Berlin Heidelberg, Berlin, Heidelberg, 2003.

[25] S. Christoph, "Distributed decision making-a unified approach," *European Journal of Operational Research*, vol. 150, no. 2, pp. 237–252, 2003.

[26] F. Sun, S. Duan, and F. Lu, "A two-level principal-agent model for schedule risk control of it outsourcing project based on genetic algorithm," in *Proceedings of the 23rd International Conference on Industrial Engineering and Engineering Management*, pp. 17-18, 2016.

[27] C. Fang and F. Marle, "A simulation-based risk network model for decision support in project risk management," *Decision Support Systems*, vol. 52, no. 3, pp. 635–644, 2012.

[28] C. Jerson, M. Annelies et al., "A multivariate approach for top-down project control using earned value management," *Decision Support Systems*, vol. 79, pp. 65–76, 2015.

[29] M. Compare, F. Martini, and E. Zio, "Genetic algorithms for condition-based maintenance optimization under uncertainty," *European Journal of Operational Research*, vol. 244, no. 2, pp. 611–623, 2015.

[30] C. García-Martínez, M. Lozano, F. Herrera, D. Molina, and A. M. Sánchez, "Global and local real-coded genetic algorithms based on parent-centric crossover operators," *European Journal of Operational Research*, vol. 185, no. 3, pp. 1088–1113, 2008.

[31] Y. Shuai, S. Bradley et al., "A new crossover approach for solving the multiple travelling salesmen problem using genetic algorithms," *European Journal of Operational Research*, vol. 228, no. 1, pp. 72–82, 2013.

[32] K. Deep and M. Thakur, "A new crossover operator for real coded genetic algorithms," *Applied Mathematics and Computation*, vol. 188, no. 1, pp. 895–911, 2007.

[33] J. H. Holland, *Adaptation in Natural and Artificial Systems: An Introductory Analysis with Applications to Biology, Control, and Artificial Intelligence*, MIT Press, Cambridge, UK, 1992.

[34] H. Ahonen, A. G. de Alvarenga, and A. R. Amaral, "Simulated annealing and tabu search approaches for the Corridor Allocation Problem," *European Journal of Operational Research*, vol. 232, no. 1, pp. 221–233, 2014.

[35] D. Zhang, Y. Liu, R. M'Hallah, and S. C. H. Leung, "A simulated annealing with a new neighborhood structure based algorithm

for high school timetabling problems," *European Journal of Operational Research*, vol. 203, no. 3, pp. 550–558, 2010.

[36] E. Rodriguez-Tello, J.-K. Hao, and J. Torres-Jimenez, "An improved simulated annealing algorithm for bandwidth minimization," *European Journal of Operational Research*, vol. 185, no. 3, pp. 1319–1335, 2008.

[37] O. Briant, D. Naddef, and G. Mounié, "Greedy approach and multi-criteria simulated annealing for the car sequencing problem," *European Journal of Operational Research*, vol. 191, no. 3, pp. 993–1003, 2008.

[38] Z. Dai and X. Zheng, "Design of close-loop supply chain network under uncertainty using hybrid genetic algorithm: a fuzzy and chance-constrained programming model," *Computers and Industrial Engineering*, vol. 88, pp. 444–457, 2015.

[39] M. A. Rahman and G. K. Venayagamoorthy, "A hybrid method for power system state estimation using Cellular Computational Network," *Engineering Applications of Artificial Intelligence*, vol. 64, pp. 140–151, 2017.

[40] N. Pérot and N. Bousquet, "Functional Weibull-based models of steel fracture toughness for structural risk analysis: estimation and selection," *Reliability Engineering & System Safety*, vol. 165, pp. 355–367, 2017.

[41] N. Wattanapongskorn and D. W. Coit, "Fault-tolerant embedded system design and optimization considering reliability estimation uncertainty," *Reliability Engineering and System Safety*, vol. 92, no. 4, pp. 395–407, 2007.

[42] S. Chatterjee and S. Bandopadhyay, "Reliability estimation using a genetic algorithm-based artificial neural network: An application to a load-haul-dump machine," *Expert Systems with Applications*, vol. 39, no. 12, pp. 10943–10951, 2012.

Hindawi
Mathematical Problems in Engineering
Volume 2017, Article ID 6859852, 9 pages
https://doi.org/10.1155/2017/6859852

Research Article

A Problem of Particulate Contamination in an Automated Assembly Machine Successfully Solved by CFD and Simple Experiments

Jatuporn Thongsri

Computer Simulation in Engineering Research Group, College of Advanced Manufacturing Innovation, King Mongkut's Institute of Technology Ladkrabang, Bangkok 10520, Thailand

Correspondence should be addressed to Jatuporn Thongsri; jatuporn.th@kmitl.ac.th

Received 12 May 2017; Revised 3 July 2017; Accepted 1 August 2017; Published 6 September 2017

Academic Editor: M. L. R. Varela

Assembly of hard disk drives (HDDs) needs to be done in an automated assembly machine (AAM) virtually free of particulate contamination that can cause them to malfunction. Fan filter units (FFUs) are installed above the AAM to reduce the number of suspended particles in the recirculating air flowing over and around them. At one time, several HDDs were found to be defective. To find out the root cause of this problem, computational fluid dynamics (CFD) was used to investigate the airflow over and around the AAM. It was found that the cause of the high particle counts was improper air speed from the FFUs. The optimal FFUs air speed needed to be in the range of 0.35–0.65 m/s in which the airflow would block out nearby airborne particles and purge away particles generated by the AAM effectively which would, in effect, reduce the particle counts down below the threshold level of class 100 clean room. A few available measurement tools at the factory were then used to perform validating measurements against the simulation results, and the validation was positive. This optimal speed range was implemented at the factory after which the level of contamination was reduced to an acceptable level.

1. Introduction

Thailand is a big producer of various electronics parts including hard disk drive (HDD). A major technical issue in manufacturing HDDs is particulate contamination. Since the slider head and spinning disk are only 3–10 nm apart during reading and writing operations, relatively big microparticles generated during the manufacturing process may lodge onto the disk and cause erroneous readings and writings. Hence, assembly of smaller parts into a fully functional HDD absolutely needs to be done in a clean room with very low airborne microparticle counts. For example, manufacturing of head stack assembly (HSA), a major component of HDD, is required to be done in class 100 of clean room. As defined in ISO class 6 of US FED STD 209E [1], this type of clean room allows no more than 100 airborne particles bigger than or equal to 0.5 μm in 1 ft^3 of air in the room. However, class 100 clean room is prohibitively costly to construct and very difficult to maintain; therefore, in real HDD production line, class 1,000 clean room equipped with fan filter units (FFUs) is employed instead. To reduce particle counts in the air above and around assembly machines (including automated assembly machine (AAM) that welds small electronic boards to the head gimbal assembly (HGA) of HSA in an HDD production line), FFUs blow away particles from them and recirculate clean air over them [2, 3]. This study was a collaborative research between the author and a few engineers at an HDD factory for the purpose of seeking out a solution for a problem of excessive particle contamination in some HDDs fabricated by the AAM at one time. The author had proposed using CFD simulation to find a solution for the problem because direct experiment was impractical and CFD simulation had already been proven to be reliable in many types of investigation.

Since the 1970s, CFD has been widely used to investigate airflow in various types of rooms, facilities, equipment, devices, and environments [4–13], but it has only been used for a few direct investigations of airflow over and around pieces of industrial machinery. Results from those investigations were very beneficial to our work and some are

mentioned here. The following are examples where CFD has been used for various purposes: an investigation of the effect of the size of smoke particles on their individual trajectory inside a vertical laminar clean room [14]; a simulation of the airflow inside a hospital operating room that led to a successful reduction of the level of contamination that, if left unaddressed, might be harmful to patients undergoing an operation in the room [15–17]; a simulation of airflow and dust control in a laneway of coal mine to provide suitable guidance for the ventilation system of emergency rescuing [18]; an evaluation of the performance of air cleaners and ventilation system of a small lecture room in order to find a way to reduce particle counts in the air inside [19]; a simulation of trajectories that small particles moved along inside an HDD in order to find the best location for placing a circulating air filter [20, 21]; a formulation of a method for controlling the level of particle contamination in a clean room for manufacturing LCD screens [22]; a solution to resolve a water condensation problem in a production line of HDD factory [23]; and an aid for a design of a wafer-making machine in a semiconductor manufacturing line that reduced particle contamination [24]. One of the previous studies successfully applied CFD to find the optimal air speed from FFUs that, after implemented, was able to reduce the level of particulate contamination on HDD parts fabricated by a welding automation machine (WAM) in an HDD factory [25]. It was a preliminary investigation that had not attempted to find the root cause of the contamination or make a comparison between the simulated results and actual measurements. This research was intended as the practical solution. This CFD investigation focused on the contamination problem of the AAM, finding the root cause of the particle contamination, validating the simulated results with the actual measurements at the factory, and seeking an effective solution to the problem. In addition, for our experiments, we purposely opted for the measurement tools that were readily available at the factory at that time so that the technicians there would be able to apply our experimental procedure easily and rapidly.

2. Theoretical Background

Airflow pattern inside the microenvironment of an AAM was determined by solving a system of partial differential conservation and turbulence equations described in the user's guide of Ansys Fluent 17.1 software [26]. The conservation equations of mass (1), momentum (2), and energy (3) can be expressed by

$$\frac{\partial \rho}{\partial t} + \frac{\partial \left(\rho u_i\right)}{\partial x_j} = 0, \tag{1}$$

$$\frac{\partial \left(\rho u_i\right)}{\partial t} + \frac{\partial \left(\rho u_i u_i\right)}{\partial x_j} = -\frac{\partial P}{\partial x_i} + F_i + \frac{\partial \left[\tau_{ij}\right]}{\partial x_j} + \frac{\partial \left(-\rho \overline{u_i' u_j'}\right)}{\partial x_j} + \frac{\partial \left(-\rho \overline{u_i'^2}\right)}{\partial x_i} + S_m, \tag{2}$$

$$\frac{\partial \left(\rho E\right)}{\partial t} + \frac{\partial \left[u_i \left(\rho E + P\right)\right]}{\partial x_i} = \frac{\partial \left(\left(k\right)_{\text{eff}} \left(\frac{\partial T}{\partial x_j}\right) + u_i \left(\tau_{ij}\right)_{\text{eff}}\right)}{\partial x_j} + S_h. \tag{3}$$

The turbulence model used in this work is transition shear-stress transport (SST). It consists of four transport equations to represent the turbulent properties of the flow. These equations include 4 parameters: turbulence kinetic energy (k), specific dissipation rate (ω), intermittency (γ), and transition momentum thickness Reynolds number ($R_{e\theta}$) that have to be set. The full forms of the 4 equations containing these parameters can be found in [26]. The Fluent CFD software solves (1)–(3) together with the 4 equations mentioned above to determine the airflow pattern.

The particle trace was calculated from a particle-force balance equation in the discrete phase model (DPM) in Fluent [27]:

$$\frac{du_p}{dt} = F_D \left(u_f - u_p\right) + g \frac{\left(\rho_p - \rho_f\right)}{\rho_p} + F_s, \tag{4}$$

where F_s stands for forces that act on the particle such as rotational force, pressure gradient force, thermoelectric force, and Brownian force. These forces do not significantly affect micron-sized particles with $\rho_p \gg \rho_f$; therefore, only drag force and Saffman's lift force were taken into account in our simulation. Saffman's lift force [28] or lift due to shear can be written by

$$\overrightarrow{F} = \frac{2K\rho_f \nu^{1/2} d_{ij} \left(\overrightarrow{u}_f - \overrightarrow{u}_p\right)}{\rho_p d_p \left(d_{lk} d_{kl}\right)^{1/4}}, \tag{5}$$

where K is 2.594 and d_{ij} is the deformation tensor.

A dispersed two-phase flow model was used to simulate particle traces. It took into account the interparticle spacing of the system, L/d_p. The type of contaminating particles that we chose to simulate was aluminum particles because they were most frequently found in the HDD factory. Their diameter was set to be 0.5 μm, and the density was set at 2,719 kg/m^3 which was approximately three orders of magnitude higher than that of air (1.225 kg/m^3). The length scale L for the smallest element of our mesh model was set at 2.5×10^{-5} m. All of these settings resulted in a value of 50 for the L/d_p term. According to a conclusion by Utikar et al. [29], fluid phase and solid phase could be considered uncoupled if the value of L/d_p was less than 100; therefore, only one-way simulation was needed for our problem. Our simulation was done with Fluent software. The transition SST model was selected as the turbulence model. This model has been widely used in the HDD industry [30]. After the airflow pattern was determined, simulated particles were released into the airstream and their trajectories were calculated. With this careful and methodical selection of simulation method and settings, we believed that the results would be sufficiently reliable for our purpose.

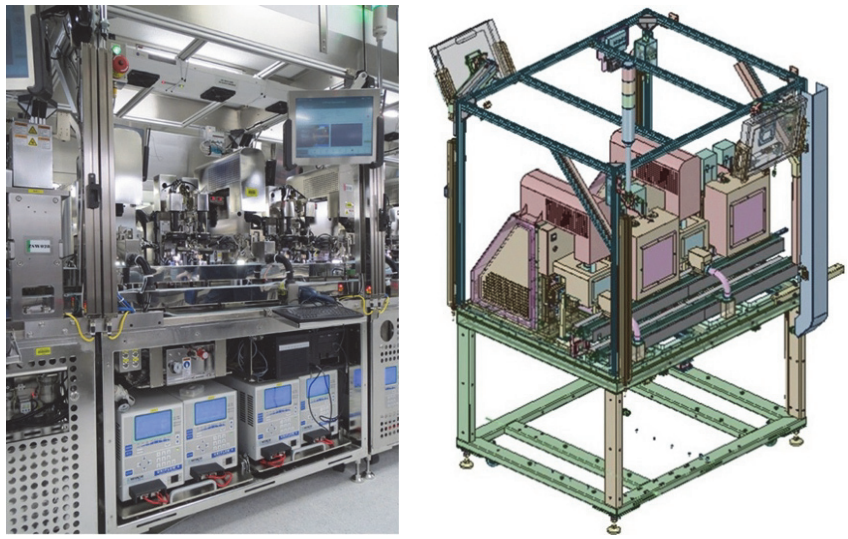

(a) (b)

Figure 1: Automated assembly machine: (a) the actual machine and (b) a solid model.

3. Methodology

3.1. Automated Assembly Machine (AAM). The AAM investigated in this study operated as an automated welder of small electronic circuits to the HGA of HSA, a major component of HDD. The AAM within has a computer system and a mobile mechanic arm. This AAM was located in a production line inside a class 1,000 clean room in the factory. Figure 1(a) shows the actual AAM and Figure 1(b) a solid model of the AAM without FFUs above it.

An FFU is a type of ventilation equipment in the shape of a rectangle of many sizes according to its usage. In this research, the size is approximately 0.60 m × 1.00 m × 0.30 m. The top side has an opening for the fan placed inside to ventilate air from above down below. The air speed exiting from the FFU can be controlled by setting the fan's speed. Within the FFU is also a HEPA filter, resulting in the exiting air that is laminar flow. The highly efficient HEPA filter, as defined by the United State Department of Energy (DOE), can filter particles sizes 0.3 μm at least 99.97%. Laminar flow is necessary for manufacturing since it can block out and purge away particles during the manufacturing process better than turbulent airflows.

The AAM consisted of 3 main parts: FFUs that blew filtered air over its microenvironment, pieces of assembling machinery, and a conveyor that carried electronic circuits, HGA, and finished product of HSA. Simplified from the AAM model in Figure 1, a working solid model of the AAM and the main airflow directions are illustrated in Figure 2.

3.2. Fluid and Mesh Models. We wanted to be able to track simulated particles as they were moving inside and outside of the AAM microenvironment; therefore, a fluid model and a mesh model were constructed, shown in Figures 3(a) and 3(b), respectively. Inside the microenvironment, the mesh model was made up of tetrahedron and hexahedron meshes,

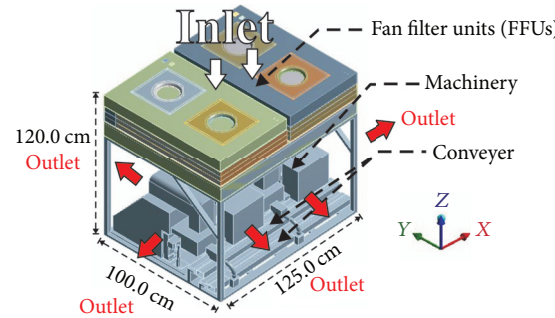

Figure 2: A model of the AAM showing directions of airflow.

but only hexahedron meshes were used outside of it. The dimensions of the air inlet were 100 × 125 cm^2 and those of the air outlets were 120 × 100 cm^2 and 120 × 125 cm^2. As for the global mesh control settings, the minimum mesh size, maximum face size, and maximum mesh size were assigned values of 0.05 mm, 36 mm, and 72 mm, respectively, with a growth rate of 1.2 and $y^+ \sim 2$. Mesh-independent analysis was performed by varying the size of the meshes at the air inlet and outlet in the range of 1–4 cm. The mesh size at the conveyor area was set to be 1 cm. The optimum mesh model, both in accuracy and computation time, was found to be consisted of 1.15 million nodes and 5.24 million.

3.3. Settings of Condition Parameters. Simulation parameters were set to correspond closely with the measured ambient conditions and FFUs air speed at the HDD factory at the time that the contamination had happened. These parameter settings were the following: pressure at 106,300 Pa, temperature at 24.5°C, and FFUs air speed at the inlet at 0.60 m/s (an average of a speed range of 0.50–0.70 m/s). These set values resulted in a nominal air change rate (ACH) of 3,564 h^{-1} and a

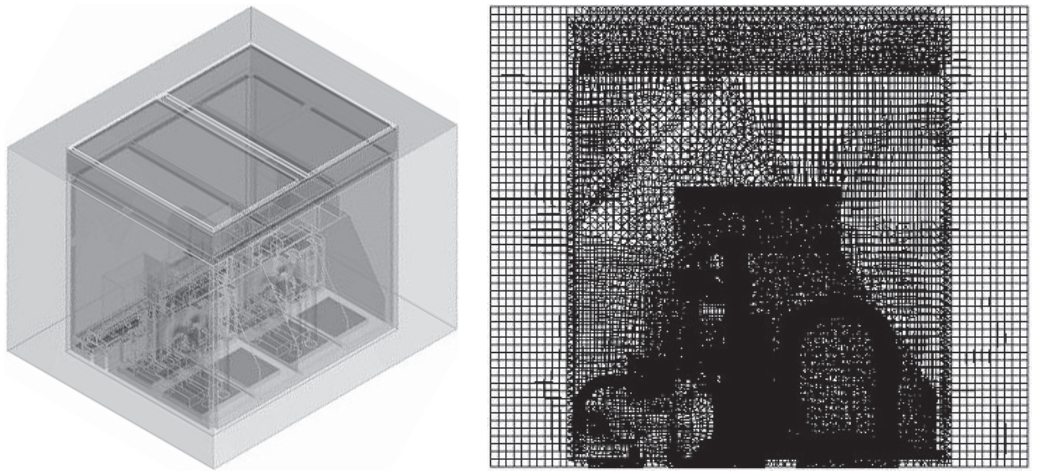

(a) (b)

Figure 3: Models of the AAM: (a) fluid model and (b) a side view of the mesh model.

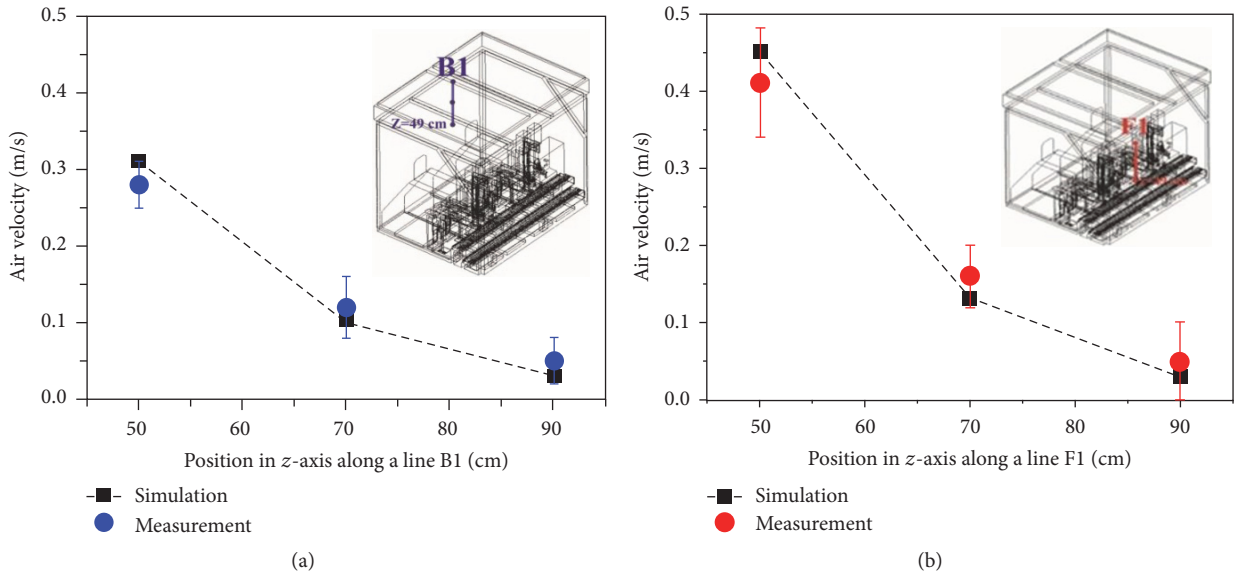

(a) (b)

Figure 4: Comparison between the simulated and measured air velocities at 3 positions at (a) the back-side surface and (b) the front-side surface of the microenvironment of the AAM.

pressure difference at the outlet of 0 Pa. The pressure-velocity coupling was set to coupled, and the spatial discretization of pressure, momentum, turbulent kinetic energy, and turbulent dissipation rate were set to be second-order upwind. All other parameters were set to default. Steady state calculation was repeated until the solution converged.

3.4. Validation. One of the best ways to observe airflow pattern in a clean room is to perform a smoke visualization test. However, we were not able to do so because CO_2 and H_2O vapors as well as those of other liquids used for this purpose might condense on the AAM and other pieces of machinery in the room and cause incalculable damage. Hence, instead of validating our simulation results with observed airflow pattern, we chose to validate them by showing that the simulated airflow velocities and directions at key places in the microenvironment of the AAM matched the actual ones closely. The actual air velocities were measured with a ±0.03 m/s-accurate hot-wire anemometer. We measured the air velocities flowing perpendicularly through 18 points at the front-side and back-side outlets while the AAM was working, three points on each of the 3 chosen imaginary lines on the surface of each outlet. At each point, twenty measurements were made and the average value was calculated. The simulated air velocities at the same positions were obtained from Fluent software by using the mesh model in Figure 3(b). It was found that the simulated air velocities and directions matched closely with the actual ones at all key places. As an example, Figure 4 shows the simulated and measured air velocities at 3 points along the imaginary lines

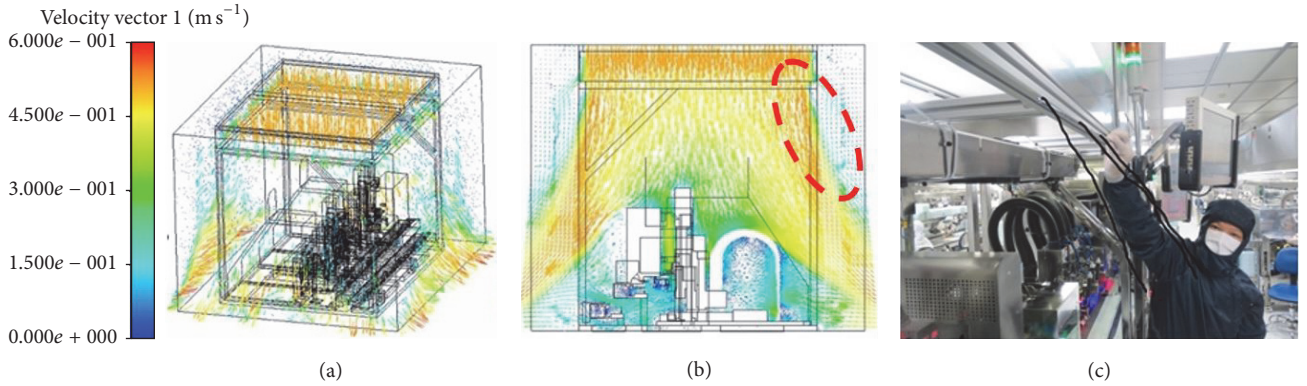

Figure 5: Velocity vectors of the airflow inside the AAM microenvironment: (a) a full view, (b) a view of a section plane near to a side, and (c) positions on the actual AAM to which some threads were attached.

B1 and F1 at (a) the back-side outlet surface and (b) the front-side outlet surface of the microenvironment, respectively. It can be clearly seen that they were closely matched. The small errors might be due to our using a constant FFUs air speed of 0.60 m/s to represent the real inconstant FFUs air speeds in the range of 0.50–0.70 m/s. The actual airflow directions were determined by observing the directions that special sewing threads were oriented in the airstream. One end of the threads was attached to the surface of each of the key locations around the AAM. This special type of thread is usually used for testing electrostatic discharge (ESD) in a clean room. It is made of conductive polyester yarn that is very light (only 60% as dense as regular thread), so its free end moves freely in an airstream. Figures 5(a) and 5(b) show simulated air velocity vectors inside the AAM microenvironment at the FFUs air speed setting of 0.60 m/s. Figure 5(a) shows a full view of the model while Figure 5(b) shows a view of a section plane near a side of the AAM. It can be clearly seen that the simulated airstream flowed down from the FFUs over the AAM and then moved along and out through the outlets at all four sides in the same directions as the actual airflow directions observed at the factory. Figure 5(c) shows a photo of several locations on the AAM where the threads were attached. The size of the threads was exaggerated to make them visible in the photo.

The comparison between the airflow near the marked area in Figure 5(b) compared to the flow direction of sewing threads in Figure 5(c) shows conformation; the air in the marked area makes the sewing threads flow out of the AAM in a systematic pattern without any random crisscross patterns as found in turbulent air. The close matches of simulated and measured air velocities and directions at all key places validated that our simulation was sufficiently reliable.

Another piece of supporting evidence for the reliability of our simulation was that one of the simulated results was positively confirmed by actual occurrences at the factory. This result indicated that particles would get trapped on the conveyor at higher FFUs air speeds. It was indirectly confirmed by a report from a technician at the factory that the level of contamination in the fabricated products became unacceptably high at higher FFUs air speed settings. These occurrences are discussed further in the light of our findings in Results and Discussion.

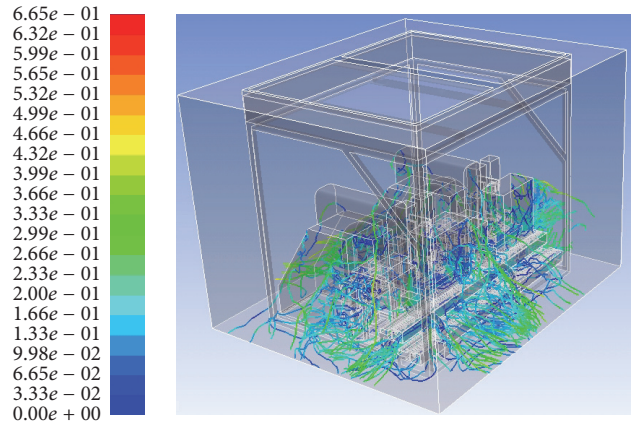

Figure 6: Traces of 300 particles released inside the AAM and carried by the airflow, color coded according to each particle residence time (s).

4. Results and Discussion

4.1. Optimum FFUs Air Speed: Contamination on the Conveyor. In order to find out how some pieces of products fabricated by the AAM at the factory got contaminated when the FFUs air speed was set at 0.60 m/s, we simulated releases of 300 spherical aluminum particles from various locations on the machine into the airstream. As can be seen in Figure 6, the simulated result shows that most of the particles got carried away through the outlets at all 4 sides of the microenvironment, but a small number of particles got pushed onto the conveyor and contaminated it. This simulation confirms a contamination problem in the AAM. We also simulated releases of larger numbers of particles at different FFUs air speeds in a slightly lower but more extended range in order to find the optimum speed that provided the least contamination. The simulation process and results are described in detail as follows.

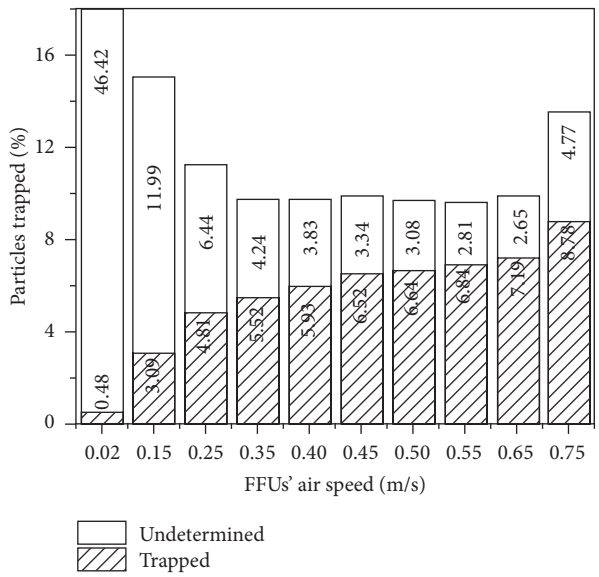

Figure 7: Percentages of aluminum particles trapped on the conveyor at different FFUs air speeds.

We wanted to know the influence of FFUs air speed on the level of contamination on the conveyor, so we simulated releases of 3,000 particles at different FFUs air speeds ranging from 0.02 to 0.75 m/s and counted the number of trapped particles at each speed. Two opposing dependencies were observed: first, the higher the air speed, the lower the number of undetermined particles; and second, the higher the air speed, the higher the number of trapped particles on the conveyor. These dependencies were indirectly confirmed by a report from an operating technician at the factory that the level of contamination increased as the FFUs air speed was set higher than 0.70 m/s. As an example, it can be seen in Figure 7 that when the FFUs air speed was set at a typical air speed in a clean room of 0.02 m/s, only 0.48% of the released particles got trapped on the conveyor while 46.42% of them were left suspended in the airstream above the AAM, and they would either fall down onto the conveyor or get purged out of the microenvironment. Undetermined means the particle is yet unknown whether it will drop onto the conveyor, float out, or still remain inside the AAM. On the other hand, when the FFUs air speed was set at 0.50 m/s, 6.64% of the released particles got trapped while only 3.08% were undetermined. This trend seems to indicate that a lower air speed was unequivocally better; however, airflow at a lower speed was not as capable at blocking out particles from intruding into the microenvironment.

To see how the level of contamination on the conveyor was higher at a higher FFUs air speed setting, we plotted the air velocity vectors and traces of 300 particles released from random locations on the AAM at different FFUs air speeds. Figure 8 shows color-coded graphic results of the simulated particle traces at two different FFUs air speeds. At a very low FFUs air speed of 0.15 m/s, the velocities of the airstreams above pushing down on the released particles to the conveyor were not much higher than those in its immediate surrounding, so the particles were pushed down only relatively lightly; that is, the directions of some of the particle traces were downward but most were lateral as can be seen in Figure 8(a). In contrast, at a very high FFUs air speed of 0.75 m/s as shown in Figure 8(b), the velocities of the airstreams moving downward were much higher than those in the immediate vicinity of the conveyor; therefore, the particles got pushed down harder onto the conveyor; that is, the directions of the traces of a larger number of particles were much steeper downward, so the released particles were more likely to get pushed down onto the conveyor and contaminate it.

Based on these simulation results and several guidelines for setting a proper FFUs air speed in a clean room [1, 31], we recommended a new optimal FFUs air speed range of 0.35–0.65 m/s as a better choice than the 0.50–0.70 m/s range previously implemented at the factory. A higher air speed would waste more energy without providing any less contamination.

4.2. Optimum FFUs Air Speed: Blocking Out Particles. We also wanted to know whether the airflow from the FFUs in this optimal speed range of 0.35–0.65 m/s would be able to block particles from entering into the AAM microenvironment, hence we simulated releases of particles moving into the microenvironment from the outside at a typical air speed observed in a production scenario in which a few technicians were moving around and speaking to each other. In order to estimate such speed, we measured the air speeds from a technician breathing and speaking repeatedly for 100 times and found that those speeds were in the range of 0.12–0.26 m/s. Knowing this, we simulated the worst case: one hundred aluminum particles moving into the AAM environment in random directions at all four sides at a speed of 0.26 m/s against the airstream from the FFUs at a speed of 0.35 m/s. The results depicted in Figure 9 show that most of the particles got blown away before they were able to enter the microenvironment, and even though a few of them were able to do so, they only stayed in it for an extremely short time and then got blown out. Their residence time in the microenvironment was certainly not long enough for them to penetrate sufficiently far into it to contaminate the AAM. Simulation trials were repeated with larger numbers of particles up to 500 and higher particle speeds up to 50 m/s. The results were the same for all cases: virtually all particles got blown away before they were able to intrude into the microenvironment of the AAM and none of them were able to stay in it long enough to contaminate the AAM. It was not surprising that the simulated particles were not able to penetrate deeply into the microenvironment even when their speeds were relatively high since their momentum was very small. Based on these results together with those in Section 4.1, we concluded that an airflow from the FFUs at a speed in the range of 0.35–0.65 m/s would be able to protect the AAM from getting contaminated by airborne particles from the outside of its microenvironment.

4.3. Optimum FFUs Air Speed: Implementation Results. Before and after the factory implemented our recommended

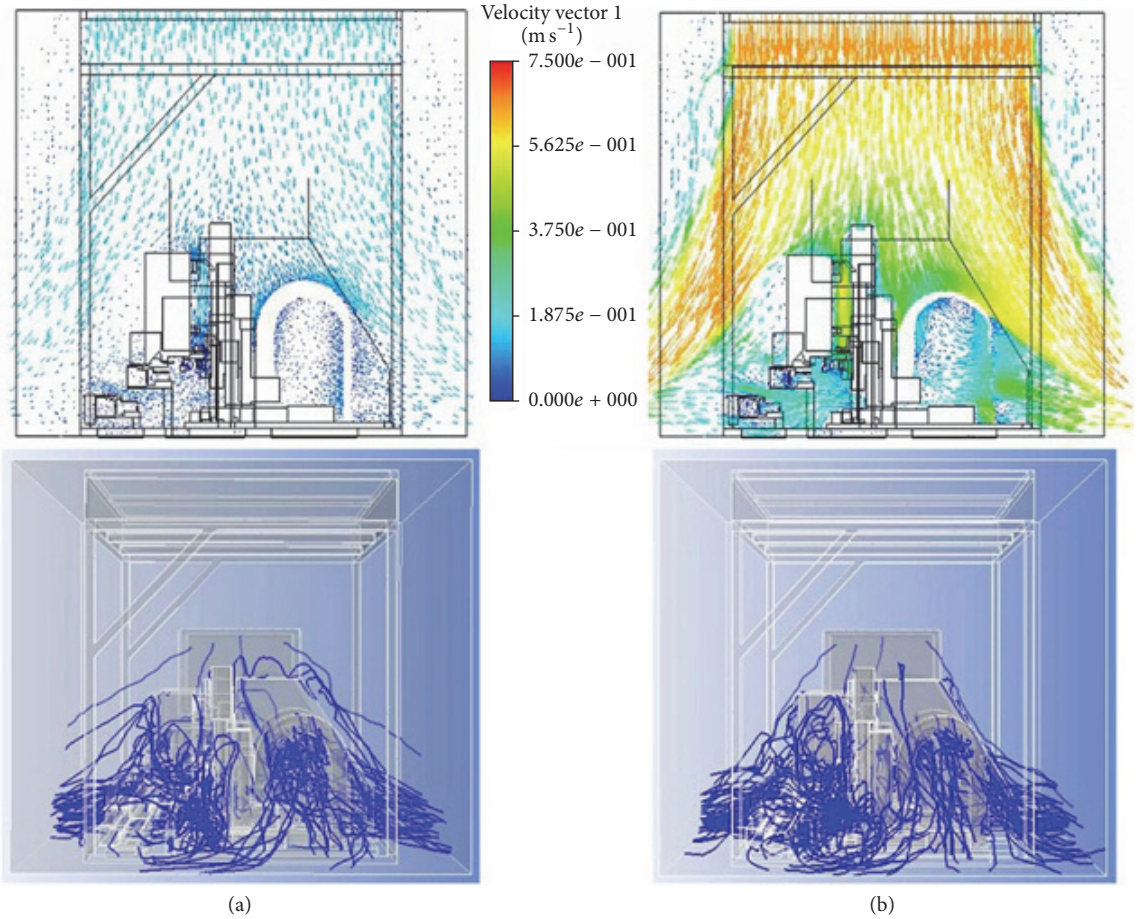

Figure 8: Velocity vectors and particle traces at FFUs air speed of (a) 0.15 m/s and (b) 0.75 m/s.

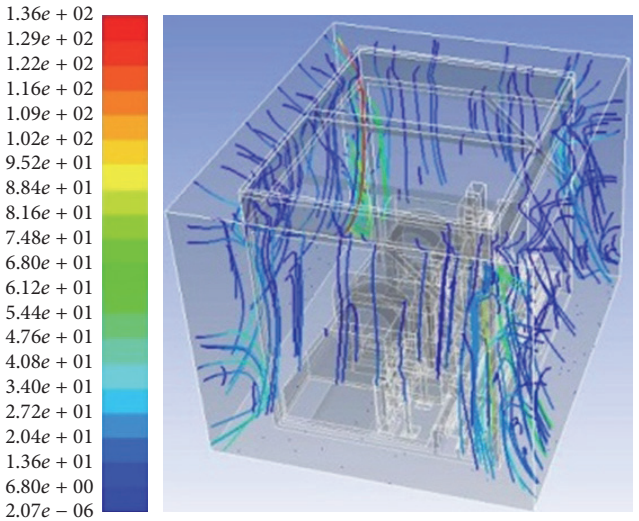

Figure 9: Traces of 100 incoming aluminum particles got blown away by the airflow from the FFUs at a speed of 0.35 m/s, color coded according to each particle residence time (s).

FFUs air speed range, we measured the concentration of 0.5 μm particles 10 times at each of the following 6 key locations around the AAM for a period of 1 minute each with a ±10% accurate laser particle counter: locations 1, 2, and 3 on the conveyor; location 4 at the front of the AAM; location 5 at the back of the AAM; and location 6 at the walkway around the AAM (see these locations and the results in Figure 10). The significance of these measured results is as follows.

First, the airstream from the FFUs kept the concentration of particles at every key location far below the threshold level of class 1,000 clean room both before and after the air speed adjustment. Moreover, it reduced the concentration at 4 out of 6 key locations down to the threshold level of class 100 of clean room and even below that after the speed adjustment. Hence, the airstream from the FFUs at a speed in our recommended range truly augmented the capability of the class 1,000 clean room in the factory to function effectively as a class 100 clean room that was ideal for HDD production. Not shown due to limited space, concentrations of 0.3 and 5.0 μm particles were also determined and found to be below the threshold level of class 1,000 of clean room.

Second, after the speed adjustment, particle concentration in every key location decreased. At the 3 locations at the conveyor, the concentrations became lower than the threshold level of class 100 clean room. Of note is that the concentration at location 4 at the front of the AAM was higher than those at location 5 at the back because there was no machine activity at the back while there were a lot of

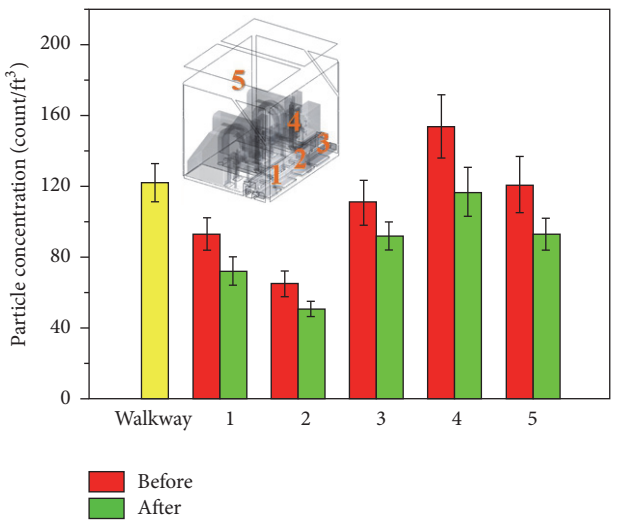

Figure 10: Variation in particle concentration at different comparative positions before and after FFUs air speeds were adjusted.

activities at the front. The particle concentration exceeded the threshold of class 100 clean room slightly only at location 4.

Third, the optimal FFUs air speed range of 0.35–0.65 m/s for the AAM that we found in this study is different from the optimum range of 0.35–0.55 m/s found for a welding automation machine (WAM) in the previous study [25]. This might be due to the difference in the height of the FFUs above each of the two machines; the WAM and its FFUs were 27.7 cm farther apart than the AAM and its FFUs were. We think that an optimal FFUs air speed for any machine crucially depends on the ambient conditions of the clean room, the shape and function of the machine, and the height of the FFUs above it.

From committing field research, we found that the root cause of overcontamination resulted from the movement of the AAM that rubbed against each other and released tiny particles. The trivial cause is particles from several activities of the operators outside the AAM and the production line. The factory resolved the problem by implementing vacuum cleaners or particle suction tools into the machines to suction the particles out of the AAM machine. This method is a waste of budget and energy since it is solving the problems at the rear end which is not a sustainable solving method. Therefore, these research results not only solve problems at the causes in a sustainable and economical manner but also save costs as well.

In the factory, there were many pieces of machinery installed next to each other in the production line (Figure 1(a)), each having its own FFUs installed above it. If CFD is used to simulate the airflow above and around all of these machines, taking into account the different heights of the FFUs above them, we are fairly sure that the level of contamination can be reduced even further.

5. Conclusion

An automate assembly machine (AAM) used to manufacture the head stack assembly (HSA) of a hard disk drive factory met the contamination problem resulting in production of HSA that did not meet standards and needs solving. The factory required that, in the problem-solving process, all machines must not be stopped. Tools and equipment should be those that the factory already owns. Experimental methods that are simple and easy to transfer to the factory's engineers should be used. We proposed a problem solver by using the computational fluid dynamics (CFD) to simulate the airflow inside the AAM and validate the CFD results using an anemometer and sewing threads. CFD results showed the airflow and particle trace, letting us know that the air flowing out of the fan filter units (FFUs), or the FFUs air speed is in the range of 0.50–0.70 m/s. This range that the factory uses is inappropriate and is too fast resulting in contamination problems. We recommended the factory to slow the rate of the FFU's air speed down to be in the range of 0.35–0.65 m/s, which is already confirmed by the CFD analysis that this method can block out particles from outside flowing inside of the AAM, and purge away particles from the inside to the outside effectively. Accelerating the FFUs air speed over the recommended range not only causes contamination problems but also is a waste of energy. We also found that the optimal range of FFUs air speed for the AAM was not the same as those for other pieces of machinery. This was most likely due to their different shape and function as well as the different height of the FFUs above each of them. The factory adapted our recommendations for usage and found that yield was increased. The research results not also resolved the AAM contamination problems in a sustainable and economical manner but also saved energy as well.

Nomenclature

AAM: Automated assembly machine
FFU: Fan filter unit
HGA: Head gimbal assembly
d_p: Diameter of particle (m)
F_s: External force (N)
L: Length scale (m)
t: Time (s)
u_p: Velocity of particle (m/s)
ρ_p: Density of particle (kg/m^3)
CFD: Computational fluid dynamics
HDD: Hard disk drive
HSA: Head stack assembly
F_D: Drag force (N)
g: Gravity (m/s^2)
P: Pressure (Pa)
u_f: Velocity of fluid (m/s)
ρ_f: Density of fluid (kg/m^3)
ν: Viscosity of fluid.

Conflicts of Interest

The author declares that there are no conflicts of interest for this article.

Acknowledgments

This research was partially supported by College of Advanced Manufacturing Innovation (AMI) and King Mongkut's Institute of Technology Ladkrabang (KMITL).

References

[1] "Cleanrooms and Associated Controlled Environments - Part 1: Classification of Air Cleanliness," ISO No. 14644-1 (1999).

[2] G. Cao, H. Awbi, R. Yao et al., "A review of the performance of different ventilation and airflow distribution systems in buildings," *Building and Environment*, vol. 73, pp. 171–186, 2014.

[3] R. Flaherty, "Clean rooms: Continuing evolution of fan filter units for clean rooms," *Filtration and Separation*, vol. 48, no. 4, pp. 33–37, 2011.

[4] P. Naphon, S. Ratchaneekorn, and J. Kurujareon, "Heat transfer and flow characteristics in the hard disk drive tester," *International Communications in Heat and Mass Transfer*, vol. 36, no. 8, pp. 820–826, 2009.

[5] Y. Luan and H. Sun, "Experimental and numerical study on the resistance performance of an axial flow cyclone separator," *Mathematical Problems in Engineering*, vol. 2015, Article ID 384524, 2015.

[6] Z. Mo, J. Xiao, and G. Wang, "Numerical research on flow characteristics around a hydraulic turbine runner at small opening of cylindrical valve," *Mathematical Problems in Engineering*, vol. 2016, Article ID 6951839, 8 pages, 2016.

[7] H. K. Ma and C. H. Chen, "Development of a divided zone method for power savings in a data center," in *Proceedings of the 29th Annual IEEE Semiconductor Thermal Measurement and Management Symposium, SEMI-THERM 2013*, pp. 33–38, San Jose, Ca, USA, March 2013.

[8] Z. Wang and T. Ren, "Investigation of airflow and respirable dust flow behaviour above an underground bin," *Powder Technology*, vol. 250, pp. 103–114, 2013.

[9] L. Jiying, "A numerical study of the indoor thermal environment in an air-conditioned large space building," in *Proceedings of the 8th International Conference on Intelligent Computation Technology and Automation, ICICTA 2015*, pp. 69–72, Jiangxi, China, June 2015.

[10] P. V. Nielsen, "Fifty years of CFD for room air distribution," *Building and Environment*, vol. 91, pp. 78–90, 2015.

[11] F. Romano, L. Marocco, J. Gustén, and C. M. Joppolo, "Numerical and experimental analysis of airborne particles control in an operating theater," *Building and Environment*, vol. 89, pp. 369–379, 2015.

[12] Y. Wang, Y. Cao, B. Liu, J. Liu, Y. Yang, and Q. Yu, "An evaluation index for the control effect of the local ventilation systems on indoor air quality in industrial buildings," *Building Simulation*, vol. 9, no. 6, pp. 669–676, 2016.

[13] Y. Z. Lun and P. C. Wang, "Numerical modelling of train aerodynamics in confined space," in *Proceedings of the 2016 IEEE Region 10 Conference, TENCON 2016*, pp. 108–115, November 2016.

[14] S.-C. Hu and C.-C. Chen, "Locating the very early smoke detector apparatus (VESDA) in vertical laminar clean rooms according to the trajectories of smoke particles," *Building and Environment*, vol. 42, no. 1, pp. 366–371, 2007.

[15] J. Liu, H. Wang, and W. Wen, "Numerical simulation on a horizontal airflow for airborne particles control in hospital operating room," *Building and Environment*, vol. 44, no. 11, pp. 2284–2289, 2009.

[16] S. Sadrizadeh, A. Tammelin, P. Ekolind, and S. Holmberg, "Influence of staff number and internal constellation on surgical site infection in an operating room," *Particuology*, vol. 13, no. 1, pp. 42–51, 2014.

[17] S. Sadrizadeh and S. Holmberg, "Effect of a portable ultra-clean exponential airflow unit on the particle distribution in an operating room," *Particuology*, vol. 18, pp. 170–178, 2015.

[18] H. Liu, S. Mao, M. Li, and J. Yue, "3D Simulation for dynamic characteristics of airflow and dust control in a laneway of coal mine," in *Proceedings of the 24th International Conference on Geoinformatics*, Galway, Ireland, August 2016.

[19] K.-C. Noh and S.-J. Yook, "Evaluation of clean air delivery rates and operating cost effectiveness for room air cleaner and ventilation system in a small lecture room," *Energy and Buildings*, vol. 119, pp. 111–118, 2016.

[20] N. Liu, Q. Zhang, and K. Sundaravadivelu, "A numerical simulation of particle trajectory in thin hard disk drive," *IEEE Transactions on Magnetics*, vol. 49, no. 6, pp. 2590–2593, 2013.

[21] J. Thongsri and V. Pongkom, "A simulation of the number of particles trapped by the circulating filter of a hard disk drive and their trajectories," *Applied Mechanics and Materials*, vol. 548-549, pp. 953–957, 2014.

[22] K.-C. Noh, H.-S. Kim, and M.-D. Oh, "Study on contamination control in a minienvironment inside clean room for yield enhancement based on particle concentration measurement and airflow CFD simulation," *Building and Environment*, vol. 45, no. 4, pp. 825–831, 2010.

[23] J. Thongsri, "A successful CFD-based solution to a water condensation problem in a hard disk drive factory," *IEEE Access*, vol. 5, pp. 10795–10804, 2017.

[24] M. Lee and S.-J. Yook, "Investigation of particulate contamination of heated wafers contained in a closed environment," *Journal of Aerosol Science*, vol. 88, pp. 148–158, 2015.

[25] J. Thongsri and M. Pimsarn, "Optimum airflow to reduce particle contamination inside welding automation machine of hard disk drive production line," *International Journal of Precision Engineering and Manufacturing*, vol. 16, no. 3, pp. 509–515, 2015.

[26] *Turbulence*, Fluent Theory Guide 17.1, 2016, Chapter 4.

[27] *Multiphase Flow*, Fluent Theory Guide 17.1, 2016, Chapter 17.

[28] *Discrete Phase*, Fluent Theory Guide 17.1, 2016, Chapter 16.

[29] R. Utikar, N. Darmawan, M. Tade et al., *Hydrodynamic simulation of cyclone separators*, INTECH, 2010.

[30] F. R. Menter, "Review of the shear-stress transport turbulence model experience from an industrial perspective," *International Journal of Computational Fluid Dynamics*, vol. 23, no. 4, pp. 305–316, 2009.

[31] T. Xu, C.-H. Lan, and M.-S. Jeng, "Performance of large fan-filter units for cleanroom applications," *Building and Environment*, vol. 42, no. 6, pp. 2299–2304, 2007.

Hindawi
Mathematical Problems in Engineering
Volume 2017, Article ID 9646303, 12 pages
https://doi.org/10.1155/2017/9646303

Research Article

Risky Multicriteria Group Decision Making Based on Cloud Prospect Theory and Regret Feedback

Yan Song,[1] Hao Yao,[1] Shuang Yao,[1] Donghua Yu,[2] and Yan Shen[3]

[1]*School of Economics and Management, Harbin Engineering University, No. 145, Nantong Street, Nangang District, Harbin 150001, China*
[2]*School of Computer Science and Technology, Harbin Institute of Technology, No. 92, Xidazhi Street, Nangang District, Harbin 150001, China*
[3]*College of Science, Harbin Engineering University, No. 145, Nantong Street, Nangang District, Harbin 150001, China*

Correspondence should be addressed to Shuang Yao; alloniam@163.com

Received 29 December 2016; Revised 12 April 2017; Accepted 26 April 2017; Published 25 May 2017

Academic Editor: M. L. R. Varela

The assessment of risky linguistic variables has significant applications in multiattribute group decision problems. This paper focuses on risky multicriteria group decision making using linguistic variable assessment and proposes a new model which considers various and differential psychological behavior and the ambiguity of linguistic variable assessment across multicriteria risks. Based on the cloud prospect value assessment, this paper proposes a cloud prospect value aggregation method and consensus degree measurement. An improved feedback adjustment mechanism based on regret theory is employed as the consistency model, which complements prospect theory. The three theoretical methods together constitute the core elements of the proposed CPD (cloud prospect value consensus degree decision) model. The feasibility and validity of the new decision making model are demonstrated with a numerical example, and feedback performance was compared with conventional direct feedback. The proposed CPD approach satisfies given consistency threshold of 0.95 and 0.98 after three and four feedback loops, respectively. Compared to the proposed CPD method, direct feedback approach needs seven and ten feedback loops under the same threshold, respectively, which shows that the proposed model increases efficiency and accuracy of group decision making and significantly reduces time cost.

1. Introduction

Multiple criteria decision making (MCDM) is an important part of modern decision science [1, 2]. Group decision making under multicriteria risk refers to decision problems whose criteria are random variables; that is, the criteria values change with the uncertain environment [3, 4]. The uncertainty is considered as risk under various states whose probabilities are known or measurable [5].

Many real-life decision making problems, such as investments, are group decision problems with multicriteria risk, often with a variety of uncertain factors and multiple uncertain states corresponding to multiple probabilities. Stock investment selection and decision making do not have exact attribute values due to the complex and uncertain environment with vagueness, ambiguity, and randomness.

Due to the complexity of the limited knowledge and decision maker (DM) perceptions, many alternative rankings occur for the uncertainty and randomness of the attribute value(s) [6]. According to their experience or related knowledge, DMs conduct fuzzy linguistic evaluations, such as "very poor," "poor," "fair," "good," and "very good." Prospect theory [7] considers DM psychological factors, which effectively corrects their maximum subjective expected utility, and has been successfully applied to individual [8, 9] and group [10–12] decision making. Therefore, to find the most desirable alternative or rank feasible alternatives to support decision making, it is critical to transform uncertain linguistic assessment, which mainly includes crisp or fuzzy numbers and their deformation.

The traditional technique for order preference by similarity to an ideal solution (TOPSIS) proposed by Hwang and

Yoon [13] is a widely used crisp number method for classical MCDM. The TOPSIS method determines a solution with the shortest distance from the ideal solution and the farthest distance from the negative-ideal solution. Similar to TOPSIS, the VIKOR method proposed by Opricovic and Tzeng [14] considers the degree of closeness to the ideal solution using an integration function based on close to ideal solution. However, neither TOPSIS nor VIKOR considers the relative importance of the distance between two different reference points.

Fuzzy numbers, derived from fuzzy set theory, have become a main stream method to represent and handle uncertain attributes [15–18]. Criteria values include interval valued fuzzy numbers (IVFNs) [19] and the combination of the interval numbers fuzzy set and soft set [20]. The fuzzy set is well suited to dealing with vagueness [21]; for example, the hesitant fuzzy soft set based on soft and hesitant fuzzy sets has been successfully applied to group decisions [22].

The cloud theory is the innovation and development of a membership function for fuzzy set theory [23]. It transforms the uncertainty qualitative language concept into quantitative values [24] and has been successfully applied to data mining [25, 26], intelligent control, and intelligent algorithm modification [27, 28].

The different knowledge and evidence available to DMs result in inconsistent evaluations. To obtain the final group opinion, DMs should coordinate inconsistency in the group decision making process. An appropriate technique is to aggregate all the individual fuzzy preference relations and consistency processing [29, 30], repeatedly modifying the decision matrix.

Regarding the linguistic variable group decision problem, DMs usually participate in the decision making process and provide subjective evaluation in three different stages. The initial decision matrix is constructed in first stage, and the criteria weights are determined and incorporated in second stage. If the initial decision matrix fails the consistency check, the decision making process turns to the third stage and the initial decision matrix is reconstructed by the DMs. This process leads to multiple repeated subjective evaluation and increases computational complexity.

Although some current methods deal with linguistic variable assessment and provide feedback adjustment to some extent, some drawbacks remain. On one hand, current linguistic variable evaluation can only be applied to real numbers or triangular fuzzy numbers, which limits its application to other decision methods [31]. When prospect theory or related methods cannot be used directly [32], a transformation from linguistic variables to number values is required. On the other hand, feedback adjustment gives DMs little useful guidance to modify the decision matrix when the group evaluation does not satisfy the consistency threshold [33]. This modification process is time-consuming and blind, particularly for risky multicriteria group decision making. The number of DM modifications can be reduced by automatic negotiation, but this can lead to deviation from the DMs original intention to reach a consensus [22]. In addition, most group decision methods handle a single state rather than multiple states.

Group decisions based on linguistic variables are widespread in practice. Although the linguistic variables are processed through triangular fuzzy numbers or fuzzy logic, the variables are in a single state [11], not the multistate, which is not risky. For example, Wang and Lee [34] generalize TOPSIS to fuzzy multiple idea group decision making in fuzzy environment with single state criteria.

The cloud model introduced in [29] transforms the uncertainty relationship from qualitative (linguistic variable) to quantitative, accommodating fuzziness and randomness of qualitative evaluation. The model integrated two domains and constructed a mapping relationship between them. The cloud model is a continuous linguistic variable method [35] that has been widely used for multicriteria group decision making [36–38].

Therefore, we propose a method based on combining the cloud model and prospect theory, which integrates the advantages of vagueness and randomness from the cloud model and risk perception from prospect theory. The proposed model incorporates the cloud prospect value aggregation method and consensus degree measurement. An improved feedback adjustment mechanism provides the consistency model. Following Peng and Yang [19], we take full advantage of the nonexpected utility theory of regret-rejoice to compensate for the prospect theory. The new feedback adjustment rules handle DM inconsistency efficiently.

This paper proposes a new group decision making method that integrates the cloud model, prospect theory, and regret theory for risky multicriteria group decision making. Focusing on the group decision problem of multicriteria risky linguistic variables, we build a method for the cloud prospect consensus degree of risky multicriteria group decision making and feedback adjustment regulation. First, we use the cloud model to convert the uncertain linguistic variable problem to a risky multicriteria decision problem. The comprehensive prospect value is calculated, and the cloud prospect decision matrix of all DMs for all alternatives is constructed based on prospect theory. Then the decision matrixes for all DMs are aggregated and their consistency is measured. Those criteria scoring less than the acceptable threshold are returned to the DMs with guidance correction information according to the least regret value, and DMs modify their decision matrix with this correction information. Finally, the method sorts the alternatives.

2. Problem Description and Theoretical Basis

Consider the group decision problem of multicriteria risk with the alternatives sets $A = \{a_1, a_2, \ldots, a_m\}$, $m \geq 2$, and the associated criteria sets $Q = \{q_1, q_2, \ldots, q_n\}$, $n > 2$, where each criterion is mutually independent. The weight vector of the criteria layer is $\omega = \{\omega_1, \omega_2, \ldots, \omega_n\}$, which satisfies the constraint $\sum_{i=1}^{n} \omega_i = 1$, $\omega_i \geq 0$, $i = 1, 2, \ldots, n$. The possible natural states $f^j = \{f_1^j, f_2^j, \ldots, f_s^j\}$ of criteria u_j have probability p_l^j under state f_l^j $(1 \leq l \leq s)$. For the set of DMs $E = \{e_1, e_2, \ldots, e_t\}$ $(t \geq 2)$, x_{ijl}^k represents the linguistic variable evaluation of alternative a_i under criteria u_j in state f_l^j. We select the optimal scheme ranking under

a cloud prospect decision framework with a higher level of consensus degree.

2.1. Cloud Model. The cloud model reflects uncertain phenomena in the field of natural and social sciences. The usual cloud model [39] includes the complete cloud, left half cloud, and right half cloud models. It is one of the most powerful tools for characterizing the linguistic atom. The variates are assumed to be uniformly normally distributed. The complete cloud produces qualitative concepts with complete features. The derivative cloud model adds one or more parameters, generating a different form of the cloud model, such as triangular, trapezoidal, Γ, and other clouds. The cloud model is usually denoted by a cloud droplet, $C(\mathrm{Ex}, \mathrm{En}, \mathrm{He})$, where Ex is the expected value, which reflects the mathematical expectation of the qualitative concept; En is the entropy, reflecting the fuzzy qualitative concept; and He is the hyper entropy, which reflects the randomness of dispersion and the degree of certainty.

A single cloud droplet does not impact overall cloud characteristics, but the cloud droplet distribution reflects the ambiguity and randomness of cloud mapping. For effective integration of ambiguity and randomness, the universal law for most basic linguistic values in natural language can be defined as follows.

Definition 1. Suppose that C is the qualitative concept of a quantitative universe U. For $\forall x \in U$, the membership degree, $\mu_C(x)$, of C is a stochastic number with a stable random tendency. The membership degree $\mu_C(x)$ of x is called the cloud on the universe U, denoted by $C(U)$; namely, $\mu_C(x) : U \to [0, 1],\ \forall x \in U$, for which $x \to \mu_C(x)$.

Definition 2. Let $\widetilde{A}$ be the qualitative concept in the universe U. A random instance x in $\widetilde{A}$, $x \in U$, satisfies $x \sim N(\mathrm{Ex}, \mathrm{En}'^2)$, $\mathrm{En}' \sim N(\mathrm{En}, \mathrm{He}^2)$. When the certainty degree of x can be expressed as $y = \exp[-(x - \mathrm{Ex})^2/2\mathrm{En}'^2]$, the distribution of x in U is called the normal cloud.

Definition 3. Let $C_1(\mathrm{Ex}_1, \mathrm{En}_1, \mathrm{He}_1)$ and $C_2(\mathrm{Ex}_2, \mathrm{En}_2, \mathrm{He}_2)$ be one-dimensional normal clouds in U. The Hamming distance between C_1 and C_2 is defined by

$$D(C_1, C_2) = \sqrt{\frac{\underline{d}^2(C_1, C_2) + \overline{d}^2(C_1, C_2)}{2}}, \tag{1}$$

where

$$\begin{aligned} &\underline{d}(C_1, C_2) \\ &\quad = \left| \left(\mathrm{Ex}_1 - 3\sqrt{\mathrm{En}_1^2 + \mathrm{He}_1^2} \right) - \left(\mathrm{Ex}_2 - 3\sqrt{\mathrm{En}_2^2 + \mathrm{He}_2^2} \right) \right|, \\ &\overline{d}^2(C_1, C_2) \\ &\quad = \left| \left(\mathrm{Ex}_1 + 3\sqrt{\mathrm{En}_1^2 + \mathrm{He}_1^2} \right) - \left(\mathrm{Ex}_2 + 3\sqrt{\mathrm{En}_2^2 + \mathrm{He}_2^2} \right) \right|. \end{aligned} \tag{2}$$

In the decision process, the number of clouds has one-to-one correspondence with the linguistic variable value in U. Therefore, most previous studies have used the golden section method to generate clouds [36]. However, this approach has some defects, so we instead use a method that can reinforce discrimination [38].

2.2. Prospect Decision Theory Based on the Cloud Model. The cloud model combines uncertainty and ambiguity. Under the cloud model and prospect decision framework, DMs evaluate the alternatives against a reference point to estimate gain or loss and are more sensitive to loss. Prospect theory was proposed in 1979. The core concept is a prospect value, which includes a value and weight function, which reflects the bounded rationality of the DMs in the decision process. Many empirical studies have found that psychological behavior plays an important role in decision analysis. Compared with expected utility theory of uncertainty decision, prospect decision theory based on the cloud model proposed the reference point on the basis of the different effect from the reference point [39].

In prospect decision theory based on the cloud model (cloud prospect decision theory), a cloud prospect decision matrix V_{ij}^k, for alternative i of attribute j, is constructed for every DM. This matrix is composed of a cloud prospect value function, $v(C)$, and a cloud prospect value weight, $\pi(p)$. The prospect decision matrix of every DM is

$$V_{ij}^k = \sum_{l=1}^{s} \sum_{z=1, z\neq i}^{m} \pi_{ijl}^k \left(p_l^j \right) v\left(C_{zjl}^k \right), \tag{3}$$

where $v(C)$ is formed by the subjective perception of the DMs [10]:

$$v\left(C_{ijl}^k \right) = \begin{cases} \left(D\left(C_{ijl}^k, C_{zjl}^k \right) \right)^{\alpha}, & C_{ijl}^k \geq C_{zjl}^k \\ -\lambda \left(D\left(C_{ijl}^k, C_{zjl}^k \right) \right)^{\gamma}, & C_{ijl}^k < C_{zjl}^k, \end{cases} \tag{4}$$

and $\pi(p)$ reflects the probability weight function considering the DM's risk attitude:

$$\pi_{ij}^k \left(p_l^j \right) = \begin{cases} \dfrac{\left(p_l^j \right)^{\tau}}{\left[\left(p_l^j \right)^{\tau} + \left(1 - p_l^j \right)^{\tau} \right]^{1/\tau}}, & C_{ijl}^k \geq C_{zjl}^k \\ \dfrac{\left(p_l^j \right)^{\delta}}{\left[\left(p_l^j \right)^{\delta} + \left(1 - p_l^j \right)^{\delta} \right]^{1/\delta}}, & C_{ijl}^k < C_{zjl}^k, \end{cases} \tag{5}$$

where C_{ijl}^k denotes the cloud evaluation of alternative i of attribute j for the kth DM. Equation (4) suggests that DM k, for the same attribute j under the same state l, compares the size of the cloud droplet for alternatives i and z ($z \neq i$) and calculates the distance between the cloud droplets, $D(C_{ijl}^k, C_{zjl}^k)$. The parameters $0 \leq \alpha \leq 1$, $0 \leq \gamma \leq 1$, which represent the degree of concavity and convexity, respectively, of the regional value function for gains and losses, control the value function, $v(C_{ijl}^k)$, of the DM's subjective perception. λ is the loss aversion coefficient. When $\lambda > 1$, the DM is more sensitive to loss, that is, loss averse.

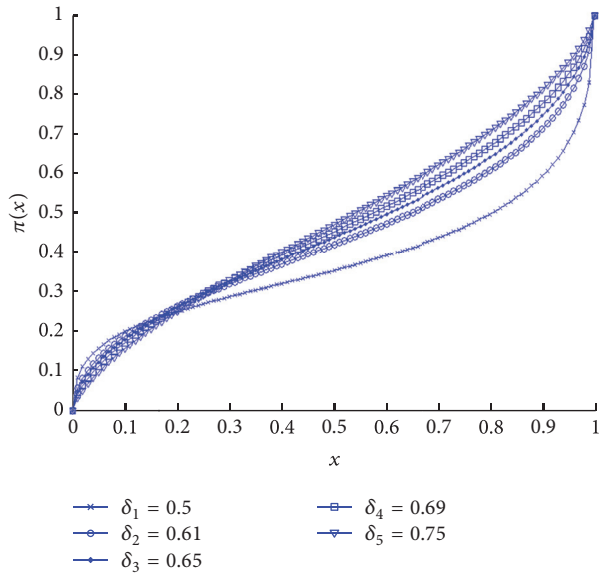

Figure 1: Effect of δ on the weight function $\pi(x)$.

The probability weight is the subjective judgment depending on the possibility P of certain events. The risk attribute coefficients τ and δ control the curvature of the prospect weight function. $\pi(P)$ is the monotone increasing function of probability P. When P is very small, the DM could overestimate the slight probability of a given incident. When P is large, $\pi(P) < P$, illustrating that DMs overlook large probability events [39]. Equation (5) shows that, for the same attribute j under the same state l, when the linguistic evaluation value C_{ijl}^k of alternative i is greater than that of alternative z, the weight function is controlled by τ, which represents the risk revenue attribute coefficient. Larger τ means more adventurous DM behavior. In contrast, δ is the risk loss attribute coefficient, and Figure 1 shows the effect of δ on $\pi(x)$.

Prospect theory states that DMs measure the gain or loss according to the distance between the result and the expectation, which is sensitive to the selection of reference points. Equations (4) and (5) use dynamic reference points, which may contain both loss and income, unlike fixed reference points that include only one of these factors. An erroneous selection could lead to deviation in the overall results.

3. Cloud Prospect Group Decision Model

Group decisions are affected by knowledge and preferences, and decisions may have to incorporate serious differences of opinion. On the basis of the cloud model and prospect decision theory, we constructed a prospect value consistency model that includes the cloud prospect value consistency degree and feedback regulation by integrating the complete decision procedure committed to solving the group decision making for the risky multiattribute linguistic variable assessment problem. Combining the randomness and ambiguity of uncertain linguistic variable assessment with DM risk attitude and bounded rationality of psychological behavior, the proposed cloud prospect decision (CPD) making model integrates the theoretical advantages of the cloud model and prospect theory.

Aggregation, consistency measurement, and consistency model are the three essential factors of the proposed CPD model, based on the cloud prospect value method. We propose an aggregation method reflecting the concentration trend and cloud prospect consensus degree measurement. The proposed improved feedback adjustable mechanism, that is, the consistency model based on regret theory, compensates for prospect theory. The three theoretical methods together constitute the core and innovation of the proposed CPD model.

3.1. Cloud Prospect Decision (CPD) Making. The proposed CPD model aggregates the DMs and constructs a prospect value consensus degree through two procedures. Essentially, it aggregates DMs and attribute levels. DM aggregation provides a comprehensive decision result for each alternative i and attribute j for multiple DMs based on the average decision value. Based on the cloud model, CPD operates at the DM level using a set of consistency thresholds to provide a preliminary correction scheme.

(1) Aggregation. Experts from a variety of professions and preferences contribute to a decision under a complicated and uncertain environment, which is the origin of the group decision. With many correlate indicators to consider, reducing and eliminating the criteria subjective weights has a significant role in reaching a high consensus degree for the decision. Therefore, the discrepant preference information of individual assessment, V_{ij}^k, should be aggregated to a collective assessment, V_{ij}^c.

The aggregation operator must satisfy the following properties:

(a) If all the assessments are the same, then the final group assessment is any one of them.

(b) The integration results are independent of the order of the experts.

(c) The group assessment opinions are the concentration trend of individual opinions.

Group assessment opinion mainly depends on the concentration trend of personal opinions. Therefore, a reasonable individual assessment integration method requires the average of multiple expert opinions. We calculate the cloud prospect decision matrix, V_{ij}^k, for each DM:

$$V_{ij}^c = \frac{\sum_{k=1}^{t} V_{ij}^k}{t}, \tag{6}$$

where t is the total number of the DMs. We use the cloud prospect decision matrix to construct the decision matrix for each alternative for each DM and extract the decision matrix for all the DMs according to the alternatives.

Finally, we use (6) to obtain V_{ij}^c for each alternative i and attribute j.

(2) Cloud Prospect Value Consistency Measurement. Classically, consensus is defined as the full and unanimous agreement of all decision makers regarding all possible alternatives [40]. However, complete agreement is not always necessary in real situations. Therefore, to obtain the maximum consensus degree among DMs on the solution set of alternatives [41], we build a CPD model:

$$\mathrm{CPD}\left(V_i^k\right) = \sqrt{\frac{1}{n}\sum_{j=1}^{n}\left(\frac{V_{ij}^k - V_{ij}^c}{\left\{\left[\max_g\left(V_{ig}^k - V_{ig}^c\right) - \min_g\left(V_{ig}^k - V_{ig}^c\right)\right] + \varepsilon\right\} * n}\right)^2}, \quad (7)$$

where ε is a correction coefficient, usually assigned a value of 1; and $g = 1, 2, \ldots, n$. The CPD of alternative i for all DMs is

$$\mathrm{CPD}\left(a_i\right) = 1 - \frac{1}{t}\sum_{k=1}^{t}\mathrm{CPD}\left(V_i^k\right). \quad (8)$$

Let the consensus degree threshold of CPD for group decisions be β. If $\mathrm{CPD}(a_i) < \beta$, then adjust a_i to minimize CPD and adjust the alternatives.

3.2. Feedback Regulation Mechanism. When the CPD does not satisfy the acceptable threshold β, the feedback regulation aims to provide corresponding adjustment suggestions to guide DM's correction. This feedback adjustment is intended to improve the efficiency of sorting decision schemes. The targeted adjustment alternative is selected by the regret-rejoice model [8]. Prospect theory makes full use of the bounded rationality and risk aversion of decision makers. Contrasting with the collective decision, there will be disparity between different assessments which will cause regret (loss) or rejoice (gain). Therefore, we take advantage of the regret concept for feedback and adjust the scheme with the known inconsistency information. Regret theory [42, 43] assumes that the DMs pay attention not only to results obtained by choosing alternatives but also to the outcome of other alternatives and avoid choosing alternatives that will make them regret.

Regret theory has been successfully applied for investment choice [44, 45] and decision making [42] and has shown that anticipated disutility from regret can have a potent effect on DMs. Thus, regret increases the regret averse attitude of an expert's willingness to adjust the scheme's assessment after knowing the difference between individual evaluation and collective evaluation until the optimal alternative ranking is finally achieved. The feedback adjustment information enables reevaluation at different state levels and includes four steps.

(1) Calculate Regret-Rejoice Value. Using V_{ij}^k, calculate the disparity between the individual and collective decision matrixes. The regret-rejoice value is

$$R\left(\Delta V\right) = 1 - e^{-\xi\Delta V}, \quad (9)$$

$$\Delta V = V_{ij}^k - V_{ij}^c, \quad (10)$$

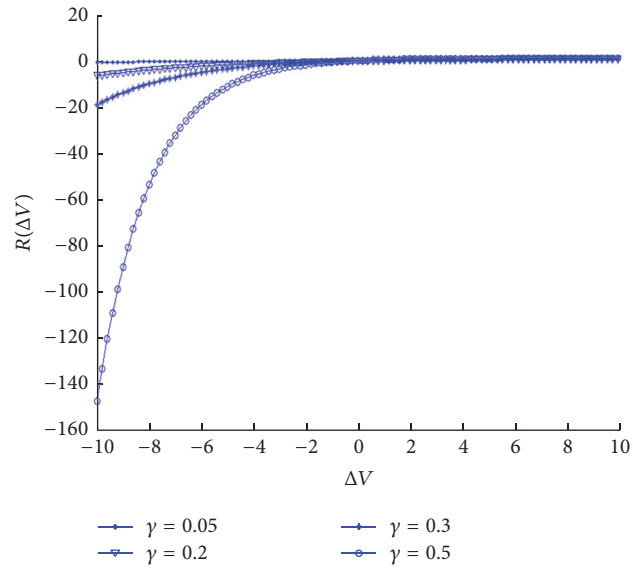

Figure 2: Effect of γ on the regret-rejoice value.

where ξ is the DM risk aversion coefficient. Larger ξ implies greater degree of DM risk aversion. Equation (10) denotes the difference between the prospect value of alternative a_i and attribute u_j for DM k. When $R(\Delta V) > 0$, $R(\Delta V)$ denotes rejoice, and when $R(\Delta V) < 0$, $R(\Delta V)$ denotes regret [19]. Similar to prospect theory, the DM is more sensitive to negative than to positive prospect, derived from psychological perception. Figure 2 shows the effect of ξ on $R(\Delta V)$.

(2) Lock the Feedback Scheme. Choose the minimum regret-rejoice value as the amended attribute of the adjustment alternative:

$$\min R\left(\Delta V\right) = \begin{cases} \min R\left(\Delta V\right) & R\left(\Delta V\right) < 0 \\ \text{or} & \\ \min R\left(\Delta V\right) & R\left(\Delta V\right) > 0. \end{cases} \quad (11)$$

Assuming V_{ij}^c to be the authoritative benchmark of the prospect value, when $\Delta V_0 < 0$, smaller values imply larger disparity between the individual and group prospect value matrixes. Smaller $R(\Delta V)$ implies more regret the DM feels for the evaluation, and larger $R(\Delta V)$ implies more desirable individual adjustment of the evaluation value.

Similarly, when $R(\Delta V) \geq 0$, larger values imply more satisfaction with the individual decision, and the DM often rejoices over underestimating the value of the alternative on the surface. However, they have known the defect of the alternative, so, the less desirable adjust the prospect value decision matrix of the alternative. Thus, they will keep the original assessment.

(3) Calculate Guidance Information for Feedback Adjustment. Compute the cloud prospect values from (3)–(5). When the feedback correction of prospect value matrix V_{ij}^k is locked, the target correction matrix is determined. If the prospect

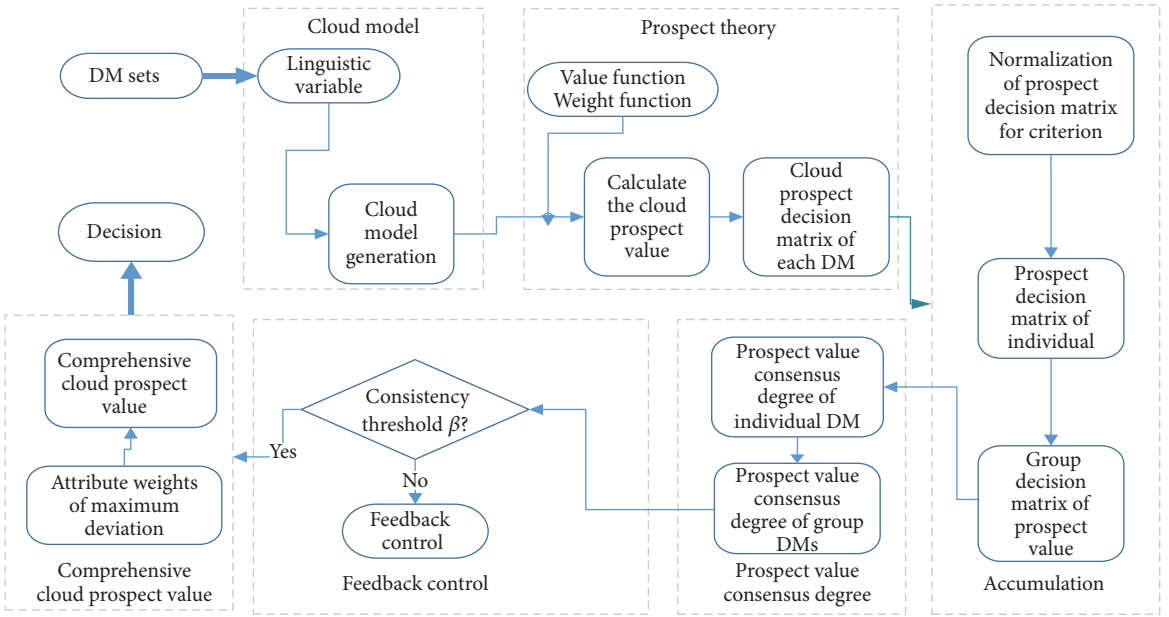

Figure 3: Group decision structure under the proposed cloud prospect and regret feedback procedure.

value $V_{ij}^k > V_{ij}^c$, then DM k should reduce x_{ijl}^k. Otherwise, the equality in (13) indicates that the DM could refuse to correct x_{ijl}^k.

If $V_{ij}^k < V_{ij}^c$, then DM k should increase x_{ijl}^k:

$$\text{if } V_{ij}^k > V_{ij}^c, \quad \text{then } \left(x_{ijl}^k\right)' \le x_{ijl}^k; \tag{12}$$

$$\text{if } V_{ij}^k = V_{ij}^c, \quad \text{then } \left(x_{ijl}^k\right)' = x_{ijl}^k; \tag{13}$$

$$\text{if } V_{ij}^k < V_{ij}^c, \quad \text{then } \left(x_{ijl}^k\right)' \ge x_{ijl}^k, \tag{14}$$

where $(x_{ijl}^k)'$ is the linguistic evaluation value after adjustment.

CPD provides a complete feedback regulation mechanism. It determines the consensus degree of the group decision at the alternative level and determines the program to be modified by comparing the CPD of all alternatives. CPD subdivides alternatives into attributes and confirms the attribute with the minimum regret-rejoice value. The feedback regulation of (12)–(14) ensures that the DMs are directed to reevaluate the alternatives and repeat all the procedures until all the alternatives satisfy β. The DMs can also refuse to reevaluate their decisions. Figure 3 shows the CPD model; Figure 4 shows the DM feedback regulation.

3.3. Decision Procedure. Under the multicriteria group decision environment, the group decision procedure based on prospect theory and the cloud model is as follows:

(1) The linguistic variables are transformed into a normal cloud model: following the DM linguistic evaluation criteria, the corresponding cloud model is combined with the effective universe, $U = [X_{\min}, X_{\max}]$, as discussed in Section 3.1.

(2) A cloud prospect decision matrix is constructed for each alternative: the cloud prospect decision matrix, $(V_{ij}^k)_{m\times n}$, is calculated for each DM for each alternative and attribute following (1)–(5).

(3) The cloud prospect decision matrixes are aggregated: we calculate the cloud prospect decision matrix of the group based on each DM's cloud prospect decision matrix.

(4) Compute the CPD: the consensus degree, CPD(e_k), is calculated for each DM. For a cloud prospect consensus degree threshold β, when CPD $\ge \beta$ for all alternatives or the DM refuses to correct x_{ijl}^k, proceed to Step (6); otherwise, proceed to Step (5).

(5) Control feedback: calculate the regret or rejoice value for all the alternatives for different criteria following (9) and (10). Lock feedback for the criteria with the minimum regret-rejoice value using (11) and provide correction and instruction information to the DMs using (12)–(14).

(6) Calculate weights to maximize deviation: the difference between individual and collective experts affects criteria weights. Maximizing deviation makes use of individual and group outputs to maximize this difference. Some criteria play an important role in the sorting of the schemes and should be endowed a larger weight coefficient. Therefore, in addition to the basic constraints, $\sum_{j=1}^n \omega_j = 1$, we add reasonable constraints to obtain optimal weight coefficients $\omega^* = (\omega_1^*, \omega_2^*, \ldots, \omega_n^*)$:

$$\max W = \sum_{i=1}^{m-1} \sum_{k=i+1}^{m} \sum_{j=1}^{n} \left|V_{ij}^c - V_{kj}^c\right| \cdot \omega_j. \tag{15}$$

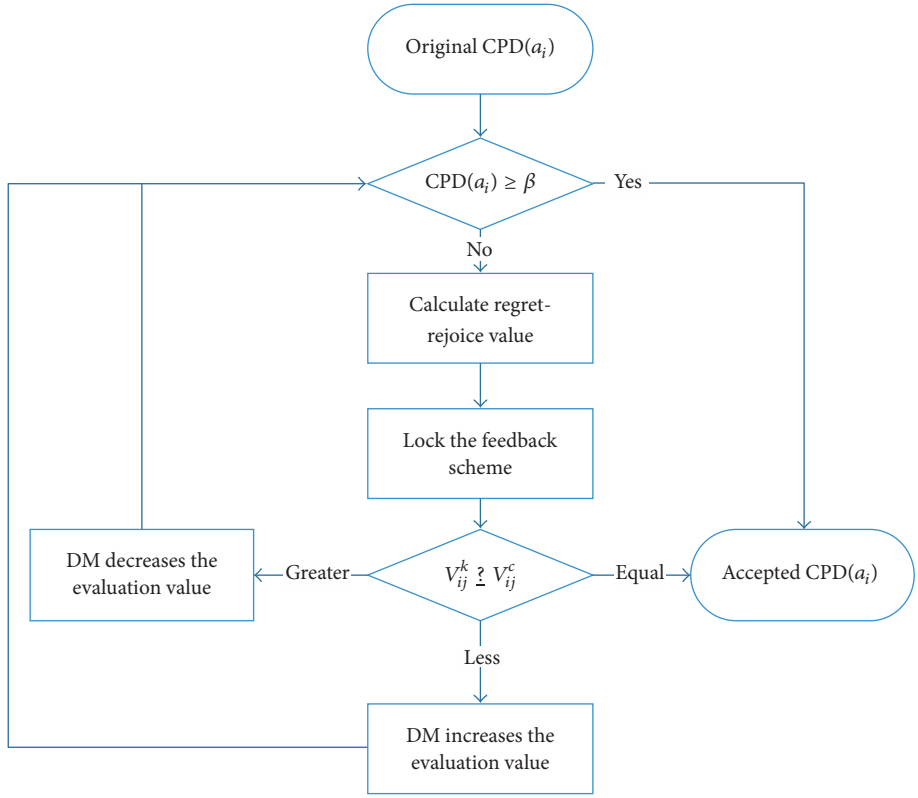

Figure 4: Feedback control diagram of DMs.

Table 1: Linguistic prospect decision matrix of e_1*.

	q_1					q_2					q_3					q_4				
	f_1^1	f_2^1	f_3^1	f_4^1	f_5^1	f_1^2	f_2^2	f_3^2	f_4^2	f_5^2	f_1^3	f_2^3	f_3^3	f_4^3	f_5^3	f_1^4	f_2^4	f_3^4	f_4^4	f_5^4
a_1	2	2	2	3	3	2	1	3	2	2	3	5	1	3	4	1	2	4	3	5
a_2	2	3	1	5	2	1	3	1	4	2	2	3	3	5	3	2	2	3	2	3
a_3	3	1	3	2	4	2	1	4	2	4	2	4	1	5	4	2	1	3	3	5
p	0.1	0.2	0.5	0.1	0.1	0.05	0.1	0.6	0.15	0.1	0.07	0.25	0.35	0.2	0.13	0.15	0.15	0.3	0.2	0.2

* e represents the first DM; f means the natural state; p represents the occurrence probability of the attribute; q_1–q_4 represent the four attributes of alternatives; a_1–a_3 mean the three alternatives.

(7) Compute the comprehensive prospect value: given the attribute weights ω_j, $j = 1, 2, \ldots, n$, for the DMs, we compute the comprehensive prospect value of each based on the comprehensive prospect value. The optimal alternative with the greatest comprehensive prospect value is

$$V_i = \sum_{j=1}^{n} \omega_j V_{ij}^c, \quad i = 1, 2, \ldots, m. \tag{16}$$

4. Numerical Analysis and Discussion

Investment in shipping vessels is one of the most important business activities in international shipping and involves large amounts of money, a long investment recovery period, and a significant risk level.

Consider a ship owner who intends to invest in one of three dry cargo ships: a_1 is a bulk carrier, a_2 is a container ship, and a_3 is a multipurpose ship. DMs evaluate the direct ($u1$), indirect ($u2$), social benefit ($u3$), and pollution loss ($u4$). Each of these four criteria is divided into five possible natural states: f_1^j = very good, f_2^j = good, f_3^j = fair, f_4^j = poor, and f_5^j = very poor. Then attribute Q has occurrence probability P under natural state f, and the linguistic evaluation set $S = \{1, 2, 3, 4, 5\}$ represents {very poor, poor, fair, good, very good}, respectively. Three experts from marketing, finance, and industry make independent linguistic evaluations, as shown in Tables 1–3.

Table 2: Linguistic prospect decision matrix of e_2.

	q_1					q_2					q_3					q_4				
	f_1^1	f_2^1	f_3^1	f_4^1	f_5^1	f_1^2	f_2^2	f_3^2	f_4^2	f_5^2	f_1^3	f_2^3	f_3^3	f_4^3	f_5^3	f_1^4	f_2^4	f_3^4	f_4^4	f_5^4
a_1	3	4	2	1	3	4	2	5	2	1	3	4	2	1	3	2	3	2	1	4
a_2	2	4	1	5	2	1	3	2	1	4	2	5	3	1	2	4	3	2	1	4
a_3	4	2	1	5	3	2	1	4	2	1	5	3	2	1	4	2	1	2	3	5
p	0.2	0.2	0.3	0.2	0.1	0.1	0.1	0.5	0.2	0.1	0.1	0.3	0.35	0.1	0.15	0.1	0.1	0.5	0.2	0.1

Table 3: Linguistic prospect decision matrix of e_3.

	q_1					q_2					q_3					q_4				
	f_1^1	f_2^1	f_3^1	f_4^1	f_5^1	f_1^2	f_2^2	f_3^2	f_4^2	f_5^2	f_1^3	f_2^3	f_3^3	f_4^3	f_5^3	f_1^4	f_2^4	f_3^4	f_4^4	f_5^4
a_1	2	4	3	1	5	2	3	4	1	2	5	3	2	1	4	2	5	1	3	4
a_2	4	2	1	5	3	2	5	4	1	2	3	5	4	1	2	1	2	3	5	4
a_3	4	1	3	2	5	2	2	2	1	4	2	3	5	4	1	4	3	5	1	2
p	0.1	0.3	0.2	0.2	0.2	0.2	0.3	0.1	0.2	0.2	0.2	0.2	0.3	0.1	0.2	0.2	0.2	0.4	0.1	0.1

Table 4: Numerical characteristics of cloud model.

Cloud model	Ex	En	He
$C_{+2}(Ex_{+2}, En_{+2}, He_{+2})$	10	2.0604	0.1309
$C_{+1}(Ex_{+1}, En_{+1}, He_{+1})$	3.82	1.2733	0.0809
$C_0(Ex_0, En_0, He_0)$	0	0.7869	0.05
$C_{-1}(Ex_{-1}, En_{-1}, He_{-1})$	−3.82	1.2733	0.0809
$C_{-2}(Ex_{-2}, En_{-2}, He_{-2})$	−10	2.0604	0.1309

The optimal dry cargo ship investment decision is made following the proposed CPD procedures described above:

(a) Linguistic variable transformation: the linguistic evaluation set is transformed to five cloud models on the universe $U = [-10, 10]$, that is, $\{C_{+2}, C_{+1}, C_0, C_{-1}, C_{-2}\}$. The numerical characteristics of the five clouds are shown in Table 4

(b) Producing the cloud prospect decision matrix: the cloud prospect decision matrix of individual V^k and group V^c is created following Steps (2) and (3). To obtain better distinction, we set $\alpha = \gamma = 0.88$, $\lambda = 2.25$, $\tau = 0.61$, and $\delta = 0.69$, (in the following matrixes, 0.0000 denotes a very small value, not necessarily 0):

$$V^1 = \begin{pmatrix} 0.7403 & 0.0142 & 0.1547 & 0.0000 \\ 1.0000 & 1.0000 & 0.0002 & 1.0000 \\ 0.0017 & 0.0000 & 1.0000 & 0.0005 \end{pmatrix}$$

$$V^2 = \begin{pmatrix} 0.7647 & 0.0000 & 1.0000 & 1.0000 \\ 1.0000 & 1.0000 & 0.0000 & 0.0034 \\ 0.0193 & 0.0250 & 0.0018 & 0.0000 \end{pmatrix},$$

$$V^3 = \begin{pmatrix} 0.0010 & 0.6907 & 0.2891 & 0.5786 \\ 0.0617 & 0.0000 & 0.1350 & 1.0000 \\ 1.0000 & 1.0000 & 1.0000 & 0.0000 \end{pmatrix},$$

$$V^C = \begin{pmatrix} -8.7761 & -10.1200 & -5.5585 & -6.1984 \\ -7.1995 & -4.9391 & -11.5442 & -3.2871 \\ -9.7045 & -7.5947 & -6.6376 & -12.4365 \end{pmatrix}. \quad (17)$$

(c) Aggregation and consistency measurement: individual and group CPDs are calculated based on a consensus degree threshold of $\beta = 0.9$ following Step (4), using (7) and (8). The original CPD of each alternative is listed in the second column of Figure 5, where the cylinders denote that the consistency degree threshold was satisfied, that is, passes consistency; and dashed rectangles represent a consistency degree below the lower limit, which do not pass the check. Although consistency does not meet the threshold in the solid rectangles, this iteration is temporarily permitted. To achieve a higher consistency threshold, all the alternatives iteratively proceed to feedback adjustment until reaching 0.98 threshold. The blue background graphic denotes the feedback adjusted attribute

(d) Feedback adjustment: following the feedback mechanism of Step (5), we compute the original CPD of each alternative, and a_1 and a_2 both do not reach the consistent degree threshold, 0.9. Since a_1 has the smallest CPD, we lock scheme a_1 as the correction alternative and then apply feedback control to satisfy the consistency degree. The specific feedback corrections are shown in Figure 5

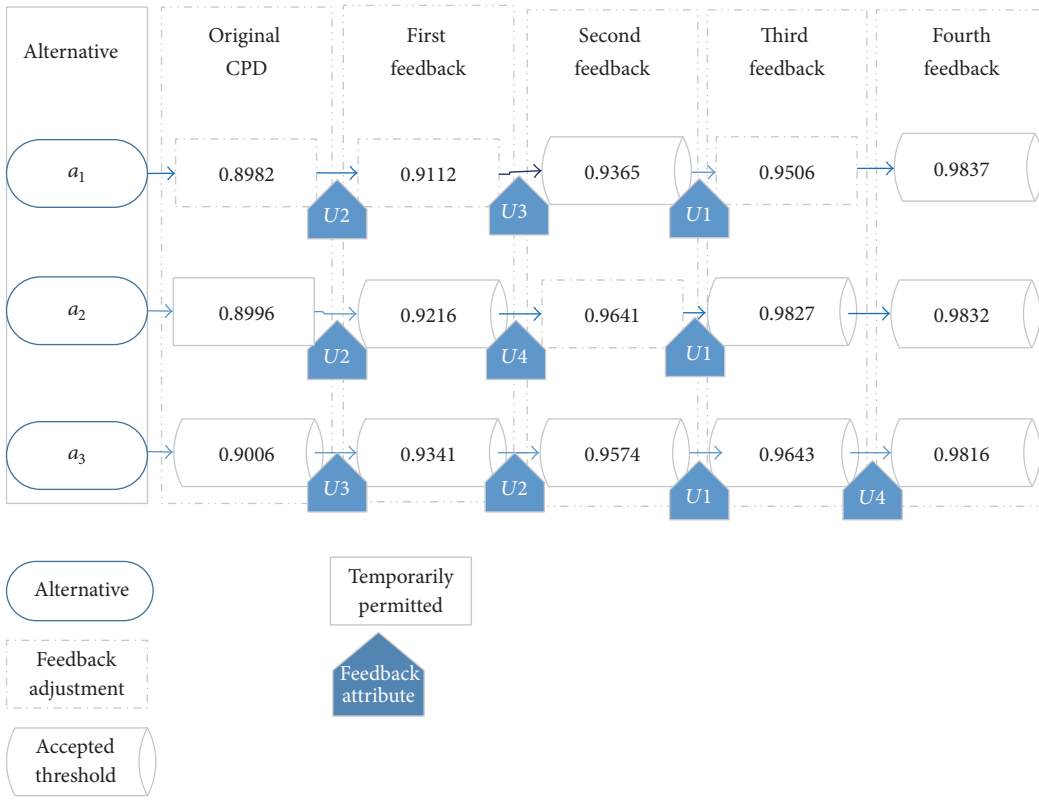

Figure 5: Feedback correction details.

(e) Feedback for alternative a_1: the feedback regulation mechanism based on regret theory includes the following:

(i) Ualculate ΔV, the difference between the individual and collection prospect value.

(ii) Use (10) to provide the psychological gap of regret or rejoice.

(iii) Calculate the regret-rejoice matrix, $R(\Delta V)$, from (9).

(iv) To better distinguish the effects, we set $\gamma = 0.5$.

Thus,

$$\Delta V_1 = \begin{pmatrix} 2.8345 & 4.8636 & 0.0542 & -5.7282 \\ 2.4006 & -13.8886 & 5.1601 & 7.3129 \\ -5.2351 & 9.0249 & -5.2142 & -1.5846 \end{pmatrix}$$

$$R(\Delta V_1) = \begin{pmatrix} 0.7576 & 0.9121 & 0.0267 & -16.5337 \\ 0.6989 & -1036.2413 & 0.9242 & 0.9742 \\ -12.7022 & 0.9890 & -12.5596 & -1.2085 \end{pmatrix}. \quad (18)$$

(f) Lock the adjustment decision maker: from (11), decision maker e_2 has the minimum regret-rejoice value to attribute q_2 (−1036.2413), which has the greatest disparity relative to the collective DMs and indicates that DM e_1 feels the maximum regret for attribute q_2. Then lock $R_{2,2}$ as the adjustment element. Provide guide information for the feedback adjustment as $V_{ij}^k(-24.9475) < V_{ij}^c(-11.0589)$ and then $(x_{iji}^k)' \geq x_{ijl}^k$; then increase $x_{2,2,3}$ from 3 to 4 under that state.

After the first correction, the individual and collective decision matrixes are

$$\left(V^1\right)' = \begin{pmatrix} -10.9416 & 0.8795 & -9.5043 & -16.6805 \\ -5.6409 & -14.2913 & -12.3644 & -6.8879 \\ -11.9936 & -3.0713 & -8.6384 & -16.4293 \end{pmatrix}$$

$$\left(V^2\right)' = \begin{pmatrix} -12.0808 & -5.9475 & -4.3984 & 1.1145 \\ -14.0602 & -6.8756 & -10.7037 & -6.5837 \\ -10.0540 & 1.4445 & -12.3211 & -22.2397 \end{pmatrix},$$

$$\left(V^3\right)' = \begin{pmatrix} -19.0112 & -1.0340 & -18.4154 & -7.7830 \\ -9.8505 & -16.5835 & -11.5341 & -8.2358 \\ 0.8503 & -0.8133 & -7.6361 & -28.3345 \end{pmatrix},$$

Table 5: Consensus for the proposed regret-rejoice feedback.

Consistency threshold	Round	Consistency	Feedback loops	Stop iteration
$\beta = 0.9$	1	0.8982	0	No
$\beta = 0.9$	2	0.9112	1	Yes
$\beta = 0.95$	3	0.9365	2	No
$\beta = 0.95$	4	0.9506	3	Yes
$\beta = 0.98$	5	0.9837	4	Yes

Table 6: Consensus for direct feedback.

Consistency threshold	Round	Consistency	Feedback loops	Stop iteration
$\beta = 0.9$	1	0.8982	0	No
$\beta = 0.9$	2	0.8991	1	No
$\beta = 0.9$	3	0.9040	2	Yes
$\beta = 0.95$	4	0.9054	3	No
$\beta = 0.95$	5	0.9257	4	No
$\beta = 0.95$	6	0.9321	5	No
$\beta = 0.95$	7	0.9435	6	No
$\beta = 0.95$	8	0.9508	7	Yes
$\beta = 0.98$	9	0.9425	8	No
$\beta = 0.98$	10	0.9739	9	No
$\beta = 0.98$	11	0.9563	10	No

$$(V^c)' = \begin{pmatrix} -14.0112 & -2.0340 & -10.7727 & -7.7830 \\ -9.8505 & -12.5835 & -11.5341 & -7.2358 \\ -7.0658 & -0.8133 & -9.5318 & -22.3345 \end{pmatrix}. \tag{19}$$

(g) First round of feedback adjustment results: after adjusting alternative a_1, $\mathrm{CPD}(a_1) = 0.9112$ and, after the first feedback adjustment, alternatives a_2 and a_3 both satisfy the threshold $\beta = 0.9$. The CPDs of all the three alternatives are improved significantly: $\mathrm{CPD}(a_2) = 0.9216$ and $\mathrm{CPD}(a_3) = 0.9341$. Thus, the first feedback causes the consistency degree of alternatives a_1, a_2, and a_3 to increase by 1.45%, 2.45%, and 3.42%, respectively

(h) High degree of consensus: to improve degree of consensus, we increased the consensus threshold to $\beta = 0.95$, requiring a further feedback. Comparing the three alternative CPDs, a_1 was further locked, and after the second feedback all the schemes except a_2 satisfied the higher threshold. Assuming that the consistency was 0.98, we repeated the procedure in procedure (e), and the iteration stopped. Figure 5 shows the detailed feedback and consistency degrees

(i) Calculating criteria weights: from Step (6), the model is

$$\begin{aligned} \max \quad & Z \\ & = 2.1392\omega_1 + 1.4769\omega_2 + 1.7881\omega_3 \\ & \quad + 2.0539\omega_4 \\ \text{s.t.} \quad & \sum_{j=1}^{4} \omega_j = 1 \\ & 0.15 \le \omega_1 \le 0.2 \\ & 0.3 \le \omega_2 \le 0.5 \\ & \omega_1 \le \omega_4 \le \omega_2 \\ & 0 < \omega_3 \le \omega_4, \end{aligned} \tag{20}$$

which provides attribute weights $\omega = [0.2, 0.3, 0.2001, 0.2999]$, and, from (16), $V = (-7.8111, -7.7813, -7.6412)$

Thus, following the maximizing principle, the optimal alternative is a_3 (multipurpose ship) and then a_2 (container ship), and the worst prospect value is a_1 (bulk carrier).

The proposed CPD method uses feedback adjustment, whereby the DMs are presented with specific feedback. The high efficiency of the proposed method is evident by comparison with direct feedback, which is the comparison of individual and group prospect decision matrices (see (12)–(14)). Consider alternative a_1 as an example, where original CPD = 0.8982. Table 5 shows the variation of an increasing consistency degree with regret-rejoice feedback, and Table 6 shows the case for direct feedback. Direct feedback requires twice the feedback to achieve the given thresholds ($\beta = 0.9$); that is, the improvement of consensus degree increases slowly. Direct feedback, after 8 feedback loops, obtains a high consensus degree, $\beta = 0.95$. However, using regret theory of feedback thought, after three loops of correction, CPD has

a higher consensus degree of 0.9506, which satisfies a higher threshold beforehand. Again, compared to the proposed CPD method, if $\beta = 0.98$, the regret feedback adjustment reaches the threshold after 4 feedback loops, whereas the direct feedback has still not reached the threshold after 10 feedback loops. Thus, the proposed CPD method shows high efficiency for the regret feedback mechanism

Consistency after regret-rejoice feedback is always improved, but consistency after direct feedback does not always increase; for example, the eighth feedback decreases. This unstable trend reduces efficiency and greatly increases the complexity of group decision making.

Thus, the proposed regret feedback method significantly reduces the number of corrections which reduces time costs and increases decision making efficiency.

5. Conclusion

We proposed a new method to address the problem of risky multiattribute group decisions, where group decision making is under a complicated and ambiguous environment. The decision attribute varies within an uncertain environment that changes with the situation. We propose formulating the group decision making process as a fuzzy linguistic variable evaluation and constructed a cloud prospect aggregation method, consistency measurement, and feedback mechanism for the consistency model. The proposed CPD model incorporates the advantages of the cloud model randomness and vagueness, prospect theory sensitivity to loss, and risk aversion based on a regret feedback mechanism to provide an organic cloud prospect consistency degree method. This fusion approach not only ensures group decision consistency but also guides the DMs to correct the decision matrix through an efficient feedback adjustment mechanism. The proposed method was verified by an algorithm example, showing the efficiency of feedback loops, consistency, and so forth.

Conflicts of Interest

The authors declare that they have no conflicts of interest.

Acknowledgments

This work was supported by the National Natural Science Foundation of China (51409065 and 71101034), the project of Provincial Natural Science Foundation (JJ2016QN0048), the project of Provincial Postdoctoral Fund (LBH-Z15047), and the project of the Provincial Youth Science Foundation (JJ2016QN0645).

References

[1] R. E. Steuer and P. Na, "Multiple criteria decision making combined with finance: a categorized bibliographic study," *European Journal of Operational Research*, vol. 150, no. 3, pp. 496–515, 2003.

[2] J. Wallenius, J. S. Dyer, P. C. Fishburn, R. E. Steuer, S. Zionts, and K. Deb, "Multiple criteria decision making, multi-attribute utility theory: recent accomplishments and what lies ahead," *Management Science*, vol. 54, no. 7, pp. 1336–1349, 2008.

[3] P. Liu and W. Li, "Risky multiobjective decision making theory and its application," *Chinese Journal of Management Science*, vol. 11, no. 6, article 1014, 2003.

[4] A. Eskandari, P. Ffolliott, and F. Szidarovszky, "Uncertainty and method choice in discrete multiobjective programming problems," *Applied Mathematics and Computation*, vol. 69, no. 2-3, pp. 335–351, 1995.

[5] F. H. Knight, *Risk, Uncertainty and Profit*, Houghton Mifflin, New York, NY, USA, 1921.

[6] J. S. H. Kornbluth, "Dynamic multi-criteria decision making," *Journal of Multi-Criteria Decision Analysis*, vol. 1, no. 2, pp. 81–92, 1992.

[7] F. Meng, C. Tan, and X. Chen, "An approach to Atanassov's interval-valued intuitionistic fuzzy multi-attribute decision making based on prospect theory," *International Journal of Computational Intelligence Systems*, vol. 8, no. 3, pp. 591–605, 2015.

[8] Z. P. Fan, X. Zhang, F. D. Chen, and Y. Liu, "Multiple attribute decision making considering aspiration-levels: a method based on prospect theory," *Computers & Industrial Engineering*, vol. 65, pp. 341–350, 2013.

[9] H. Hansson and C. J. Lagerkvist, "Decision making for animal health and welfare: integrating risk-benefit analysis with prospect theory," *Risk Analysis*, vol. 34, no. 6, pp. 1149–1159, 2014.

[10] Y. Dong, N. Luo, and H. Liang, "Consensus building in multiperson decision making with heterogeneous preference representation structures: a perspective based on prospect theory," *Applied Soft Computing Journal*, vol. 35, pp. 898–910, 2015.

[11] X. H. Li and X. H. Chen, "Extension of the TOPSIS method based on prospect theory and trapezoidal intuitionistic fuzzy numbers for group decision making," *Journal of Systems Science and Systems Engineering*, vol. 23, no. 2, pp. 231–247, 2014.

[12] N. Zhang, Z. Fang, and X. Liu, "Grey situation group decision-making method based on prospect theory," *The Scientific World Journal*, vol. 2014, Article ID 703597, 7 pages, 2014.

[13] C. L. Hwang and K. Yoon, *Multiple Attribute Decision Making: Methods and Applications*, Springer, New York, NY, USA, 1981.

[14] S. Opricovic and G. H. Tzeng, "Compromise solution by MCDM methods: a comparative analysis of VIKOR and TOPSIS," *European Journal of Operational Research*, vol. 156, no. 2, pp. 445–455, 2004.

[15] L. A. Zadeh, "Fuzzy sets," *Information and Control*, vol. 8, no. 3, pp. 338–353, 1965.

[16] F. Chiclana, F. Herrera, and E. Herrera-Viedma, "Integrating three representation models in fuzzy multipurpose decision making based on fuzzy preference relations," *Fuzzy Sets and Systems*, vol. 97, no. 1, pp. 33–48, 1998.

[17] H. Behret, "Group decision making with intuitionistic fuzzy preference relations," *Knowledge-Based Systems*, vol. 70, pp. 33–43, 2014.

[18] H. Liao, Z. Xu, X.-J. Zeng, and D.-L. Xu, "An enhanced consensus reaching process in group decision making with intuitionistic fuzzy preference relations," *Information Sciences*, vol. 329, pp. 274–286, 2016.

[19] X. D. Peng and Y. Yang, "Algorithms for interval-valued fuzzy soft sets in stochastic multi-criteria decision making based on regret theory and prospect theory with combined weight," *Applied Soft Computing*, vol. 54, pp. 1–16, 2016.

[20] X. Yang, T. Y. Lin, J. Yang, Y. Li, and D. Yu, "Combination of interval-valued fuzzy set and soft set," *Computers & Mathematics with Applications*, vol. 58, no. 3, pp. 521–527, 2009.

[21] D. F. Li, "Multiattribute decision making models and methods using intuitionistic fuzzy sets," *Journal of Computer & System Sciences*, vol. 70, no. 1, pp. 73–85, 2005.

[22] F. Q. Wang, X. Li, and X. H. Chen, "Hesitant fuzzy soft set and its applications in multicriteria decision making," *Journal of Applied Mathematics*, vol. 2014, Article ID 643785, 10 pages, 2014.

[23] L. I. De-Yi, C. Y. Liu, D. U. Yi, and X. Han, "Artificial intelligence with uncertainty," *Journal of Software*, vol. 15, no. 11, article 2, 2004.

[24] L. Deyi, M. Haijun, and S. Xuemei, "Membership clouds and membership cloud generators," *Journal of Computer Research and Development*, vol. 32, no. 6, pp. 15–20, 1995.

[25] W. Shuliang, L. Deren, S. Wenzhong, L. Deyi, and W. Xinzhou, "Cloud model-based spatial data mining," *Geographical Information Science*, vol. 9, no. 2, pp. 67–78, 2003.

[26] Y. Weng and Z. Zhongying, "Pattern mining for time series based on cloud theory pan-concept-tree," in *Proceedings of the International Conference on Rough Sets and Current Trends in Computing*, 2004.

[27] Z. Yunfang, D. Chaohua, and C. Weirong, "Adaptive probabilities of crossover and mutation in genetic algorithms based on cloud generators," *Journal of Computational Information Systems*, vol. 1, no. 4, pp. 671–678, 2005.

[28] P. Lv, L. Yuan, and J. Zhang, "Cloud theory-based simulated annealing algorithm and application," *Engineering Applications of Artificial Intelligence*, vol. 22, no. 4-5, pp. 742–749, 2009.

[29] D. Li, C. Liu, and W. Gan, "A new cognitive model: cloud model," *International Journal of Intelligent Systems*, vol. 24, no. 3, pp. 357–375, 2009.

[30] L. Y. Zhang, T. Li, and X. H. Xu, "Consensus model for multiple criteria group decision making under intuitionistic fuzzy environment," *Knowledge-Based Systems*, vol. 57, pp. 127–135, 2014.

[31] F. Meng and X. Chen, "An approach to uncertain linguistic multi-attribute group decision making based on interactive index," *International Journal of Uncertainty, Fuzziness and Knowledge-Based Systems*, vol. 23, no. 3, pp. 319–344, 2015.

[32] P. Liu, F. Jin, X. Zhang, Y. Su, and M. Wang, "Research on the multi-attribute decision-making under risk with interval probability based on prospect theory and the uncertain linguistic variables," *Knowledge-Based Systems*, vol. 24, no. 4, pp. 554–561, 2011.

[33] S. L. Wang, *Spatial data mining and knowledge discovery based on data field and cloud model [dissertation]*, Wuhan University, 2002.

[34] Y. J. Wang and H. S. Lee, "Generalizing TOPSIS for fuzzy multiple-criteria group decision-making," *Computers & Mathematics with Applications*, vol. 53, no. 11, pp. 1762–1772, 2007.

[35] J. Ren, "Linguistic-stochastic multi-criterion decision-making method based on cloud model," *Computer Integrated Manufacturing Systems*, vol. 18, no. 12, pp. 2792–2797, 2012.

[36] J.-Q. Wang, P. Lu, H.-Y. Zhang, and X.-H. Chen, "Method of multi-criteria group decision-making based on cloud aggregation operators with linguistic information," *Information Sciences*, vol. 274, pp. 177–191, 2014.

[37] J.-Q. Wang, J.-J. Peng, H.-Y. Zhang, T. Liu, and X.-H. Chen, "An uncertain linguistic multi-criteria group decision-making method based on a cloud model," *Group Decision and Negotiation*, vol. 24, no. 1, pp. 171–192, 2015.

[38] K. Zhao, J. W. Gao, Z. Q. Qi, and C. B. Li, "Multi-criteria risky-decision-making approach based on prospect theory and cloud model," *Control and Decision*, vol. 30, no. 3, pp. 395–402, 2015.

[39] A. Tversky and D. Kahneman, "Advances in prospect theory: cumulative representation of uncertainty," *Journal of Risk and Uncertainty*, vol. 5, no. 4, pp. 297–323, 1992.

[40] J. Kacprzyk and M. Fedrizzi, "A 'soft' measure of consensus in the setting of partial (fuzzy) preferences," *European Journal of Operational Research*, vol. 34, no. 3, pp. 316–325, 1988.

[41] X. Chen, H. Zhang, and Y. Dong, "The fusion process with heterogeneous preference structures in group decision making: a survey," *Information Fusion*, vol. 24, pp. 72–83, 2015.

[42] D. E. Bell, "Regret in decision making under uncertainty," *Operations Research*, vol. 30, pp. 961–981, 1982.

[43] G. Loomes and R. Sugden, "Regret theory: an alternative theory of rational choice under uncertainty," *The Economic Journal*, vol. 92, no. 368, pp. 805–824, 1982.

[44] A. Muermann, O. S. Mitchell, and J. M. Volkman, "Regret, portfolio choice, and guarantees in defined contribution schemes," *Insurance: Mathematics & Economics*, vol. 39, no. 2, pp. 219–229, 2006.

[45] S. Michenaud and B. Solnik, "Applying regret theory to investment choices: currency hedging decisions," *Journal of International Money and Finance*, vol. 27, no. 5, pp. 677–694, 2008.

Hindawi
Mathematical Problems in Engineering
Volume 2017, Article ID 6738139, 13 pages
https://doi.org/10.1155/2017/6738139

Research Article

Modeling and Simulation Study of Designer's Bidirectional Behavior of Task Selection in Open Source Design Process

Shuo Zhang[1,2] and Yingzi Li[3]

[1]*School of Economics and Management, North China Electric Power University, Beijing 102206, China*
[2]*Beijing Key Laboratory of New Energy and Low-Carbon Development, North China Electric Power University, Beijing 102206, China*
[3]*Donlinks School of Economics and Management, University of Science and Technology Beijing, Beijing 100083, China*

Correspondence should be addressed to Yingzi Li; liyz@ustb.edu.cn

Received 9 January 2017; Revised 25 April 2017; Accepted 2 May 2017; Published 24 May 2017

Academic Editor: M. L. R. Varela

Open source design (OSD) is an emerging mode of product design. In OSD process, how to select right tasks directly influences the efficiency and quality of task completion, hence impacting the whole evolution process of OSD. In this paper, designer's bidirectional behavior of task selection integrating passive selection based on website recommendation and autonomous selection is modeled. First, the model of passive selection behavior by website recommendation is proposed with application of collaborative filtering algorithm, based on a three-dimensional matrix including information of design agents, tasks, and skills; second, the model of autonomous selection behavior is described in consideration of factors such as skill and incentive; third, the model of bidirectional selection behavior is described integrating the aforementioned two selection algorithms. At last, contrast simulation analysis of bidirectional selection, passive selection based on website recommendation, and autonomous selection is proposed with ANOVA, and results show that task selection behavior has significant effect on OSD evolution process and that bidirectional selection behavior is more effective to shorten evolution cycle according to the experiment settings. In addition, the simulation study testifies the model of bidirectional selection by describing the task selection process of OSD in microperspective.

1. Introduction

Open source design (OSD), also called mass collaborative product development (MCPD), is an emerging design mode in recent years. In OSD process, many volunteer designers with different knowledge autonomously contribute to product development, as well as product creation, design, test, and even popularization by means of open network platform [1]. OSD is in rapid development with advantage of high innovation, low cost, and high customer satisfaction. Thus, OSD gradually becomes an important complementary mode of traditional collaborative product development (CPD) [2]. Different from the top-down organization mode of traditional CPD, the organization of OSD is in bottom-up self-organized structure, and OSD including organization and project/product is in continuous evolution [3]. Moreover, OSD can make full use of the emergence of design originality, as well as sharing in technology, resource, and knowledge between designers.

At present, Open Source Software (OSS) is the most successful application of OSD, and some open source communities (OSC) that coexist with OSS are in effective operation like Linux, Apache, Mozilla, and so on [4]. Meanwhile, OSD has been applied in industrial product design [5]. By this mode, the new product originality or CAD model is released to public by volunteer designers or enterprises, and many OSC members will complete it collaboratively by Internet. New ideas and products are constantly emerging in some famous innovation OSC such as Open Source Car, Prosthetics Project, and Lego Mindstorms [6–8]. These cases show that OSD is influencing product design mode deeply and comprehensively.

In OSD process, task selection is an important phase, in which designers endeavor to select appropriate tasks

to promote design process effectively. If this phase is not worked well, it may be a bottleneck that restricts efficiency and quality of task execution. To select matched tasks from numerous candidates, designers perform selection behaviors in consideration of many relevant subjective and objective factors, such as individual preference, technical ability, and motivators. However, there is little research on task selection of OSD process. On this aspect, designers' behaviors are described effectively and expressly from microperspectives in detail by theory of Complex Adaptive System (CAS) and agent modeling [9]. As a result, task selection behavior of designers in OSD process is studied based on CAS in this paper.

The rest of the paper is organized as follows. In Section 2, related work on task selection study of OSD and related area is discussed. In Section 3, bidirectional behavior of task selection integrating passive and autonomous selection methods is proposed. In Section 4, simulation experiments based on an engineering design case of cell phone are designed, and related simulations are carried out to make contrastive analysis of different selection behaviors and analyze designers' bidirectional behaviors of task selection during OSD process from microscopic view. In Section 5, the highlights and future work are represented.

2. Related Work

In OSD process, it is a key point to select tasks matched to designers, which can improve the efficiency and success rate of open source project. However, there is little research on designers' task selection behaviors in OSD with quantitative model and algorithm. As regards to selection problem, there are abundant researches such as recommendation and task allocation. Therefore, relative studies on web service recommendation and task allocation are discussed for reference.

2.1. Research on Web Service Recommendation. The ongoing rapid expansion of the Internet greatly increases the necessity of effective recommendation systems for filtering the abundant information [10]. A recommendation system, which is widely applied in web service such as online shopping, e-resource services, and social network activities, aims to provide users with personalized online product or service recommendations to handle the increasing online information overload problem [11]. Collaborative filtering (CF) is widely employed for making web service recommendation [12]. CF-based web service recommendation, which attempts to predict what information will meet a user's needs from the neighborhoods of like-minded people or similar items, aims to recommend users products, services, resources, and so on, to best satisfy their requirements [13]. There are usually millions of customers and products in web service recommendation system, which is similar to OSD system. Hence, the recommendation models such as CF are of great value on task recommendation research of OSD. According to web service recommendation system, users' selection behaviors during OSD process can be described by system's recommendation algorithm.

2.1.1. Recommendation Research on Online Shopping. To attract more customers and provide them good service to select satisfactory products, many e-commerce enterprises, such as Amazon, develop recommendation systems to recommend customers products which they probably need [14].

Rodrigues and Ferreira [15] propose a hybrid recommendation system that combines content-based, collaborative filtering, and data mining techniques, to surpass recommendation difficulties of low efficiency and quality to provide customer right products. In addition, a novel recommendation system using collaborative filtering algorithm is implemented in Apache Hadoop leveraging MapReduce paradigm for Bigdata, and the Amazon dataset is used for the product recommendations [16]. Online personalized product ranking is also extensively discussed in the literature of recommendation systems and considered beneficial to both consumers and e-retailers. Zhang et al. [17] propose a new approach called Ranking with Prediction Uncertainty to improve the accuracy of personalized product ranking based on collaborative filtering techniques. Arguing that current approaches are suboptimal in terms of matching tasks and contributors' individual interests and capabilities, Geiger and Schader [18] advocate the introduction of personalized task recommendation mechanisms in crowdsourcing information systems and contribute to a conceptual foundation for the design of such mechanisms by conducting a systematic review of the corresponding academic literature. Moreover, the multicriteria based CF presents a possibility of providing accurate recommendations by considering the user preferences in multiple aspects. Hence, Nilashi et al. [19] propose new recommendation methods using Adaptive Neuro-Fuzzy Inference Systems (ANFIS) and Self-Organizing Map (SOM) clustering to improve predictive accuracy of criteria CF, in which SOM enables generating high quality clusters of dataset and ANFIS is used for discovering knowledge (fuzzy rules) from users' ratings in multicriteria dataset. In recommendation system, the sparsity problem usually occurs in the transaction data, which makes it difficult to identify reliable neighbors, resulting in less effective recommendations. Therefore, Choi et al. [20] suggest a means to derive implicit rating information from the transaction data of an online shopping mall and then propose a new user similarity function, which computes the user similarity of two users if they rated similar items, to mitigate the sparsity problem.

2.1.2. Recommendation Research on e-Resource Service. Recommendation systems are information filtering tools that aspire to predict the rating for users and items, predominantly from big data to recommend their likes. This makes recommendation system essentially a central part of e-commerce applications. In e-resource service area, the emergence of the online media sharing sites (e.g., YouTube, Youku, and Hulu) has introduced new challenges in program recommendation in online networks, and personalized recommendation services can effectively solve this problem to assist users in classifying users with similar interests.

Katarya and Verma [21] suggest an improved movie recommendation system through data clustering and computational intelligence, applying hybrid of k-means and cuckoo

search to the Movielens dataset. However, there is a bottleneck that the amount of available viewing logs and user friendship networks are too limited to design effective recommendation algorithms. Thus, Li et al. [22] propose a novel recommendation model which turns to the social networks and mine user preferences information expressed in microblogs for evaluating the similarity between online movies and TV episodes, to bridge the gap between domains of movie and TV watchers with social network activities. In addition, García-Cumbreras et al. [23] present a novel application of Sentiment Analysis by categorizing users according to the average polarity of their comments, use these categories as attributes in CF algorithms, and prove this solution can provide a more reliable prediction by generating a new corpus of opinions on movies obtained from the Internet Movie Database. In consideration of annotation information, Wei et al. [24] propose a hybrid movie recommendation approach using tags and rating, to improve recommendation accuracy. On the other hand, music recommendation is a research topic of increasing interest since online music platforms have become rapidly popular. However, some important problems, such as the difficulty of extracting content information from music, must be addressed in order to give reliable recommendations. Sánchez-Moreno et al. [25] propose a recommendation method based on playing coefficients to deal with gray sheep and sparsity problems without needing user attributes, content data, and explicit ratings from users, and the proposal is proved to outperform the methods that make use of user attributes. Meanwhile, content personalization is a long-standing problem for online news services. Bai et al. [26] study the problem of news personalization by leveraging usage information that is external to the news service, propose a novel approach applying user profiles that are built based on the past interactions of the user with a web search engine, and extensively test it on real-world datasets obtained from Yahoo. Resources in cloud computing platforms such as Amazon, Google AppEngine, and Microsoft Azure provide a new space of mobile search to improve the availability of cloud resources. On this aspect, Zhao et al. [27] propose a hybrid filtering mechanism to eliminate irrelevant or less relevant results for personalized mobile search, which combines content-based filtering and collaborative filtering to make use of the user's query history and communication history of social network.

2.1.3. Recommendation Research on Social Network Activities. The rapid growth of social network services has produced a considerable amount of data, called big social data. Big social data are helpful for improving personalized recommendation systems because these enormous data have various characteristics. Therefore, many personalized recommendation systems based on big social data have been proposed.

Seo et al. [28] introduce an appropriate measure to calculate the closeness between users in a social circle, namely, the friendship strength, proposing a friendship strength-based personalized recommendation system that recommends topics or interests users might have in multidomain environments order by analyzing big social data, using Twitter in particular. Based on collaborative filtering methods, Shahmohammadi et al. [29] propose directed proximity measures for activity prediction and recommendation both for pairs of users without any interaction background and also for user pairs with the activity background and perform experiments on the dataset of different Facebook activity networks including like, comment, post, and share networks, showing that the proposed collaborative methods deal with the activity prediction.

In social networks, a commonly adopted recommendation method takes advantage of the tastes of a user's trust neighbors and recommends resources which his/her neighbors have bought or evaluated. It will perform poorly for the inactive users who have few trust neighbors. Social tagging has become increasingly prevalent on the Internet, which provides an effective way for users to organize, manage, share, and search for various kinds of resources. Guo et al. [30] try to find users' similar neighbors using tag information which is not only from users' photos but also from their favorite photos and the common friend information, propose a group recommendation scheme utilizing users' trust neighbors and similar neighbors' tastes, and do the experiments on a real-world Flickr dataset and obtain a promising result especially for inactive users. Zheng and Li [31] investigate the importance and usefulness of tag and time information when predicting users' preference and examine how to exploit such information to build an effective resource-recommendation model, carrying out empirical research with data from a real-world dataset to show that tag and time information can well express users' taste and that better performances can be achieved if such information is integrated into collaborative filtering.

With the rapid development of web service technology and cloud computing environments, more and more service providers supply web services with the same features. To solve the service discovery problem, Lin et al. [32] propose a trustworthy two-phase web service discovery mechanism based on QoS (Quality of Service) and CF, which discovers and recommends the needed web services effectively for users in the distributed environment, and also solve the problem of services with incorrect QoS information. In the constantly changing business environment, organizations must exploit effective and efficient methods of preserving, sharing, and reusing knowledge in order to help knowledge workers find task-relevant information. Hence, Lai and Liu [33] propose hybrid recommendation methods based on a knowledge flow model, which integrates KF mining, sequential rule mining, and CF techniques to understand knowledge workers' task-needs and the ways they reference documents, and recommend codified knowledge.

2.1.4. Cold Start Problem of Collaborative Filtering in Recommendation System. Although collaborative filtering (CF) is widely used for recommendation systems, it suffers from complete cold start (CCS) problem where no rating records are available and incomplete cold start (ICS) problem where only a small number of rating records are available for some new items or users in the system.

Wei et al. [34] propose two recommendation models to solve the CCS and ICS problems for new items, which are based on a framework of tightly coupled CF approach and

deep learning neural network, and the experiment results on Netflix movie recommendation show the tight coupling of CF approach and deep learning neural network is feasible and very effective for cold start item recommendation. Meanwhile, Kim et al. [35] propose a collaborative filtering method to provide an enhanced recommendation quality derived from user-created tags, in which collaborative tagging is employed as an approach in order to grasp and filter users' preferences for items, and experimental results show that the proposed algorithm offers significant advantages in terms of both improving the recommendation quality for sparse data and dealing with cold start users as compared to existing work. Recommending items to new users generally creates a sense of belonging and loyalty and encourages them to frequently utilize recommendation systems. Chen et al. [36] propose a cold start recommendation method for the new user that integrates a user model with trust and distrust networks to identify trustworthy users, whose suggestions are then aggregated to provide useful recommendations for cold start new users, and experiments based on the well-known Epinions dataset demonstrate the efficacy of the proposed method. Given that the relational characteristics between items can provide much useful information during the recommendation process, Lv et al. [37] propose an item recommendation method based on a domain ontology and genetic algorithm (GA), obtain data relations between items by using all the item relations in the ontology and GA, and utilize the data relations as the basis of the online top-n item recommendations to solve the cold start problem.

2.2. Research on Task Allocation. It is a kind of passive behaviors for customers to select products or services by recommendation system, which endeavors to provide accurate recommendations by prediction. Nevertheless, customers usually surf the web and select products or services on their own initiative, instead of recommendations by system. In this case, autonomous selection is an important type of task selection in OSD. However, there is little research on autonomous selection of tasks. Compared to autonomous selection, which is performed personally, task allocation is usually brought out from an overall perspective of systems or workflows. In spite of this, the two behaviors are both in consideration of matching attributes between individuals and tasks. Hence, the research on task allocation is considerable reference for autonomous selection study. Some research on task allocation is abstracted as follows.

Ul Hassan and Curry [38] provide a conceptual framework to study the minimum-cost maximum reliability assignment problem with online combinatorial optimization and online learning on spatial crowdsourcing, which provides new insights into the combinatorial assignment strategies when the objective is to maximize reliability and minimize costs. Brahmbhatt and Camorlinga [39] leverage the existing similarity between disease epidemics and distributed system services and evaluate several factors on the SARS pandemics from a CAS perspective, which provides several insights and inspiration used to develop an algorithm for the task assignment problem in a distributed system. To assign workers to tasks effectively, Nembhard and Bentefouet [40] investigate the operational decision-making processes including selecting workers from a pool, grouping workers based on individual characteristics, and assigning groups to tasks and model worker productivity to include skill knowledge obtained by learning-by-doing and learning-by-transfer. To handle scheduling of tasks on heterogeneous systems, Akbari and Rashidi [41] propose an algorithm based on multiobjective scheduling cuckoo optimization algorithm to reduce execution time allowing for maximum parallelization, which is effectively implemented on a large number of random graphs and real-world application graphs with wide range characteristics. On the research of workflow execution dynamics in distributed environments, Yun et al. [42] formulate a generic problem considering both workflow mapping and task scheduling to minimize the end-to-end delay of workflows and propose an integrated solution to improve the workflow performance. Moreover, Shao et al. [43] study knowledge workforce assigning problem in software projects from three essential project management perspectives, timeliness, effectiveness, and efficiency, explore ideal workforce composites focused on productivity and quality with different scenarios of workload ratio, and propose an analytical model and a metaheuristic approach based on particle swarm optimization. In addition, Brown et al. [44] conduct a laboratory experiment to examine how task difficulty and different types of performance feedback (none, individual, and relative) affect individuals' selection and find that participants exhibit a strong better-than-average bias in assessing their relative skills on easy tasks and a moderate worse-than-average bias in assessing their relative skills on difficult tasks. As a multiobjective problem including time, cost, quality, and risk, the optimal allocation of distributed manufacturing resources is a challenging task for supply chain deployment. Zhang et al. [45] present an improved variant of the Teaching-Learning-Based Optimization algorithm to concurrently evaluate, select, and sequence the candidate distributed manufacturing resources allocated to subtasks comprising the supply chain. Yu et al. [46] incorporate the synergy effect between products in supplier selection process and propose a negotiation protocol including combinatorial procurement auction protocol and multibilateral bargaining protocol, by which both the purchasing company and suppliers can express their preferences on the synergy effect between products in negotiation process.

3. Task Selection of Bidirectional Behavior

During OSD process, designers contribute to product design by performing different and complex behaviors, such as task setting, release, selection, execution, interruption, collaboration, and screening, which directly drive the design process and influence product evolution as well as OSC evolution. In the numerous different kinds of behaviors, task selection behavior is a most essential one. Before task execution, designers need to select appropriate tasks which can obviously promote the evolution of OSD. Otherwise, subsequent execution of tasks, which are selected not matched to designers, will encounter more difficulties, thus affecting

quality and efficiency of OSD evolution. As a result, it has been a key issue on how to select tasks that are effectively matched to design agents. There are mainly two ways on task selection in OSD, which are passive selection based on website recommendation and autonomous selection based on task information [10, 38]. Although website recommendation provides much convenience to designers while selecting tasks, it is a type of passive selection behaviors for designers, by which the recommended tasks may not fully meet designers' requirement if the historical data are sparse or cannot reflect designers' preference. On the other hand, autonomous selection based on task information is a type of behaviors on designers' own initiative, but this selection is not effective in the condition of numerous tasks released in OSD process, which are too many for designers to autonomously select best matched tasks. Moreover, designers select tasks often considering both website recommendation and autonomous selection while contributing to OSD. As a result, the bidirectional selection behavior in consideration of both recommendation and autonomous selection is proposed in this paper. To correctly describe the bidirectional behavior, the designer is defined as design agent by the methodology of agent modeling which is proposed in preliminary study [9]. The model of bidirectional selection is built as follows.

3.1. Passive Behavior of Task Selection Based on Website Recommendation. According to this way, design agent selects task only based on recommendation service of website. In this case, the recommendation algorithm for task selection is key important. There are considerable researches on recommendation algorithms in related areas such as e-commerce [10, 11, 14]. In this paper, collaborative filtering algorithm is applied to recommend tasks to designers, which describes task recommendation mechanism based on a three-dimensional matrix including information on design agent, task, and skills. In the mechanism, the similarity between target agent and other design agent is firstly calculated based on evaluation information of tasks, skill information of agents, and skill demand information of tasks; secondly, some design agents are selected as recommendation agents whose similarities with target agent are relatively higher; thirdly, tasks which are completed by the recommendation agents and have not been selected by target agent are chosen into task recommendation list; then, each evaluation value of the task list by target agent is predicted, by which the task list is ordered; at last, a number of tasks which are selected from highest to lowest based on predicted evaluation values are recommended to target agent.

3.1.1. Three-Dimensional Matrix for Recommendation. The three-dimensional matrix is composed of information on design agent, task, and skill, which includes designer-task 0-1 matrix, designer-task evaluation matrix, designer-skill 0-1 matrix, designer-skill 0-1 matrix, designer-skill matrix, task-skill 0-1 matrix, and task-skill demand value matrix, as shown in Figure 1.

In Figure 1, D_i $(i = 1, 2, \ldots, n)$ denotes design agent, and n is the number of design agents; T_j $(j = 1, 2, \ldots, m)$ denotes the task of OSD, and m is the number of tasks; S_k $(k = 1, 2, \ldots, l)$ denotes the skill item, and l is the number of skill items.

$DT = (dt_{ij})$ $(dt_{ij} \in \{0, 1\})$ denotes designer-task 0-1 matrix, in which $dt_{ij} = 1$ means that D_i has completed T_j while $dt_{ij} = 0$ means that D_i has not selected T_j.

$DT' = (dt'_{ij})$ denotes designer-task evaluation matrix, in which dt'_{ij} represents the evaluation value of T_j by D_i after D_i completes it. If D_i does not select T_j, $dt_{ij} = 0 \Rightarrow dt'_{ij} = 0$.

$DS = (ds_{ik})$ $(ds_{ik} \in \{0, 1\})$ denotes designer-skill 0-1 matrix, in which $ds_{ik} = 1$ means that D_i masters skill item S_k while $ds_{ik} = 0$ means that D_i does not master S_k.

$DS' = (ds'_{ik})$ denotes designer-skill matrix, in which ds'_{ik} represents the level of D_i in S_k. If D_i does not master S_k, $ds_{ik} = 0 \Rightarrow ds'_{ik} = 0$.

$TS = (ts_{jk})$ $(ts_{jk} \in \{0, 1\})$ denotes task-skill 0-1 matrix, in which $ts_{jk} = 1$ means that it requires skill item S_k to execute T_j while $ds_{ik} = 0$ means that it does not.

$TS' = (ts'_{jk})$ denotes task-skill matrix, in which ts'_{jk} is the lower limit for S_k to execute T_j. If the execution of T_j does not require S_k, $ts_{jk} = 0 \Rightarrow ts'_{jk} = 0$.

3.1.2. Recommendation of Similar Design Agents

(1) Similarity between Design Agents. Similarity is a key factor to measure the similar degree between design agents and target agent. Based on corresponding references [32, 35], the similarity between target agent D_i and design agent $D_{i'}$ is calculated as formula (1)

$$\mathrm{Sim}(D_i, D_{i'}) = \frac{\sum \left(dt'_{ij} - \overline{DT_i^{ii'}}\right)\left(dt'_{i'j} - \overline{DT_{i'}^{ii'}}\right)}{\sqrt{\sum \left(dt'_{ij} - \overline{DT_i^{ii'}}\right)^2 \sum \left(dt'_{i'j} - \overline{DT_{i'}^{ii'}}\right)^2}},$$
$$\text{s.t.} \quad \begin{cases} \sum_{j=1}^{m} dt_{ij} dt_{i'j} \geq \Delta_t \\ \sum_{k=1}^{l} ds_{ik} ds_{i'k} \geq \Delta_s, \end{cases} \tag{1}$$

where Δ_t is the lower bound constraint for number of tasks completed by both D_i and $D_{i'}$; Δ_s is the lower bound constraint for number of skill items that both D_i and $D_{i'}$ master; $\overline{DT_i^{ii'}}$ is the mean evaluation value of tasks by D_i, which both D_i and $D_{i'}$ have rated, $\overline{DT_i^{ii'}} = \sum_{j=1}^{m} dt_{ij} dt_{i'j} dt'_{ij} / \sum_{j=1}^{m} dt_{ij} dt_{i'j}$; $\overline{DT_{i'}^{ii'}}$ is the mean evaluation value of tasks by $D_{i'}$, which both D_i and $D_{i'}$ have rated, $\overline{DT_{i'}^{ii'}} = \sum_{j=1}^{m} dt_{ij} dt_{i'j} dt'_{i'j} / \sum_{j=1}^{m} dt_{ij} dt_{i'j}$.

The value of the task evaluated by D_i is calculated as formula (2), which considers factors of time and incentive

$$dt'_{ij} = \alpha \frac{rt_j^T}{at_{ij} + rt_j^T} + (1 - \alpha) \frac{aw_{ij}/at_{ij}}{aw_{ij}/at_{ij} + aw_j^T/rt_j^T}, \tag{2}$$

where rt_j^T is rated completion time of task T_j; at_{ij} is the actual completion time of task T_j by D_i; aw_j^T is rated bonus after

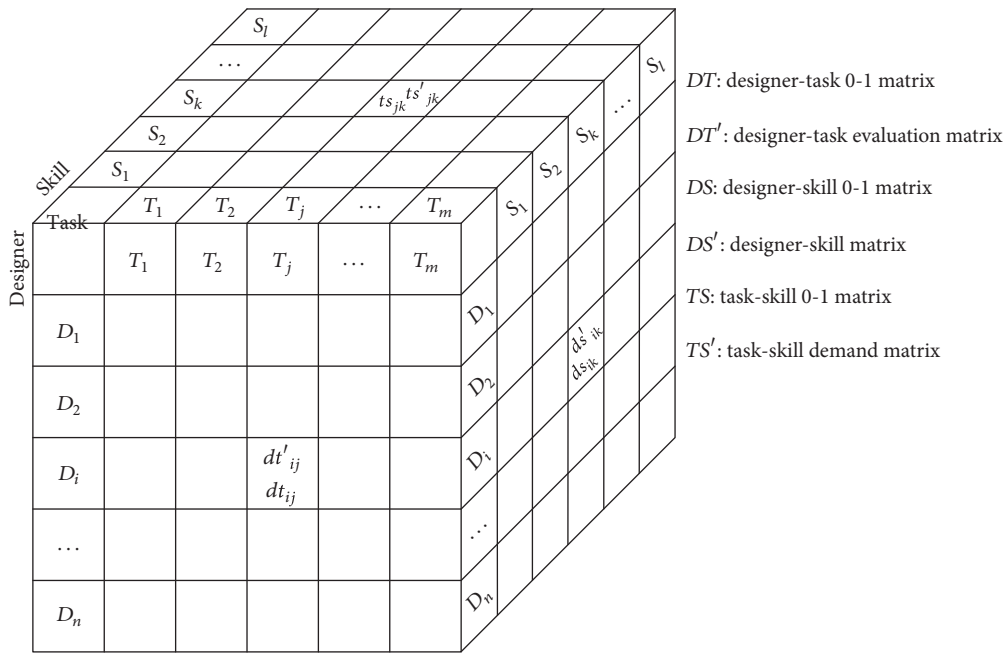

Figure 1: Three-dimensional matrix.

completion of task T_j; aw_{ij} is actual bonus after completion of task T_j by D_i; α is weight, $\alpha \in [0, 1]$.

(2) Screening Similar Design Agent. Design agent $D_{i'}$, whose similarity $\mathrm{Sim}(D_i, D_{i'})$ with D_i is one of K maximum similarities of the candidates, will be selected into recommendation set $\mathrm{KNN} = \{D_1, D_2, \ldots, D_K\}$.

(3) Prediction for Task Evaluation. Task T_j $(dt_{i'j} = 1, dt_{ij} = 0)$, which is not performed by D_i while completed and evaluated by $D_{i'}$ $(D_{i'} \in \mathrm{KNN})$, will be selected to calculate the predicted evaluation value fdt'_{ij} if performed by D_i, as formula (3)

$$fdt'_{ij} = \overline{DT_i} + \frac{\sum_{D_{i'}}^{\mathrm{KNN}} \mathrm{Sim}\left(D_i, D_{i'}\right)\left(dt'_{i'j} - \overline{DT_{i'}^{ii'}}\right)}{\sum_{D_{i'}}^{\mathrm{KNN}} \mathrm{Sim}\left(D_i, D_{i'}\right)}. \quad (3)$$

After the calculation, task T_j, whose predicted evaluation value fdt'_{ij} is one of the N maximum values of the candidate tasks, will be selected into recommendation task set RT_i, which is recommended to D_i.

(4) Cold Start Problem. If D_i never performs any task before $(\forall dt_{ij} = 0)$, D_i cannot be recommended for any task applying aforementioned algorithms without task evaluation data, which is the so-called cold start problem. To figure out the issue, a model to calculate incentive coefficient in consideration of incentive factor is proposed, which is applied to recommend D_i tasks, as formula (4)

$$e_{ij} = \frac{aw_j^T}{rt_j^T} \times \frac{aw_j^T}{aw_i^D} = \frac{\left(aw_j^T\right)^2}{rt_j^T aw_i^D},$$
$$\text{s.t.} \quad \sum_{k=1}^{l} ds_{ik} ts_{jk} \geq \Delta_s^{dt}, \quad (4)$$

where aw_i^D is cumulative bonus of D_i and Δ_s^{dt} is the lower bound constraint for number of skill items to perform T_j.

After the calculation, task T_j, whose incentive coefficient by D_i is one of the N maximum values of the candidate tasks, will be selected into recommendation task set RT_i, which is recommended to D_i.

3.2. Autonomous Selection according to Task Information. In OSD process, design agent often autonomously selects tasks from task series that OSC releases to public in consideration of some factors such as skill and incentive. To select satisfactory tasks, design agent performs the behavior by fitness f_{ij} as formula (5)

$$f_{ij} = \beta \times r_{ij} + (1 - \beta) \times e_{ij}, \quad (5)$$

where r_{ij} is similarity between D_i and T_j; e_{ij} is incentive coefficient to execute the task as formula (4); β is weight, $\beta \in [0, 1]$.

The calculation of r_{ij} is as formula (6)

$$r_{ij} = \frac{\sum_{k=1}^{l} \left(ds_{ik} ts_{jk}\right) \left(ds'_{ik} - \overline{DS_i^{ij}}\right) \left(ts'_{jk} - \overline{TS_j^{ij}}\right)}{\sqrt{\sum_{k=1}^{l} \left(ds_{ik} ts_{jk}\right) \left(ds'_{ik} - \overline{DS_i^{ij}}\right)^2 \sum_{k=1}^{l} \left(ds_{ik} ts_{jk}\right) \left(ts'_{jk} - \overline{TS_j^{ij}}\right)^2}} \quad (6)$$

$$\text{s.t.} \quad \sum_{k=1}^{l} ds_{ik} ts_{jk} > 0,$$

where $\overline{DS_i^{ij}}$ is mean value of D_i on S_k ($ds_{ik} = 1, ts_{jk} = 1$), $\overline{DS_i^{ij}} = \sum_{k=1}^{l} ds_{ik} ts_{jk} ds'_{ik} / \sum_{k=1}^{l} ds_{ik} ts_{jk}$, and $\overline{TS_j^{ij}}$ is mean requirement of T_j on S_k ($ds_{ik} = 1, ts_{jk} = 1$), $\overline{TS_j^{ij}} = \sum_{k=1}^{l} ds_{ik} ts_{jk} ts'_{jk} / \sum_{k=1}^{l} ds_{ik} ts_{jk}$.

By calculation as formula (5), task T_j, whose fitness f_{ij} is one of the N maximum values of the candidate tasks, will be selected into task set ST_i for autonomous selection.

3.3. Bidirectional Behavior of Task Selection. During OSD process, task array RT_i, which is recommended for D_i based on the three-dimensional recommendation algorithm, may not meet D_i's actual requirement for sparse data or designers' special preference. Meanwhile, D_i probably cannot select optimal task only by autonomous selection because of large number of tasks which cannot be traversed one by one. To figure out the problem, designers often take full account of both website recommendation and autonomous selection to perform task selection behavior, which is called bidirectional behavior of task selection. This kind of selection behavior is proposed to guarantee the tasks more in line with requirements of D_i. According to the methodology of bidirectional selection behavior, the selection process is calculated as follows.

(1) D_i calculates f_{ij} of each task T_j according to formula (5) in RT_i, which is obtained by the model of website recommendation.

(2) D_i integrates RT_i and ST_i which is obtained by the model of autonomous selection into one task array BT_i and rearranges the task series according to f_{ij}.

(3) D_i selects task T_j, whose f_{ij} is one of the N maximum values of BT_i, into task set FT_i for execution.

4. Simulation Study of Bidirectional Selection Behavior

4.1. Simulation Experiment Setting. According to the model of bidirectional selection behavior proposed in Section 3, simulation study is carried out to testify the efficiency of bidirectional behavior on OSD evolution.

Based on the model and the simulation platform [9], the simulation study is carried out according to a cell phone design scenario abstracted from corresponding references [47–49]. In this scenario, cell phone is composed of many components, such as front cover, rear cover, main board, keyboard, battery, screen, receiver, microphone, antenna, Wi-Fi, and camera. These components are independent but relative. For example, front cover, rear cover, and screen are independent in function design, but compatible in assembling, so the relationship among the three parts should be taken into account. Based on the scenario derived from the references, the relationship of module tasks is set in the simulation platform as shown in Figure 2.

Figure 2 is mainly composed of two icons, which are *Task* and *Info*, respectively. *Task* denotes two types of tasks which are initial module task and collaboration task in OSD process. Initial module task, shown as T_i ($i = 0, 1, 2, \ldots, 19$), is the basic composition of OSD project, which is divided and packaged according to product function as well as skill requirement, such as front cover, rear cover, and main board of a cell phone. Meanwhile, collaboration task, shown as T_i ($i > 19$), is generated if design agent asks for collaboration while executing initial module tasks. During OSD process, each task, no matter initial module task or collaboration task, can be selected by design agents autonomously. *Info* shows the information of tasks that are connected directly, such as task triggering time and precedence relationship between tasks. In addition, Table 1 lists some important parameters, which quantify task requirement and rewards for design agents. In this scenario, the number of skill items is set as 3.

Besides, some key parameters in the simulation are initialized as shown in Table 2, in which *S*1, *S*2, and *S*3 are three comparison scenarios corresponding to passive behavior of selection by recommendation, autonomous selection behavior, and bidirectional selection behavior, respectively. According to the parameter settings, each scenario is simulated 100 times, obtaining 100 data samples for comparative analysis.

4.2. ANOVA of Three Task Selection Behaviors. In this section, Analysis of Variance (ANOVA) is carried out to analyze if task selection behavior influences OSD process and bidirectional behavior is best effective of the three. In this way, the analysis can be applied as assistant decision of task selection in OSD process. The hypothesis for ANOVA is as follows.

H_0: $\mu_1 = \mu_2 = \mu_3$ (task selection behavior has no effect on evolution cycle of OSD)

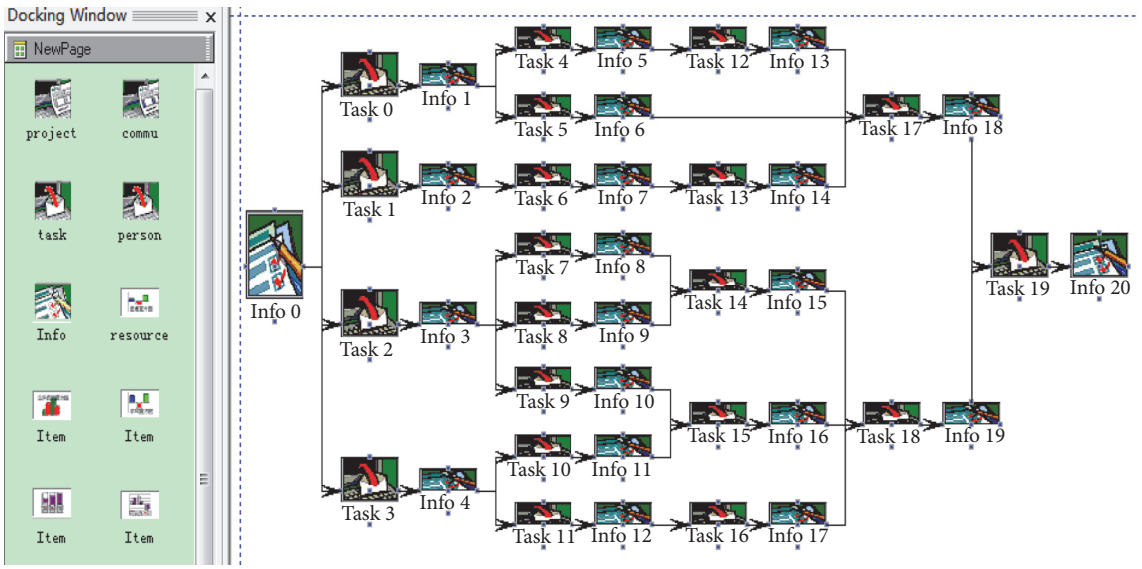

Figure 2: Module task relationship of the scenario.

Table 1: Parameters of task requirement and rewards for design agent.

Task ID	0	1	2	3	4	5	6	7	8	9
Matrix of skill demand	6.26	5.148	27.617	4.263	25.522	16.358	26.001	12.857	14.106	7.669
	3.048	8.416	10.769	8.104	11.663	15.208	10.85	22.561	28.413	0.138
	17.775	13.931	20.516	6.793	28.474	3.164	3.596	5.155	3.253	16.934
Rated bonus	16.6	17.1	16.5	18.1	21.2	17.5	9.6	9.1	10	18.1
Task ID	10	11	12	13	14	15	16	17	18	19
Matrix of skill demand	15.629	20.203	7.088	16.334	23.616	9.666	19.539	13.936	13.301	22.179
	23.029	28.172	19.139	3.754	14.665	1.196	21.834	25.224	3.539	12.78
	22.335	26.397	24.824	2.134	21.044	22.271	21.92	21.208	29.694	7.338
Rated bonus	12.1	12.3	14.3	13.6	18.1	15.5	28	20.1	20.5	20

Table 2: Partial parameters of simulation experiment.

Parameter name	Parameter setting
Scenario	$S1$, $S2$, $S3$
Community scale (number of agents)	200
Task selection method for each scenario	$S1$: passive behavior of task selection by recommendation $S2$: autonomous selection behavior $S3$: bidirectional selection behavior
Simulation time	300 (100/scenario)

H_1: $\mu_1 \neq \mu_2 \neq \mu_3$ (task selection behavior has significant effect on evolution cycle of OSD)

According to the hypothesis, ANOVA is applied with SPSS to process the data of three scenarios which are extracted from simulation experiments, as shown in Table 4.

The results of ANOVA show that task selection behavior has significant effect on evolution cycle of OSD. $\mu_1 = 391.52$ (mean value of evolution cycle in $S1$) is significantly longer than that of $S2$ and $S3$. Data analysis of evolution process in $S1$ shows that task recommendation does not do well at the beginning of OSD process because there is not enough information on task evaluation for recommendation, which is the main reason that results in longer evolution cycle. $\mu_2 = 373.1$ (mean value of evolution cycle in $S2$) is significantly shorter than $S1$'s cycle but longer than that of $S3$. The main reason is that the scale of design tasks in $S2$ is not quite large which is not difficult for design agent to autonomously select compatible tasks. $\mu_3 = 364.81$ (mean value of evolution cycle in $S3$) is significantly shorter than that of $S2$ and $S3$. The main reason is that design agent can select more matched tasks in combination with website recommendation and autonomous selection. As a result, compared with $S1$ and $S2$, $S3$ is more effective to promote evolution process of OSD.

Simulation study shows that task selection behavior of design agent has significant effect on evolution process of OSD. In this experiment with moderate task scale, the bidirectional behavior of task selection is more effective to shorten evolution cycle. However, it should be testified which selection behavior is more effective if task scale is much larger in further study.

Table 3: Task selection of A_{13}.

Order	Simulation step	Task recommendation				Autonomous selection			Final selection		
		Task number	Task ID	fdt'_{ij}	f_{ij}	Task number	Task ID	f_{ij}	Task number	Task ID	f_{ij}
1	0	4	3	1.389110	0.304965	3	2	0.730274	3	2	0.730274
			1	1.239946	0.376856		1	0.376856		0	0.686295
			2	1.024853	0.730274		3	0.304965		1	0.376856
			0	0.784246	0.686295						
2	149	1	6	0.050432	0.269533	1	6	0.269533	1	6	0.269533
3	157	1	14	0.113611	0.269073	1	14	0.269073	1	14	0.269073
4	176	2	484	0.008573	0.240730	1	485	0.24942	2	485	0.249420
			485	0.005935	0.249420					484	0.240730
5	188	2	13	0.076980	0.128854	2	15	0.222744	2	15	0.222744
			15	0.060707	0.222744		13	0.128854		13	0.128854
6	254	1	17	0.125698	0.271574	1	17	0.271574	1	17	0.271574
7	286	1	18	0.100443	0.208817	1	18	0.208817	1	18	0.208817
8	315	1	19	0.104335	0.182663	1	19	0.182663	1	19	0.182663

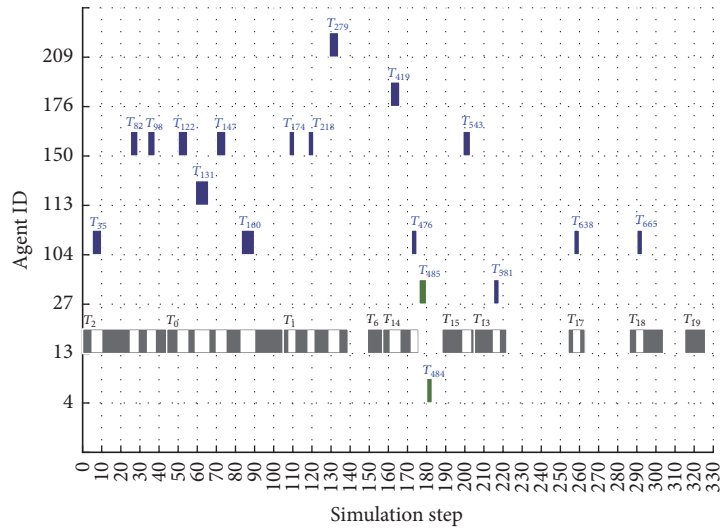

Figure 3: Task selection and execution flow of A_{13}.

4.3. Simulation Analysis of Bidirectional Selection Process. According to previous analysis, bidirectional behavior of task selection is testified to be the best of three behaviors of task selection based on simulation experiment setting. To describe and analyze designer's bidirectional behavior of task selection integrating website recommendation and autonomous selection during OSD process, a data set is extracted from data sample of *S*3. The data set records the task selection behaviors of design agent A_{13} in OSD process. The task selection of A_{13} is shown as Table 3 and Figure 3.

As shown in Table 3, A_{13} performs bidirectional behaviors of task selection for 8 times during this OSD process. In each time, the bidirectional selection behavior contains 3 phases: website recommendation, autonomous selection, and integrated selection. Firstly, the system recommends A_{13} some tasks which are sorted by website recommendation according to formula (3); secondly, A_{13} chooses some tasks autonomously from OSS and sorts them according to formula (5); meanwhile, corresponding values of tasks that are recommended are also calculated based on formula (5); at last, A_{13} integrates the tasks that are recommended or autonomously chosen, sorts them by values based on formula (5), and selects tasks in descending order, which is also the order of task execution subsequently. Table 3 shows the detailed data for bidirectional selection behavior of A_{13}.

As shown in Figure 3, vertical axis denotes design agent ID, and horizontal axis denotes simulation step of OSD. During the whole process, A_{13} selects and executes 28 tasks, including 10 module tasks (T_2, T_0, T_1, T_6, T_{14}, T_{15}, T_{13}, T_{17}, T_{18}, and T_{19}) which are shown as gray blocks, and 18 collaboration tasks (T_{35}, T_{82}, T_{98}, T_{122}, T_{131}, T_{147}, T_{160}, T_{174}, T_{218}, T_{279}, T_{419}, T_{476}, T_{485}, T_{484}, T_{543}, T_{581}, T_{638}, and T_{665}) which are shown as blue or green blocks (blue ones represent online collaboration tasks; green ones represent offline collaboration tasks) [9].

Table 4: ANOVA of task selection behaviors.

(a) Descriptives

					Sample			
	N	Mean	Std. deviation	Std. error	95% confidence interval for mean		Minimum	Maximum
					Lower bound	Upper bound		
1	100	391.520000	23.3949317	2.3394932	386.877938	396.162062	334.0000	451.0000
2	100	373.100000	25.8732341	2.5873234	367.966189	378.233811	293.0000	432.0000
3	100	364.810000	22.5266150	2.2526615	360.340231	369.279769	310.0000	423.0000
Total	300	376.476667	26.3800901	1.5230552	373.479401	379.473932	293.0000	451.0000

(b) Test of homogeneity of variances

Sample			
Levene statistic	df1	df2	Sig.
1.025	2	297	.360

(c) ANOVA

Sample					
	Sum of squares	df	Mean square	F	Sig.
Between groups	37381.487	2	18690.743	32.521	.000
Within groups	170695.350	297	574.732		
Total	208076.837	299			

(d) Multiple comparisons

Dependent variable: sample						
LSD						
(I) group	(J) group	Mean difference (I-J)	Std. error	Sig.	95% confidence interval	
					Lower Bound	Upper Bound
1	2	18.4200000*	3.3903741	.000	11.747800	25.092200
	3	26.7100000*	3.3903741	.000	20.037800	33.382200
2	1	−18.4200000*	3.3903741	.000	−25.092200	−11.747800
	3	8.2900000*	3.3903741	.015	1.617800	14.962200
3	1	−26.7100000*	3.3903741	.000	−33.382200	−20.037800
	2	−8.2900000*	3.3903741	.015	−14.962200	−1.617800

*The mean difference is significant at the .05 level.

During collaboration process, A_{13} collaborates with A_{150} for 7 times (T_{82}, T_{98}, T_{122}, T_{147}, T_{174}, T_{218}, and T_{543}), A_{104} for 5 times (T_{35}, T_{160}, T_{476}, T_{638}, and T_{665}), A_{27} for 2 times (T_{485} and T_{581}), A_4 (T_{484}), A_{113} (T_{131}), A_{176} (T_{419}), and A_{209} (T_{279}) for 1 time, respectively. In this simulation, design agent's bidirectional selection behavior as well as execution behavior in OSD process is described in detail.

Compared to Table 3, tasks (T_{35}, T_{82}, T_{98}, T_{122}, T_{131}, T_{147}, T_{160}, T_{174}, T_{218}, T_{279}, T_{419}, T_{476}, T_{543}, T_{581}, T_{638}, and T_{665}) that are blue blocks are not in selection list of Table 3, indicating that they are not selected by A_{13}. This is because that these tasks are generated by A_{13} itself while executing module tasks but encountering exception for collaboration, corresponding to the blank blocks of module tasks in Figure 3, and that they are not released to public but directly sent to corresponding design agents for online collaboration.

The simulation describes the process of designer's bidirectional selection behavior in microperspective and proves that the model of bidirectional selection is effective in OSD process by simulation analysis with the table and figure aforementioned.

5. Conclusions

5.1. Contributions. It is a tough issue for designers to select tasks completely fit to them in OSD process, which also directly impacts the efficiency of OSD evolution. Thus, designers' bidirectional behavior of task selection integrating passive selection of website recommendation and autonomous selection is modeled in this paper. Passive selection behavior based on website recommendation is modeled with application of collaborative filtering algorithm to recommend tasks to designers by predication, which describes recommendation process based on a three-dimensional matrix including information on design agent, task, and skills; autonomous selection behavior is described in consideration of factors such as skill and incentive; the bidirectional selection model integrates the aforementioned two selection

algorithms to describe designers' selection behaviors who usually select tasks in consideration of both OSD recommendation and autonomous selection. By simulation comparison of bidirectional selection, passive selection based on website recommendation, and autonomous selection with ANOVA, analysis is carried out to show that task selection behavior has significant effect on OSD evolution process and that bidirectional selection behavior is more effective to shorten evolution cycle according to the experiment settings on community scale and task number. In addition, the simulation study shows the process of task selection in microperspective and testifies the model of bidirectional selection.

5.2. Implications. In OSD (e.g., SourceForge, NetBeans) [50, 51], there are millions of projects/products/tasks provided to designers for selection and contribution. For designers, it is really difficult to find right one from mass abundant tasks and also costs time, which may block their contributions to OSD. For OSD, it is a key issue how to guarantee the projects/products/tasks matching to designers. Therefore, the bidirectional selection method is proposed to solve the problems.

On the one hand, it will provide designers much convenience to select right tasks by OSD recommendation. Besides, it will provide designers more personalized services on project/product/task selection including both recommendation and autonomous selection. On the other hand, it will provide OSD managers useful advice on how to match designers and projects/products/tasks in consideration of factors such as skill and incentive, by bidirectional selection simulation, which will help coordinate resources of OSD and promote the development of projects/products/tasks effectively. In addition, the findings prove that agent-based modeling and simulation can be taken as an approach to study the open source design process. In this paper, designer's selection behavior is abstracted by agent modeling, which represents both his/her subjective factors (e.g., incentive) and objective factors (e.g., skill) while making decisions. Meanwhile, the selection process is described by agent simulation, which describes not only individual's decision process, but also OSD's evolution process. As a result, the proposed bidirectional selection method can be applied in practice benefiting both designers and OSD.

5.3. Future Work. Although the bidirectional selection method is proved to provide much convenience in task selection of OSD, there are some limitations to solve. First, the algorithm cannot work effectively if the number of designers and tasks is too huge, because the paper does not provide a corresponding method to solve this problem. Second, more factors should be considered in the bidirectional selection algorithm to help designers select more proper tasks and provide more effective advice on matching tasks and designers as well as promoting OSD evolution.

In future work, intelligence algorithms such as genetic algorithm will be added to solve the problem of large number of tasks and designers. Besides, more simulation experiments, in consideration of more complex factors, such as designers' preference, community scale, and task number, will be designed and carried out to study which selection scheme is more effective to product design as well as OSD evolution.

Conflicts of Interest

The authors declare that there are no conflicts of interest regarding the publication of this paper.

Authors' Contributions

Shuo Zhang and Yingzi Li contributed equally to this work.

Acknowledgments

This contribution is based upon the research work supported by the National Natural Science Foundation of China no. 71601078, Humanities and Social Sciences of Education Ministry in China no. 16YJC630060, the Social Science Fund of Beijing no. 16GLC070, and the Fundamental Research Funds for the Central Universities no. 2016MS72.

References

[1] Don Tapscott and A. D. Williams, *Wikinomics: How Mass Collaboration Changes Everything*, Portfolio Hardcover, 2006.

[2] E. V. Hippel, *Democratizing Innovation: The Evolving Phenomenon of User Innovation*, vol. 55, MIT Press, pp. 63-78, 2005.

[3] J. H. Panchal and M. Fathianathan, "Product realization in the age of mass collaboration," in *Proceedings of ASME International Design Engineering Technical Conferences and Computers and Information in Engineering Conference*, pp. 219–229, 2008.

[4] K. Crowston and J. Howison, "Hierarchy and centralization in free and open source software team communications," *Knowledge, Technology & Policy*, vol. 18, no. 4, pp. 65–85, 2006.

[5] C. Kohtala, "Addressing sustainability in research on distributed production: An integrated literature review," *Journal of Cleaner Production*, vol. 106, pp. 654–668, 2015.

[6] G. Müller-Seitz and G. Reger, "Networking beyond the software code? an explorative examination of the development of an open source car project," *Technovation*, vol. 30, no. 11-12, pp. 627–634, 2010.

[7] B. Rolandsson, M. Bergquist, and J. Ljungberg, "Open source in the firm: Opening up professional practices of software development," *Research Policy*, vol. 40, no. 4, pp. 576–587, 2011.

[8] R. J. Davies et al., "A user driven approach to develop a cognitive prosthetic to address the unmet needs of people with mild dementia," *Pervasive & Mobile Computing*, vol. 5, no. 3, pp. 253–267, 2009.

[9] S. Zhang, Y. Li, and X. Zhang, "Agent behavior-based simulation study on mass collaborative product development process," *Mathematical Problems in Engineering*, vol. 2015, Article ID 689383, 10 pages, 2015.

[10] L. Lü, M. Medo, C. H. Yeung, Y. Zhang, Z. Zhang, and T. Zhou, "Recommender systems," *Physics Reports*, vol. 519, no. 1, pp. 1–49, 2012.

[11] J. Lu, D. S. Wu, M. S. Mao, W. Wang, and G. Zhang, "Recommender system application developments: a survey," *Decision Support Systems*, vol. 74, pp. 12–32, 2015.

[12] J. Liu, M. Tang, Z. Zheng et al., "Location-aware and personalized collaborative filtering for web service recommendation,"

IEEE Transactions on Services Computing, vol. 9, no. 5, pp. 686–699, 2016.

[13] Y.-Y. Shih and D.-R. Liu, "Product recommendation approaches: Collaborative filtering via customer lifetime value and customer demands," *Expert Systems with Applications*, vol. 35, no. 1-2, pp. 350–360, 2008.

[14] R. Zhang and T. Tran, "An information gain-based approach for recommending useful product reviews," *Knowledge and Information Systems*, vol. 26, no. 3, pp. 419–434, 2011.

[15] F. Rodrigues and B. Ferreira, "Product recommendation based on shared customer's behaviour," *Procedia Computer Science*, vol. 100, pp. 136–146, 2016.

[16] P. A. Riyaz and S. M. Varghese, "A scalable product recommendations using collaborative filtering in hadoop for bigdata," *Procedia Technology*, vol. 24, pp. 1393–1399, 2016.

[17] M. Zhang, X. Guo, and G. Chen, "Prediction uncertainty in collaborative filtering: Enhancing personalized online product ranking," *Decision Support Systems*, vol. 83, pp. 10–21, 2016.

[18] D. Geiger and M. Schader, "Personalized task recommendation in crowdsourcing information systems—current state of the art," *Decision Support Systems*, vol. 65, no. 1, pp. 3–16, 2014.

[19] M. Nilashi, O. B. Ibrahim, and N. Ithnin, "Hybrid recommendation approaches for multi-criteria collaborative filtering," *Expert Systems with Applications*, vol. 41, no. 8, pp. 3879–3900, 2014.

[20] K. Choi, Y. Suh, and D. Yoo, "Extended collaborative filtering technique for mitigating the sparsity problem," *International Journal of Computers Communications & Control*, vol. 11, no. 5, p. 631, 2016.

[21] R. Katarya and O. P. Verma, "An effective collaborative movie recommender system with cuckoo search," *Egyptian Informatics Journal*, 2016.

[22] H. Li, J. Cui, B. Shen, and J. Ma, "An intelligent movie recommendation system through group-level sentiment analysis in microblogs," *Neurocomputing*, vol. 210, pp. 164–173, 2016.

[23] M. Á. García-Cumbreras, A. Montejo-Ráez, and M. C. Díaz-Galiano, "Pessimists and optimists: improving collaborative filtering through sentiment analysis," *Expert Systems with Applications*, vol. 40, no. 17, pp. 6758–6765, 2013.

[24] S. Wei et al., "A hybrid approach for movie recommendation via tags and ratings," *Electronic Commerce Research & Applications*, vol. 18, pp. 83–94, 2016.

[25] D. Sánchez-Moreno, A. B. Gil González, M. D. Muñoz Vicente, V. F. López Batista, and M. N. Moreno García, "A collaborative filtering method for music recommendation using playing coefficients for artists and users," *Expert Systems with Applications*, vol. 66, pp. 234–244, 2016.

[26] X. Bai, B. Barla Cambazoglu, F. Gullo, A. Mantrach, and F. Silvestri, "Exploiting search history of users for news personalization," *Information Sciences*, pp. 125–137, 2017.

[27] F. Zhao, F. Yan, H. Jin, L. T. Yang, and C. Yu, "Personalized mobile searching approach based on combining content-based filtering and collaborative filtering," *IEEE Systems Journal*, pp. 1–9, 2015.

[28] Y. D. Seo, Y. Kim, E. Lee, and D. Baik, "Personalized recommender system based on friendship strength in social network services," *Expert Systems with Applications*, vol. 69, pp. 135–148, 2017.

[29] A. Shahmohammadi, E. Khadangi, and A. Bagheri, "Presenting new collaborative link prediction methods for activity recommendation in Facebook," *Neurocomputing*, vol. 210, pp. 217–226, 2016.

[30] C. Guo, B. Li, and X. Tian, "Flickr group recommendation using rich social media information," *Neurocomputing*, vol. 204, pp. 8–16, 2016.

[31] N. Zheng and Q. Li, "A recommender system based on tag and time information for social tagging systems," *Expert Systems with Applications*, vol. 38, no. 4, pp. 4575–4587, 2011.

[32] S. Y. Lin et al., "A trustworthy QoS-based collaborative filtering approach for web service discovery," *Journal of Systems & Software*, vol. 93, no. 4, pp. 217–228, 2014.

[33] C. H. Lai and D. R. Liu, "Integrating knowledge flow mining and collaborative filtering to support document recommendation," *Journal of Systems and Software*, vol. 82, no. 12, pp. 2023–2037, 2009.

[34] J. Wei, J. He, K. Chen, Y. Zhou, and Z. Tang, "Collaborative filtering and deep learning based recommendation system for cold start items," *Expert Systems with Applications*, vol. 69, pp. 29–39, 2017.

[35] H. N. Kim. et al., "Collaborative filtering based on collaborative tagging for enhancing the quality of recommendation," *Commerce Research & Applications*, vol. 9, no. 1, pp. 73–83, 2010.

[36] C. C. Chen, Y. H. Wan, M. C. Chung, and Y. C. Sun, "An effective recommendation method for cold start new users using trust and distrust networks," *Information Sciences*, vol. 224, no. 2, pp. 19–36, 2013.

[37] G. Lv, C. Hu, and S. Chen, "Research on recommender system based on ontology and genetic algorithm," *Neurocomputing*, vol. 187, pp. 92–97, 2016.

[38] U. Ul Hassan and E. Curry, "Efficient task assignment for spatial crowdsourcing," *Expert Systems with Applications*, vol. 58, no. C, pp. 36–56, 2016.

[39] P. Brahmbhatt and S. G. Camorlinga, "Epidemiology-based task assignment algorithm for distributed systems," *Procedia Computer Science*, vol. 95, pp. 428–435, 2016.

[40] D. A. Nembhard and F. Bentefouet, "Selection, grouping, and assignment policies with learning-by-doing and knowledge transfer," *Computers and Industrial Engineering*, vol. 79, pp. 175–187, 2015.

[41] M. Akbari and H. Rashidi, "A multi-objectives scheduling algorithm based on cuckoo optimization for task allocation problem at compile time in heterogeneous systems," *Expert Systems with Applications*, vol. 60, no. C, pp. 234–248, 2016.

[42] D. Yun, C. Q. Wu, and Y. Gu, "An integrated approach to workflow mapping and task scheduling for delay minimization in distributed environments," *Journal of Parallel and Distributed Computing*, vol. 84, pp. 51–64, 2015.

[43] B. B. M. Shao, P.-Y. Yin, and A. N. K. Chen, "Organizing knowledge workforce for specified iterative software development tasks," *Decision Support Systems*, vol. 59, no. 1, pp. 15–27, 2014.

[44] J. L. Brown, S. Farrington, and G. B. Sprinkle, "Biased self-assessments, feedback, and employees' compensation plan choices," *Accounting Organizations & Society*, vol. 54, pp. 45–59, 2016.

[45] W. Zhang, S. Zhang, S. Guo, Y. Yang, and Y. Chen, "Concurrent optimal allocation of distributed manufacturing resources using extended teaching-learning-based optimization," *International Journal of Production Research*, vol. 55, no. 3, pp. 718–735, 2016.

[46] C. Yu, T. N. Wong, and Z. Li, "A hybrid multi-agent negotiation protocol supporting supplier selection for multiple products with synergy effect," *International Journal of Production Research*, pp. 1–20, 2016.

[47] Q. Le and J. H. Panchal, "Modeling the effect of product architecture on mass-collaborative processes," *Journal of Computing & Information Science in Engineering*, vol. 11, no. 1, pp. 333–359, 2011.

[48] K. Hölttä, E. S. Suh, and O. D. Weck, "Tradeoff between modularity and performance for engineered systems and products," in *Proceedings of the International Conference on Engineering Design: Engineering Design & the Global Economy Engineers (ICED '05)*, Australia, 2005.

[49] K. Hölttä-Otto and O. de Weck, "Degree of modularity in engineering systems and products with technical and business constraints," *Concurrent Engineering Research and Applications*, vol. 15, no. 2, pp. 113–125, 2007.

[50] O. Temizkan and R. L. Kumar, "Exploitation and exploration networks in open source software development: an artifact-level analysis," *Journal of Management Information Systems*, vol. 32, no. 1, pp. 116–150, 2015.

[51] T. Zhang, J. Chen, G. Yang, B. Lee, and X. Luo, "Towards more accurate severity prediction and fixer recommendation of software bugs," *Journal of Systems and Software*, vol. 117, no. C, pp. 166–184, 2016.